Lecture Notes in Engineering

Edited by C. A. Brebbia and S. A. Orszag

1

J. C. F. Telles

The Boundary Element Method Applied to Inelastic Problems

Springer-Verlag
Berlin Heidelberg New York Tokyo

Lecture Notes in Engineering

The Springer-Verlag Lecture Notes provide rapid (approximately six months), refereed publication of topical items, longer than ordinary journal articles but shorter and less formal than most monographs and textbooks. They are published in an attractive yet economical format; authors or editors provide manuscripts typed to specifications, ready for photo-reproduction.

The Editorial Board

Lecture Notes in Engineering

Edited by C.A. Brebbia and S.A. Orszag

1

J.C.F. Telles

The Boundary Element Method Applied to Inelastic Problems

Springer-Verlag
Berlin Heidelberg New York Tokyo 1983

Author
J.C.F. Telles, M.Sc., Ph.D.
Professor Adjunto,
COPPE – Univ. Federal do Rio de Janeiro,
Programa de Engenharia Civil,
Caixa Postal 68506,
21944 – Rio de Janeiro,
Brazil

ISBN-13: 978-3-540-12387-3 e-ISBN-13: 978-3-642-45562-9
DOI: 10.1007/978-3-642-45562-9

Library of Congress Cataloging in Publication Data
Telles, J. C. Faria (José Claudio Faria), 1950-
The boundary element method for inelastic problems.
(Lecture notes in engineering ; 1)
Bibliography: p.
1. Plasticity. 2. Boundary value problems.
I. Title. II. Series.
TA418.14.T44 1983 620.1'1233 83-685

2061/3020-543210

FOREWORD

These notes correspond to a research project carried out at Southampton University while I was on leave from the Federal University of Rio de Janeiro.

The main object of the work is the application of the direct boundary element method for the solution of nonlinear material problems. To this end, the elastic formulation of the technique is first introduced by considering two and three-dimensional problems employing the fundamental solutions corresponding to the infinite and semi-infinite spaces. Thus, in addition to the known Kelvin and Mindlin solutions, the complete fundamental solution due to a unit point load within the half-plane is presented and its implementation discussed in detail, including the results of some classical examples.

Three alternative formulations - initial strain, initial stress and fictitious forces - are discussed for 3-D and 2-D inelastic problems. The numerical implementation of the first two approaches is then presented for two-dimensional problems, including the half-plane fundamental solution.

Different applications of the inelastic boundary element equations to pure elastoplastic analysis are presented. The initial strain formulation is implemented with the von Mises yield criterion and employs a simple solution technique. The initial stress implementation is more general and can handle four different yield criteria, with two different solution routines. A common feature of the alternative implementations is that they are all incremental - iterative processes, capable of performing iterations by using a single recursive expression, relating stresses to the plastic strains and the initial elastic solution.

Finally, the implementation of the B.E. technique to viscoplasticity and creep is accomplished by using the initial stress equations in conjunction with an Euler time integration procedure.

Several examples are presented to outline the accuracy and applicability of the different formulations, these involve elastoplastic, creep and viscoplastic problems.

I wish to express my sincere gratitude to Dr. C. A. Brebbia for his stimulating influence in this work and also to the other members of his research group: W. Mansur, L. Wrobel, W. Venturini, P. Georgiou, M. Kavanagh and J. Waters for many invaluable discussions and useful suggestions.

A special mention is deserved for my wife, Elvira, without whose patience and understanding this work would not have been possible.

The financial support provided by the Federal University of Rio de Janeiro and the Brazilian National Council for Scientifical and Technological Development (C.N.Pq.) is also greatly acknowledged.

Southampton, September 1981 J. C. F. Telles

TABLE OF CONTENTS

NOTATION

u_j		displacement components
p_j		traction components
ε_{ij}		total strain components
σ_{ij}		stress components
ε^a_{ij}		inelastic strain components
σ^a_{ij}		"initial stress" due to ε^a_{ij}
b_j		body force components
$\hat{\theta}$	=	$\varepsilon^a_{11} + \varepsilon^a_{22} + \varepsilon^a_{33}$ for 3-D and plane strain $\varepsilon^a_{11} + \varepsilon^a_{22}$ for plane stress
u^*_{ij}, p^*_{ij} ε^*_{jki}, σ^*_{jki} u^*_{ijk}, p^*_{ijk} $\varepsilon^*_{ijk\ell}$, $\sigma^*_{ijk\ell}$		components of the tensors corresponding to the fundamental solutions
E, G		Young's and shear moduli
ν		Poisson's ratio
$\bar{\nu}$	=	$\nu/(1+\nu)$
Γ		boundary of the body
Ω		domain of the body (open region)
k		work hardening parameter
σ_e, ε_e, ε^a_e		equivalent stress, equivalent total strain and equivalent inelastic strain respectively
δ_{ij}		Kronecker delta symbol
Φ		material function to be determined experimentally
σ_o		uniaxial yield stress
c'		cohesion of the material

ϕ'	angle of internal friction
H'	slope of the uniaxial static curve plotted as stress versus plastic strain
γ, K	material parameters
$(\bar{r}, \bar{\theta})$	cylindrical coordinate system
s	load point
q	field point
r	distance between s and q
$\bar{\Gamma}$	traction-free surface of half-space or half-plane
s'	image of s with respect to $\bar{\Gamma}$
R	distance between s' and q
$\delta(s, q)$	Dirac delta function
(r, ϕ)	cylindrical coordinate system based at s
t	time
n_j	direction cosines of outward normal to the boundary of the body
η	intrinsic coordinate associated with 2-D boundary element
ξ_i	homogeneous coordinates associated with 2-D internal cell

CHAPTER 1

INTRODUCTION AND MOTIVATION

1.1 Introduction

Numerical methods for the solution of problems related to continuum mechanics have been investigated by engineers and physical scientists for many years. Quite generally, such methods can be classified in three main categories; finite differences, finite elements and boundary elements. The former is probably the first successfully applied numerical method and is usually derived by direct application of a difference operator corresponding to the governing differential equation of the problem. This operation is carried out at a series of points (nodes) within the domain of the body and generates a narrow banded system of equations relating the value of the unknown function at such nodal points to the boundary conditions at selected points over the boundary. These equations can then be solved by a direct procedure in linear problems or iteratively for nonlinear cases. This last feature, i.e. the possibility of easily extending the technique to deal with geometric and material nonlinear problems, is a direct consequence of the simple concept involved in its implementation and partly justifies the great deal of attention that has been given to the technique[11], [12]. The method, however, possesses some drawbacks which are immediately apparent when problems with complicated boundary geometries are attempted. In addition, simplicity pays its price when relatively accurate solutions are desired for the technique usually requires a large number of nodal points to represent realistically the actual solution to the problem. Consequently, it is not surprising that finite

difference methods have become superseded by more sophisticated techniques such as those pertaining to the finite element category.

The finite element method [13, 14] is by far the most popular numerical method nowadays. The domain of the body is subdivided into a collection of connected subdomains, of rather simple shape, called finite elements. Trial functions, usually polynomials, are then chosen to locally approximate the actual behaviour of the solution. These functions are uniquely defined in terms of the approximated values of the solution (and possibly its derivatives) at certain nodal points located inside or on the boundary of each element. A "best fit" for the approximation is then obtained through the application of some weighted residual technique or variational principle (such as energy minimization), leading to a normally banded and symmetric system of equations which involves the unknown values of the approximated solution at the nodal points. The method is, without doubt, computationally more efficient than the early finite difference approach and during the last twenty years has reached such a stage of development that a very wide range of linear and nonlinear unsolved engineering problems are now amenable to solutions within the context of this powerful numerical method [15, 16].

There are, however, many classes of problems for which finite elements do not behave satisfactorily and this has led researchers to look for alternative techniques such as those based on integral equations.

In these modern techniques, the governing differential equation of the problem, which involves the behaviour of the unknown solution inside and on the surface of the domain, is transformed into an integral equation defined over the surface, thus enabling the reduction of the

dimensionality of the problem by one. The surface may then be discretized into a number of boundary elements over which polynomial functions, of the type used in finite elements, are introduced to interpolate the values of the approximated solution between the nodal points. This allows for the evaluation of the relevant integrals, usually by some numerical process, resulting in a final system of equations which, although fully populated, is of much smaller size than the finite element counterpart.

Methods included in the above pattern are here designated boundary element methods [1, 2], for they reduce the approximation of the solution to the boundary by using an "element" type discretization. However, "boundary integral equation" methods [3, 4] is also a common name broadly found in the literature.

Boundary element methods present important features that plainly justify the increasing popularity achieved in recent years; (i) reduced set of equations, (ii) simple data preparation to run a problem, (iii) infinite or semi-infinite problems are properly modelled, (iv) accurate selective calculation of internal stresses and displacements and (v) great resolution for stress concentration problems are some of the main characteristics. Such methods, themselves, can be classified into two groups [5] : indirect and direct. This classification, perhaps over simplified, helps to outline the main differences in the approaches most used today.

In the indirect formulation, the integral equations are expressed entirely in terms of a unit singular solution of the differential equation, distributed over the boundary, with specific unknown densitites. Such density functions have no physical significance, but once their values have been obtained, the displacements

and stresses can be readily computed. Numerical algorithms based on this approach have been described for elastic problems by Jaswom and Symm [4], Butterfield and Banerjee [18], Watson [17], Mendelson [6] and many others.

In the direct procedure, the unknown functions appearing in the integral equations are the actual physical variables of the problem (such as tractions and boundary displacements in elasticity). The internal stresses and displacements are directly computed afterwards by using the boundary values obtained through the solution of the system of equations. Elastic applications of this technique have been described by Rizzo [19], Cruse [20 - 22], Lachat and Watson [23], Brebbia [1, 2], Nakaguma [25] and others.

The key to the implementation of these methods is the adoption of a singular solution (fundamental solution) to the corresponding differential equation of the problem. Such fundamental solution, in elastic applications of the type described by Rizzo [19] and Cruse [20], is usually the one due to Lord Kelvin (see Love [26]) and corresponds to a unit point load applied within the infinite medium. Alternative formulations, of the same type, have been presented by Nakaguma [25] and Cruse [27], where fundamental solutions that satisfy certain special boundary conditions were used. The former applied Mindlin's [44] singular solution for half-space problems and the latter a special Green's function for cracked plates. In these references the advantages of using such particular fundamental solutions were pointed out for the corresponding specific applications.

The present work is mainly concerned with the application of the direct boundary element method to nonlinear material problems. The

complete formulation for two and three dimensional inelastic problems is presented. In addition, the fundamental solution corresponding to a unit point load applied within the half-plane is introduced and implemented together with the Kelvin solution for two dimensional problems involving plasticity, creep and viscoplasticity.

The bibliography on boundary elements has grown at a rapidly accelerated rate during the last few years and it will be difficult to give credit to the many authors that have contributed to it. References [1 - 4] and [28 - 43] include many of the most important works published up to now and also indicate the present stage in development of the techniques. A brief historical account of the publications related to nonlinear material applications is given in the next Section.

1.2 Literature Survey - Nonlinear Applications

Although elastic (numerical) applications of integral equations were already known in the 1960's, it was only during the last decade that the first publications on nonlinear material problems appeared. The first publication on this subject was due to Swedlow and Cruse [5] in 1971. The article was concerned with the generalization of the strain hardening elastoplastic constitutive equations, previously presented by the first author, to compressible and anisotropic plastic flow, and presented an extended form of Somigliana's identity including plastic strain rates. In addition, the starting boundary integral equation for the direct boundary element formulation was first introduced, for three dimensional problems, but examples were not shown nor the integral expression for internal stresses was given. The authors, however, pointed out the existence of a domain integral which accounts

for the plastic strains contribution to the formulation.

This early work was taken up by Riccardella [7] in 1973, who implemented the von Mises yield criterion (isotropic hardening) for two dimensional problems using piecewise constant interpolation for the plastic strains. The complete integral expression for stresses at internal points was not presented due to the author's recognition of a singularity in the plastic strain integral. Instead, this apparent difficulty was correctly avoided by first integrating analytically the plastic strain term and then obtaining the derivatives also in closed form. A direct consequence of the procedure was that interpolation functions other than constant could not be easily implemented. By using a rather cumbersome implicit solution technique, some examples were solved and the author concluded that, although not entirely successful, the results were encouraging. This work deserves considerable credit, not only for being the first of its kind, but also because it laid the numerical basis for much of the work that followed. Linear boundary elements, for instance, were first presented together with the analytical expressions for the free term. Also, the closed form integrals for the plastic strain term remained the only correct expressions available until recently.

During the same period, Mendelson [6] presented and discussed different integral formulations for elastoplastic problems; namely indirect, direct and a direct biharmonic formulation therein called semidirect approach. Partial solutions to some elastoplastic examples were presented, including a trivial closed form expression for the torsion problem of a circular shaft and some early numerical results for an edge-notched beam under pure bending. The latter was solved by using the so-called semidirect formulation. By contrast with

the previous references, the direct formulation was presented including the integral expressions for the internal stresses (two and three dimensional problems). Such expressions, however, were later seen to be incorrect due to the way in which the plastic strain term was considered.

In 1975 an extension of the above work was presented by Mendelson and Albers [8]. In this paper the numerical results for the torsion problem of a bar with square cross section were presented within the context of the direct formulation (warping function) and the deformation theory of plasticity. Ideal plasticity and strain hardening were considered, and a comparison of results with finite difference solutions indicated the powerfulness of the technique. The paper also produced some further results for the beam problem presented before, but in addition to the complete solution obtained by the semidirect formulation, an attempt to apply the direct procedure was presented with inconclusive results.

Two years later Mukherjee [9] presented a theoretical paper concerned with the proper care in reducing the three dimensional direct boundary element formulation to the plane strain case. In this work he partially corrected the equations presented in references [6, 8] and produced modified versions for the kernels of the plastic strain integrals. Such modifications are entirely based on the incompressibility of the plastic strains, consequently, cannot be valid for plasticity problems in which plastic dilation is allowed (plastic potentials type Druker-Prager or Mohr-Coulomb) to occur. An application of the formulation to obtain closed form solutions for some simple problems was also discussed in [45] by the same author and a co-worker.

Still in 1977, Chaudonneret [54] used a direct boundary element formulation for the viscoplastic analysis of a notched plate. In her study, original constitutive equations developed at O.N.E.R.A. (France) were employed and a confirmation of the results was obtained experimentally. Also, the integral equations presented were based on an "initial stress" form of the viscoplastic strains influence and the numerical implementaion was carried out using linear boundary elements and constant rectangular cells for integrating the nonlinear term. It is worth mentioning that Riccardella's procedure for obtaining the internal stresses was probably used, since the corresponding integral expressions presented in the paper were still not correct.

The following year saw a major contribution towards the proper inelastic boundary element formulation; Bui [10] presented a paper in which he points out the appropriate concept (originally due to Mikhlin [33]) for the derivative of the singular integral of the inelastic term. Here, the three dimensional integral expressions are discussed and the author indicates the existence of a free term in the integral equation for internal stresses which was not considered in any of the previous publications. This free term, however, does not ease the numerical implementation, because the associated domain integral (inelastic term) still has to be evaluated in the principal value sense. Nevertheless, it was the very first time the correct integral expression was proposed.

Recognition of the above work led Mukherjee and Kumar [48] to adopt the procedure previously described by Riccardella. In this paper they succeeded in performing time dependent inelastic analysis of some plane stress examples using power law creep and the recently developed constitutive relations due to Hart (metallic media). The

solution procedure employed was a predictor-corrector time integration scheme coupled with piecewise constant spatial interpolation for both, boundary unknowns and inelastic strains.

One year after (1979), Telles and Brebbia [46] produced the complete boundary element formulation for three and two dimensional plasticity problems. The correct expressions for internal stresses were given, including the proper derivatives of the singular domain integrals. In their work, emphasis was given to the numerical implementation of the integral equations and a simple procedure for numerically computing the principal value of the plastic strain integrals, together with the corresponding free terms, was proposed. Such procedure is based on the application of a uniform plastic strain field to the discretized integral equations and allows for the implementation of higher order internal cells. This work did not show any solutions for engineering examples, but the possibility of correctly employing higher order representation for the inelastic strains was demonstrated for the first time.

As it is seen, the 1970's saw a great deal of controversy with respect to the correctness of the boundary element formulation. In the beginning of the present decade, however, the technique was already capable of solving many practical problems using more sophisticated numerical implementations. As early as 1980, for instance, Telles and Brebbia [49] employed the direct boundary element method to solve some elastoplastic problems in two dimensions (plane stress and plane strain). An "initial strain" form of the inelastic term was considered and the formulation was capable of handling incompressible plastic strains using the isotropic von Mises yield criterion with strain hardening, ideal plasticity and strain softening behaviour. The

numerical implementation was accomplished by using linear interpolation functions for both, boundary elements and internal cells. In this work the potentialities of boundary elements for inelastic analysis were highlighted by comparing the results with finite element solutions for the same problems.

In another publication by the same authors [52], an"initial stress" formulation was introduced with four different yield criteria (Tresca, Mises, Mohr-Coulomb and Drucker-Prager). The possibility of plastic dilation was therefore considered. In addition, alternative direct boundary element formulations were also discussed; namely initial strain, initial stress and fictitious tractions and body forces approach. Among the different applications presented is the geotechnical problem of a deep tunnel which clearly demonstrates the suitability of boundary elements for inelastic infinite medium problems.

Still in 1980 a somewhat approximated boundary element formulation was presented by Banerjee and Cathie [50]. In this paper they correct a previous unsuccessful formulation [47] proposed by the first author and co-worker. The original feature presented is concerned with the calculation of the internal stresses; here, instead of using the integral expression, the authors compute internal displacements and apply a numerical differentiation scheme of the type used in finite differences or finite elements. Such procedure is obviously less accurate, and more importantly requires extra computer time for the operations. The direct consequences are already apparent in the examples presented. An attempt to optimise the number of operations per iteration cycle was also discussed by Cathie [51], but in spite of this effort it was later proved that the procedure is computationally inefficient [56].

Another improvement in an early formulation was presented by Morjaria and Mukherjee [55], where the (already mentioned) implementation previously described by the second author and colleague [48] was made more efficient by employing linear boundary elements and an Euler-type time integration scheme. The inelastic term, however, was still spatially interpolated in constant piecewise form. In this publication some further examples (plane stress) are solved, including a plate with an elliptic cutout; comparisons with the previous attempt reveal substantial improvement in computer efficiency.

In 1981 the first successful formulations employing fundamental solutions that satisfy particular boundary conditions are introduced. Telles and Brebbia [56] implement the half-plane singular solution in the context of the different formulations previously proposed by them. In this work finite and semi-infinite plasticity problems are solved with great resolution, and this is achieved without boundary discretization over the traction-free surface of the semi-plane. Another interesting implementation was presented by Morjaria and Mukherjee [57] where an indirect and biharmonic boundary element formulation is presented in conjunction with the fundamental solution for planar bodies with cutouts (circular and elliptic). This biharmonic formulation is here applied to solve one of the author's previous examples and also to the challenging problem of a cracked plate simulated by a narrow elliptic cutout.

The above advanced implementations clearly indicate the advantages of adopting different fundamental solutions for the corresponding different types of problems.

A further development is also presented by Telles and Brebbia [58] where they introduce a viscoplastic boundary element implementation

which is capable of handling plasticity, creep and viscoplasticity in a unified approach. In this reference the Perzyna's constitutive model for elastic/viscoplastic material behaviour is adopted with four different yield criteria. The solution routine employed is a simple Euler time integration scheme with time step limiting considerations. The examples shown illustrate the capabilities of boundary elements in these classes of time dependent nonlinear problems.

1.3 Layout of Notes

CHAPTER 2 gives an outline of the basic theory which is used throughout this work. A review of the small strain theory of elasticity is first presented and this is followed by some basic concepts of plasticity, viscoplasticity and creep illustrated by the corresponding uniaxial behaviour. The chapter also presents the differential equations which govern continuum inelastic problems and introduces two alternative forms of representing the inelastic contribution, i.e.,initial strain and initial stress.

CHAPTER 3 is entirely concerned with elastic problems and the complete boundary element formulation using the fundamental solutions due to Kelvin [26] is reviewed. A formulation of the technique for half-plane type problems is also introduced through the adoption of a fundamental solution satisfying the traction-free condition over the surface of the semi-plane. This fundamental solution has been presented by Melan [79] in terms of stresses only, hence this solution is first extended to compute displacements which are needed to apply the direct boundary element method. In addition, a correction in one of the original formulae by Melan is effectuated and the complete

expressions for the boundary element computation of stresses at internal points are presented.

The numerical implementation is discussed in detail and the application of the half-plane formulation to solve some classical problems is included.

CHAPTER 4 introduces the boundary element equations for inelastic problems. Somigliana's identity for displacements [26] is extended to handle inelastic strains by following two different procedures, the first leads to an initial strain form and the second to an initial stress representation.

A proper procedure for obtaining the integral equations for stresses at interior points is presented and the complete boundary element equations for 3-D and 2-D problems including the half-plane implementation are discussed in detail. This includes three alternative formulations; initial strain, initial stress and fictitious tractions and body forces. In addition, the spatial discretization of the equations is introduced and a simple and efficient semi-analytical integration scheme is applied for the domain integrals of the inelastic terms.

CHAPTER 5 is concerned with the application of the inelastic boundary element equations to solve plasticity problems. The yield condition presented in Chapter 2 is extended to general continuum problems and the von Mises yield criterion [60-64, 68-71] is first introduced in conjunction with the initial strain equations. Also, a solution algorithm [63] based on these expressions is presented and discussed in detail, including a series of examples and comparisons with existing results.

In order to extend the range of applications, general stress-strain relations for post yield behaviour are introduced in incremental form. This is accomplished by considering four different yield criteria; namely [76] Tresca, von Mises, Mohr-Coulomb and Drucker-Prager. Such relations are seen to be particularly useful when the initial stress equations are employed, hence two different algorithms for stepwise plasticity solutions are presented and implemented for the initial stress formulations.

At the end of the chapter examples and comparisons with alternative solutions are presented and these also include applications of the half-plane fundamental solution.

CHAPTER 6 is devoted to the application of the boundary element technique to time-dependent nonlinear material problems. The uniaxial models presented in Chapter 2 are employed in equivalent or effective form to generate the constitutive equations and a unified procedure, capable of handling viscoplasticity and creep is presented. In addition, the procedure is also applicable to simulating pure elastoplastic solutions through the consideration of long term load increments followed by stationary conditions.

The solution technique employed is an explicit Euler single-step [106-108] process which is introduced in conjunction with time step limiting considerations for stability. Also, a series of examples is presented to outline the accuracy and applicability of the formulation, including elastoplastic, creep and viscoplastic problems.

CHAPTER 7 presents a general discussion on the various aspects of the different solution techniques employed here, together with the concluding remarks for the present research.

CHAPTER 2

BASIC THEORY

2.1 Introduction

This chapter is partly devoted to introducing some basic concepts of the theory which is going to be used in the subsequent chapters of this work. Although the major concern of these notes is with the application of the boundary element method to nonlinear material problems, the chapter starts by briefly reviewing some basic concepts of the small strain theory of elasticity. These concepts can be taken from any standard text on the subject [26, 61, 68, 69, 75] and are therefore presented without need for further comments.

In the later sections of the chapter; plasticity, viscoplasticity and creep are introduced through the examination of the uniaxial stress-strain curve of inelastic materials. The differences between these inelastic material idealizations are then illustrated and discussed.

Towards the end, the basic differential equations which characterize continuum inelastic problems are presented following two different representations; namely initial strain and initial stress, depending on whether the inelastic terms are considered as "initial strains" or "initial stresses".

2.2 Theory of Elasticity

Throughout this work the so-called Cartesian tensor notation is used. This notation is not only a time saver in writing long

expressions, but is also extremely useful in derivation and in the proof of theorems. Such notation makes use of subscript indices (1, 2, 3) to represent (x, y, z) and also renders summation symbols unnecessary when the same letter subscript occurs twice in a term. Hence, in three dimensions,

$$a_i a_i = a_1^2 + a_2^2 + a_3^2 \tag{2.2.1}$$

and

$$a_{kk} = a_{11} + a_{22} + a_{33}.$$

In addition, the permutation symbol e_{ijk} and the Kronecker delta symbol δ_{ij} will be used, i.e.

$$e_{ijk} = \begin{cases} 0 & \text{when any two indices are equal;} \\ +1 & \text{when } i, j, k \text{ are } 1, 2, 3 \text{ or an even permutation of } 1, 2, 3; \\ -1 & \text{when } i, j, k \text{ are an odd permutation of } 1, 2, 3. \end{cases} \tag{2.2.2}$$

and

$$\delta_{ij} = \begin{cases} 1 & \text{if } i = j \\ 0 & \text{if } i \neq j \end{cases}$$

Herein, unless otherwise stated (locally), subscripts are assumed to have a range of three in three dimensional problems whereas for two dimensions (plane stress and plane strain) this range is only two. In this section, however, only three dimensional expressions are considered.

The external forces acting at any instant on a body are classified in two kinds : body forces and surface forces.

Body forces act on the elements of volume or mass inside the body, e.g., gravity. These forces will be reckoned per unit volume. Surface forces act on the bounding surface of the body and will be reckoned per unit area of the surface across which they act. Such forces are designated tractions.

If one considers an infinitesimal rectangular parallelepiped surrounding a given point within the body, it readily follows that static equilibrium of forces and moments requires satisfaction of the following equation

$$\sigma_{ij,i} + b_j = 0 \tag{2.2.3}$$

where the components of the stress tensor are represented by σ_{ij} and b_j stands for the components of the body force. Space derivatives are indicated by a comma,i.e., $\partial\sigma_{ij}/\partial x_i = \sigma_{ij,i}$.

Furthermore, if there are no body moments applied, equilibrium conditions also leads to

$$\sigma_{ij} = \sigma_{ji} \quad . \tag{2.2.4}$$

If the six different components of the stress tensor are assumed to be known at a certain point, the equivalent tractions (p_i) acting on any plane through this point can be computed by

$$p_i = \sigma_{ji} n_j \tag{2.2.5}$$

where n_j represents the direction cosines of the normal to the plane.

Regardless to the state of stress at a given point, one can always choose a special set of axes through the point in such a way

that the shear stress components vanish when the stresses are referred to it. The directions of these special axes are called principal directions and the normal stress acting on each plane perpendicular to the principal directions are called principal stresses.

The principal directions can be obtained by considering the following relation

$$p_i = \lambda n_i \tag{2.2.6}$$

which indicates that the traction vector is parallel to the normal vector.

Substitution of (2.2.6) into (2.2.5) leads to

$$(\sigma_{ij} - \lambda\delta_{ij})n_i = 0 \ . \tag{2.2.7}$$

Equation (2.2.7) represents a system of three linear homogeneous equations which for $\sigma_{ij} \neq 0$ must admit a non trivial solution ($n_i n_i = 1$). Consequently,

$$|\sigma_{ij} - \lambda\delta_{ij}| = 0 \tag{2.2.8}$$

or, in expanded form

$$\lambda^3 - I_1 \lambda^2 - I_2\lambda - I_3 = 0 \tag{2.2.9}$$

where

$$\begin{aligned} I_1 &= \sigma_{kk} \\ I_2 &= \frac{1}{2}(\sigma_{ij}\sigma_{ij} - \sigma_{ii}\sigma_{jj}) = \frac{1}{2}\sigma_{ij}\sigma_{ij} - \frac{1}{2} I_1^2 \\ I_3 &= \frac{1}{6} e_{ijk}e_{pqr}\sigma_{ip}\sigma_{jq}\sigma_{kr} \end{aligned} \tag{2.2.10}$$

The principal stresses (roots of the cubic equation (2.2.9)) are physical quantities whose values do not depend on the coordinate system in which the components of stress where initially given. They are, therefore, invariants of the stress state at the point. A direct consequence is that I_1, I_2 and I_3 are also scalar invariants with respect to any rotation of the Cartesian reference axis.

It can be demonstrated that the three principal directions are mutually perpendicular. Hence, if the reference axes are chosen to coincide with the principal axes of stress,

$$\begin{aligned} I_1 &= \sigma_1 + \sigma_2 + \sigma_3 \\ I_2 &= -(\sigma_1\sigma_2 + \sigma_2\sigma_3 + \sigma_3\sigma_1) \\ I_3 &= \sigma_1\sigma_2\sigma_3 \end{aligned} \tag{2.2.11}$$

where σ_1, σ_2 and σ_3 are the principal stresses.

It is convenient in plasticity theory to split the stress tensor into two parts, one called the spherical stress tensor and the other the stress deviator or deviatoric stress tensor. The spherical stress tensor ($\bar{\sigma}_{ij}$) is related to the mean stress as follows

$$\bar{\sigma}_{ij} = \frac{1}{3}\,\sigma_{kk}\,\delta_{ij} = \frac{I_1}{3}\,\delta_{ij} \tag{2.2.12}$$

and the components of the deviatoric stress tensor are given by

$$S_{ij} = \sigma_{ij} - \bar{\sigma}_{ij} = \sigma_{ij} - \frac{I_1}{3}\,\delta_{ij}\ . \tag{2.2.13}$$

The principal directions of the stress deviator tensor are the same as those of the stress tensor and it is usually easier to

compute the principal deviator stresses (S_k) then to calculate σ_k. If λ now denotes any one of the principal deviator stresses, a derivation similar to that of equation (2.2.9) yields

$$\lambda^3 - J_2\lambda - J_3 = 0 \tag{2.2.14}$$

where J_1, J_2 and J_3 are the scalar invariants of the stress deviator analogous to those given in (2.2.10), but now calculated with S_{ij} instead of σ_{ij}. Hence,

$$\begin{aligned} J_1 &= 0 \\ J_2 &= \frac{1}{2} S_{ij}S_{ij} \\ J_3 &= \frac{1}{3} S_{ij}S_{jk}S_{ki} \end{aligned} \tag{2.2.15}$$

Equation (2.2.14) can be solved explicitly by the following substitution [76]

$$\lambda = 2\left(\frac{J_2}{3}\right)^{\frac{1}{2}} \sin\alpha \tag{2.2.16}$$

which leads to

$$2\left(\frac{J_2}{3}\right)^{\frac{3}{2}} \left[4\sin^3\alpha - 3\sin\alpha\right] = J_3 \,. \tag{2.2.17}$$

The expression in square brackets is equal to $-\sin3\alpha$, thus

$$\sin3\alpha = -\frac{J_3}{2}\left(\frac{3}{J_2}\right)^{\frac{3}{2}} \,. \tag{2.2.18}$$

Assuming that the first solution is obtained with 3α in the range $\pm \pi/2$ (i.e.- $\pi/6 \leq \alpha \leq \pi/6$), the other two solutions of (2.2.18) are found by the cyclic nature of $\sin(3\alpha + 2n\pi)$. This furnishes the three independent roots of (2.2.14), namely

$$S_k = 2\left(\frac{J_2}{3}\right)^{\frac{1}{2}} \sin\alpha_k \tag{2.2.19}$$

where for $S_1 > S_2 > S_3$ one has $\alpha_1 = \alpha + \frac{2}{3}\pi$, $\alpha_2 = \alpha$ and $\alpha_3 = \alpha + \frac{4}{3}\pi$. Note that the principal stresses can be calculated by the simple relation

$$\sigma_k = S_k + \frac{\sigma_{\ell\ell}}{3} \quad . \tag{2.2.20}$$

In addition, $-\frac{\pi}{6} \leq \alpha \leq \frac{\pi}{6}$ is also a stress invariant which can be used as an alterantive to J_3 in representing the stress state at a point.

Under the action of forces, a body is displaced from its original configuration. If x_i denotes the position of a point P of the body in its initial state and $x_i + u_i$ denotes the position of the same point when the body is deformed, u_i represents the displacement components and is a function of x_i. If the displacements are such that their first derivatives are so small that the square and product of the partial derivatives of u_i are negligible, then strains can be represented by the Cauchy's infinitesimal strain tensor.

$$\varepsilon_{ij} = \frac{1}{2}(u_{i,j} + u_{j,i}) \quad . \tag{2.2.21}$$

In general, during the deformation process, any small element of the body is changed in shape, translated and rotated. Consider the point P' in the neighbourhood of P with coordinates $x_i + dx_i$. Avoiding rigid body translations, the relative displacement of P' with respect to P is given by

$$du_i = u_{i,j}dx_j \tag{2.2.22}$$

which can be further written as

$$du_i = \frac{1}{2}(u_{i,j} + u_{j,i})dx_j - \frac{1}{2}(u_{j,i} - u_{i,j})dx_j \tag{2.2.23}$$

or

$$du_i = \varepsilon_{ij}dx_j - \omega_{ij}dx_j \ , \tag{2.2.24}$$

where ω_{ij} is the rotation tensor of the infinitesimal displacement field, i.e.,

$$\omega_{ij} = \frac{1}{2}(u_{j,i} - u_{i,j}) \ . \tag{2.2.25}$$

From the above it is seen that although the displacements uniquely define the components of the strain tensor, the inverse problem is not so straightforward. In the first place, strains represent pure deformation, whereas displacements include rigid body motion which has no effect on the strains. This problem can, however, be made unique by specifying the rigid body motion (i.e. displacement and rotation) at some point of the body. A more difficult problem is encountered in calculating the displacements from strains using equation (2.2.21). Here, a system of six differential equations for the three unknown functions u_i is obtained, and consequently one must expect a not possible solution unless some additional conditions are satisfied. These conditions are given by the compatibility equations and are found in standard texts on elasticity. They are as follows

$$\varepsilon_{ij,k\ell} + \varepsilon_{k\ell,ij} - \varepsilon_{ik,j\ell} - \varepsilon_{j\ell,ik} = 0 \ . \tag{2.2.26}$$

Equation (2.2.26) is a necessary and sufficient condition that the strain components give single-valued displacements for simply connected regions. For multiply connected regions, however, this condition is necessary but generally not sufficient.

It should be emphasized that all the relations presented so far are independent of material properites, consequently, they hold

for both elastic and inelastic material behaviour.

For an isotropic elastic material in which there is no change in temperature, Hooke's law relating stresses and strains can be stated in the form

$$\sigma_{ij} = 2G\varepsilon_{ij} + \frac{2G\nu}{1-2\nu}\,\varepsilon_{kk}\delta_{ij} \tag{2.2.27}$$

or inversely

$$\varepsilon_{ij} = \frac{1}{2G}\left(\sigma_{ij} - \frac{\nu}{1+\nu}\,\sigma_{kk}\delta_{ij}\right) \tag{2.2.28}$$

where ν is Poisson's ratio and G is the shear modulus.

The shear modulus can be related to the Young's modulus and ν as follows

$$G = \frac{E}{2(1+\nu)} \,. \tag{2.2.29}$$

Alternatively expression (2.2.27) can be written more concisely as

$$\sigma_{ij} = C_{ijk\ell}\varepsilon_{k\ell} \tag{2.2.30}$$

in which $C_{ijk\ell}$ is the fourth-order isotropic tensor of elastic constants given by

$$C_{ijk\ell} = \frac{2G\nu}{1-2\nu}\,\delta_{ij}\delta_{k\ell} + G(\delta_{ik}\delta_{j\ell} + \delta_{i\ell}\delta_{jk}) \,. \tag{2.2.31}$$

Equations (2.2.3), (2.2.21) and (2.2.27) represent a set of 15 equations for 6 stresses, 6 strains and 3 displacements which can be further manipulated. A straightforward procedure is to substitute equation (2.2.21) into (2.2.27) to obtain stresses in terms of displacement gradients, and then substitute the result into equation

(2.2.3) to obtain three second order partial differential equations for the three displacement components. The result of these operations is the well-known Navier equation which may be written in the following form

$$G u_{j,kk} + \frac{G}{1-2\nu} u_{k,kj} + b_j = 0 \ . \tag{2.2.32}$$

This equation is particularly convenient when displacement boundary conditions are specified. By using equations (2.2.21) and (2.2.27) as before, but now substituting into equation (2.2.5) for boundary points, the traction boundary conditions are obtained as

$$\frac{2G\nu}{1-2\nu} u_{k,k} n_i + G(u_{i,j} + u_{j,i}) n_j = p_i \tag{2.2.33}$$

where n_j stands for the direction cosines of the outward normal to the boundary of the body.

It is interesting to note that since the equilibrium condition is now expressed in terms of displacements in equation(2.3.32), the compatibility equations are no longer required. The displacement u_i is solved from the Navier equation to satisfy the boundary conditions. After u_i is known throughout the body, the strains are obtained by equation (2.2.21),and the stresses are calculated by Hooke's law.

The solution of equation (2.2.32) by the direct boundary element method is the object of Chapter three of this work.

2.3 Inelastic Behaviour of Materials

In the theory of elasticity reviewed in the last section of this chapter, there were two controlling factors : complete recovery of the unstrained configuration when the loads are removed and the

dependence of the deformations only on the final stresses, not on the previous load history or strain path. In plasticity, these two factors are not realised.

Plasticity is possibly defined as a property which enables a material to be deformed continuously and permanently without rupture during the application of stresses exceeding the elastic limit of the material. Thus, residual strains are expected to occur on removal of the load and furthermore the final deformation depends not only on the final stresses, but also on the path stress history from the beginning of yield.

The problem of formulating physical relations describing the actual behaviour of a material during plastic flow is a very complex one. This complexity is due to the non-linearity and irreversibility of the deformation processes and to a number of phenomena which occur only after the material becomes plastic. The yield characteristics of many materials, for instance, are modified by the rate of straining, with the resistance to deformation increasing markedly with the speed of loading (viscous effect). On the other hand, creep of metals is one example where deformations will occur (usually at elevated temperatures) with extended periods of time under constant stress. In order to simplify the present discussion, it is here considered some possible approximate diagrams that may represent the behaviour of a specimen stressed in simple tension or compression.

An elastic perfectly plastic material is shown in figure 2.3.1. Here, as the stress in the loaded specimen is increased, from O towards A , an elastic recoverable strain takes place until the stress reaches the value $\sigma = Y$, when a plastic strain is superimposed

and further deformation will occur under constant yield stress. If, after a point B has been reached, the specimen is unloaded, the path O - A - B is not retraced due to the irreversibility of plastic deformation, but the stress point will follow the line B - C parallel to O - A. Stressing the specimen in compression will therefore lead to point C for which the compressive yield stress $\sigma = -Y$ is attained. Thereafter the specimen deforms under constant value of yield stress and point D may be reached allowing for the entire cycle to be repeated.

A more complex situation occurs when hardening/softening effects are taken into account. This can be seen in figure 2.3.2 where simplified linear hardening is characterized by a constant modulus E_T. After reaching the point A for which $\sigma = Y$, a further increase of stress is now required to induce further deformation. When the specimen is unloaded from the point B, the stress point moves along the line B - C as before, but it is known from experiments that the compressive yield stress will vary depending on the previous deformation history, thus $|\sigma_B| \neq |\sigma_C|$ in general and this is referred to in the literature as the Bauschinger effect.

There are several simplified models used to describe the Bauschinger effect. At one extreme it is assumed that the elastic unloading range will be double the initial yield stress (kinematic hardening). Hence,

$$\sigma_C = \sigma_B - 2Y \ . \tag{2.3.1}$$

At the other extreme there is the isotropic hardening theory which assumes that the mechanism that produces hardening acts equally in tension and compression, thus

$$\sigma_C = -\sigma_B \ . \tag{2.3.2}$$

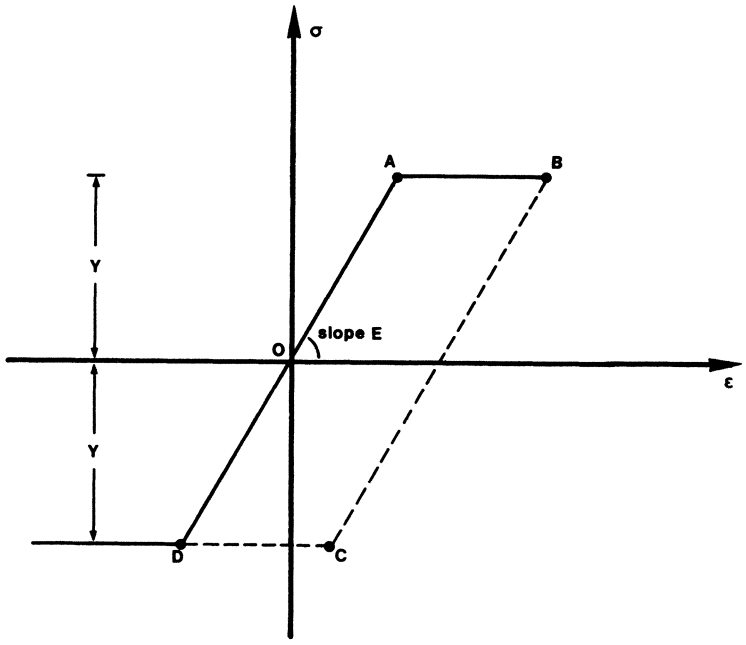

Fig. 2.3.1 Uniaxial stress-strain diagram for an elastic perfectly plastic material.

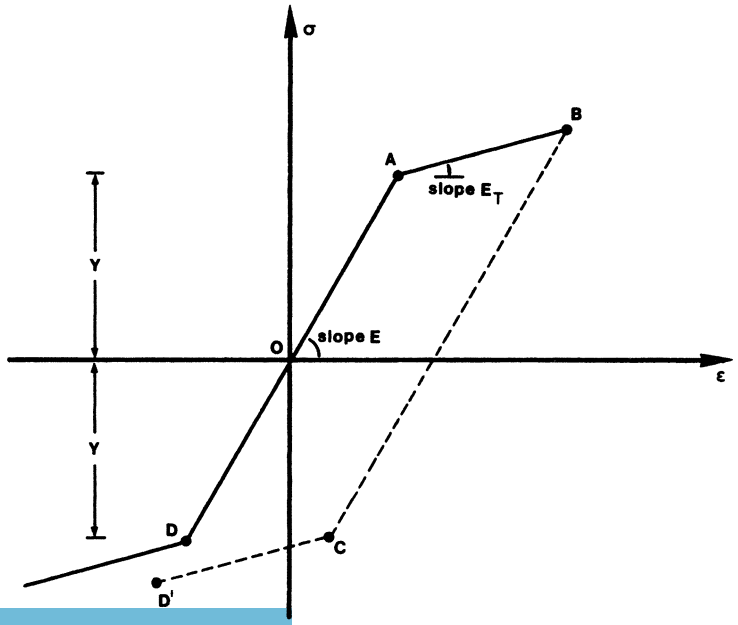

Fig. 2.3.2 Uniaxial stress-strain diagram for a hardening material.

Actually, neither theory accurately represents the hardening effects in reverse loading. The kinematic model, though more accurate in this situation, tends to overcorrect for the Bauschinger effect [63] and the isotropic model does not take into account such anisotropic behaviour. The latter, however, is mathematically simpler and consequently has been most frequently used. Furthermore, the drawback involved in the isotropic hardening theory can be overcome by making use of the fraction model [77], also known as the overlay model [78]. In this model a material particle is considered to be composed of various portions which can be represented by subelements connected in parallel showing isotropic hardening behaviour in plastic deformation. By assigning different properties to each subelement and assuming that all subelements are subjected to the same total strain, the proper material behaviour can be simulated as closely as possible, including the Bauschinger effect.

If only one subelement is chosen, the isotropic hardening theory is obtained. However, if necessary, the model can also describe kinematic hardening behaviour by making a suitable choice of the number of subelements, their size and isotropic hardening rules. This means that the kinematic model is no longer needed, and consequently attention will be given in the subsequent parts of this work to the isotropic hardening theory. Thus, from now on $\sigma \geq 0$ is always implied for simplicity.

Assuming that the total strain ε is subdivided into an elastic strain ε^e and a plastic strain ε^p, one gets

$$\varepsilon = \varepsilon^e + \varepsilon^p \tag{2.3.3}$$

where

$$\varepsilon^e = \frac{\sigma}{E} \quad . \tag{2.3.4}$$

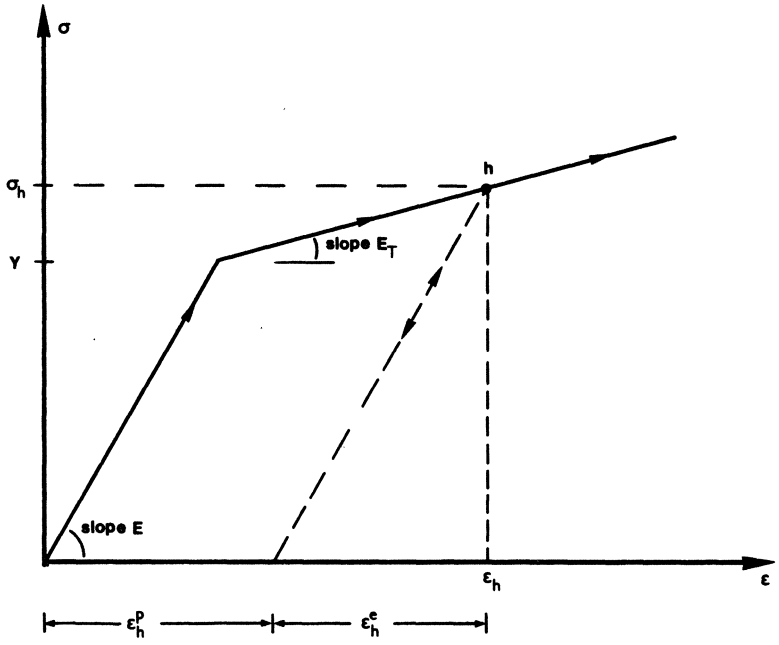

Fig. 2.3.3 Uniaxial stress-strain diagram showing elastic and plastic strains.

With reference to figure 2.3.3 it is seen that pure elastic behaviour is obtained for initial loading when

$$\sigma - Y < 0 \ . \tag{2.3.5}$$

Once σ exceeds Y, however, this condition changes such that σ is tested against the yield stress σ_o as follows

$$\sigma - \sigma_o < 0 \tag{2.3.6}$$

where σ_o has the initial value Y and varies according to a certain rule as plastic flow progresses.

For the case depicted in figure 2.3.3 it is easily seen that

$$\sigma_o = Y + \frac{E_T}{1 - \frac{E_T}{E}} \varepsilon^p \ . \qquad (2.3.7)$$

In order to keep the present discussion sufficiently general, the above expression can be related to the work hardening hypothesis by assuming that σ_o is a function of a hardening parameter k which represents the total plastic work; namely,

$$k = \int \sigma \, d\varepsilon^p \ . \qquad (2.3.8)$$

Hence,

$$\sigma_o = g\left(\int \sigma \, d\varepsilon^p \right) \qquad (2.3.9)$$

and

$$\frac{dg}{dk} = \frac{1}{\sigma} \frac{dg}{d\varepsilon^p} = \frac{H'}{\sigma} \qquad (2.3.10)$$

where H' is the slope of the uniaxial curve replotted as stress versus plastic strain.

Equation (2.3.7), which corresponds to linear work hardening, can therefore be written as

$$\sigma_o = Y + H' \varepsilon^p \qquad (2.3.11)$$

in which for this case H' is a constant given by

$$H' = \frac{E_T}{1 - \frac{E_T}{E}} \qquad (2.3.12)$$

Recalling the condition presented in (2.3.6), plastic behaviour is possible if the following condition or criterion is satisfied

$$F(\sigma, k) = \sigma - \sigma_o = 0 \qquad (2.3.13)$$

where $F(\sigma, k)$ is a yield function subjected to the restriction

$$F(\sigma, k) \leq 0 \ . \qquad (2.3.14)$$

It was mentioned before that some materials present pronounced rate dependent plastic behaviour. Within the context of the classical or inviscid theory of plasticity, however, time independence is a basic assumption and this makes a simultaneous description of plastic and rheologic effects impossible. Such a unified description is the object of the viscoplastic theory.

Every material shows more or less pronounced viscous properties. In some problems these properties can be neglected without any real effect in the results, but in other problems this influence may be essential and the important feature of the inelastic behaviour is the time dependence of the deformation process. Thus, in such cases, the inelastic strains will depend on the time stress history as well as on the path stress history. Consequently, different results will be obtained for different loading paths and different durations of the loading processes.

In the present work, the elastic/viscoplastic model due to Perzyna [72 - 74] has been adopted. This model assumes that the material exhibits viscous properties in the plastic region only, which means that $F < 0$ represents a pure elastic behaviour. Moreover, the yield criterion of equation (2.3.13) is still valid as an initial condition, now designated static yield criterion. In spite of these common features, viscoplasticity allows for

$$F(\sigma, k) > 0 \qquad (2.3.15)$$

which is impossible in the so-called inviscid theory of plasticity.

The uniaxial plastic strain for rate dependent plastic materials is given in rate form as follows

$$\dot{\varepsilon}^p = \gamma < \Phi\left(\frac{F}{\sigma_o}\right) > \tag{2.3.16}$$

where the dot indicates time derivative, γ is a material parameter possibly function of time, temperature, etc. and

$$< \Phi\left(\frac{F}{\sigma_o}\right) > = \begin{cases} 0 & \text{for } F \leq 0 \\ \Phi\left(\frac{F}{\sigma_o}\right) & \text{for } F > 0 \ . \end{cases} \tag{2.3.17}$$

The function Φ is selected from experimental results and different types have been proposed [72], e.g.,

$$\begin{aligned} &\Phi(X) = X^n \ ; \ \Phi(X) = X \ ; \ \Phi(X) = \exp X - 1 \\ &\Phi(X) = \sum_{\alpha=1}^{N} A_\alpha (\exp X^\alpha - 1) \ ; \ \Phi(X) = \sum_{\alpha=1}^{N} B_\alpha X^\alpha \ . \end{aligned} \tag{2.3.18}$$

Equation (2.3.16) clearly indicates that the rate of increase of the inelastic strain is a function of the excess stress above the static yield criterion. This function of the excess stress generates the viscoplastic strain rate according to a predetermined viscosity law which is better illustrated by means of the rheological model of figure 2.3.4.

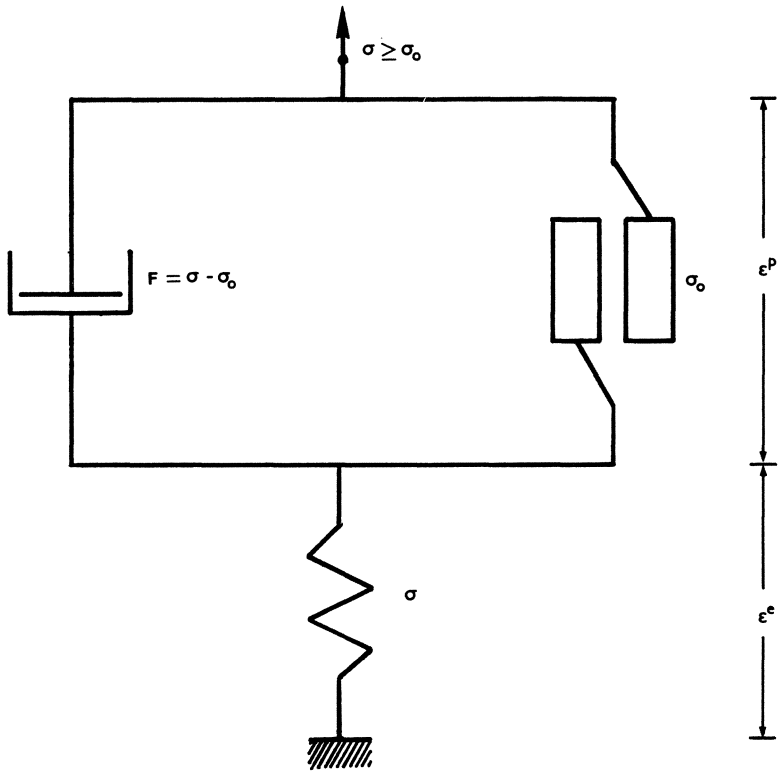

Fig. 2.3.4 Rheological model for elastic/viscoplastic behaviour.

In this mechanical model, the friction slider is assumed to sustain all the stress σ up to $\sigma = \sigma_o$, when it then becomes active and slides for $\sigma > \sigma_o$. When this happens, the excess stress $\sigma - \sigma_o$ is carried by the (possibly nonlinear) dashpot which generates the viscoplastic strain. The elastic part of the total strain is instantaneously given by the elastic spring.

It should be noticed that in general the dashpot and the slider may have properties that depend on the viscoplastic strain ($H' \neq 0$). Thus, after some time under constant applied σ, the slider tends to become rigid again and an asymptotic static configuration ($\dot{\varepsilon}^p = 0$)

is achieved providing satisfaction of the static yield criterion.

In order to demonstrate the equivalence of the rheological model and equation (2.3.16), consider the equilibrium condition ($\sigma \geq \sigma_o$)

$$\sigma = F + \sigma_o \tag{2.3.19}$$

where F represents the stress acting on the dashpot and σ_o is the part that corresponds to the friction slider.

The stress in the viscous dashpot is related to the viscoplastic strain rate as follows

$$F = \mu \dot{\varepsilon}^p = \mu(\dot{\varepsilon} - \dot{\varepsilon}^e) \tag{2.3.20}$$

where μ denotes the damping parameter of the dashpot.

Substituting (2.3.20) into (2.3.19) and rearranging gives

$$\dot{\varepsilon} = \dot{\varepsilon}^e + \frac{1}{\mu}(\sigma - \sigma_o) \tag{2.3.21}$$

which reads

$$\dot{\varepsilon} = \dot{\varepsilon}^e + \dot{\varepsilon}^p \ . \tag{2.3.22}$$

Hence,

$$\dot{\varepsilon}^p = \frac{1}{\mu}(\sigma - \sigma_o) \tag{2.3.23}$$

which corresponds to equation (2.3.16) if

$$\mu = \frac{\sigma_o}{\gamma} \tag{2.3.24}$$

and

$$\Phi\left(\frac{F}{\sigma_o}\right) = \frac{F}{\sigma_o} \ . \tag{2.3.25}$$

It is interesting to study some closed form solutions to equation (2.3.21). For simplicity, assume that $H' = 0$ $(\sigma_o = Y)$ and that the uniaxial model is subjected to a constant total strain rate. Thus, equation (2.3.21) becomes

$$\dot{\varepsilon} = \frac{\dot{\sigma}}{E} + \frac{\gamma}{Y}(\sigma - Y) \tag{2.3.26}$$

and leads to the following linear differential equation

$$\dot{\sigma} + \frac{\gamma E}{Y}\sigma = E(\dot{\varepsilon} + \gamma) \tag{2.3.27}$$

where $\dot{\varepsilon}$ = constant.

The solution of equation (2.3.27) is given by

$$\sigma = Y\left(\frac{\dot{\varepsilon}}{\gamma} + 1\right) + C\exp\left(-\frac{\gamma E}{Y}t\right) \tag{2.3.28}$$

in which t denotes time and C depends on the initial conditions.

If at $t = 0$, $\varepsilon = Y/E$ and $\varepsilon^p = 0$, the following expression for the stress arises

$$\sigma = \frac{Y\dot{\varepsilon}}{\gamma}\left[1 - \exp\left(-\frac{\gamma E}{Y}t\right)\right] + Y \tag{2.3.29}$$

which can also be written in terms of strain instead of time as follows (see figure 2.3.5).

$$\sigma = \frac{Y\dot{\varepsilon}}{\gamma}\left\{1 - \exp\left[\frac{\gamma}{\dot{\varepsilon}}\left(1 - \frac{E\varepsilon}{Y}\right)\right]\right\} + Y\ . \tag{2.3.30}$$

Alternatively, one can assume that initially an instantaneous $\varepsilon = \frac{Y}{E}\left(\frac{\dot{\varepsilon}}{\gamma} + 1\right)$ is applied and then the total strain increases at a constant rate. In this case the above expression greatly simplifies and the stress remains constant throughout, i.e.,

$$\sigma = Y\left(\frac{\dot{\varepsilon}}{\gamma} + 1\right)\ . \tag{2.3.31}$$

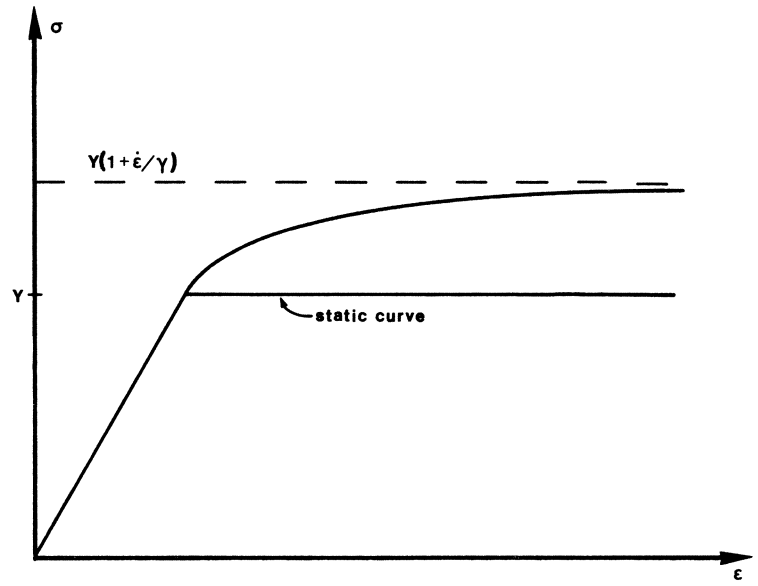

Fig. 2.3.5 Uniaxial stress-strain curve for $\dot{\varepsilon}$ = constant
($t = 0 \rightarrow \varepsilon = Y/E$)

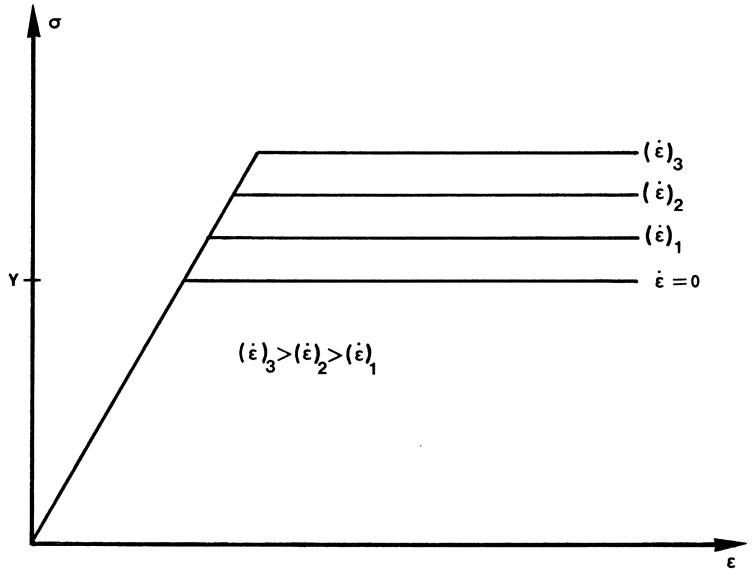

Fig. 2.3.6 Uniaxial stress-strain curve for $\dot{\varepsilon}$ = constant.

$\left[t = 0 \rightarrow \varepsilon = \frac{Y}{E} \left(\frac{\dot{\varepsilon}}{\gamma} + 1 \right) \text{ instantaneously applied} \right]$

This case is illustrated in figure 2.3.6.

It is instructive now to point out an important distinction between the inviscid theory of plasticity and the viscoplastic theory adopted here. For pure plasticity, the yield condition presented in (2.3.13) leads to a necessary condition for plastic behaviour to occur. Once the stress point is satisfying the equation $F = 0$, a loading criterion can be defined $(H' > 0)$, depending on what happens next, i.e.,

$F = 0$, $\dot{\sigma} < 0$ represents unloading (leads to an elastic state);

$F = 0$, $\dot{\sigma} > 0$ represents loading (leads to another plastic state).

In viscoplasticity, however, the case $F > 0$ exists and consequently viscoplastic behaviour will continue to occur completely independent of whether $\dot{\sigma} \gtrless 0$.

An intersting feature of the elastic/viscoplastic model is that for slow incremental loading processes, the results obtained by the classical theory of plasticity are approached (provided the stationary state $F = 0$ is possible). This has been mentioned before when describing the rheological model and is indeed observable in figure 2.3.6. When this is the case, clearly the function Φ and the parameter γ become immaterial, the latter acting just as a time scale factor which renders time a fictitious variable.

Such features can be better explained by rewriting equation (2.3.16) in the following form $(F \gtrless 0)$

$$\dot{\varepsilon}^p = \gamma \, \Phi \left(\frac{F}{\sigma_o} \right) \tag{2.3.32}$$

which after rearranging gives

$$F = \sigma_o \, \Phi^{-1}\left(\frac{\dot{\varepsilon}^p}{\gamma} \right) \tag{2.3.33}$$

or

$$F = \sigma_o \, \Phi^{-1}\left(\frac{\dot{\varepsilon} - \dot{\sigma}/E}{\gamma} \right) . \tag{2.3.34}$$

For slow incremental loading processes, the rates become vanishingly small along the loading path, thus $F = 0$ is approximately attained throughout. In practical terms, one can think of a discrete loading programme in which sufficiently small load increments are applied instantaneously. After each load increment, the load is kept constant and a stationary state is allowed to occur (i.e., the friction slider "locks" again in the rheological model). In this fashion, the complete loading path can be followed with the statical yield condition being satisfied at a number of discrete points along the path.

In the simple uniaxial behaviour discussed here, increments of any size can be applied because the result at the final point is always the same. This is not the same for continuum problems; in such cases, stress redistribution usually occurs, hence the same stress path may not be obtained. Consequently, small increments must always be kept in mind for the general case.

With reference to the mechanical model of figure 2.3.4, it is immediately apparent that on removal of the dashpot - assuming $\mu = 0$ (i.e. $\gamma \to \infty$) - a pure elastoplastic problem is simulated and only instantaneous response is obtained. Here, the restriction $\sigma \leq \sigma_o$ is readily found necessary in order to maintain equilibrium. Another useful simulation can be obtained by assuming that instead of the dashpot, the friction slider is removed (i.e., $\sigma_o = 0$). In this case, the mechanical model retains its rheological properties and

corresponds to the well-known Maxwell model where a linear dashpot is associated in series with a spring. Therefore, by assuming nonlinear properties to the dashpot, the so-called secondary or steady creep of metals [66, 67, 63, 65] can be equally represented in this comprehensive model. This matter will be dealt with in what follows.

There is experimental evidence that some metals, usually at elevated temperature, deform continuously with time under constant load. This phenomenon is designated creep and the time dependent strain originated in the process is called creep strain. A typical uniaxial curve of creep strain (ε^c) versus time under constant load is shown in figure 2.3.7. The first part, AB, where the creep rate decreases rapidly, is known as primary or transient creep. This portion is usually recoverable with time after unloading. The second stage, BC, is associated with a constant creep rate and consequently called steady or secondary creep. In this stage, creep leaves permanent strain. The final stage, CD, known as tertiary creep, is characterized by a rapid increase in the creep rate and leads quickly to rupture. Tertiary creep is greatly affected by the reduction in the cross-sectional area at large strains. This fact, allied to the usual short duration of the primary stage, generally leads to interest in the secondary creep only, though the primary part cannot always be neglected.

In constant stress tests, it is customary to represent the creep strain by a general equation of the form

$$\varepsilon^c = g(\sigma, t, T) \qquad (2.3.35)$$

where T is temperature.

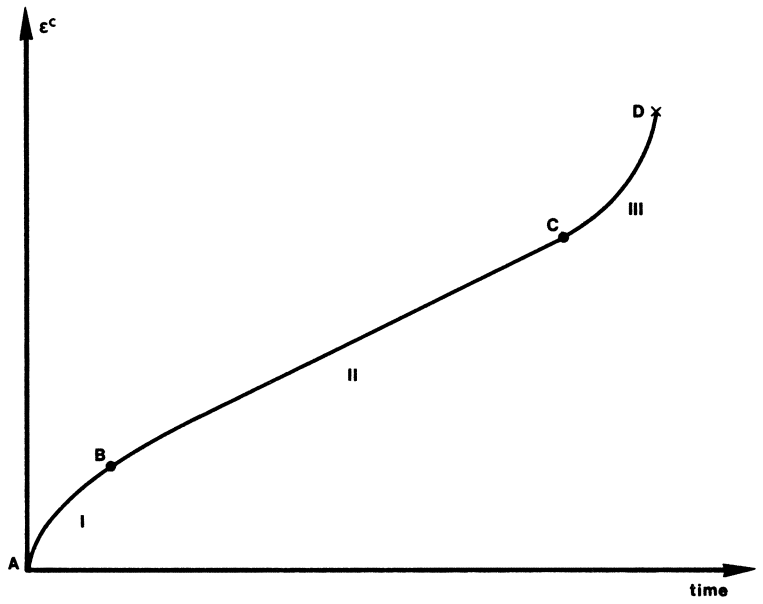

Fig. 2.3.7 Typical uniaxial creep curve under constant load.

A good review of the different types of relations proposed for equation (2.3.35) is given in [66]. In tests of short duration, primary creep predominates. A commonly used expression to represent this primary creep is

$$\varepsilon^c = B\,\sigma^n\,t^{k+1}\,. \tag{2.3.36}$$

For the secondary part, the following representation has been preferred

$$\varepsilon^c = K\,\sigma^m\,t \tag{2.3.37}$$

where B, K, m, n and k are temperature dependent material parameters.

Generalization of the above equations to include time varying stress is a questionable assumption commonly made. Here, it is the strain rate at any time which is of interest. Thus, equation (2.3.36) gives the time hardening expression

$$\dot{\varepsilon}^c = (k+1)B\,\sigma^n\,t^k \tag{2.3.38}$$

and equation (2.3.37) reduces to the well-known Norton's law, i.e.,

$$\dot{\varepsilon}^c = K\,\sigma^m\ . \tag{2.3.39}$$

Equation (2.3.39) seems to be acceptable for materials which only exhibits secondary creep and has been widely applied in many practical problems. Note that this equation together with the elastic strain rate $(\dot{\sigma}/E)$ can be simulated by the nonlinear Maxwell model mentioned before.

For short term problems, equation (2.3.38) can be substituted by its strain hardening counterpart. This can be done by expressing t from equation (2.3.36) as a function of ε^c and σ, and then substituting the result in expression (2.3.38). The final expression is

$$\dot{\varepsilon}^c = (k+1)B^{\frac{1}{k+1}}\,\sigma^{\frac{n}{k+1}}(\varepsilon^c)^{\frac{k}{k+1}} \tag{2.3.40}$$

For constant stress the above equation is the same as (2.3.38), but for time varying stress, different results will be obtained. Experimental data seem to agree better with the strain hardening approach. This is true especially for very short time tests [66]. A shortcoming of both relations is that they do not predict the reversal of the creep strain after unloading. Here, the use of overlay type models [77, 78], appears to be promising.

Throughout this brief exposition only $\sigma \geq 0$ was considered. It should be kept in mind that for $\sigma < 0$ a negative creep or plastic strain ($|\sigma| \geq \sigma_o$) will be generated instead. The expressions remain valid if only the absolute values are considered. The reason for keeping $\sigma \geq 0$ will be more evident in Chapters 5 and 6 where the generalization for multiaxial stress states will be presented and the relations discussed here will be readily applied in equivalent or effective form.

2.4 Governing Equations

In the present section the basic differential equations for continuum inelastic problems are introduced. In order to keep a unified notation, these equations are presented in rate form. This is a natural procedure for time dependent problems such as viscoplasticity and creep. For classical plasticity, it should be emphasized that pure incremental quantities could be equally used, since the relations are homogeneous in time due to the lack of time dependent effects. Plasticity, however, can be associated to a time-like parameter which is in fact independent of the time scale.

Within the context of small strain theory, the total strain rate for inelastic problems is assumed to be represented by

$$\dot{\varepsilon}_{ij} = \frac{1}{2}(\dot{u}_{i,j} + \dot{u}_{j,i}) = \dot{\varepsilon}^{e}_{ij} + \dot{\varepsilon}^{a}_{ij} \qquad (2.4.1)$$

where $\dot{\varepsilon}^{e}_{ij}$ and $\dot{\varepsilon}^{a}_{ij}$ are respectively the elastic and inelastic parts of the total strain rate tensor.

Herein, by inelastic strains one means any kind of strain field which can be considered as "initial strains", i.e.,

$$\dot{\varepsilon}^{a}_{ij} = \dot{\varepsilon}^{p}_{ij} + \dot{\varepsilon}^{c}_{ij} + \dot{\varepsilon}^{T}_{ij} \qquad (2.4.2)$$

$\dot{\varepsilon}^{p}_{ij}$ - plastic or viscoplastic strain rate.

$\dot{\varepsilon}^{c}_{ij}$ - creep strain rate

$\dot{\varepsilon}^{T}_{ij}$ - thermal strain rate.

The equilibrium conditions presented in (2.2.3) can now be written in rate form as

$$\dot{\sigma}_{ij,i} + \dot{b}_{j} = 0 \ . \qquad (2.4.3)$$

Equation (2.4.3) is valid in the interior of the body. The same condition when applied to the boundary surface, leads to the following rate version of equation (2.2.5),

$$\dot{p}_{i} - \dot{\sigma}_{ij}\, n_{j} = 0 \qquad (2.4.4)$$

where n_{j} stands for the direction cosines of the outward normal to the boundary of the body.

If inelastic strains are considered as initial strains, the application of Hooke's law to the elastic part of the total strain rate tensor results in the following expression for the stress rate components

$$\dot{\sigma}_{ij} = 2G(\dot{\varepsilon}_{ij} - \dot{\varepsilon}^{a}_{ij}) + \frac{2G\nu}{1-2\nu}\,(\dot{\varepsilon}_{\ell\ell} - \dot{\hat{\theta}})\delta_{ij} \qquad (2.4.5)$$

in which $\dot{\hat{\theta}} = \dot{\varepsilon}^{a}_{kk}$

The above expression can be rewritten in terms of initial stresses

$$\dot{\sigma}_{ij} = 2G\dot{\varepsilon}_{ij} + \frac{2G\nu}{1-2\nu}\dot{\varepsilon}_{kk}\,\delta_{ij} - \dot{\sigma}^{a}_{ij} \tag{2.4.6}$$

where $\dot{\sigma}^{a}_{ij}$ represents the components of the "initial stresses" given by

$$\dot{\sigma}^{a}_{ij} = 2G\,\dot{\varepsilon}^{a}_{ij} + \frac{2G\nu}{1-2\nu}\dot{\hat{\theta}}\,\delta_{ij}\,. \tag{2.4.7}$$

The substitution of equation (2.4.5) into (2.4.3) and (2.4.4), together with equation (2.4.1) gives [65]

$$\dot{u}_{j,\ell\ell} + \frac{1}{1-2\nu}\dot{u}_{\ell,\ell j} = 2(\dot{\varepsilon}^{a}_{ij,i} + \frac{\nu}{1-2\nu}\dot{\hat{\theta}}_{,j}) - \frac{\dot{b}_j}{G} \tag{2.4.8}$$

and

$$\dot{p}_i + 2G(\dot{\varepsilon}^{a}_{ij}\,n_j + \frac{\nu}{1-2\nu}\dot{\hat{\theta}}\,n_i) = \frac{2G\nu}{1-2\nu}\dot{u}_{\ell,\ell}\,n_i + G(\dot{u}_{i,j} + \dot{u}_{j,i})n_j\,. \tag{2.4.9}$$

Equation (2.4.8) is an extended form of the Navier equation presented in eqn. (2.2.32) and (2.4.9) represents its traction boundary conditions (see eqn. (2.2.33)). The above expressions can alternatively be written in the following form

$$\dot{u}_{j,\ell\ell} + \frac{\nu}{1-2\nu}\dot{u}_{\ell,\ell j} = -\frac{\dot{\bar{b}}_j}{G} \tag{2.4.10}$$

and

$$\dot{\bar{p}}_i = \frac{2G\nu}{1-2\nu}\dot{u}_{\ell,\ell}\,n_i + G(\dot{u}_{i,j} + \dot{u}_{j,i})n_j \tag{2.4.11}$$

where $\dot{\bar{b}}_j$ and $\dot{\bar{p}}_i$ are pseudobody forces and pseudotractions given by

$$\dot{\bar{b}}_j = \dot{b}_j - 2G(\dot{\varepsilon}^{a}_{ij,i} + \frac{\nu}{1-2\nu}\dot{\hat{\theta}}_{,j}) = \dot{b}_j - \dot{\sigma}^{a}_{ij,i} \tag{2.4.12}$$

and

$$\dot{\bar{p}}_i = \dot{p}_i + 2G(\dot{\varepsilon}^{a}_{ij}\,n_j + \frac{\nu}{1-2\nu}\dot{\hat{\theta}}\,n_i) = \dot{p}_i + \dot{\sigma}^{a}_{ij}\,n_j\,. \tag{2.4.13}$$

One can notice that equation (2.4.10) represents a set of three quasi-linear partial differential equations for the displacement rates

(inelastic terms appear on the right-hand-side). Therefore, provided the inelastic strain rates are known, the same argument presented at the end of Section 2.2 still applies.

Expressions (2.4.1) - (2.4.13) have been presented for three dimensional bodies. For plane problems, these equations can also be used (i, j, k, ℓ = 1, 2) with $\dot{\hat{\theta}} = \dot{\varepsilon}^a_{11} + \dot{\varepsilon}^a_{22} + \dot{\varepsilon}^a_{33}$ in plane strain and ν replaced by $\bar{\nu} = \nu/(1+\nu)$ with $\dot{\hat{\theta}} = \dot{\varepsilon}^a_{11} + \dot{\varepsilon}^a_{22}$ in plane stress.

Different procedures for the boundary element solution of the above equations will be presented in these notes. The various formulations will be seen to stem from the equations introduced in this section and consequently the names initial strain and initial stress will be broadly used to indicate their corresponding integral equations. This remark may appear unnecessary, but it is here included to avoid confusion with some early finite element formulations where the names initial strain/stress were used to indicate the way in which plastic strain increments are calculated from the constitutive equations [15]. In these formulations, the so-called initial strain is unable to handle ideal plasticity. This restriction, of course, does not apply to the formulations presented here.

CHAPTER 3

BOUNDARY ELEMENT FORMULATION FOR ELASTIC PROBLEMS

3.1 Introduction

This chapter is primarily intended to show how an elasticity problem, governed by the Navier equation (2.2.32) and with prescribed boundary conditions, can be reduced to a suitable integral equation amenable to numerical solution within the framework of the direct boundary element method. Hence, the basic reciprocal relations are first deduced, leading to the so-called Somigliana's identity for dispacements [32, 26]. Next, the complete boundary element formulation using the fundamental solution due to Kelvin is reviewed. A new formulation of the technique for half-plane type problems is also introduced through the adoption of a fundamental solution satisfying the traction-free condition over the surface of the semi-plane. A subsequent section is entirely concerned with the numerical implementation of the method and the last section presents the application of the half-plane formulation to some classical problems.

3.2 Somigliana's Identity

In order to clarify the subsequent ideas, an initial remark is now due; throughout these notes the concept of regular region will be used in the sense defined by Kellogg [31]. More specifically, regular regions are always implied here, and these represent regions bounded by regular surfaces (not necessarily smooth or Liapunov everywhere) which may have corners or edges, provided they are not too sharp [4]. The extension of this concept to infinite or semi-infinite regions will be discussed in another section of this chapter.

Consider a body defined by $\Omega + \Gamma$ (Γ is the boundary and Ω is the domain as shown in figure 3.2.1) which is in a state of equilibrium under some prescribed loads and displacements. This state is here represented by the set σ_{ij}, ε_{ij}, u_i, p_i and b_i.

Let us now assume a domain Ω^* with boundary Γ^* which contains the body $\Omega + \Gamma$ under consideration (see figure 3.2.2). As before, this new region is considered to be in an equilibrium state now denoted by σ^*_{ij}, ε^*_{ij}, etc. If elastic properties remain valid in both cases, the following integral statement can be inferred by simple symmetry of the tensors involved.

$$\int_{\Omega} \sigma^*_{ij}\, \varepsilon_{ij}\, d\Omega = \int_{\Omega} \sigma_{ij}\, \varepsilon^*_{ij}\, d\Omega \quad . \tag{3.2.1}$$

Integrating by parts both sides of (3.2.1) and using expressions (2.2.21) and (2.2.3), comes

$$\int_{\Omega} b^*_i\, u_i\, d\Omega + \int_{\Gamma} p^*_i\, u_i\, d\Gamma = \int_{\Omega} b_i\, u^*_i\, d\Omega + \int_{\Gamma} p_i\, u^*_i\, d\Gamma \tag{3.2.2}$$

which corresponds to Betti's second reciprocal work theorem.

Equation (3.2.2) can be further modified by assuming that the body force components b^*_i correspond to positive unit point loads applied at point $s \in \Omega^*$ in each of the three ortogonal directions given by the unit vectors p_i. This can be represented as follows

$$b^*_j = \delta(s, q) P_j \tag{3.2.3}$$

where $\delta(s, q)$ represents the Dirac delta function, s is the singular point (load point) and $q \in \Omega^*$ is a field point.

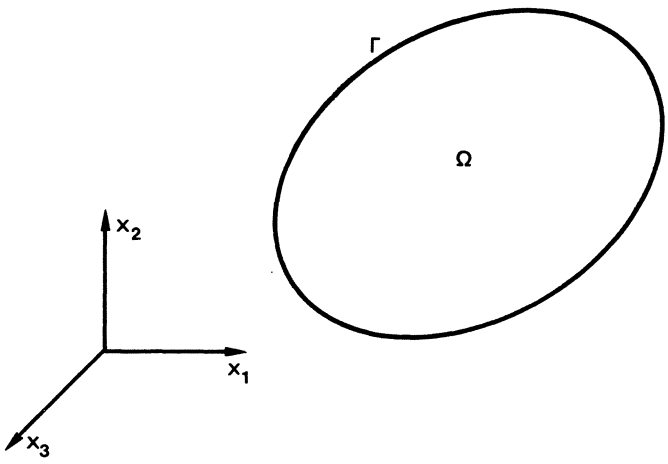

Fig. 3.2.1 Three dimensional body with volume Ω and boundary Γ.

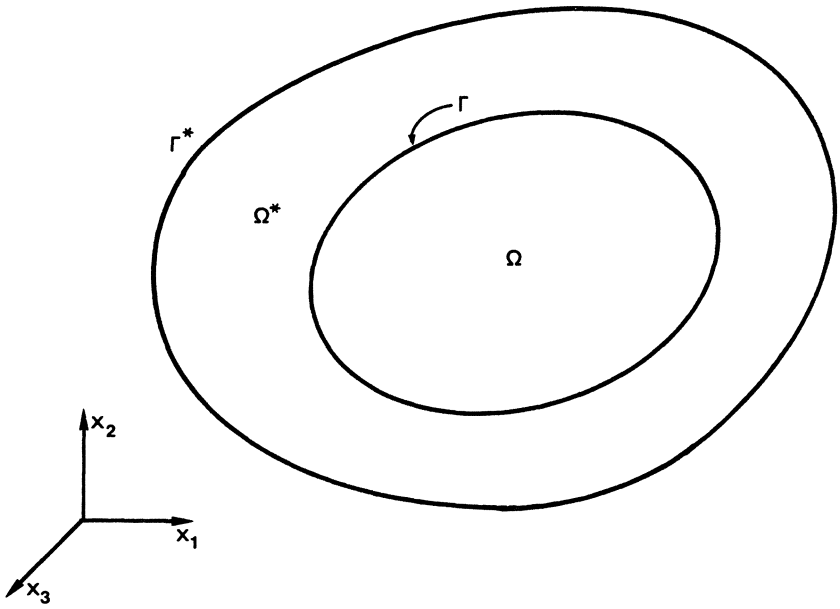

Fig. 3.2.2 General region $\Omega^* + \Gamma^*$ containing the body $\Omega + \Gamma$ with the same elastic properties.

The Dirac delta function has the following properties

$$\delta(s, q) = 0 \quad , \quad \text{if} \quad s \neq q$$

$$\delta(s, q) = \infty \quad , \quad \text{if} \quad s = q \tag{3.2.4}$$

$$\int_{\Omega^*} g(q)\ \delta(s, q)\ d\Omega^*(q) = g(s).$$

Therefore, if $s \in \Omega$, the first integral in eqn. (3.2.2) can be represented as

$$\int_{\Omega} b_i^*\ u_i\ d\Omega = u_i(s)\ P_i\ . \tag{3.2.5}$$

Furthermore, if each point load is taken as independent, the starred displacements and tractions can be written in the form

$$\begin{aligned} u_j^* &= u_{ij}^*(s, q)\ P_i \\ p_j^* &= p_{ij}^*(s, q)\ P_i \end{aligned} \tag{3.2.6}$$

where $u_{ij}^*(s, q)$ and $p_{ij}^*(s, q)$ represent the displacements and tractions in the j direction at point q corresponding to a unit point force acting in i direction (P_i) applied at point s.

From the above it is seen that equation (3.2.2) can be rewritten to represent the three separate components of the displacement at s in the form

$$u_i(s) = \int_{\Gamma} u_{ij}^*(s,Q)\ p_j(Q)\ d\Gamma(Q) - \int_{\Gamma} p_{ij}^*(s,Q)\ u_j(Q)\ d\Gamma(Q) + \int_{\Omega} u_{ij}^*(s,q)\ b_j(q)\ d\Omega(q) \tag{3.2.7}$$

where here and in what follows; $s, q \in \Omega$ and $S, Q \in \Gamma$.

Equation (3.2.7) is known as Somigliana's identity for displacements [32] and was here obtained by reciprocity with a singular solution of the Navier equation satisfying

$$Gu^*_{j,kk} + \frac{G}{1-2\nu} u^*_{k,kj} + \delta(s, q)P_j = 0 \ . \qquad (3.2.8)$$

Thus, solutions of the above equation are called fundamental solutions.

Equation (3.2.7) can alternatively be obtained through weighted residual considerations [1, 2]. Such procedure possesses the advantage of being more general and permits a straightforward extension to more complex differential equations. This technique is going to be applied in Chapter 4 where the inelastic boundary element formulation is presented. A common feature of both procedures is that they involve operations such as integrating by parts (equations (3.2.1) - (3.2.2)) with the singular delta function, and this may create some concern regarding to the final result. Here we recall reference [80], page 317, which reads :

"Whatever its theoretical limitations, the δ function is a useful device which, at worst, can be used formally provided the answers to which it leads are subsequently checked experimentally or by independent analysis". Therefore, equation (3.2.7) will be obtained through a formal procedure in the next section. This will be performed after the presentation of the different fundamental solutions adopted here.

3.3 Fundamental Solutions

Following the definition of fundamental solution introduced in the last section (see eqn. (3.2.8)), the different singular solutions

of the Navier equation considered here are now presented and classified according to the region $\Omega^* + \Gamma^*$ involved (see fig. 3.2.2).

In the first class considered, Ω^* is assumed to be an infinite elastic medium and consequently Γ^* is taken to infinity. This case corresponds to the fundamental solution due to Kelvin [26], and the appropriate expressions for the fundamental displacements and tractions defined in equations (3.2.6) are given by [1, 2]

$$u^*_{ij}(s, q) = \frac{1}{16\pi(1-\nu)Gr}\left\{(3-4\nu)\delta_{ij} + r_{,i}\, r_{,j}\right\} \tag{3.3.1}$$

for 3-D problems,

$$u^*_{ij}(s,q) = \frac{-1}{8\pi(1-\nu)G}\left\{(3-4\nu)\ \ln(r)\ \delta_{ij} - r_{,i}\, r_{,j}\right\} \tag{3.3.2}$$

for 2-D plane strain problems,

$$p^*_{ij}(s,q) = \frac{-1}{4\alpha\pi(1-\nu)r^{\alpha}}\left\{\left[(1-2\nu)\delta_{ij} + \beta\, r_{,i}\, r_{,j}\right]\frac{\partial r}{\partial n} - (1-2\nu)(r_{,i}n_j - r_{,j}n_i)\right\} \tag{3.3.3}$$

$\alpha = 2, 1$; $\beta = 3, 2$ for 3-D and 2-D plane strain respectively. Also, $r = r(s, q)$ represents the distance between the load point s and the field point q and its derivatives are taken with reference to the coordinates of q, i.e.,

$$r = (r_i r_i)^{\frac{1}{2}}$$

$$r_i = x_i(q) - x_i(s) \tag{3.3.4}$$

$$r_{,i} = \frac{\partial r}{\partial x_i(q)} = \frac{r_i}{r} \ .$$

In addition, the strains (ε^*_{jk}) at any point q due to a unit point load applied at s in i direction can be written as

$$\varepsilon^*_{jki}(s, q) = \frac{-1}{8\alpha\pi(1-\nu)Gr^{\alpha}} \left\{(1-2\nu)(r_{,k}\delta_{ij} + r_{,j}\delta_{ik}) - r_{,i}\delta_{jk} + \beta r_{,i}r_{,j}r_{,k}\right\} \tag{3.3.5}$$

and the stresses,

$$\sigma^*_{jki}(s, q) = \frac{-1}{4\alpha\pi(1-\nu)r^{\alpha}} \left\{(1-2\nu)(r_{,k}\delta_{ij} + r_{,j}\delta_{ki} - r_{,i}\delta_{jk}) + \beta r_{,i}r_{,j}r_{,k}\right\} . \tag{3.3.6}$$

The plane strain expressions are valid for plane stress if ν is replaced by $\bar{\nu} = \nu/(1+\nu)$.

In order to illustrate some features of this fundamental solution, and also to clarify subsequent matters, the passage from 3-D to 2-D plane strain will be commented. It is immediately apparent that the displacements u^*_{ij} for 3-D problems vanish as $r \to \infty$. This is not the same for 2-D; in this case, $u^*_{ij} \to -\infty$ as $r \to \infty$ due to the logarithm of r included in expression (3.3.2). Such behaviour of the 2-D case is entirely consistent and by all means expected. On physical grounds, for instance, one can consider the case of a semi-infinite bar extending from $x(A) = 0$ to $x(B) \to \infty$. If the extremity B is assumed to be fixed, a positive axial load applied at A would produce a state of constant strains. Consequently, by integration, $u(A) \to \infty$. Alternatively, if the displacement at a third point C is subtracted as a rigid body motion (i.e., extremity B is not taken as a reference any more) and this point is at a finite distance from A; $u(A)$ would be finite and $u(C) = 0$, but $u(B) \to -\infty$.

This simple analysis clearly indicates the physical nature of expression (3.3.2) and can be used to justify the passage from 3-D to 2-D by integrating the former with respect to $x_3(s)$. Thus, consider the following alternative expression for displacements in the 3-D case

$$\hat{u}^*_{ij}(s, q) = u^*_{ij} - \bar{u}^*_{ij} = \frac{1}{16\pi(1-\nu)G}\left\{(3-4\nu)\delta_{ij}\left[\frac{1}{r} - \frac{1}{\bar{r}}\right] + \frac{r_{,i}r_{,j}}{r}\right\} \qquad (3.3.7)$$

where u^*_{ij} was given by expression (3.3.1) and $\bar{u}^*_{ij} = u^*_{ij}(s, \bar{q})$ represents the displacements at a certain point $\bar{q}$, lying on a perpendicular to the load direction i passing through s . Also,

$$x_3(\bar{q}) = x_3(q) \qquad (3.3.8)$$

and

$$\bar{r} = r(s, \bar{q}) = (r_3^2 + 1)^{\frac{1}{2}}. \qquad (3.3.9)$$

Expression (3.3.7) can be used to find the two dimensional fundamental displacements as follows

$$\left[u^*_{ij}(s,q)\right]_{2-D} = \int_{-\infty}^{\infty} \hat{u}^*_{ij}(s,q)\, dx_3(s) \qquad (3.3.10)$$
$$(i,j = 1,2)$$

where the integrals involved are $\left(r = (r_1^2 + r_2^2)^{\frac{1}{2}}\right)$

$$\int_{-\infty}^{\infty} \left\{ \frac{1}{(r_3^2 + r^2)^{\frac{1}{2}}} - \frac{1}{(r_3^2 + 1)^{\frac{1}{2}}} \right\} dr_3 = -2\ln(r) \qquad (3.3.11)$$

and

$$r_i r_j \int_{-\infty}^{\infty} \frac{1}{(r_3^2 + r^2)^{\frac{3}{2}}}\, dr_3 = \frac{2r_i r_j}{r^2} = 2r_{,i}r_{,j} . \qquad (3.3.12)$$

The above results can readily be seen to produce expression (3.3.2). Note that the displacements are zero at $\bar{q}$ (depending on the direction of the load).

The second class of fundamental solutions adopted corresponds to half-space problems. In this case the Kelvin region is subdivided by an infinite horizontal plane $\bar{\Gamma}$ and its lower part is considered as $\Omega^* + \Gamma^*$. Thus, the region of interest becomes a semi-infinite medium with the plane part of Γ^* being represented by the surface $\bar{\Gamma}$. This lower half-space is always assumed to contain the region $\Omega + \Gamma$ and the plane $x_1 = 0$ is taken to be the boundary surface $\bar{\Gamma}$ which is here considered free from tractions (see figure 3.3.1).

The stress distribution due to point loads applied within the isotropic half-plane was presented by Melan [79]. The solution to the equivalent three dimensional problem was given by Mindlin [44] who produced not only the stresses, but also the corresponding displacements due to concentrated loads acting inside the half-space. The application of Mindlin's fundamental solution to boundary elements has been reported by Nakaguma [25] and the purpose of the present section is to present the complete solution to Melan's problem (including displacements), allowing for its general application to the boundary element technique.

Following Mindlin's procedure [44], it is seen that the complete half-space fundamental solution can be obtained by superposition of eighteen nuclei of strain (see Love [26]) derived from Kelvin's solution (six for each of the three components of the force). Also, the first singular solution employed in each load direction is found to be the single Kelvin solution presented in expressions (3.3.1) to (3.3.6) for

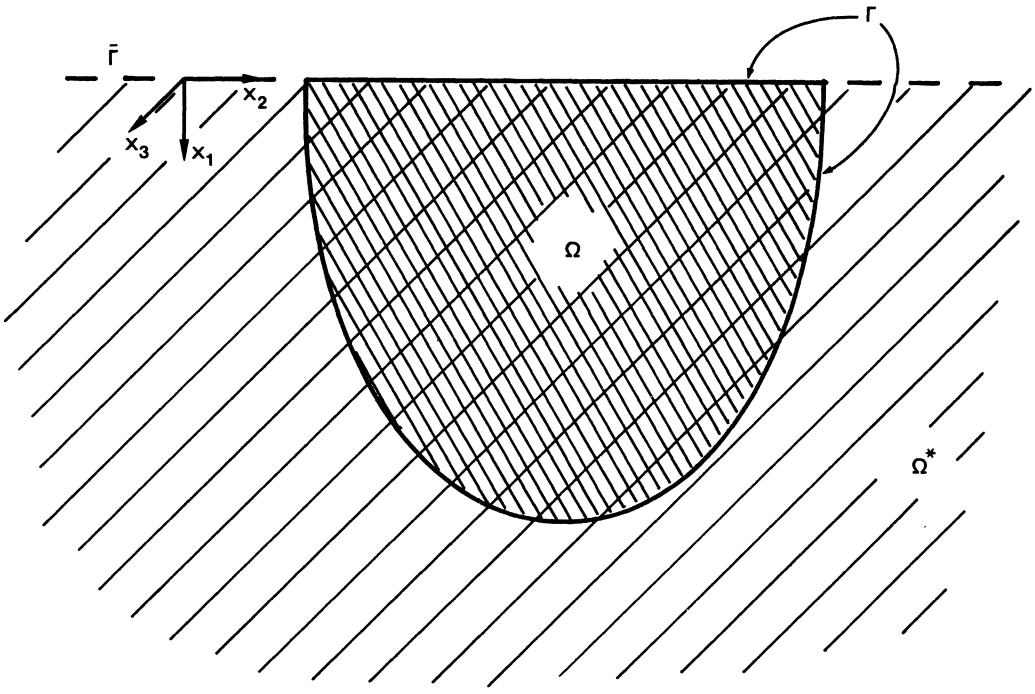

Fig. 3.3.1 Body $\Omega + \Gamma$ located within the semi-infinite space $x_1 \geq 0$.

3-D. All the other nuclei involve the coordinates of the image of the load point with respect to the surface $\bar{\Gamma}$. This provides satisfaction of the traction-free condition over the surface of the semi-infinite space. Therefore, this class of solutions can be written as

$$( )^* = ( )^k + ( )^c \qquad (3.3.13)$$

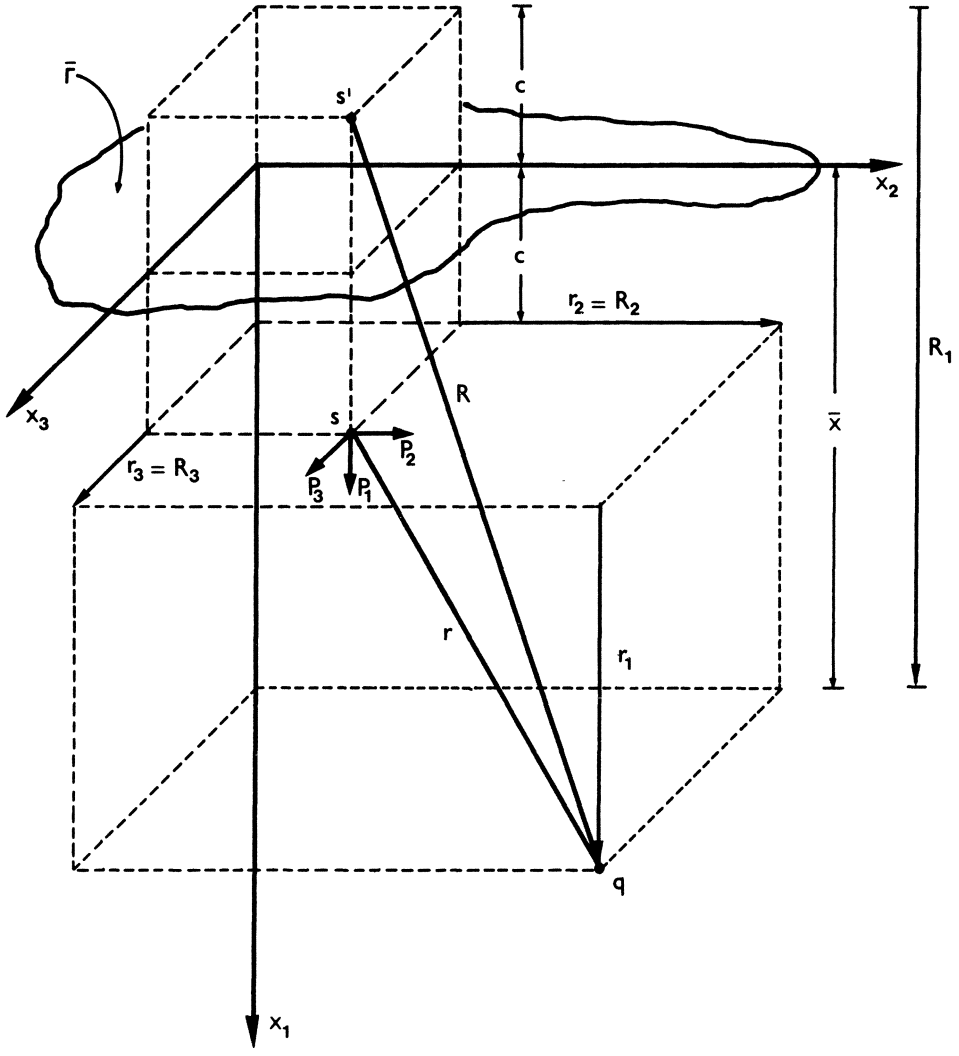

Fig. 3.3.2 Unit point loads applied within the half-space ($|P_1| = |P_2| = |P_3| = 1$) .

where $( )^k$ and $( )^c$ stand for Kelvin part (expressions (3.3.1) - (3.3.6) for 3-D and 2-D) and complementary part respectively.

In what follows, in order to avoid unnecessary repetition, only the complementary part of the solutions will be discussed. But it is always implied that the total expressions for the fundamental solutions are given by relation (3.3.13).

The complete set of expressions for the 3-D displacements and stresses are presented in Mindlin's paper. In order to obtain the plane strain fundamental displacements, the integration procedure already demonstrated for the Kelvin problem can be used. Therefore, the relevant 3-D complementary displacements required are now presented

$$u_{11}^c = \bar{K}_d \left\{ \frac{8(1-\nu)^2 - (3-4\nu)}{R} + \frac{(3-4\nu)R_1^2 - 2c\bar{x}}{R^3} + \frac{6c\bar{x}R_1^2}{R^5} \right\}$$

$$u_{12}^c = \bar{K}_d \, r_2 \left\{ \frac{(3-4\nu)r_1}{R^3} - \frac{4(1-\nu)(1-2\nu)}{R(R+R_1)} + \frac{6c\bar{x}R_1}{R^5} \right\} \qquad (3.3.14)$$

$$u_{21}^c = \bar{K}_d \, r_2 \left\{ \frac{(3-4\nu)r_1}{R^3} + \frac{4(1-\nu)(1-2\nu)}{R(R+R_1)} - \frac{6c\bar{x}R_1}{R^5} \right\}$$

$$u_{22}^c = \bar{K}_d \left\{ \frac{1}{R} + \frac{(3-4\nu)r_2^2}{R^3} + \frac{2c\bar{x}}{R^3}\left[1 - \frac{3r_2^2}{R^2}\right] + \frac{4(1-\nu)(1-2\nu)}{R+R_1}\left[1 - \frac{r_2^2}{R(R+R_1)}\right] \right\}$$

where with reference to figure 3.3.2 (i = 1, 2, 3)

$$r = (r_i r_i)^{\frac{1}{2}}$$

$$R = (R_i R_i)^{\frac{1}{2}}$$

$$r_i = x_i(q) - x_i(s)$$

$$R_i = x_i(q) - x_i(s') \qquad (3.3.15)$$

$$c = x_1(s) \geq 0$$

$$\bar{x} = x_1(q) \geq 0$$

$$\bar{K}_d = 1/[16\pi(1-\nu)G] \quad .$$

Integration of expressions (3.3.14) requires some laborious algebraic operations. The integrals involved were computed with the aid of reference [81] and are presented in table 3.3.1. Thus, with reference to figure 3.3.3, the complementary part of the plane strain displacements can be obtained. They are as follows

$$u_{11}^c = K_d \left\{ -[8(1-\nu)^2 - (3-4\nu)] \ln R + \frac{[(3-4\nu)R_1^2 - 2c\bar{x}]}{R^2} + \frac{4c\bar{x}R_1^2}{R^4} \right\}$$

$$u_{12}^c = K_d \left\{ \frac{(3-4\nu)r_1 r_2}{R^2} + \frac{4c\bar{x}R_1 r_2}{R^4} - 4(1-\nu)(1-2\nu)\theta \right\} \qquad (3.3.16)$$

$$u_{21}^c = K_d \left\{ \frac{(3-4\nu)r_1 r_2}{R^2} - \frac{4c\bar{x}R_1 r_2}{R^4} + 4(1-\nu)(1-2\nu)\theta \right\}$$

$$u_{22}^c = K_d \left\{ -[8(1-\nu)^2 - (3-4\nu)] \ln R + \frac{[(3-4\nu)r_2^2 + 2c\bar{x}]}{R^2} - \frac{4c\bar{x}r_2^2}{R^4} \right\}$$

$$\int_{-\infty}^{\infty} f(r_1, r_2, r_3, R_1)dr_3 = F(r_1, r_2, R_1)$$

f	F
$R = (R_i R_i)^{\frac{1}{2}}$; i=1, 2, 3	$R = (R_i R_i)^{\frac{1}{2}}$; i=1, 2
$\frac{1}{R}$ (†)	$2 \ln\left(\frac{1}{R}\right)$
$\frac{1}{R^3}$	$\frac{2}{R^2}$
$\frac{1}{R^5}$	$\frac{4}{3}\frac{1}{R^4}$
$\frac{1}{R^7}$	$\frac{16}{15}\frac{1}{R^6}$
$\frac{1}{R+R_1}$	$\frac{2R_1}{R_2}\arctan\left(\frac{R_1}{R_2}\right) + 2 \ln\left(\frac{1}{R}\right)$
$\frac{1}{R(R+R_1)}$	$-\frac{2}{R_2}\arctan\left(\frac{R_1}{R_2}\right)$
$\frac{1}{R(R+R_1)^2}$	$\frac{2}{R_2^2} + \frac{2R_1}{R_2^3}\arctan\left(\frac{R_1}{R_2}\right)$
$\frac{1}{R(R^2-R_1^2)}$	$\frac{2}{R_1 R_2}\arctan\left(\frac{R_1}{R_2}\right)$
$\frac{2R_1^2}{R(R^2-R_1^2)}$	$\frac{4R_1}{R_2}\arctan\left(\frac{R_1}{R_2}\right)$
$\frac{2R_1}{R^2-R_1^2}$	0
$\frac{2R_1^2}{R(R^2-R_1^2)^2}$	$\frac{2}{R_2^2} + \frac{2}{R_1 R_2}\left(\frac{R_1^2}{R_2^2} - 1\right)\arctan\left(\frac{R_1}{R_2}\right)$
$\frac{2R_1}{(R^2-R_1^2)^2}$	0

† $\frac{1}{R}$ is replaced by $\left(\frac{1}{R} - \frac{1}{\bar{R}}\right)$ for integration. See expression (3.3.11).

Table 3.3.1 Some useful integrals.

where the notation presented in (3.3.15) is used (i = 1, 2) and

$$\theta = \arctan(R_2/R_1)$$
$$K_d = 1/[8\pi(1-\nu)G] \quad . \tag{3.3.17}$$

The stresses corresponding to unit forces acting inside the half-plane can be taken from Melan's paper [79]. It should be noted that while checking Melan's formulae, a mistake was found in the expression for σ^c_{222} . This error does not appear to have been corrected in the past and is often repeated in recent publications such as [82]. The correct complementary parts of the stresses (plane strain) are given by

$$\sigma^c_{111} = - K_s \left\{ \frac{(3\bar{x} + c)(1-2\nu)}{R^2} + \frac{2R_1(R_1^2 + 2c\bar{x}) - 4\bar{x}r_2^2(1-2\nu)}{R^4} - \frac{16c\bar{x}\, R_1 r_2^2}{R^6} \right\}$$

$$\sigma^c_{121} = - K_s r_2 \left\{ - \frac{(1-2\nu)}{R^2} + \frac{2[\bar{x}^2 - 2c\bar{x} - c^2 + 2\bar{x}R_1(1-2\nu)]}{R^4} + \frac{16c\bar{x}\, R_1^2}{R^6} \right\}$$

$$\sigma^c_{221} = - K_s \left\{ \frac{(\bar{x} + 3c)(1-2\nu)}{R^2} + \frac{2[R_1(r_2^2 + 2c^2) - 2cr_2^2 + 2\bar{x}r_2^2(1-2\nu)]}{R^4} + \frac{16c\bar{x}\, R_1 r_2^2}{R^6} \right\} \tag{3.3.18}$$

$$\sigma^c_{112} = - K_s r_2 \left\{ \frac{(1-2\nu)}{R^2} - \frac{2[c^2 - \bar{x}^2 + 6c\bar{x} - 2\bar{x}R_1(1-2\nu)]}{R^4} + \frac{16c\bar{x}\, r_2^2}{R^6} \right\}$$

$$\sigma^c_{122} = - K_s \left\{ \frac{(3\bar{x} + c)(1-2\nu)}{R^2} + \frac{2\left[(2c\bar{x} + r_2^2)R_1 - 2\bar{x}R_1^2(1-2\nu)\right]}{R^4} \right.$$

$$\left. - \frac{16c\bar{x}R_1 r_2^2}{R^6} \right\}$$

$$\sigma^c_{222} = - K_s r_2 \left\{ \frac{3(1-2\nu)}{R^2} + \frac{2\left[r_2^2 - 4c\bar{x} - 2c^2 - 2\bar{x}R_1(1-2\nu)\right]}{R^4} \right.$$

$$\left. + \frac{16c\bar{x}\, R_1^2}{R^6} \right\}$$

where

$$K_s = 1/\left[4\pi(1-\nu)\right] \quad . \tag{3.3.19}$$

The corresponding tractions and strains can be computed from (3.3.18) by using the relations

$$p^c_{ij} = \sigma^c_{jki}\, n_k \tag{3.3.20}$$

and

$$\varepsilon^c_{jki} = \frac{1}{2G}\left[\sigma^c_{jki} - \nu\, \sigma^c_{\ell\ell i}\, \delta_{jk}\right] \quad . \tag{3.3.21}$$

For plane stress ν is replaced by $\bar{\nu}$ in formulae (3.3.16) to (3.3.21). From now on this remark will be valid for all the tensors related to the different fundamental solutions adopted here. Consequently, only plane strain expressions will be shown.

It is interesting to note that the complementary expressions do not present any singularities within the actual region $x_1 \geq 0$ when $c > 0$ (i.e., when the load point is located inside Ω^*). For the case when the load point lies at the surface $\bar{\Gamma}$ $(c \to 0)$, it is easily

s load point

q field point

s' image of s

$|P_1| = |P_2| = 1$

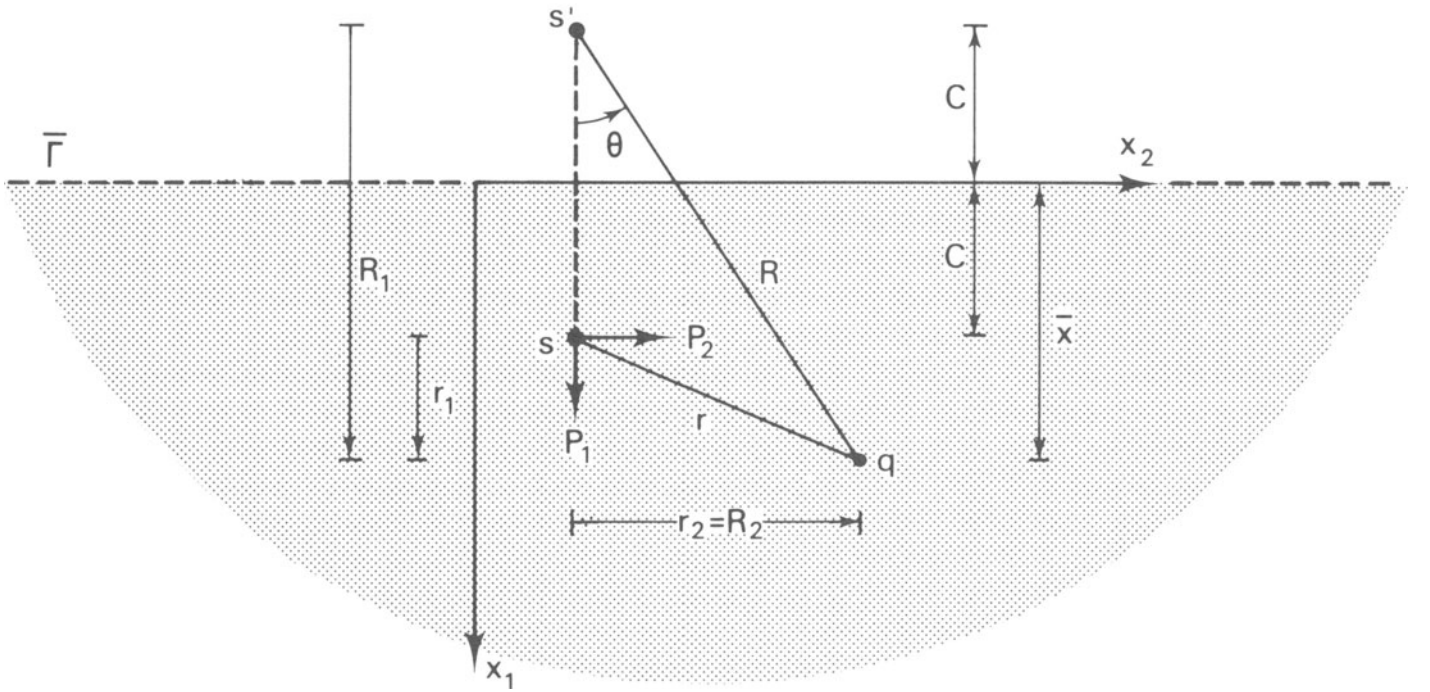

Fig. 3.3.3 Unit Point Loads Applied within the Half-Plane.

seen that the complementary expressions together with the Kelvin solution (see relation (3.3.13)), produce the complete solution to the problem of Boussinesq-Cerruti [44, 26] in 3-D or Flamant's problem [75, 26] in 2-D. The 3-D case was discussed by Nakaguma [25] and the fundamental displacements and tractions for the 2-D case are as follows ($s \in \bar{\Gamma}$)

$$\begin{aligned} u^*_{11} &= - K'_d \left\{ 2(1-\nu) \ln r - r^2_{,1} \right\} \\ u^*_{12} &= - K'_d \left\{ (1-2\nu)\theta - r_{,1} r_{,2} \right\} \\ u^*_{21} &= - K'_d \left\{ - (1-2\nu)\theta - r_{,2} r_{,1} \right\} \\ u^*_{22} &= - K'_d \left\{ 2(1-\nu) \ln r - r^2_{,2} \right\} \end{aligned} \tag{3.3.22}$$

and

$$p^*_{ij} = - \frac{2}{\pi r} \left\{ r_{,i} r_{,j} \frac{\partial r}{\partial n} \right\} \tag{3.3.23}$$

where

$$K'_d = 1/(2\pi G). \tag{3.3.24}$$

In addition, the fundamental strains and stresses are given by

$$\varepsilon^*_{jki} = \frac{-1}{\pi G r} \left\{ r_{,i} r_{,j} r_{,k} - \nu \, r_{,i} \, \delta_{jk} \right\} \tag{3.3.25}$$

and

$$\sigma^*_{jki} = \frac{-2}{\pi r} r_{,i} r_{,j} r_{,k} \tag{3.3.26}$$

The above expressions clearly indicate that as $c \to 0$ the half-plane fundamental solution still produces singularities of the same order as the corresponding Kelvin fundamental solution, the same argument is valid for 3-D [25]. It is important to note that the

traction-free condition over the surface of the half-plane is now provided by the occurrence of $\partial r/\partial n$ in expression (3.3.23) (i.e., $\partial r/\partial n = 0$ for $s, q \in \bar{\Gamma}$) .

Once the fundamental solutions have been presented, Somigliana's identity can be obtained by following a more formal procedure. Recalling the integral statement (3.2.1), one can always write

$$\int_{\Omega_\varepsilon} \sigma^*_{ij}(s, q)\, \varepsilon_{ij}(q)\, d\Omega(q) = \int_{\Omega_\varepsilon} \sigma_{ij}(q)\, \varepsilon^*_{ij}(s, q)\, d\Omega(q) \qquad (3.3.27)$$

where Ω_ε is the domain that arises from Ω by removing a ball of radius ε and surface $\bar{\Gamma}_\varepsilon$ centred at the load (singular) point s (see figure 3.3.4)).

Within Ω_ε the tensors corresponding to the fundamental solution are never singular ($s \notin \Omega_\varepsilon$). Consequently, assuming that $\varepsilon_{ij}(q)$ and $\sigma_{ij}(q)$ are both continuous and bounded for any point $q \in \Omega$, integrating by parts as before leads to

$$\begin{aligned} \int_{\Gamma+\bar{\Gamma}_\varepsilon} p^*_i(s, Q)\, u_i(Q)\, d\Gamma(Q) = & \int_{\Gamma+\bar{\Gamma}_\varepsilon} u^*_i(s, Q)\, p_i(Q)\, d\Gamma(Q) \\ & + \int_{\Omega_\varepsilon} u^*_i(s, q)\, b_i(q)\, d\Omega(q) \end{aligned} \qquad (3.3.28)$$

Considering now the integrals defined over $\bar{\Gamma}_\varepsilon$, one can easily verify that

$$\lim_{\varepsilon \to 0} \int_{\bar{\Gamma}_\varepsilon} u^*_i(s, Q)\, p_i(Q)\, d\Gamma(Q) = 0 \; . \qquad (3.3.29)$$

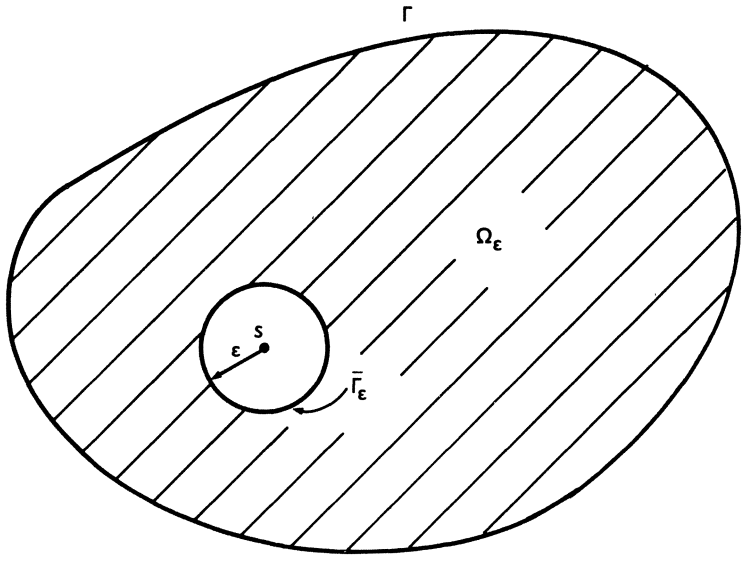

Fig. 3.3.4 Singular point s removed from Ω by an auxiliary spherical boundary.

The same can not be said for the first boundary integral in equation (3.3.28). The corresponding $\bar{\Gamma}_\varepsilon$ integral can be written as follows

$$\int_{\bar{\Gamma}_\varepsilon} p_i^*(s, Q)\, u_i(Q)\, d\Gamma(Q) = \int_{\bar{\Gamma}_\varepsilon} p_i^*(s, Q)\left[u_i(Q) - u_i(s)\right] d\Gamma(Q) + u_i(s) \int_{\bar{\Gamma}_\varepsilon} p_i^*(s, Q)\, d\Gamma(Q) \tag{3.3.30}$$

where from the assumption of continuity of $u_i(q)$ one gets

$$\lim_{\varepsilon \to 0} \int_{\bar{\Gamma}_\varepsilon} p_i^*(s, Q)\left[u_i(Q) - u_i(s)\right] d\Gamma(Q) = 0 \quad . \tag{3.3.31}$$

The last integral in (3.3.30) can be computed from a starting assumption. Since the fundamental solutions correspond to unit point loads applied at s, it is readily seen that

$$\int_{\bar{\Gamma}_\varepsilon} p_i^*(s, Q)\, d\Gamma(Q) = P_j \int_{\bar{\Gamma}_\varepsilon} p_{ij}^*(s, Q)\, d\Gamma(Q) = \delta_{ij} P_j \qquad (3.3.32)$$

which leads to

$$u_i(s) \int_{\bar{\Gamma}_\varepsilon} p_i^*(s, Q)\, d\Gamma(Q) = u_i(s) P_i \ . \qquad (3.3.33)$$

Expression (3.3.33) is independent of the radius ε and can obviously be verified by analytical integration of the different fundamental solutions.

From the above it is seen that by taking the limit as $\varepsilon \to 0$ and considering each of the P_i terms to act independently, Somigliana's identity for displacements is obtained in the form of equation (3.2.7).

3.4 Stresses at Internal Points

Equation (3.2.7) is a continuous representation of displacements at any point $s \in \Omega$. Consequently, the stress state at this point can be obtained by combining the derivatives of eqn. (3.2.7) with respect to the coordinates of s to produce the strain tensor and then substituting the result into Hooke's law (see Chapter 2, equations (2.2.21) and (2.2.27)). The final expression is as follows

$$\sigma_{ij}(s) = \int_\Gamma u_{ijk}^*(s, Q)\, p_k(Q)\, d\Gamma(Q) - \int_\Gamma p_{ijk}^*(s, Q)\, u_k(Q)\, d\Gamma(Q) + \int_\Omega u_{ijk}^*(s, q)\, b_k(q)\, d\Omega(q) \ . \qquad (3.4.1)$$

Note that differentiation was carried out directly inside the integrals. This is obviously possible for the boundary integrals, but the body force term needs a proper proof. This matter will be taken up in Chapter 4 where the inelastic formulation is presented and a strong demonstration of the validity of this procedure will be discussed.

For the Kelvin fundamental solution, the new tensors are written as

$$u^*_{ijk} = - \sigma^*_{ijk} \tag{3.4.2}$$

$$\begin{aligned} p^*_{ijk} = \frac{G}{2\alpha\pi(1-\nu)r^\beta} \Big\{ & \beta \frac{\partial r}{\partial n} \big[(1-2\nu)\delta_{ij} r_{,k} + \\ & + \nu(\delta_{ik} r_{,j} + \delta_{jk} r_{,i}) - \gamma r_{,i} r_{,j} r_{,k}\big] \\ & + \beta\nu(n_i r_{,j} r_{,k} + n_j r_{,i} r_{,k}) + \\ & (1-2\nu)\ (\beta n_k r_{,i} r_{,j} + n_j \delta_{ik} + n_i \delta_{jk}) \\ & - (1-4\nu) n_k \delta_{ij} \Big\} \end{aligned} \tag{3.4.3}$$

where $\alpha = 2, 1$; $\beta = 3, 2$; $\gamma = 5, 4$ for 3-D and 2-D respectively. Note that the substitution

$$\frac{\partial r}{\partial x_i(s)} = - r_{,i} = - \frac{\partial r}{\partial x_i(q)} \tag{3.4.4}$$

was already effectuated.

The complementary expressions for the tensors corresponding to the half-plane fundamental solution are obtained by

$$u^c_{ijk} = G\left(\frac{\partial u^c_{ik}}{\partial x_j} + \frac{\partial u^c_{jk}}{\partial x_i}\right) + \frac{2G\nu}{1-2\nu}\frac{\partial u^c_{\ell k}}{\partial x_\ell}\delta_{ij} \tag{3.4.5}$$

and

$$p^c_{ijk} = G\left[\frac{\partial \sigma^c_{kmi}}{\partial x_j} + \frac{\partial \sigma^c_{kmj}}{\partial x_i} + \frac{2\nu}{1-2\nu}\frac{\partial \sigma^c_{km\ell}}{\partial x_\ell}\delta_{ij}\right]n_m \tag{3.4.6}$$

where the above derivatives are taken with reference to the coordinates of the load point. These derivatives are listed below for completeness

$$\frac{\partial u^c_{11}}{\partial x_1} = \frac{K_d}{R^2}\left\{\left[3(3-4\nu) - 8(1-\nu)^2\right]R_1 - 2\bar{x} + \frac{\left[4\bar{x}R_1 + 12c\bar{x} - 2(3-4\nu)R_1^2\right]}{R^2}R_1 - \frac{16c\bar{x}R_1^3}{R^4}\right\}$$

$$\frac{\partial u^c_{12}}{\partial x_1} = \frac{K_d}{R^2}r_2\left\{4(1-\nu)(1-2\nu) - (3-4\nu) + \frac{\left[4\bar{x}(2c+\bar{x}) - 2(3-4\nu)R_1r_1\right]}{R^2} - \frac{16c\bar{x}R_1^2}{R^4}\right\}$$

$$\frac{\partial u^c_{21}}{\partial x_1} = \frac{K_d}{R^2}r_2\left\{-(3-4\nu) - 4(1-\nu)(1-2\nu) - \frac{\left[2(3-4\nu)R_1r_1 + 4\bar{x}(2c+\bar{x})\right]}{R^2} + \frac{16c\bar{x}R_1^2}{R^4}\right\} \tag{3.4.7}$$

$$\frac{\partial u^c_{22}}{\partial x_1} = \frac{K_d}{R^2}\left\{2\bar{x} - \left[8(1-\nu)^2 - (3-4\nu)\right]R_1 - \frac{\left[4\bar{x}r_2^2 + 2R_1((3-4\nu)r_2^2 + 2c\bar{x})\right]}{R^2} + \frac{16c\bar{x}R_1r_2^2}{R^4}\right\}$$

$$\frac{\partial u^c_{11}}{\partial x_2} = \frac{K_d}{R^2}r_2\left\{8(1-\nu)^2 - (3-4\nu) + \frac{2\left[(3-4\nu)R_1^2 - 2c\bar{x}\right]}{R^2} + \frac{16c\bar{x}R_1^2}{R^4}\right\}$$

$$\frac{\partial u^c_{12}}{\partial x_2} = \frac{K_d}{R^2}\left\{ 4(1-\nu)(1-2\nu)R_1 + (3-4\nu)r_1 - \frac{\left[2(3-4\nu)R_1 r_1 - 12c\bar{x}\right]R_1}{R^2} - \frac{16c\bar{x}R_1^3}{R^4} \right\} \qquad (3.4.7)\ \text{cont.}$$

$$\frac{\partial u^c_{21}}{\partial x_2} = \frac{K_d}{R^2}\left\{ -4(1-\nu)(1-2\nu)R_1 - (3-4\nu)r_1 + \frac{\left[2(3-4\nu)r_1 r_2^2 + 4c\bar{x}R_1\right]}{R^2} - \frac{16c\bar{x}R_1 r_2^2}{R^4} \right\}$$

$$\frac{\partial u^c_{22}}{\partial x_2} = \frac{K_d}{R^2} r_2 \left\{ 8(1-\nu)^2 - 3(3-4\nu) + \frac{2\left[(3-4\nu)r_2^2 + 6c\bar{x}\right]}{R^2} - \frac{16c\bar{x}r_2^2}{R^4} \right\}$$

$$\frac{\partial \sigma^c_{111}}{\partial x_1} = -\frac{K_s}{R^2}\left\{ (1-2\nu) + \frac{2\left[2c\bar{x} + R_1(3R_1 + 2\bar{x} - (3\bar{x}+c)(1-2\nu))\right]}{R^2} - \frac{8\left[2c\bar{x}r_2^2 + R_1(R_1(R_1^2+2c\bar{x}) + 4\bar{x}r_2^2\nu)\right]}{R^4} + \frac{96c\bar{x}R_1^2 r_2^2}{R^6} \right\}$$

$$\frac{\partial \sigma^c_{121}}{\partial x_1} = -\frac{K_s}{R^4} r_2 \left\{ 2r_1 - 4\nu(R_1 + 2\bar{x}) + 8R_1 \frac{\left[2\bar{x}R_1 + 6c\bar{x} - \bar{x}^2 + c^2 - 2\bar{x}R_1(1-2\nu)\right]}{R^2} - \frac{96c\bar{x}R_1^3}{R^4} \right\}$$

$$\frac{\partial \sigma^c_{221}}{\partial x_1} = -\frac{K_s}{R^2}\left\{ 3(1-2\nu) + \frac{2\left[2c^2 - r_2^2 + R_1(4c - (\bar{x}+3c)(1-2\nu))\right]}{R^2} + \frac{8\left[r_2^2(2c\bar{x} + R_1^2 - 2\bar{x}R_1(1-2\nu)) - 2c^2R_1^2\right]}{R^4} - \frac{96c\bar{x}R_1^2 r_2^2}{R^6} \right\} \qquad (3.4.8)$$

$$\frac{\partial \sigma^c_{112}}{\partial x_1} = -\frac{K_s}{R^4} r_2 \left\{ 2(2\bar{x} - R_1)(1-2\nu) - 4(c + 3\bar{x}) + \frac{8\left[2\bar{x}r_2^2 + R_1(6c\bar{x} - 2\bar{x}R_1(1-2\nu) + c^2 - \bar{x}^2)\right]}{R^2} - \frac{96c\bar{x}R_1 r_2^2}{R^4} \right\}$$

$$\frac{\partial \sigma^c_{122}}{\partial x_1} = -\frac{K_s}{R^2} \left\{ (1-2\nu) + \frac{2\left[2c\bar{x} + r_2^2 + R_1(2\bar{x} - (7\bar{x} + c)(1-2\nu))\right]}{R^2} - \frac{8\left[2c\bar{x}r_2^2 + R_1(2\bar{x}r_2^2 + (2c\bar{x} + r_2^2)R_1 - 2\bar{x}R_1^2(1-2\nu))\right]}{R^4} + \frac{96c\bar{x}R_1^2 r_2^2}{R^6} \right\}$$

$$\frac{\partial \sigma^c_{222}}{\partial x_1} = -\frac{K_s}{R^4} r_2 \left\{ 4\nu(3R_1 + 2\bar{x}) - 2(7R_1 + 2\bar{x}) + \frac{8R_1\left[4\bar{x}R_1(1-\nu) + 8c\bar{x} - r_2^2 + 2c^2\right]}{R^2} - \frac{96c\bar{x}R_1^3}{R^4} \right\}$$

$$\frac{\partial \sigma^c_{111}}{\partial x_2} = -\frac{K_s}{R^4} r_2 \left\{ 2(7\bar{x} + c)(1-2\nu) + \frac{4\left[2R_1(R_1^2 + 6c\bar{x}) - 4\bar{x}r_2^2(1-2\nu)\right]}{R^2} - \frac{96c\bar{x}R_1 r_2^2}{R^4} \right\} \qquad \text{(3.4.8) cont.}$$

$$\frac{\partial \sigma^c_{121}}{\partial x_2} = -\frac{K_s}{R^2} \left\{ (1-2\nu) - \frac{2\left[\bar{x}^2 - 2c\bar{x} - c^2 + (1-2\nu)(r_2^2 + 2\bar{x}R_1)\right]}{R^2} + \frac{8\left[r_2^2(\bar{x}^2 - 2c\bar{x} - c^2 + 2\bar{x}R_1(1-2\nu)) - 2c\bar{x}R_1^2\right]}{R^4} + \frac{96c\bar{x}R_1^2 r_2^2}{R^6} \right\}$$

$$\frac{\partial \sigma^c_{221}}{\partial x_2} = -\frac{K_s}{R^4} r_2 \left\{ -2(5-6\nu)r_1 + \frac{8\left[R_1(r_2^2 + 2c^2 - 4c\bar{x}) - 2cr_2^2 + 2\bar{x}r_2^2(1-2\nu)\right]}{R^2} + \frac{96c\bar{x}R_1 r_2^2}{R^4} \right\}$$

$$\frac{\partial \sigma^c_{112}}{\partial x_2} = -\frac{K_s}{R^2}\left\{-(1-2\nu) + \frac{2\left[(r_2^2 - 2\bar{x}R_1)(1-2\nu) + c^2 - \bar{x}^2 + 6c\bar{x}\right]}{R^2} - \frac{8\left[12c\bar{x} + c^2 - \bar{x}^2 - 2\bar{x}R_1(1-2\nu)\right]r_2^2}{R^4} + \frac{96c\bar{x}r_2^4}{R^6}\right\}$$

$$\frac{\partial \sigma^c_{122}}{\partial x_2} = -\frac{K_s}{R^4} r_2 \left\{2(3\bar{x} + c)(1-2\nu) - 4R_1 + \frac{8R_1\left[6c\bar{x} + r_2^2 - 2\bar{x}R_1(1-2\nu)\right]}{R^2} - \frac{96c\bar{x}R_1 r_2^2}{R^4}\right\} \qquad (3.4.8)\ \text{cont.}$$

$$\frac{\partial \sigma^c_{222}}{\partial x_2} = -\frac{K_s}{R^2}\left\{-3(1-2\nu) - \frac{2\left[3r_2^2 - 4c\bar{x} - 2c^2 - (2\bar{x}R_1 + 3r_2^2)(1-2\nu)\right]}{R^2} + \frac{8\left[r_2^2(r_2^2 - 4c\bar{x} - 2c^2 - 2\bar{x}R_1(1-2\nu)) - 2c\bar{x}R_1^2\right]}{R^4} + \frac{96c\bar{x}R_1^2 r_2^2}{R^6}\right\}.$$

It should be noticed that equation (3.4.1) can be further modified when the half-plane fundamental solution is used. This will be discussed in the section that follows.

3.5 Boundary Integral Equation

In the preceeding sections the derivation of Somigliana's identity has been presented without need for distinction between the different fundamental solutions employed. In this section, however, it is instructive to consider first the Kelvin solution and then extend the complete formulation to half-space type problems where full advantage of the traction-free condition can be taken.

Considering the Kelvin case, Somigliana's identity is not satisfactory for obtaining solutions unless the boundary displacements and tractions are known throughout the boundary Γ (body forces are always assumed to be prescribed). Therefore it is interesting to

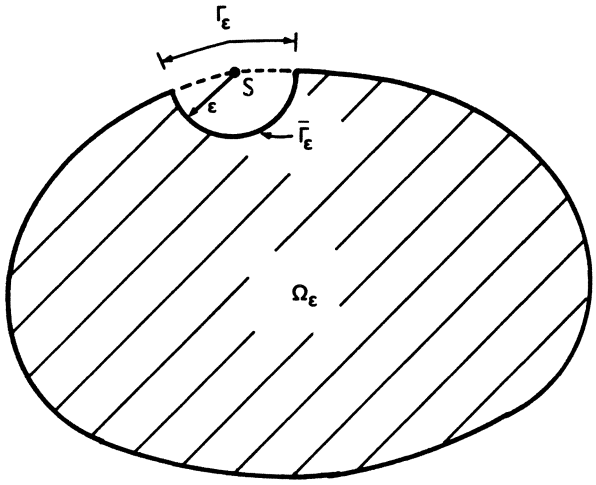

Fig. 3.5.1 Singular point S removed from Γ by part of a spherical boundary.

examine the limiting form of equation (3.3.28) as $s \to S (S \in \Gamma$ as conventioned in eqn.(3.2.7)). Assuming that the body can be represented as shown in figure 3.5.1, this limiting form can be written as follows [24]

$$\int_{\Gamma-\Gamma_\varepsilon+\bar{\Gamma}_\varepsilon} p^*_{ij}(S, Q)\, u_j(Q)\, d\Gamma(Q) = \int_{\Gamma-\Gamma_\varepsilon+\bar{\Gamma}_\varepsilon} u^*_{ij}(S, Q)\, p_j(Q)\, d\Gamma(Q) + \int_{\Omega_\varepsilon} u^*_{ij}(S, q)\, b_j(q)\, d\Gamma(q) \tag{3.5.1}$$

where the assumption that each P_i is acting independently was already made.

Let us now study separately the limit of each integral in (3.5.1) as $\varepsilon \to 0$. The first integral can be written as

$$\lim_{\varepsilon\to 0} \int_{\Gamma-\Gamma_\varepsilon+\bar{\Gamma}_\varepsilon} p^*_{ij}(S, Q)\, u_j(Q)\, d\Gamma(Q) = \lim_{\varepsilon\to 0} \int_{\bar{\Gamma}_\varepsilon} p^*_{ij}(S, Q)\, u_j(Q)\, d\Gamma(Q) + \lim_{\varepsilon\to 0} \int_{\Gamma-\Gamma_\varepsilon} p^*_{ij}(S, Q)\, u_j(Q)\, d\Gamma(Q) \tag{3.5.2}$$

where from the first integral on the right-hand-side comes

$$\lim_{\varepsilon\to 0}\int_{\bar{\Gamma}_\varepsilon} p^*_{ij}(S,\,Q)\,u_j(Q)\,d\Gamma(Q) = \lim_{\varepsilon\to 0}\int_{\bar{\Gamma}_\varepsilon} p^*_{ij}(S,\,Q)\left[u_j(Q) - u_j(S)\right]d\Gamma(Q) + \lim_{\varepsilon\to 0}\left\{ u_j(S)\int_{\bar{\Gamma}_\varepsilon} p^*_{ij}(S,\,Q)\,d\Gamma(Q)\right\} . \tag{3.5.3}$$

Clearly, the first integral on the right of (3.5.3) vanishes from the condition of continuity of $u_j(Q)$ and the second integral allows for the representation

$$C_{ij}(S) = \lim_{\varepsilon\to 0}\int_{\bar{\Gamma}_\varepsilon} p^*_{ij}(S,\,Q)\,d\Gamma(Q) \tag{3.5.4}$$

Going back to expression (3.5.2), the second integral on the right-hand-side is seen to be taken in the Cauchy principal value sense [28]. The remaining integrals in expression (3.5.1) present no special singularities and can be interpreted in the normal sense of integration. Therefore, as $\varepsilon \to 0$, the following equation arises

$$C_{ij}(S)\,u_j(S) + \int_\Gamma p^*_{ij}(S,\,Q)\,u_j(Q)\,d\Gamma(Q) = \int_\Gamma u^*_{ij}(S,\,Q)\,p_j(Q)\,d\Gamma(Q) + \int_\Omega u^*_{ij}(S,\,q)\,b_j(q)\,d\Omega(q) \tag{3.5.5}$$

where the integral on the left-hand-side is to be interpreted in the sense of Cauchy principal value.

Equation (3.5.5) is valid for 3-D or 2-D, it provides a relation that must be satisfied between surface displacements, surface tractions and body forces in an elastic body. Taking into consideration that the body force term is always known, when boundary conditions are prescribed this equation becomes a boundary integral equation for the unknown boundary data. This important feature is the one that makes it most attractive and can be fully explored for numerical solutions.

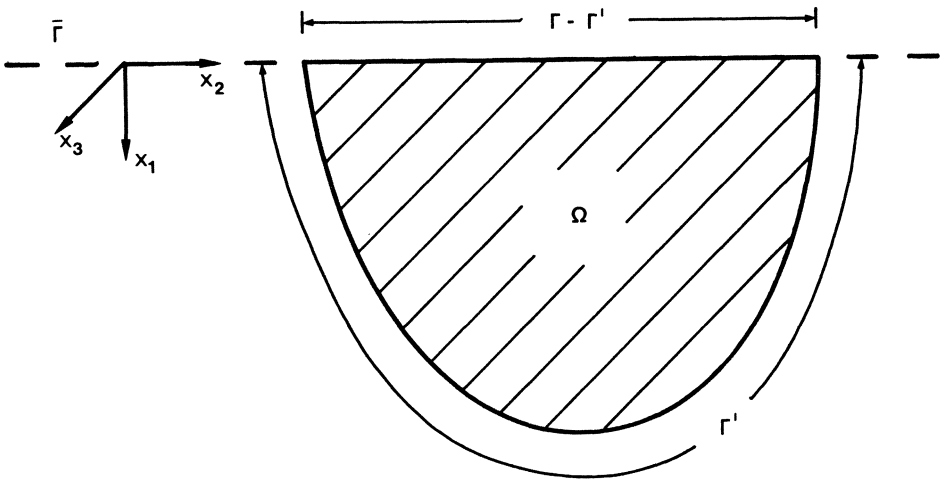

Fig. 3.5.2 Body with part of its boundary Γ coinciding with the surface of the semi-infinite space.

The coefficient $C_{ij}(S)$ was defined in (3.5.4). If the tangent plane at S is continuous, $C_{ij}(S) = \delta_{ij}/2$ but if this is not the case, closed form expressions for this coefficient have been presented in references [7, 83] for 2-D and 3-D. For practical applications, however, it will be seen later that C_{ij} together with the corresponding principal value can be indirectly computed by applying equation (3.5.5) to represent rigid body movements.

Equation (3.5.5) is the starting equation for the boundary element technique using the Kelvin fundamental solution. For half-space type solutions, it is interesting to start by reviewing Somigliana's identity to point out an important simplification in this equation which was not mentioned before. If the body that is being analysed presents part of its boundary coinciding with the surface of the semi-infinite space $\bar{\Gamma}$ (see figure 3.5.2), the integral over this part which involves p^*_{ij} vanishes identically because of the traction-free condition included into the fundamental solution. Consequently, Somigliana's

identity can be rewritten as follows (3-D or 2-D)

$$u_i(s) = \int_{\Gamma} u^*_{ij}(s, Q)\, p_j(Q)\, d\Gamma(Q) - \int_{\Gamma'} p^*_{ij}(s, Q)\, u_j(Q)\, d\Gamma(Q) + \int_{\Omega} u^*_{ij}(s, q)\, b_j(q)\, d\Omega(q) \qquad (3.5.6)$$

where Γ' represents the part of Γ in which $x_1 > 0$.

In addition, equation (3.5.6) can also be specialised for load points located on the surface of the half-space $\Gamma - \Gamma'$ without any further modification. This is because when $c = 0$ the singularity which occurs in the first integral on the right-hand-side of (3.5.6) can be integrated in the usual sense. Furthermore, if the problem to be analysed satisfies the traction-free condition ($p_j(Q) = 0$) over some part of $\Gamma - \Gamma'$, this weak singularity is also removed, allowing for load points along such part of the boundary to be considered as internal points.

As it will be seen later, the above described characteristic of the half-space formulation plays an important role in its application to the boundary element method.

Due to the non-singular nature of the complementary expressions (see formulae (3.3.16) -(3.3.20)), specialisation of equation (3.5.6) for load points located along the boundary Γ' creates exactly the same singularities obtained for the single Kelvin formulation. Therefore, the following equation is obtained

$$C_{ij}(S)\, u_j(S) + \int_{\Gamma'} p^*_{ij}(S, Q)\, u_j(Q)\, d\Gamma(Q) = \int_{\Gamma} u^*_{ij}(S, Q)\, p_j(Q)\, d\Gamma(Q) + \int_{\Omega} u^*_{ij}(S, q)\, b_j(q)\, d\Omega(q) \qquad (3.5.7)$$

in which the integral on the left-hand-side is to be interpreted in the Cauchy principal value sense and the expression of $C_{ij}(S)$ corresponds only to the Kelvin part of the fundamental solution. Hence, $C_{ij} = \delta_{ij}/2$ on smooth surfaces and can be taken from other references otherwise [7, 83].

The special case when the load point is located at the intersection of Γ' and $\bar{\Gamma}$ can also be handled by equation (3.5.7). However, in this case limiting relations are involved resulting in a different expression for C_{ij}. This exception does not create any difficulty and the proper expression for C_{ij} can be obtained by applying equation (3.5.7) to represent rigid body movements.

In conclusion, equation (3.5.7) can in general be quoted as representing the specialisation of (3.5.6) for any boundary load point if $C_{ij} = \delta_{ij}$ when referring to the boundary $\Gamma - \Gamma'$.

Following the procedure presented in Section 3.4, the derivatives of equation (3.5.6) with respect to the coordinates of the load point can be combined with Hooke's law to obtain a particular version of equation (3.4.1)

$$\sigma_{ij}(s) = \int_{\Gamma} u^*_{ijk}(s, Q)\, p_k(Q)\, d\Gamma(Q) - \int_{\Gamma'} p^*_{ijk}(s, Q)\, u_k(Q)\, d\Gamma(Q) + \int_{\Omega} u^*_{ijk}(s, q)\, b_j(q)\, d\Omega(q) \,. \tag{3.5.8}$$

Note that if the problem to be analysed satisfies the traction free condition $p_k(Q) = 0$ over some part of the boundary $\Gamma - \Gamma'$, stresses at boundary points located on this part of the boundary can also be computed by equation (3.5.8). In this case s is replaced by S in the above equation on condition that $S \in$ traction free part of $\Gamma - \Gamma'$.

Although body forces have been considered in the equations presented so far, in the following sections this term will not be included for simplicity. However, it is worth mentioning that the domain integral involved can be avoided in many practical cases by using some alternative procedures. Lachat and Watson [23], for instance, use superposition with a particular solution which includes only the body force term. A more interesting procedure is presented by Rizzo and Shippy [84] where the possibility of transforming the body force integral into a surface integral is presented. This procedure is applicable to some of the most common types of body forces, such as constant gravitational load, centrifugal load due to a fixed axis of rotation and the effect of a steady-state temperature distribution. A unified procedure for such cases (3-D and 2-D) has been recently presented by Danson [85], in which the Galerkin vector corresponding to the fundamental solution is employed.

3.6 Infinite and Semi-Infinite Regions

Throughout the derivations presented in this chapter, bounded bodies were always considered. In this section the validity of the previous expressions (Kelvin fundamental solution) will be extended to external problems in infinite regular regions. As before, we borrow this concept from Kellogg [31]. Thus, infinite regular region means a region bounded by a regular surface (hence a bounded surface), and containing all sufficiently distant points. In addition, the same extension will be seen applicable to problems related to the semi-infinite space with or without cavities. Consequently, the ideas will be generalized to include such cases.

The extension of equation (3.5.5) to infinite regular regions is not valid without further hypotheses on the functions involved. Such hypotheses are concerned with the behaviour of the functions on an infinitely distant surface and are referred to as regularity conditions.

Let ρ be the radius of a sphere of surface Γ_ρ and centred at S, which encloses the cavity (or cavities) of the external problem depicted in figure 3.6.1.

Equation (3.5.5) can be written for the region within Γ and Γ_ρ as follows

$$C_{ij}(S)\, u_j(S) + \int_\Gamma p^*_{ij}(S, Q)\, u_j(Q)\, d\Gamma(Q) + \int_{\Gamma_\rho} p^*_{ij}(S, Q)\, u_j(Q)\, d\Gamma(Q) = \int_\Gamma u^*_{ij}(S, Q)\, p_j(Q)\, d\Gamma(Q) + \int_{\Gamma_\rho} u^*_{ij}(S, Q)\, p_j(Q)\, d\Gamma(Q) . \tag{3.6.1}$$

Clearly, if the limiting case $\rho \to \infty$ is considered, equation (3.6.1) can be expressed in terms of boundary integrals over Γ alone if

$$\lim_{\rho\to\infty} \int_{\Gamma_\rho} \left[p^*_{ij}(S, Q)\, u_j(Q) - u^*_{ij}(S, Q)\, p_j(Q)\right] d\Gamma(Q) = 0 . \tag{3.6.2}$$

For 3-D problems, one has $(Q \in \Gamma_\rho)$

$$d\Gamma(Q) = |J|\, d\phi d\theta \quad \text{with} \quad |J| = O(\rho^2) ;$$

$$u^*_{ij}(S, Q) = O(\rho^{-1}) ; \tag{3.6.3}$$

$$p^*_{ij}(S, Q) = O(\rho^{-2})$$

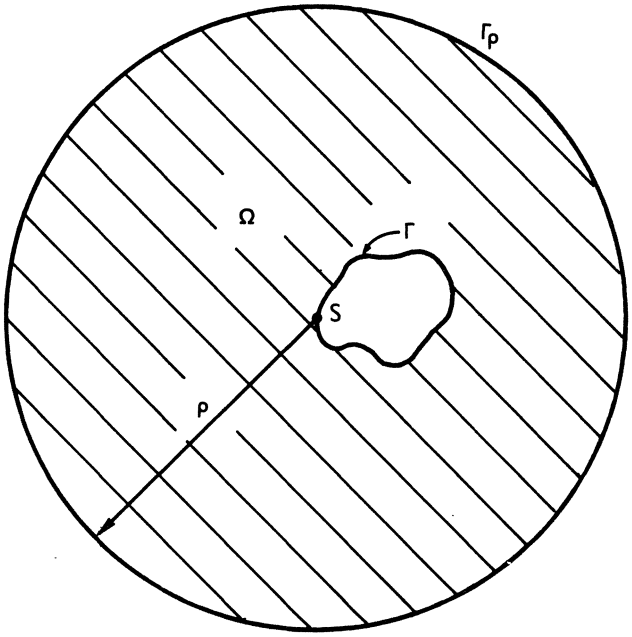

Fig. 3.6.1 Infinite region with cavity.

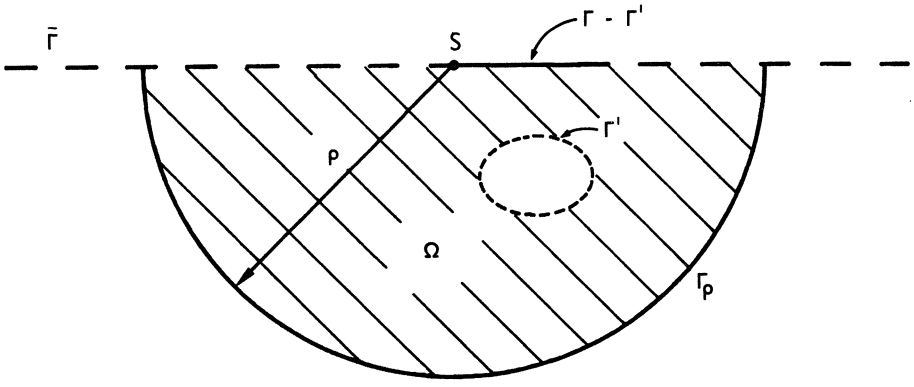

Fig. 3.6.2 Semi-infinite region with or without cavities.

where $O(\ )$ represents the asymptotic behaviour as $\rho \to \infty$.

Therefore, if at most $u_j(Q)$ and $p_j(Q)$ have the behaviour ρ^{-1} and ρ^{-2} at infinity, the regularity conditions (3.6.2) are satisfied. Notice that if the total load applied over the boundary of the cavity is not self equilibrated, Saint-Venant's principle [68] gives that $u_j(Q)$ and $p_j(Q)$ will behave like the fundamental solution corresponding to a concentrated force in the direction of the resultant load. Thus, $u_j(Q) = O(\rho^{-1})$ and $p_j(Q) = O(\rho^{-2})$ are obtained and they ensure that each term of (3.6.2) vanishes separately from the other.

For 2-D problems, the equivalent of (3.6.3) is given by

$$d\Gamma(Q) = |J|\, d\phi \quad \text{with} \quad |J| = O(\rho);$$

$$u^*_{ij}(S, Q) = \begin{cases} O(\ln(\rho) + 1), & i = j; \\ O(1), & i \neq j; \end{cases} \tag{3.6.4}$$

$$p^*_{ij}(S, Q) = O(\rho^{-1}) \ .$$

From the above it is seen that in order to guarantee that each term of (3.6.2) vanishes separately, one needs $u_j(Q) = O(\rho^{-1})$ and $p_j(Q) = O(\rho^{-2})$ as before [3]. This case however, does not correspond to the behaviour of the fundamental solution at infinity. Based on the same argument as for 3-D, one can substitute $u_j(Q)$ and $p_j(Q)$ by the tensors corresponding to the 2-D fundamental solution and indeed verify that equation (3.6.2) is satisfied. The only difference now is that the two terms do not approach zero separately, but they cancel each other as $\rho \to \infty$.

The above discussion strongly suggests that the regularity conditions are always satisfied if $u_i(Q)$ and $p_i(Q)$ behave at most like the corresponding fundamental solution at infinity. This statement is also verified for semi-infinite problems where the half-space and half-plane fundamental solutions dictate the corresponding conditions. In these applications, the interesting case in which part of the boundary $\bar{\Gamma}$ is loaded - e.g. figure 3.6.2 - can also be included.

In conclusion, provided the regularity conditions are satisfied, problems of cavities in the external region can be represented by (see figure 3.6.1).

$$C_{ij}(S)\, u_j(S) + \int_{\Gamma} p^*_{ij}(S, Q)\, u_j(Q)\, d\Gamma(Q) = \int_{\Gamma} u^*_{ij}(S, Q)\, p_j(Q)\, d\Gamma(Q) \qquad (3.6.5)$$

for infinite regions (Kelvin), and also

$$C_{ij}(S)\, u_j(S) + \int_{\Gamma'} p^*_{ij}(S, Q)\, u_j(Q)\, d\Gamma(Q) = \int_{\Gamma} u^*_{ij}(S, Q)\, p_j(Q)\, d\Gamma(Q) \qquad (3.6.6)$$

for semi-infinite regions which may have a loaded boundary $\Gamma - \Gamma'$ (see figure 3.6.2).

The conclusions reached in this section are obviously valid for Somigliana's identity and also guarantee stronger regularity in the expressions for stresses at internal points. Note that for an external cavity problem the integral equations are of the same form as for the internal region counterpart, the difference being given by

the normal n which is taken as pointing into the cavity.

3.7 Numerical Implementation

In this section a general numerical procedure for the solution of boundary value problems in solid mechanics will be described. In order to concentrate the attention to the main aspects of the process, the different forms of boundary integral equation introduced in the previous sections will be represented in a unified manner as follows (body forces are omitted for simplicity)

$$C_{ij}(S)\, u_j(S) + \int_\Gamma p^*_{ij}(S, Q)\, u_j(Q)\, d\Gamma(Q) = \int_\Gamma u^*_{ij}(S, Q)\, p_j(Q)\, d\Gamma(Q) \qquad (3.7.1)$$

where depending on the fundamental solution employed (infinite or semi-infinite space) the appropriate expression for $C_{ij}(S)$ and the substitution of Γ by Γ' in the first integral are implied.

Instead of attempting closed form solutions to equation (3.7.1), which is a difficult task and only attainable for simple geometries and boundary conditions, a suitable numerical approach is here employed. The basic steps involved in this approach constitute the numerical essence of the boundary element technique (see [1 - 4]), they are summarized below :

(a) The boundary Γ is discretized into a series of elements over which displacements and tractions are chosen to be piecewise interpolated between the element nodal points;

(b) Equation (3.7.1) is applied in discretized form to each nodal point S of the boundary Γ and the integrals are computed (usually by a numerical quadrature scheme)

over each boundary element. A system of N linear algebraic equations involving the set of N nodal tractions and N nodal displacements is therefore obtained;

(c) Boundary conditions are imposed and consequently N nodal values (traction or displacement in each direction per node) are prescribed. The system of N equations can therefore be solved by standard methods to obtain the remaining boundary data.

Values of displacements and stresses at any selected internal point s can readily be computed by numerical quadrature using the appropriate equations (i.e. eqns. (3.2.7) and (3.4.1) or eqns. (3.5.6) and (3.5.8)) also in discretized fashion. Note that non-zero body forces can be included by a simple numerical integration scheme, which leads to an additional contribution to the independent term of the system of equations, and a similar contribution to the internal displacements and stresses.

In what follows each of the above steps will be more closely examined for the two dimensional case, but the generalization to three dimensional problems is straightforward.

For the discretization of equation (3.7.1), the boundary Γ is approximated by using a series of elements. The Cartesian coordinates $\underset{\sim}{x}^{(j)}$ of points located within each element Γ_j are expressed in terms of interpolation functions $\underset{\sim}{M}$ and the nodal coordinates $\underset{\sim}{x}^{(m)}$ of the element by the following matrix relation

$$\underset{\sim}{x}^{(j)} = \underset{\sim}{M}\, \underset{\sim}{x}^{(m)} \tag{3.7.2}$$

In a similar way, boundary displacements and tractions are approximated over each element through interpolation functions $\underset{\sim}{N}$

$$\underset{\sim}{u}^{(j)} = \underset{\sim}{N}\, \underset{\sim}{u}^{(n)}$$
$$\underset{\sim}{p}^{(j)} = \underset{\sim}{N}\, \underset{\sim}{p}^{(n)} \tag{3.7.3}$$

where $\underset{\sim}{u}^{(n)}$ and $\underset{\sim}{p}^{(n)}$ contain the nodal displacements and tractions respectively. Note that the superscript m in equation (3.7.2) refers to the number of boundary points required to define the geometry of each boundary element whereas the superscript n in (3.7.3) refers to the number of boundary nodes to which the nodal values of displacements and tractions are associated. These numbers may be different in general.

Assuming that the boundary Γ is discretized into L elements Γ_j, the substitution of (3.7.3) into eqn. (3.7.1) leads to

$$\underset{\sim}{C}(S_i)\, \underset{\sim}{u}(S_i) + \sum_{j=1}^{L} \left(\int_{\Gamma_j} \underset{\sim}{p}^{*}\, \underset{\sim}{N}\, d\Gamma \right) \underset{\sim}{u}^{(n)} = \sum_{j=1}^{L} \left(\int_{\Gamma_j} \underset{\sim}{u}^{*}\, \underset{\sim}{N}\, d\Gamma \right) \underset{\sim}{p}^{(n)} \tag{3.7.4}$$

for a boundary node S_i.

Since the two dimensional interpolation functions $\underset{\sim}{N}$ are usually expressed in terms of the homogeneous coordinate η, it is necessary to transform the element of surface $d\Gamma$ from the global Cartesian system (see eqn. 3.7.2) to this intrinsic system of coordinates

$$d\Gamma = |J|\, d\eta \tag{3.7.5}$$

where the Jacobian of the transformation is given by

$$|J| = \sqrt{\left(\frac{dx_1}{d\eta} \right)^2 + \left(\frac{dx_2}{d\eta} \right)^2} \,. \tag{3.7.6}$$

In simple cases, the integrals presented in equation (3.7.4) can be computed analytically. In general, however,numerical integration schemes often lead to a more efficient procedure and can be applied to higher order interpolation functions without any difficulty. The special case when a singular node S_i lies on the element Γ_j requires some additional care and this will be dealt with later on. For the normal cases when $S_i \notin \Gamma_j$, the integrals in (3.7.4) can readily be replaced by summations of the form

$$\begin{aligned} \int_{\Gamma_j} \underset{\sim}{p}^* \underset{\sim}{N}\, d\Gamma &= \int_{-1}^{1} \underset{\sim}{p}^* \underset{\sim}{N}\, |J|\, d\eta = \sum_{k=1}^{K} |J|_k\, W_k\, (\underset{\sim}{p}^* \underset{\sim}{N})_k \\ \int_{\Gamma_j} \underset{\sim}{u}^* \underset{\sim}{N}\, d\Gamma &= \int_{-1}^{1} \underset{\sim}{u}^* \underset{\sim}{N}\, |J|\, d\eta = \sum_{k=1}^{K} |J|_k\, W_k\, (\underset{\sim}{u}^* \underset{\sim}{N})_k \end{aligned} \qquad (3.7.7)$$

where K is the number of Gaussian type integration points and W_k is the weighting factor associated with them.

From the application of equation (3.7.4) to all NN boundary nodes, a final system of $2NN$ equations arises

$$(\underset{\sim}{C} + \hat{\underset{\sim}{H}})\, \underset{\sim}{u} = \underset{\sim}{G}\, \underset{\sim}{p} \qquad (3.7.8)$$

where vectors $\underset{\sim}{u}$ and $\underset{\sim}{p}$ contain all displacements and tractions at the boundary nodes and the quasi-diagonal matrix $\underset{\sim}{C}$ can be incorporated into $\hat{\underset{\sim}{H}}$ to form a matrix $\underset{\sim}{H}$. Thus,

$$\underset{\sim}{H}\, \underset{\sim}{u} = \underset{\sim}{G}\, \underset{\sim}{p} \; . \qquad (3.7.9)$$

It should be noticed that for the total computation of matrix $\underset{\sim}{H}$, the leading diagonal submatrices which correspond to the free term C_{ij} plus the principal value integral (see eqns. (3.5.5) and (3.5.7)) can be calculated by imposing to eqn. (3.7.9) the condition

that rigid body translations result in zero tractions. Therefore, considering finite regions, two independent translations [22] such as $u_i = \delta_{i1}$ and $u_i = \delta_{i2}$ can be applied, resulting in the following relation

$$\underset{\sim}{H}_{pq}\ \underset{\sim}{u}_{q} = \underset{\sim}{0} \qquad (p, q = 1, 2, \ldots\ldots, NN) \tag{3.7.10}$$

in which $\underset{\sim}{H}_{pq}$ represents the 2×2 submatrices of $\underset{\sim}{H}$ and $\underset{\sim}{u}_{q}$ is readily substituted by

$$\underset{\sim}{u}_{q} = \underset{\sim}{I} \qquad (q = 1, 2, \ldots., NN) \tag{3.7.11}$$

where $\underset{\sim}{I}$ is the identity matrix of order 2.

Equation (3.7.10) allows for the computation of the leading diagonal submatrices of $\underset{\sim}{H}$ in the form (summation not implied)

$$\underset{\sim}{H}_{\alpha\alpha} = - \sum_{\substack{q=1 \\ q \neq \alpha}}^{NN} \underset{\sim}{H}_{\alpha q} \ . \qquad (\alpha = 1, 2, \ldots\ldots, NN) \tag{3.7.12}$$

Expression (3.7.12) is valid for finite bodies, for infinite or semi-infinite regions, however, a further term must be added. With reference to Section 3.6, one can readily verify that since $\underset{\sim}{u}_{q} = O(1)$, the regularity conditions at infinity are no longer satisfied. Consequently, the following expression has to be considered in such cases

$$C_{ij}(S)\, u_j + u_j \int_{\Gamma} p^*_{ij}(S, Q)\, d\Gamma(Q) + \lim_{\rho \to \infty} u_j \int_{\Gamma_\rho} p^*_{ij}(S, Q)\, d\Gamma(Q) = 0 \tag{3.7.13}$$

where u_j corresponds to any rigid body translation and $S \in \Gamma$.

As discussed before (see Section 3.2), since the tensor $p^*_{ij}(S, Q)$ corresponds to a positive unit point load applied in i direction, the condition of equilibrium within the region $\Omega^* + \Gamma^*$ leads to

$$\lim_{\rho\to\infty} \int_{\Gamma_\rho} p^*_{ij}(S, Q)\, d\Gamma(Q) = -\delta_{ij} \qquad (3.7.14)$$

in which Γ_ρ is the boundary of a circular region for the infinite space (2-D Kelvin fundamental solution) or a semi-circular region for the semi-infinite space (half-plane fundamental solution).

Substituting expression (3.7.14) into (3.7.13) for the rigid body translations employed in equation (3.7.10), and discretizing gives (summation not implied)

$$\underset{\sim}{H}_{\alpha\alpha} = \underset{\sim}{I} - \sum_{\substack{q=1 \\ q\neq\alpha}}^{NN} \underset{\sim}{H}_{\alpha q} \quad . \qquad (\alpha = 1, 2, \ldots\ldots NN) \qquad (3.7.15)$$

Expressions (3.7.12) and (3.7.15) provide useful means of computing the leading diagonal submatrices of $\underset{\sim}{H}$, avoiding analytical evaluation of the coefficients C_{ij} and the principal value integrals.

By applying the $2NN$ specified boundary conditions, equation (3.7.9) can be reordered and the final system of equations arises

$$\underset{\sim}{A}\ \underset{\sim}{y} = \underset{\sim}{f} \qquad (3.7.16)$$

where $\underset{\sim}{A}$ is a fully populated matrix of order $2NN$, vector $\underset{\sim}{y}$ is formed by the unknown displacements and tractions and the contribution of the prescribed values is included into vector $\underset{\sim}{f}$.

It should be pointed out that for computational purposes, the assemble of matrix $\underset{\sim}{A}$ is performed directly from the element integrals, without actually forming matrices $\underset{\sim}{H}$ and $\underset{\sim}{G}$. In addition, symmetric bodies under symmetric loads can be considered without discretization of the symmetry axes [7]. This is accomplished by an automatic condensation process which integrates over reflected elements and performs the final assemble of matrix $\underset{\sim}{A}$ already in reduced size.

Once that nodal values of boundary displacements and tractions are known, internal displacements and stresses can be computed by the corresponding equations also in discretized form. Here, since there are no singular integrals to be computed, simple standard numerical quadrature schemes can be used throughout.

It is interesting to note that the use of a half-plane fundamental solution renders the discretization of the traction-free part of the boundary $x_1 = 0$ unnecessary; the displacements and stresses along this part of the surface being computed as internal points. This feature, apart from generating a smaller system of equations, avoids any numerical approximation over the free-surface. Therefore, semi-infinite or finite sized problems can be handled with equal ease.

Among the different types of elements that can be employed in the numerical discretization of the integral equations [2, 24], the linear element has been found to give acceptable accuracy without requiring much computer effort for the solution of the examples presented here. Henceforth, the numerical implementation of this element will be discussed in more detail. The geometry of the element is represented by a straight line and with reference to figure 3.7.1,

$|J| = \ell/2$. Also, the relevant matrices of equations (3.7.2) and (3.7.3) are given by

$$\underset{\sim}{M} = \underset{\sim}{N} = \left[\underset{\sim}{I}\, N_1 \quad \underset{\sim}{I}\, N_2\right] \tag{3.7.17}$$

where $N_1 = \frac{1}{2}(1-\eta)$, $N_2 = \frac{1}{2}(1+\eta)$ and the corresponding vectors $\underset{\sim}{x}^{(m)}$ $\underset{\sim}{u}^{(n)}$ and $\underset{\sim}{p}^{(n)}$ are formed by subvectors $\left[{}^{i}(\ )_1 \ {}^{i}(\ )_2\right]^T$ for each node i = 1, 2 located at the extremities of the element (see figure 3.7.1).

From the above it is seen that the integrals presented in equation (3.7.4) give rise to two element matrices $\underset{\sim}{h}$ and $\underset{\sim}{g}$ (corresponding to $\underset{\sim}{H}$ and $\underset{\sim}{G}$ respectively) of order 2×4 in the following form

$$\begin{aligned} \underset{\sim}{h} &= \frac{\ell}{2}\int_{-1}^{1} \left[\underset{\sim}{p}^{*} N_1 \quad \underset{\sim}{p}^{*} N_2\right] d\eta \\ \underset{\sim}{g} &= \frac{\ell}{2}\int_{-1}^{1} \left[\underset{\sim}{u}^{*} N_1 \quad \underset{\sim}{u}^{*} N_2\right] d\eta \end{aligned} \tag{3.7.18}$$

which allows for numerical integration as shown in (3.7.7).

For the special case of the singular node being coincident with one of the end nodes of the element, the coefficients of matrix $\underset{\sim}{g}$ can be computed analytically to avoid more sophisticated numerical integration schemes. Considering the Kelvin fundamental solution, the following expression is obtained

$$g_{ij}^{kn} = c_2 \left\{ c_1 \ell\left[\delta_{kn} + \frac{1}{2} - \ln(\ell)\right]\delta_{ij} + \frac{\ell_i \ell_j}{\ell} \right\} \tag{3.7.19}$$

$$(i, j, k, n = 1, 2)$$

where the subscripts i and j indicate the position of the coefficient in the 2×2 submatrix k of $\underset{\sim}{g}$ and n indicates the singular node. Also,

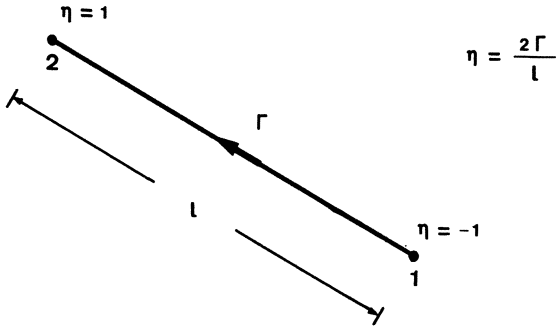

Fig. 3.7.1 Linear element and definition of intrinsic coordinate η .

$$c_1 = 3 - 4\nu$$
$$c_2 = 1/[16\pi\ (1-\nu)G] \qquad (3.7.20)$$
$$\ell_i = {}^2x_i - {}^1x_i \ .$$

Since the complementary tensors of the half-plane fundamental solution are non-singular when $c \neq 0$, expression (3.7.19) can be used for the singular part of the integrals, while the remaining part is integrated numerically. For the case when $c = 0$, both parts added up (see (3.3.22)) for integration and the resulting expression is given by

$$g_{ij}^{kn} = \bar{c}_2 \left\{ \bar{c}_1 \ell [\delta_{kn} + \frac{1}{2} - \ln(\ell)]\delta_{ij} + \frac{\ell_i \ell_j}{\ell} + \alpha(1-\delta_{ij})\ell\ \theta\ \bar{c}_3 \right\} \qquad (3.7.21)$$

where

$$\bar{c}_1 = 2(1-\nu)$$

$$\bar{c}_2 = 1/(4\pi G)$$

$$\bar{c}_3 = 1 - 2\nu \qquad (3.7.22)$$

$$\theta = \arctan(\ell_2/\ell_1) \qquad (-\pi/2 \leq \theta \leq \pi/2)$$

$$\alpha = \begin{cases} -1 & \text{for } j = 1 \\ 1 & \text{for } j = 2 \end{cases}$$

For the computation of displacements at internal points, each element contributes with two matrices $\underset{\sim}{h}$ and $\underset{\sim}{g}$ of the form presented in (3.7.18). The same pattern is valid for internal stresses, where the corresponding element matrices $\underset{\sim}{h}'$ and $\underset{\sim}{g}'$ are now 3×4 . In this case, the 2×2 matrices $\underset{\sim}{p}^*$ and $\underset{\sim}{u}^*$ are substituted by their counterparts $'\underset{\sim}{p}^*$ and $'\underset{\sim}{u}^*$ which are of order 3×2 . Note that only the three different components of stress are computed and the sequence chosen here is σ_{11}, σ_{12} and σ_{22} .

With reference to the numerical integrals, four Gauss points have been found to produce acceptable precision in many cases. This number, however, can be increased to six if the element is located very near to the singular node or internal point.

In order to simulate properly traction discontinuities over the boundary, the concept of double nodes has been adopted here. This consists of having two boundary nodes with exactly the same coordinates without any boundary element in between. Such procedure has been thoroughly discussed in a previous paper by the present author and colleagues [86], and the reader is referred to it for further explanations. The only limitation of this concept is when both nodes have a displacement component in the same direction prescribed as a boundary condition.

This generates a singular matrix $\underset{\sim}{A}$ (such possibility would violate the displacement continuity condition). Nevertheless, all the other combinations are possible.

An alternative procedure capable of handling the special case mentioned above has been proposed by Chaudonneret [87].

Finally, it should be noted that stresses at boundary nodes can easily be computed by using the values of the interpolated displacements and tractions over the boundary elements. Such procedure does not require any integration and is presented in Appendix B for the inelastic case. The expressions are valid for elastic problems if one makes $\dot{\varepsilon}^{a}_{ij} = 0$ and substitutes the rates by the corresponding accumulated values of the variables.

3.8 Examples - Half-Plane Formulation

Applications of the Kelvin formulation described here have been reported by the present author and co-workers in references [86, 88]. In these papers, boundary element solutions for a series of examples are discussed and compared with analytical and finite element results. Among the applications, the practical problem of the stress analysis of a dam is presented and discussed in conjunction with finite element results for the same problem. Not only here, but in all the examples the boundary element technique was found to produce accurate and efficient solutions.

Herein, in order to save space, we shall restrict ourselves to the original aspects of the present work. Therefore, to outline the applicability of the elastic formulation, some examples solved by the half-plane implementation are compared with analytical results in what follows.

Example 3.8.1- The first example consists of a linear traction distribution over a finite part of the boundary of a semi-infinite medium (figure 3.8.1). The problem was solved by discretizing the loaded part of the surface using two boundary elements only and results were computed at five internal points.

Analytical results to this problem were presented in [82] and are here compared in tables 3.8.1 and 3.8.2. Due to the well known non-uniqueness of displacements in two dimensional analysis,the vertical displacements are given with reference to the corresponding displacement of node 2.

Node	$u-^{2}u$	v	
1	-4.476	-10.400	B.E.M.
2	0.	5.200	
3	-27.649	10.400	
1	-4.476	-10.400	EXACT
2	0.	5.200	
3	-27.649	10.400	
	m × 10^2		

Table 3.8.1 Linear traction distribution problem. Displacements at boundary nodes.

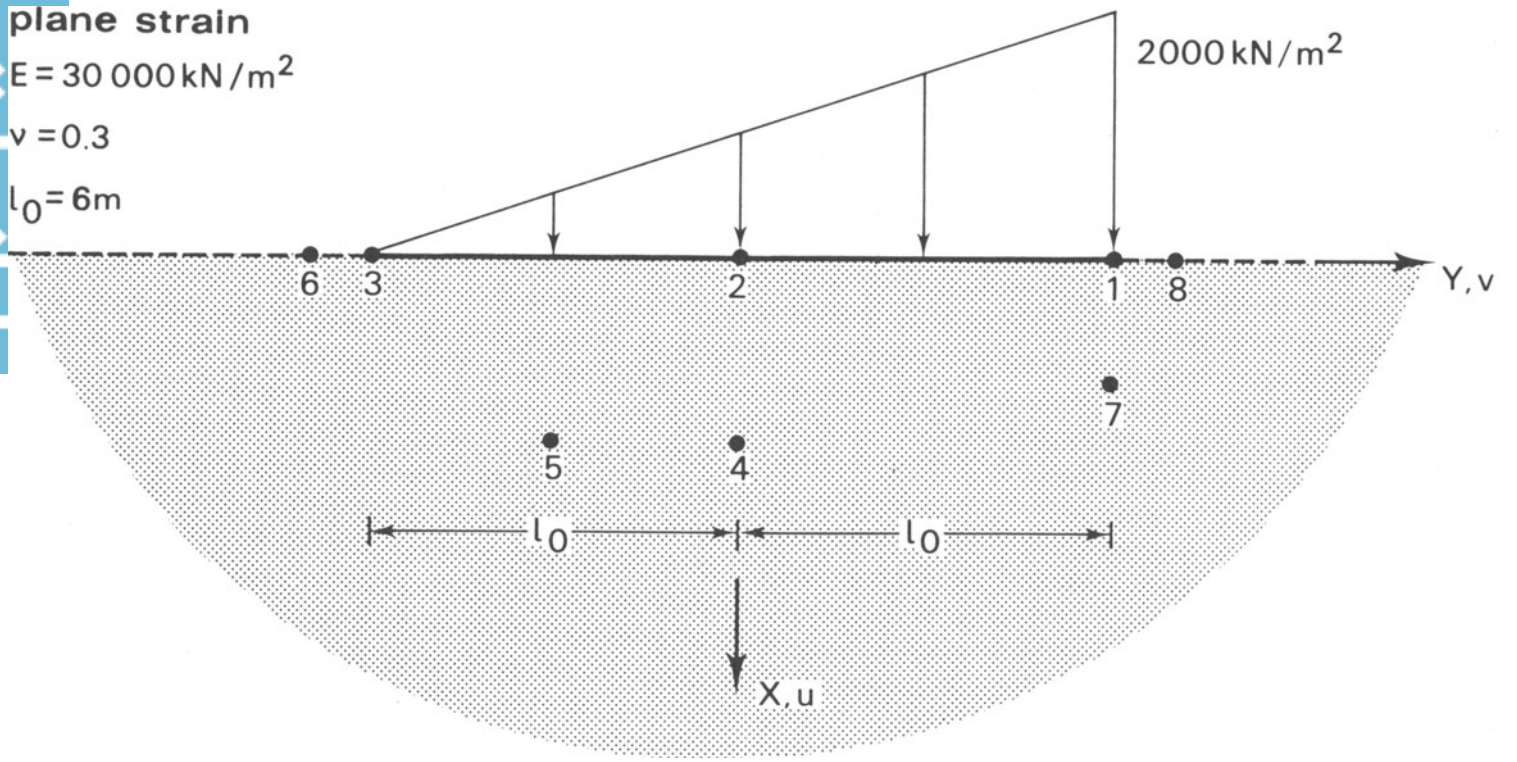

Fig. 3.8.1 Linear traction distribution problem. Boundary element discretization and internal points.

Point	$u-^2u$	v	σ_x	σ_y	σ_{xy}	
4	-6.251	-0.768	-959.48	-450.18	225.09	B.E.M.
5	-16.429	0.217	-514.78	-388.96	260.13	
6	-31.022	10.400	0.	0.	0.	
7	-8.394	-0.430	-894.86	-511.73	-487.48	
8	-14.719	-10.400	0.	0.	0.	
4	-6.251	-0.768	-959.48	-450.18	225.09	EXACT
5	-16.429	0.217	-514.78	-388.96	260.13	
6	-31.022	10.400	0.	0.	0.	
7	-8.394	-0.430	-894.86	-511.73	-487.48	
8	-14.719	-10.400	0.	0.	0.	
	$m \times 10^2$		kN/m^2			

Table 3.8.2 Linear traction distribution problem. Results at internal points.

Note that the exact agreement of the results is to be expected. Although linear interpolation functions are not exact for the boundary displacements, their contribution is removed from the analysis by the very nature of the fundamental solution.

Example 3.8.2 - The next classical example is a rigid flat punch indented into the half-plane. The punch is considered to be perfectly smooth and indentation was carried out by prescribing the flat punch displacements. Boundary element analysis was performed by discretizing half of the contact surface into twelve unequally sized boundary elements. The thirteen boundary nodes were located along the discretized boundary according to the formula,

$$y = \frac{6.5(1-\alpha)}{\alpha}$$

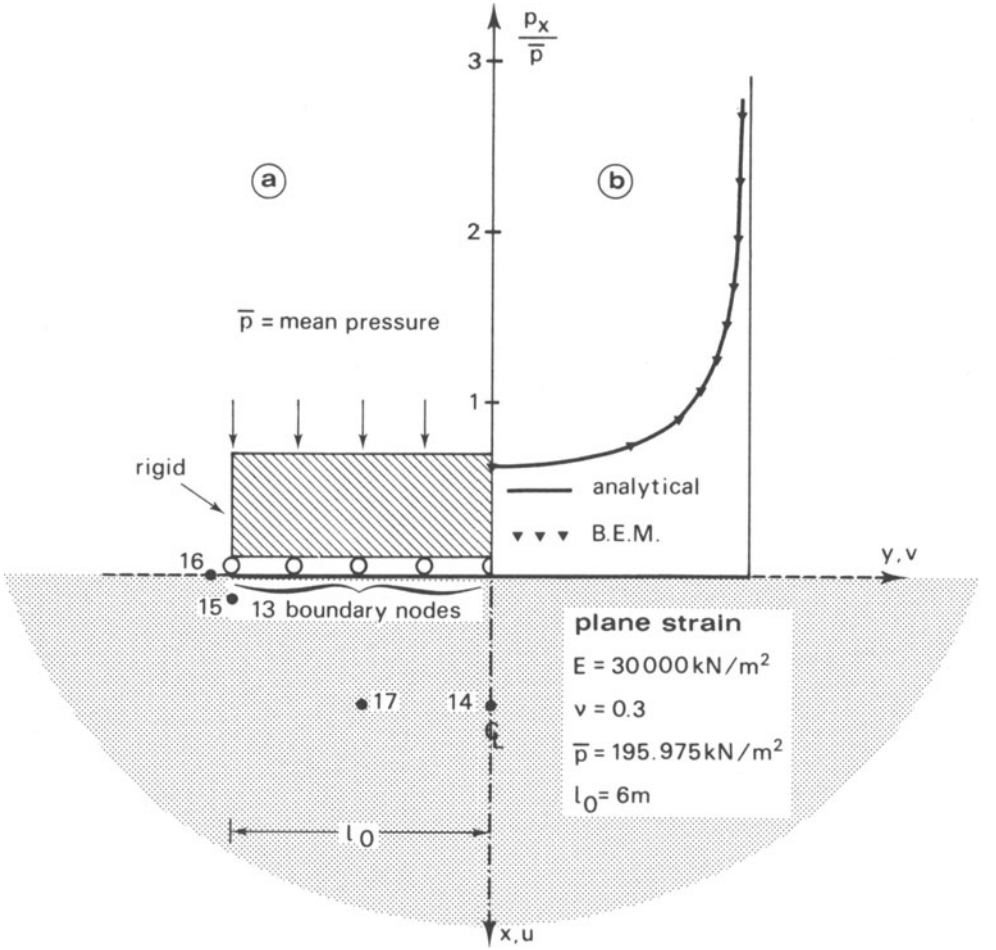

Fig. 3.8.2 Smooth punch problem. (a) problem geometry.
(b) contact stresses along the discretized boundary.

where α is the node number.

Additional results were obtained at four internal points (see figure 3.8.2a). Note that as discussed in Section 3.7, symmetry was considered by a direct condensation process which automatically integrates over reflected elements not requiring any boundary discretization of the symmetry axis.

Contact stresses along the discretized boundary are compared with analytical results [82] in figure 3.8.2b. Apart from some traction perturbation over the tiny element connected to node thirteen, the singularity at the edge of the punch does not seem to have disturbed the results. This is also confirmed by the accuracy of the computations at internal points presented in Table 3.8.3.

Point	$u-{}^1u$	v	σ_x	σ_y	σ_{xy}	
14	-0.724	0.	-133.92	-89.28	0.	B.E.M.
15	-0.826	-1.210	-330.64	-113.16	107.93	
16	-1.824	-2.038	0.	0.	0.	
17	-0.908	-0.234	-151.87	-77.69	-3.14	
14	-0.735	0.	-133.91	-89.27	0.	EXACT
15	-0.842	-1.208	-326.47	-114.43	110.50	
16	-1.841	-2.038	0.	0.	0.	
17	-0.917	-0.234	-152.00	-77.67	-3.35	
	$m \times 10^2$		kN/m^2			

Table 3.8.3 Smooth punch problem. Results at internal points.

Example 3.8.3 - In the third application of the formulation a semi-infinite plate with a circular hole near the straight boundary is studied. The problem is here considered under two different loading cases, unit normal pressure applied over the surface of the hole and simple tension $\bar{\sigma}_y$ parallel to the straight edge. In both cases, the stress σ_y along the traction-free straight boundary is compared with analytical results presented by Jeffery [89] and Mindlin [90] respectively.

The relatively small distance between the centre of the hole and the straight surface is 1.34 times the radius of the circle. For the boundary element analysis only the surface of the hole needs discretization and due to symmetry only half of this surface was considered.

Results for the first loading case (see figure 3.8.3) were computed at a series of points (considered as internal points) located along the straight boundary and 24 boundary elements of equal size were used to represent half the circle with the same area.

The second loading case was analysed by simple superposition; tractions p_y equal to the scalar product of the simple tension and the unit normal to the surface of the hole were applied to the circular boundary and the corresponding results superimposed onto the constant stress field $\bar{\sigma}_y$.

To illustrate the convergence of the method the results for 6, 12 and 24 boundary element discretizations of the half circle are compared with analytical results in figure 3.8.4.

It is worth mentioning that if the distance between the hole

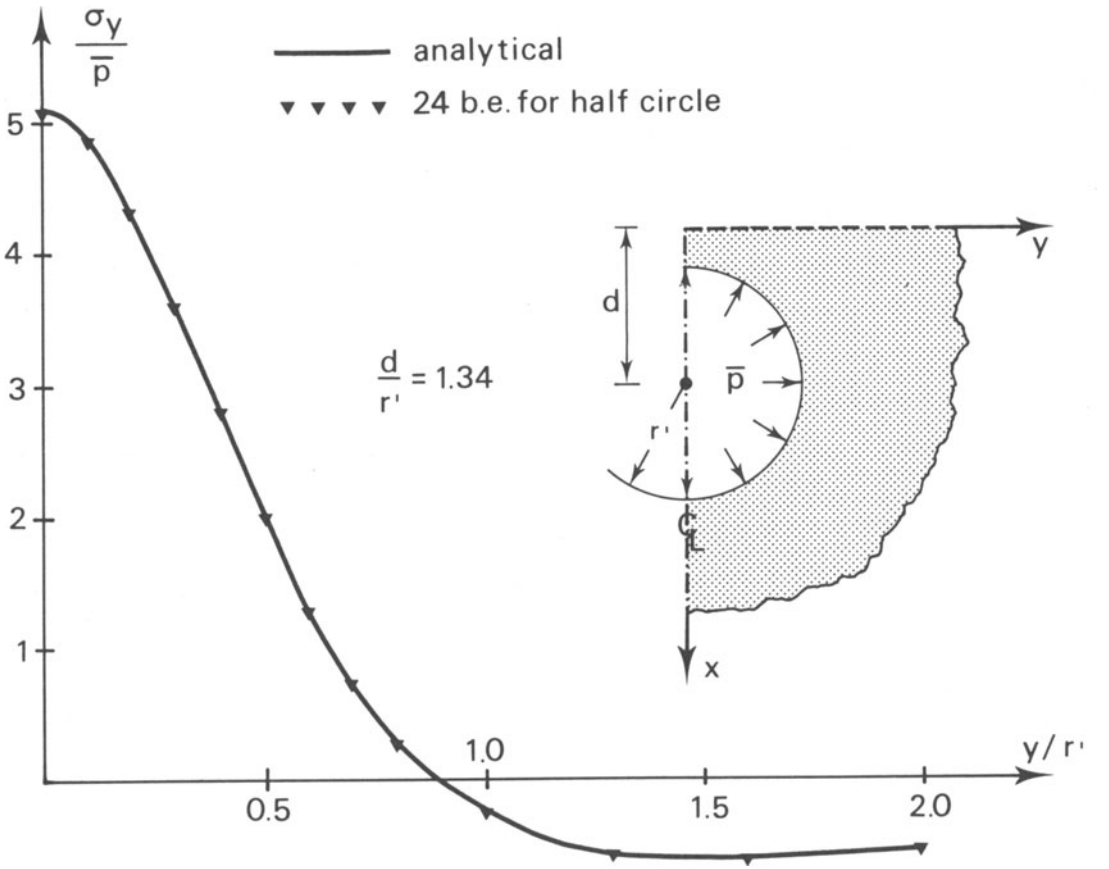

Fig. 3.8.3 Circular hole near straight boundary under uniform pressure. Stress σ_y along the traction-free straight boundary.

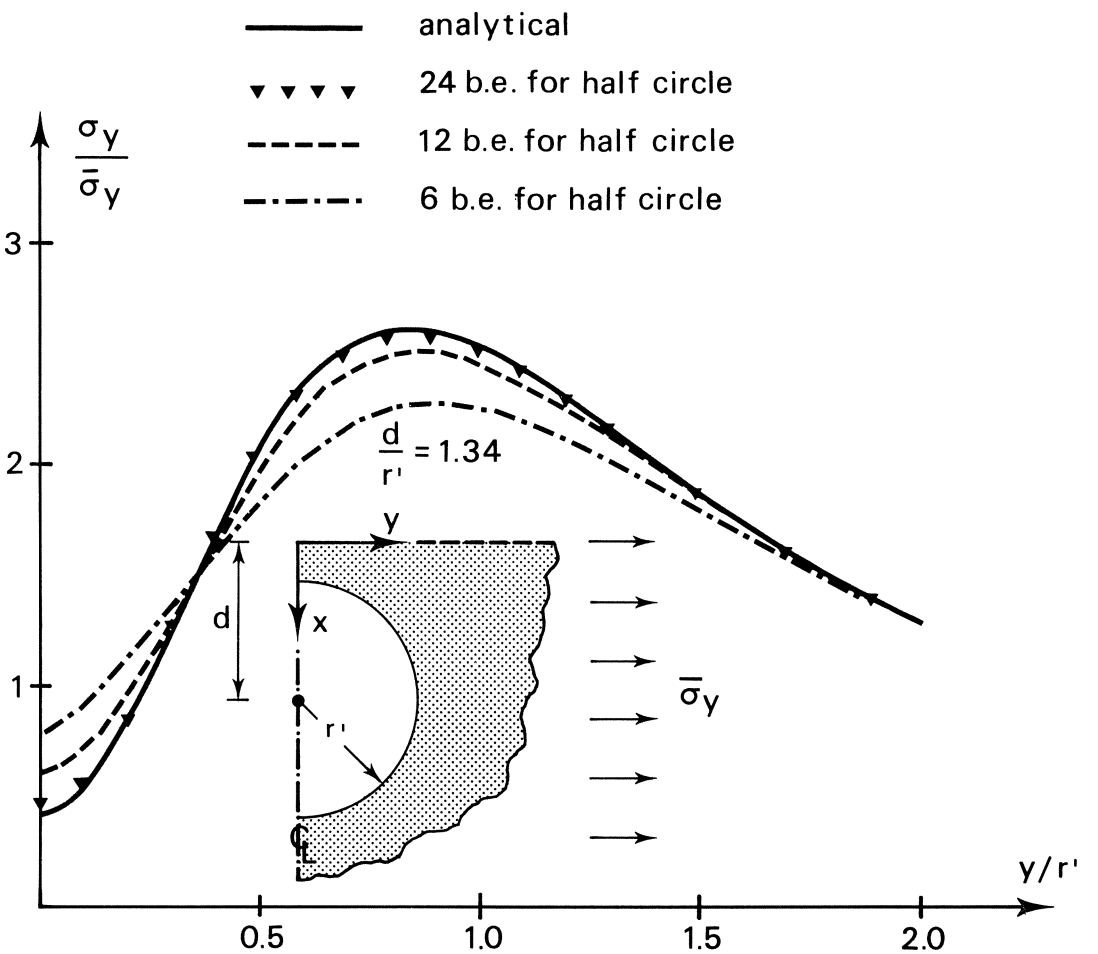

Fig. 3.8.4 Circular hole near the straight boundary under remote tension. Stress σ_y along the traction-free straight boundary.

and the straight edge were larger, fewer boundary elements would be required for the same accuracy of results. With reference to the first loading case, for $d/r' = 1.81$, 12 boundary elements produced an error at the peak stress of about - 2.7%, whereas for $d/r' = 1.34$ this error was - 6.5%.

The examples shown here illustrate some of the possible applications of the half-plane formulation. It is evident that such problems are more efficiently solved by this procedure than using the Kelvin fundamental solution which requires defining a series of elements on the traction-free surface. The number of these elements, in principle, needs to extend to infinity or at least should be large enough to produce accurate solutions. Special elements extending to infinity have been proposed [91] to reduce such large discretization of the free-surface, but they require further tests to validate their application. The most accurate and computationally more efficient technique is to use the half-plane fundamental solution which eliminates the need for any numerical approximation over the free-surface.

CHAPTER 4

BOUNDARY ELEMENT EQUATIONS FOR INELASTIC PROBLEMS

4.1 Introduction

This chapter presents the starting equations for the different inelastic formulations adopted here. An extended form of Somigliana's identity is first presented by following the procedure introduced in Chapter 3. Here, the weighted residual technique is also applied to arrive at an equivalent statement.

By considering first the Kelvin fundamental solution, a proper procedure for obtaining the complete integral expression for stresses at internal points is presented and a discussion about alternative boundary element formulations for 3-D and 2-D problems is included. The half-plane expressions are then introduced and the extension of the equations to handle inelastic problems is accomplished. Finally, the spatial discretization is introduced and the equations are expressed in matrix form.

4.2 Somigliana's Identity for Inelastic Problems

In order to start the present section, expression (3.3.27) of Chapter 3 will be rewritten for 3-D problems as follows [5]

$$\int_{\Omega_\varepsilon} \sigma^*_{ij}(s, q)\, \dot{\varepsilon}^e_{ij}(q)\, d\Omega(q) = \int_{\Omega_\varepsilon} \dot{\sigma}_{ij}(q)\, \varepsilon^*_{ij}(s, q)\, d\Omega(q) \quad (4.2.1)$$

where $\dot{\varepsilon}^e_{ij}(q)$ represents the elastic part of the total strain rate

tensor (see eqn. (2.4.1)). This statement is now in a more general form in which only the appropriate part of the total strain rate tensor is involved. Note that it is obtained by simple symmetry considerations as before (see statement (3.2.1)).

Recalling Chapter 2 expression (2.4.1), one gets

$$\dot{\varepsilon}^{e}_{ij} = \dot{\varepsilon}_{ij} - \dot{\varepsilon}^{a}_{ij} \quad , \tag{4.2.2}$$

which leads to

$$\int_{\Omega_\varepsilon} \sigma^{*}_{ij}(s, q)\, \dot{\varepsilon}_{ij}(q)\, d\Omega(q) = \int_{\Omega_\varepsilon} \dot{\sigma}_{ij}(q)\, \varepsilon^{*}_{ij}(s, q)\, d\Omega(q) + \int_{\Omega_\varepsilon} \sigma^{*}_{ij}(s, q)\, \dot{\varepsilon}^{a}_{ij}(q)\, d\Omega(q) \quad . \tag{4.2.3}$$

The first integral terms in both sides of expression (4.2.3) can now be integrated by parts as in Chapter 3 while the last integral remains unchanged. The following expression then arises

$$\int_{\Gamma+\bar{\Gamma}_\varepsilon} p^{*}_{i}(s, Q)\, \dot{u}_{i}(Q)\, d\Gamma(Q) = \int_{\Gamma+\bar{\Gamma}_\varepsilon} u^{*}_{i}(s, Q)\, \dot{p}_{i}(Q)\, d\Gamma(Q) + \int_{\Omega_\varepsilon} u^{*}_{i}(s, q)\, \dot{b}_{i}(q)\, d\Omega(q) + \int_{\Omega_\varepsilon} \sigma^{*}_{ij}(s, q)\, \dot{\varepsilon}^{a}_{ij}(q)\, d\Omega(q) \quad , \tag{4.2.4}$$

which taking the limit as $\varepsilon \to 0$ (see figure 3.3.4) and assuming each P_j to act separately, gives an extended form of equation (3.2.7)

$$\dot{u}_{i}(s) = \int_{\Gamma} u^{*}_{ij}(s, Q)\, \dot{p}_{j}(Q)\, d\Gamma(Q) - \int_{\Gamma} p^{*}_{ij}(s, Q)\, \dot{u}_{j}(Q)\, d\Gamma(Q) + \int_{\Omega} u^{*}_{ij}(s, q)\, \dot{b}_{j}(q)\, d\Omega(q) + \int_{\Omega} \sigma^{*}_{jki}(s, q)\, \dot{\varepsilon}^{a}_{jk}(q)\, d\Omega(q) \quad . \tag{4.2.5}$$

Equation (4.2.5) is the Somigliana's identity for inelastic problems, it was here obtained by following the same procedure presented in Chapter 3. This equation is valid for 3-D inelastic problems using the fundamental solution due to Kelvin. For half-space type problems (fundamental solution due to Mindlin), the same simplification indicated in the last chapter can be applied leading to the inelastic counterpart of equation (3.5.6). For 2-D problems, however, special attention must be given to the inelastic strain rate integral [9], and this will be thoroughly discussed in other sections of this chapter.

In Chapter 3 Section 3.2 it was mentioned that Somigliana's identity could be obtained by the weighted residual technique. The advantage of using a weighted residual procedure is that one can start from the beginning with the idea of finding a numerical solution to the actual problem [1, 2]. Thus, the technique brings some physical insight into the numerical solution of the differential equations and more importantly, since it is general, a unified procedure capable of relating the boundary element method to other numerical methods (such as finite elements and finite differences) is obtained.

The basic steps for this procedure will be outlined in what follows, for further details the reader is referred to [1, 2] where a complete discussion about the technique is presented.

We seek an approximate solution to the equilibrium equation presented in Chapter 2 (eqn. (2.4.3))

$$\dot{\sigma}_{ij,i} + \dot{b}_j = 0 \tag{4.2.6}$$

with boundary conditions

$$\dot{u}_i = \dot{\bar{u}}_i \quad \text{on} \quad \Gamma'_1 \tag{4.2.7}$$

$$\dot{p}_i = \dot{\bar{p}}_i \quad \text{on} \quad \Gamma'_2$$

where $\Gamma'_1 + \Gamma'_2 = \Gamma$.

For an assumed solution, $\dot{u}_j$, the error introduced can be minimized by writing the following weighted residual statement

$$\int_\Omega (\dot{\sigma}_{jk,j} + \dot{b}_k)u^*_k \, d\Omega = \int_{\Gamma'_2} (\dot{p}_k - \dot{\bar{p}}_k)u^*_k \, d\Gamma + \int_{\Gamma'_1} (\dot{\bar{u}}_k - \dot{u}_k)p^*_k \, d\Gamma \tag{4.2.8}$$

where u^*_k and p^*_k correspond to the displacements and surface tractions of the weighting field. Note that

$$p^*_k = \sigma^*_{jk} \, n_j \tag{4.2.9}$$

with n_j being the direction cosines of the outward normal to the boundary of the body.

If the same material constants (E, G and ν) are valid for the approximating and the weighting fields, the first term in equation (4.2.8) can be integrated by parts to give

$$-\int_\Omega \dot{\sigma}_{jk} \, \varepsilon^*_{jk} \, d\Omega + \int_\Omega \dot{b}_k \, u^*_k \, d\Omega = -\int_{\Gamma'_2} \dot{\bar{p}}_k \, u^*_k \, d\Gamma - \int_{\Gamma'_1} \dot{p}_k \, u^*_k \, d\Gamma + \int_{\Gamma'_1} (\dot{\bar{u}}_k - \dot{u}_k)p^*_k \, d\Gamma \ . \tag{4.2.10}$$

Recalling expression (2.4.6) of Chapter 2, one gets

$$\dot{\sigma}_{ij} = \dot{\sigma}^{e}_{ij} - \dot{\sigma}^{a}_{ij} \tag{4.2.11}$$

where $\dot{\sigma}^{e}_{ij} = C_{ijk\ell}\,\dot{\varepsilon}_{k\ell}$ (see expression (2.2.31)).

Expression (4.2.11) can be substituted into equation (4.2.10) as follows

$$\begin{aligned} -\int_{\Omega} \dot{\sigma}^{e}_{jk}\,\varepsilon^{*}_{jk}\,d\Omega + \int_{\Omega} \dot{\sigma}^{a}_{jk}\,\varepsilon^{*}_{jk}\,d\Omega + \int_{\Omega} \dot{b}_{k}\,u^{*}_{k}\,d\Omega = -\int_{\Gamma'_2} \dot{\bar{p}}_{k}\,u^{*}_{k}\,d\Gamma \\ -\int_{\Gamma'_1} \dot{p}_{k}\,u^{*}_{k}\,d\Gamma + \int_{\Gamma'_1} (\dot{\bar{u}}_{k} - \dot{u}_{k})p^{*}_{k}\,d\Gamma\ , \end{aligned} \tag{4.2.12}$$

and again the first term can be integrated by parts to give

$$\begin{aligned} \int_{\Omega} \sigma^{*}_{jk,j}\,\dot{u}_{k}\,d\Omega + \int_{\Omega} \dot{\sigma}^{a}_{jk}\,\varepsilon^{*}_{jk}\,d\Omega + \int_{\Omega} \dot{b}_{k}\,u^{*}_{k}\,d\Omega = -\int_{\Gamma'_2} \dot{\bar{p}}_{k}\,u^{*}_{k}\,d\Gamma \\ -\int_{\Gamma'_1} \dot{p}_{k}\,u^{*}_{k}\,d\Gamma + \int_{\Gamma'_2} \dot{u}_{k}\,p^{*}_{k}\,d\Gamma + \int_{\Gamma'_1} \dot{\bar{u}}_{k}\,p^{*}_{k}\,d\Gamma\ . \end{aligned} \tag{4.2.13}$$

The above equation can now be written in general form as

$$\begin{aligned} \int_{\Omega} b^{*}_{k}\,\dot{u}_{k}\,d\Omega = \int_{\Gamma} u^{*}_{k}\,\dot{p}_{k}\,d\Gamma - \int_{\Gamma} p^{*}_{k}\,\dot{u}_{k}\,d\Gamma + \int_{\Omega} u^{*}_{k}\,\dot{b}_{k}\,d\Omega \\ + \int_{\Omega} \varepsilon^{*}_{jk}\,\dot{\sigma}^{a}_{jk}\,d\Omega \end{aligned} \tag{4.2.14}$$

where the substitution $\sigma^{*}_{jk,j} = -\,b^{*}_{k}$ was made.

Proceeding as in Section 3.2, one can assume that the weighting field is the solution to the fundamental problem (eqn. (3.2.8))

which allows for b_k^* to be given by expression (3.2.3). Thus, for each unit point load P_i, the following equation is obtained

$$\dot{u}_i(s) = \int_\Gamma u_{ij}^*(s, Q)\, \dot{p}_j(Q)\, d\Gamma(Q) - \int_\Gamma p_{ij}^*(s, Q)\, \dot{u}_j(Q)\, d\Gamma(Q) + \int_\Omega u_{ij}^*(s, q)\, \dot{b}_j(q)\, d\Omega(q) + \int_\Omega \varepsilon_{jki}^*(s, q)\, \dot{\sigma}_{jk}^a(q)\, d\Omega(q) \,. \tag{4.2.15}$$

Equation (4.2.15) is the initial stress counterpart of equation (4.2.5). Consequently, as discussed before, if the half-space fundamental solution is adopted, Γ can be substituted by Γ' in the second boundary integral. An interesting feature of the initial stress form is that, in contrast with the initial strain equation (4.2.5), the reduction to 2-D problems is accomplished by simply keeping the subscripts with a range of two. In both cases, however, the specialization for $s \to S$ $(S \in \Gamma)$ can be performed as in pure elastic analysis. Therefore, the following expression is obtained

$$C_{ij}(S)\, \dot{u}_j(S) + \int_\Gamma p_{ij}^*(S, Q)\, \dot{u}_j(Q)\, d\Gamma(Q) = \int_\Gamma u_{ij}^*(S, Q)\, \dot{p}_j(Q)\, d\Gamma(Q) + \int_\Omega u_{ij}^*(S, q)\, \dot{b}_j(q)\, d\Omega(q) + \int_\Omega \sigma_{jki}^*(S, q)\, \dot{\varepsilon}_{jk}^a(q)\, d\Omega(q) \tag{4.2.16}$$

where the last integral can be substituted by

$$\int_\Omega \varepsilon_{jki}^*(S, q)\, \dot{\sigma}_{jk}^a(q)\, d\Omega(q) \tag{4.2.17}$$

for the initial stress formulation.

It is worth mentioning that the initial stress and initial strain equations are entirely equivalent. This will be proved in Section 4.4 where a complete discussion about the alternative boundary element formulations is presented.

4.3. Internal Stresses

Of fundamental importance for the stepwise solution of nonlinear material problems is the calculation of stresses at internal points. In order to combine both, accuracy and computational efficiency, it has been demonstrated by Telles and Brebbia [56] that the proper integral equation should be used in preference to computing displacements at internal points and differentiating them numerically as it is done in finite differences or finite elements.

The correct integral equations for stresses at internal points have been presented in previous papers by the present author. Since its derivation requires the derivative of the singular integral of the inelastic term and this had often led to incorrect expressions in the past [6, 9, 45, 47, 54], a proper procedure for obtaining these equations is presented in this section. It is the author's belief that this will enlighten the general concept originally due to Mikhlin [33] which has been applied in references [10, 46].

In order to simplify the presentation, only the Kelvin fundamental solution will be considered in conjunction with the initial stress equation. Also, from now on the initial notation will be somewhat simplified allowing equation (4.2.15) to be written as follows

$$\dot{u}_i = \int_\Gamma u^*_{ij}\, \dot{p}_j \, d\Gamma - \int_\Gamma p^*_{ij}\, \dot{u}_j \, d\Gamma + \int_\Omega u^*_{ij}\, \dot{b}_j \, d\Omega + \int_\Omega \varepsilon^*_{jki}\, \dot{\sigma}^a_{jk} \, d\Omega \, . \tag{4.3.1}$$

From the application of Hooke's law to the elastic part of the total strain rate tensor comes the following expression for the stress rates (see eqn. (2.4.6) of Chapter 2)

$$\dot{\sigma}_{ij} = G\left(\frac{\partial \dot{u}_i}{\partial x_j} + \frac{\partial \dot{u}_j}{\partial x_i}\right) + \frac{2G\nu}{1-2\nu}\frac{\partial \dot{u}_k}{\partial x_k}\delta_{ij} - \dot{\sigma}^a_{ij} \quad . \qquad (4.3.2)$$

Stresses at points located within the body can be computed by substituting equation (4.3.1) into equation (4.3.2) on condition that the space derivatives present in (4.3.2) be taken with reference to the coordinates of the load point. As in the elastic case, such differentiation can be applied directly to the fundamental solution tensors for the first three integrals of (4.3.1). However, the last one needs further examination; in a more formal representation, this integral should be written in the following form

$$V_i = \lim_{\varepsilon \to 0} \int_{\Omega_\varepsilon} \varepsilon^*_{jki}\, \dot{\sigma}^a_{jk}\, d\Omega \qquad (4.3.3)$$

where Ω_ε arises from Ω by removing a ball of radius ε centred at the load point s (see Chapter 3 figure 3.3.4).

The proper expression for the derivative of V_i can therefore be written as

$$\frac{\partial V_i}{\partial x_m} = \lim_{\varepsilon \to 0}\left\{\frac{\partial}{\partial x_m}\int_{\Omega_\varepsilon} \varepsilon^*_{jki}\, \dot{\sigma}^a_{jk}\, d\Omega\right\} \qquad (4.3.4)$$

For simplicity and without loss of generality, the two dimensional case will be carried out. In this case ε represents the radius of a circle and one can define a cylindrical coordinate system $(\bar{r}, \bar{\theta})$ based at the point $0 \equiv s$ as shown in figure 4.3.1a. In this system of coordinates the tensor ε^*_{jki} can be represented by

$$\frac{1}{r(\bar{r}, \bar{\theta})}\psi_{jki}(\phi) \qquad (4.3.5)$$

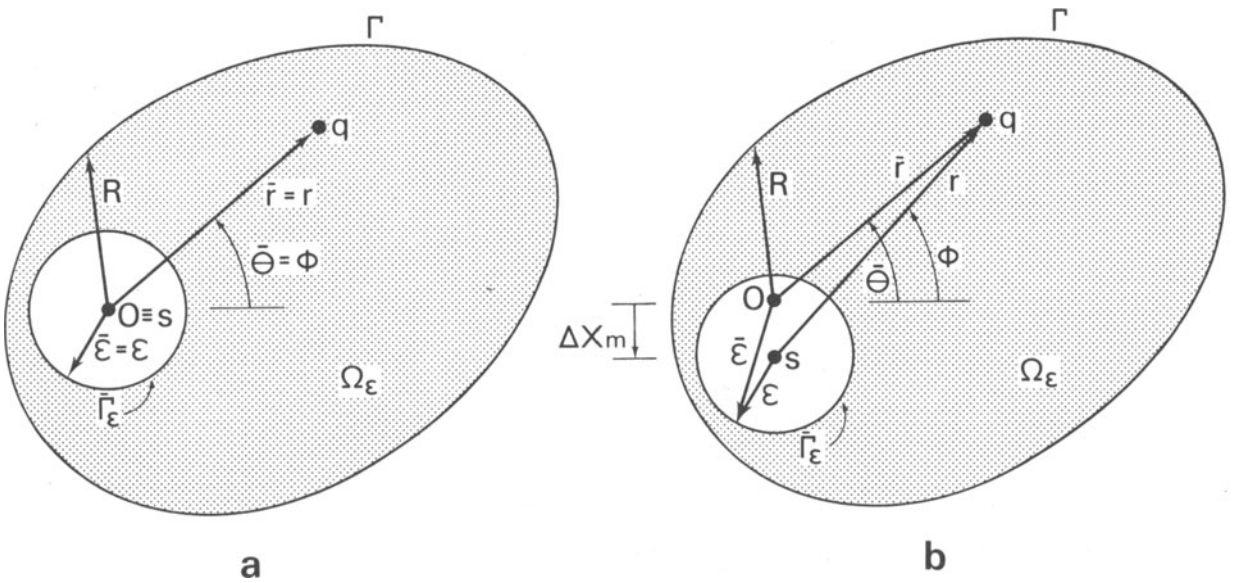

Fig. 4.3.1 Cylindrical coordinate system based at $O \equiv s$ and effect of increment in the rectangular coordinate x_m of s.

where for the case depicted in figure 4.3.1a one has $r(\bar{r}, \bar{\theta}) = \bar{r}$ and $\phi(\bar{r}, \bar{\theta}) = \bar{\theta}$, but if a small increment in the rectangular coordinate x_m of the singular point is given, not only r and ϕ become different from $\bar{r}$ and $\bar{\theta}$ but also $\bar{\Gamma}_\varepsilon$ is shifted (see figure 4.3.1b), indicating their dependence on the coordinates of the load point.

Expression (4.3.4) is now of the form

$$\frac{\partial V_i}{\partial x_m} = \int_0^{2\pi} \lim_{\varepsilon \to 0} \left\{ \frac{\partial}{\partial x_m} \int_{\bar{\varepsilon}}^{R(\bar{\theta})} \frac{\psi_{jki}}{r} \overset{\bullet}{\sigma}{}^a_{jk} \, \bar{r} \, d\bar{r} \right\} d\bar{\theta} \qquad (4.3.6)$$

which allows for the application of Leibnitz formula† to the term between brackets, i.e.

$$\frac{\partial}{\partial x_m} \int_{\bar{\varepsilon}}^{R} \frac{\psi_{jki}}{r} \overset{\bullet}{\sigma}{}^a_{jk} \, \bar{r} \, d\bar{r} = \int_{\bar{\varepsilon}}^{R} \frac{\partial}{\partial x_m} \left(\frac{\psi_{jki}}{r} \right) \overset{\bullet}{\sigma}{}^a_{jk} \, \bar{r} \, d\bar{r} - \frac{\psi_{jki}}{r(\bar{\varepsilon}, \bar{\theta})} \overset{\bullet}{\sigma}{}^a_{jk} \, \bar{\varepsilon} \frac{\partial \bar{\varepsilon}}{\partial x_m} \, . \qquad (4.3.7)$$

Taking into consideration that $0 \equiv s$ and $r(\bar{\varepsilon}, \bar{\theta}) = \varepsilon$, the substitution of expression (4.3.7) in (4.3.6) gives

$$\frac{\partial V_i}{\partial x_m} = \int_0^{2\pi} \lim_{\varepsilon \to 0} \int_{\varepsilon}^{R(\phi)} \frac{\partial}{\partial x_m} \left(\frac{\psi_{jki}}{r} \right) \overset{\bullet}{\sigma}{}^a_{jk} \, r \, dr \, d\phi - \overset{\bullet}{\sigma}{}^a_{jk}(s) \int_0^{2\pi} \psi_{jki} \cos(r, x_m) d\phi \qquad (4.3.8)$$

---

† Leibnitz formula gives that

$$\frac{d}{d\alpha} \int_{\phi_1(\alpha)}^{\phi_2(\alpha)} F(x, \alpha) dx = \int_{\phi_1(\alpha)}^{\phi_2(\alpha)} \frac{\partial F}{\partial \alpha} dx - F(\phi_1, \alpha) \frac{d\phi_1}{d\alpha} + F(\phi_2, \alpha) \frac{d\phi_2}{d\alpha}$$

where $\dot{\sigma}^a_{jk}(s)$ represents the value of the initial stress rate at the singular point.

Finally, one has to study the existence of the first integral in expression (4.3.8) which can be further written as

$$\int_0^{2\pi} \lim_{\varepsilon\to 0} \int_\varepsilon^R \frac{\partial}{\partial x_m}\left(\frac{\psi_{jki}}{r}\right)\dot{\sigma}^a_{jk}\, r\, dr\, d\phi = \int_0^{2\pi} \lim_{\varepsilon\to 0} \left\{ \bar{\psi}_{jkim} \int_\varepsilon^R \left(\dot{\sigma}^a_{jk} - \dot{\sigma}^a_{jk}(s)\right)\frac{1}{r}\, dr \right\} d\phi \tag{4.3.9}$$

$$+ \dot{\sigma}^a_{jk}(s)\int_0^{2\pi} \bar{\psi}_{jkim}\, \ln(R)\, d\phi - \lim_{\varepsilon\to 0} \left\{ \dot{\sigma}^a_{jk}(s)\, \ln(\varepsilon) \int_0^{2\pi} \bar{\psi}_{jkim}\, d\phi \right\}$$

where $\bar{\psi}_{jkim}(\phi) = r^2 \frac{\partial}{\partial x_m}\left(\frac{\psi_{jki}}{r}\right)$, and it is assumed that $\dot{\sigma}^a_{jk}$ satisfies a Hölder condition [31, 28] at s such that

$$\left|\dot{\sigma}^a_{jk}(q) - \dot{\sigma}^a_{jk}(s)\right| \leq A\, r^\alpha \tag{4.3.10}$$

where A and α are positive constants.

Clearly, the first two terms on the right-hand-side of (4.3.9) are convergent and the last one requires that

$$\int_0^{2\pi} \bar{\psi}_{jkim}\, d\phi = 0\,. \tag{4.3.11}$$

A condition which is fulfilled by an intrinsic property of $\bar{\psi}_{jkim}$. Therefore, the proof is complete and one can transform expression (4.3.8) back to the rectangular coordinate system as follows

$$\frac{\partial V_i}{\partial x_m} = \int_\Omega \frac{\partial \varepsilon^*_{jki}}{\partial x_m}\, \dot{\sigma}^a_{jk}\, d\Omega - \dot{\sigma}^a_{jk}(s) \int_{\Gamma_1} \varepsilon^*_{jki}\, r_{,m}\, d\Gamma \tag{4.3.12}$$

in which the first integral is to be interpreted in the sense of Cauchy principal value, Γ_1 defines a circle of unit radius centred at the load point and $r_{,m}$ is the derivative of r with reference to the coordinates of the field point. Note that $r_{,m} = -\partial r/\partial x_m$.

It is worth mentioning that the derivative of the body force rate integral can be investigated by the same procedure. In this case, due to the weaker singularity of u^*_{ij}, the free term (corresponding to the Γ_1 integral) vanishes when $\varepsilon \to 0$.

Expression (4.3.12) is also valid for three dimensional problems with Γ_1 representing the surface of a unit sphere. In both cases the corresponding Γ_1 integral can be computed in closed form and directly substituted in equation (4.3.2). In addition, since σ^*_{jki} and ε^*_{jki} present singularities of the same order, the same concept applies for the initial strain formulation. Therefore, the complete set of equations for two and three dimensional problems (Kelvin) is presented in the next section.

4.4 Alternative Boundary Element Formulations

In this section different formulations using the Kelvin fundamental solutions are discussed.

4.4.1 Initial Strain - The adoption of an initial strain formulation for three dimensional inelastic problems leads to the following equation (see Section 4.2).

$$C_{ij}\,\dot{u}_j = \int_\Gamma u^*_{ij}\,\dot{p}_j\,d\Gamma - \int_\Gamma p^*_{ij}\,\dot{u}_j\,d\Gamma + \int_\Omega u^*_{ij}\,\dot{b}_j\,d\Omega + \int_\Omega \sigma^*_{jki}\,\dot{\varepsilon}^a_{jk}\,d\Omega \ . \tag{4.4.1}$$

Equation (4.4.1) is assumed valid for any location of the load point (interior or boundary points), provided C_{ij} and the second boundary integral on the right-hand-side are properly interpreted as known from the elastic application of the technique.

Under this assumption, the stress rates at interior points can be computed by use of expressions (2.4.1) and (2.4.5) of Chapter 2. The derivative of equation (4.4.1) yields ($C_{ij} = \delta_{ij}$)

$$\frac{\partial \dot{u}_i}{\partial x_m} = \int_\Gamma \frac{\partial u^*_{ij}}{\partial x_m} \dot{p}_j \, d\Gamma - \int_\Gamma \frac{\partial p^*_{ij}}{\partial x_m} \dot{u}_j \, d\Gamma + \int_\Omega \frac{\partial u^*_{ij}}{\partial x_m} \dot{b}_j \, d\Omega + \int_\Omega \frac{\partial \sigma^*_{jki}}{\partial x_m} \dot{\varepsilon}^a_{jk} \, d\Omega - \dot{\varepsilon}^a_{jk} \int_{\Gamma_1} \sigma^*_{jki} \, r_{,m} \, d\Gamma \tag{4.4.2}$$

where the fourth integral is to be interpreted in the principal value sense and the last integral is to be performed over the surface of a unit sphere centred at the singular point. Note that the derivatives are taken with respect to the load point; as before these are indicated explicitly to differentiate from the comma notation which is taken with reference to the field point.

The last integral in equation (4.4.2) can now be computed

$$- \dot{\varepsilon}^a_{jk} \int_{\Gamma_1} \sigma^*_{jki} \, r_{,m} \, d\Gamma = \frac{1}{15(1-\nu)} \left[(8-10\nu) \, \dot{\varepsilon}^a_{im} - (1-5\nu) \dot{\varepsilon}^a_{\ell\ell} \, \delta_{im} \right] . \tag{4.4.3}$$

In what follows the reader is referred to the end of this section for the components of the new tensors related to the fundamental solutions.

The above expressions together with (2.4.1) and (2.4.5) allow for the determination of the internal stresses

$$\dot{\sigma}_{ij} = \int_{\Gamma} u^*_{ijk}\, \dot{p}_k\, d\Gamma - \int_{\Gamma} p^*_{ijk}\, \dot{u}_k\, d\Gamma + \int_{\Omega} u^*_{ijk}\, \dot{b}_k\, d\Omega$$
$$+ \int_{\Omega} \sigma^*_{ijk\ell}\, \dot{\varepsilon}^a_{k\ell}\, d\Omega - \frac{2G}{15(1-\nu)} \left[(7-5\nu)\dot{\varepsilon}^a_{ij} + (1+5\nu)\dot{\varepsilon}^a_{\ell\ell}\, \delta_{ij}\right] \tag{4.4.4}$$

where the last two terms represent the influence of the inelastic strains.

For plane strains the procedure is analogous, the only difference being the fact that the inelastic strain rate integrals still have to take into consideration the work performed in the third direction ($\sigma^*_{33i}\, \dot{\varepsilon}^a_{33}$) . This effect is easily incorporated through some particular assumptions such as incompressibility of the inelastic strains (valid for creep and plasticity of metals) or the isolated case of thermal strains [9]. These cases lead to what follows

$$C_{ij}\, \dot{u}_j = \int_{\Gamma} u^*_{ij}\, \dot{p}_j\, d\Gamma - \int_{\Gamma} p^*_{ij}\, \dot{u}_j\, d\Gamma + \int_{\Omega} u^*_{ij}\, \dot{b}_j\, d\Omega + \int_{\Omega} \hat{\sigma}^*_{jki}\, \dot{\varepsilon}^a_{jk}\, d\Omega \tag{4.4.5}$$

in which

$$\hat{\sigma}^*_{jki} = \sigma^*_{jki} + \frac{2\nu\delta_{jk}\, r,_i}{4\pi(1-\nu)r} \quad \text{if} \quad \dot{\hat{\theta}} = 0 \quad \text{(see section 2.4)} \tag{4.4.6}$$

or

$$\hat{\sigma}^*_{jki} = \sigma^*_{jki} - \frac{\nu\delta_{jk}\, r,_i}{4\pi(1-\nu)r} \quad \text{if} \quad \dot{\varepsilon}^a_{jk} = \dot{\varepsilon}^T_{jk} = \alpha\dot{T}\delta_{jk} \tag{4.4.7}$$

where α is the coefficient of linear thermal expansion and $\dot{T}$ is the temperature rate.

The corresponding internal stress rates are computed by

$$\dot{\sigma}_{ij} = \int_{\Gamma} u^*_{ijk}\, \dot{p}_k\, d\Gamma - \int_{\Gamma} p^*_{ijk}\, \dot{u}_k\, d\Gamma + \int_{\Omega} u^*_{ijk}\, \dot{b}_k\, d\Omega + \int_{\Omega} \hat{\sigma}^*_{ijk\ell}\, \dot{\varepsilon}^a_{k\ell}\, d\Omega + f_{ij}(\dot{\varepsilon}^a_{k\ell}) \tag{4.4.8}$$

where the last integral is to be taken in the Cauchy principal value sense and if $\dot{\hat{\theta}} = 0$

$$\hat{\sigma}^*_{ijk\ell} = \sigma^*_{ijk\ell} + \frac{G}{2\pi(1-\nu)r^2}\left[4\nu\, r_{,i}\, r_{,j}\delta_{k\ell} - 2\nu\,\delta_{ij}\,\delta_{k\ell}\right] ;$$
$$f_{ij} = -\frac{G}{4(1-\nu)}\left[2\,\dot{\varepsilon}^a_{ij} + (1-4\nu)\dot{\varepsilon}^a_{\ell\ell}\,\delta_{ij}\right] . \tag{4.4.9}$$

For pure thermal strains one has

$$\hat{\sigma}^*_{ijk\ell} = \sigma^*_{ijk\ell} - \frac{G}{2\pi(1-\nu)r^2}\left[2\nu r_{,i}\, r_{,j}\,\delta_{k\ell} - \nu\,\delta_{ij}\,\delta_{k\ell}\right] ;$$
$$f_{ij} = -\frac{G(1+\nu)}{1-\nu}\,\alpha\,\dot{T}\,\delta_{ij} . \tag{4.4.10}$$

Plane stress problems can also be solved by using equations (4.4.5) and (4.4.8) with $\hat{\sigma}^*_{jki} = \sigma^*_{jki}$, $\hat{\sigma}^*_{ijk\ell} = \sigma^*_{ijk\ell}$, ν replaced by $\bar{\nu}$ in all $(\,)^*$ tensors and the free term in (4.4.8) being given by

$$f_{ij} = -\frac{G}{4(1-\bar{\nu})}\left[2\,\dot{\varepsilon}^a_{ij} + \dot{\varepsilon}^a_{\ell\ell}\,\delta_{ij}\right] . \tag{4.4.11}$$

4.4.2 Initial Stress - In order to discuss the initial stress formulation, let us merely study the plastic strain rate integral presented in equation (4.4.1). Recalling expressions (3.3.5) and (3.3.6) we see that

$$\int_\Omega \sigma^*_{jki}\,\dot{\varepsilon}^a_{jk}\,d\Omega = \int_\Omega C_{jkrs}\,\varepsilon^*_{rsi}\,\dot{\varepsilon}^a_{jk}\,d\Omega \tag{4.4.12}$$

by simple inspection of expression (2.2.31) we can make,

$$C_{jkrs} = C_{rsjk} \tag{4.4.13}$$

moreover

$$C_{rsjk}\,\dot{\varepsilon}^{a}_{jk} = \dot{\sigma}^{a}_{rs} \tag{4.4.14}$$

where $\dot{\sigma}^{a}_{rs}$ was given in Chapter 2 expression (2.4.7).

Thus,

$$\int_{\Omega} \sigma^{*}_{jki}\,\dot{\varepsilon}^{a}_{jk}\,d\Omega = \int_{\Omega} \varepsilon^{*}_{jki}\,\dot{\sigma}^{a}_{jk}\,d\Omega\ . \tag{4.4.15}$$

Hence the initial stress equation is seen to be equivalent to the initial strain. For plane strain problems the demonstration follows the same pattern and the corresponding expression is

$$\int_{\Omega} \hat{\sigma}^{*}_{jki}\,\dot{\varepsilon}^{a}_{jk}\,d\Omega = \int_{\Omega} \varepsilon^{*}_{jki}\,\dot{\sigma}^{a}_{jk}\,d\Omega\ . \tag{4.4.16}$$

In both cases the internal stresses can be computed by

$$\dot{\sigma}_{ij} = \int_{\Gamma} u^{*}_{ijk}\,\dot{p}_{k}\,d\Gamma - \int_{\Gamma} p^{*}_{ijk}\,\dot{u}_{k}\,d\Gamma + \int_{\Omega} u^{*}_{ijk}\,\dot{b}_{k}\,d\Omega + \int_{\Omega} \varepsilon^{*}_{ijk\ell}\,\dot{\sigma}^{a}_{k\ell}\,d\Omega + g_{ij}(\dot{\sigma}^{a}_{k\ell}) \tag{4.4.17}$$

where the integral of the initial stress term is in the principal value sense and the expressions for the free term are of the following form

$$g_{ij} = -\frac{1}{15(1-\nu)}\left[(7-5\nu)\dot{\sigma}^{a}_{ij} + (1-5\nu)\dot{\sigma}^{a}_{\ell\ell}\,\delta_{ij}\right] \quad \text{for 3-D} \tag{4.4.18}$$

and

$$g_{ij} = -\frac{1}{8(1-\nu)}\left[2\dot{\sigma}^{a}_{ij} + (1-4\nu)\dot{\sigma}^{a}_{\ell\ell}\,\delta_{ij}\right] \quad \text{for 2-D plane strain.} \tag{4.4.19}$$

It is worth noting that for plane strains the initial stress integrals do not require the contribution of the work performed in the third

direction, nor the particular assumptions concerning $\dot{\varepsilon}^a_{ij}$ need to be made. This is because $\varepsilon^*_{33i} = 0$ and the effect of $\dot{\varepsilon}^a_{33}$ is already included into the components of $\dot{\sigma}^a_{ij}$. As a consequence, plane stress problems can be handled by the plane strain expressions with the replacement of ν by $\bar{\nu}$ being the only modification.

4.4.3 Fictitious Tractions and Body Forces - The last integral presented in equation (4.4.1) can be written in terms of the derivatives of u^*_{ij} as follows

$$\int_\Omega \sigma^*_{jki}\, \dot{\varepsilon}^a_{jk}\, d\Omega = \int_\Omega \left\{ G(u^*_{ij,k} + u^*_{ik,j}) + \frac{2G\nu}{1-2\nu}\, u^*_{i\ell,\ell}\, \delta_{jk} \right\} \dot{\varepsilon}^a_{jk}\, d\Omega \qquad (4.4.20)$$

which after integrating by parts gives the identity

$$\int_\Omega \sigma^*_{jki}\, \dot{\varepsilon}^a_{jk}\, d\Omega = \int_\Gamma u^*_{ij}\, 2G\left(\dot{\varepsilon}^a_{jk}\, n_k + \frac{\nu}{1-2\nu}\, \dot{\varepsilon}^a_{\ell\ell}\, n_j \right) d\Gamma$$
$$- \int_\Omega u^*_{ij}\, 2G\left(\dot{\varepsilon}^a_{jk,k} + \frac{\nu}{1-2\nu}\, \dot{\varepsilon}^a_{\ell\ell,j} \right) d\Omega \,. \qquad (4.4.21)$$

The substitution of (4.4.21) in (4.4.1) gives as a result

$$C_{ij}\, \dot{u}_j = \int_\Gamma u^*_{ij}\, \dot{\bar{p}}_j\, d\Gamma - \int_\Gamma p^*_{ij}\, \dot{u}_j\, d\Gamma + \int_\Omega u^*_{ij}\, \dot{\bar{b}}_j\, d\Omega \qquad (4.4.22)$$

where $\dot{\bar{b}}_j$ and $\dot{\bar{p}}_j$ were given in Chapter 2 expressions (2.4.12) and (2.4.13) respectively.

Therefore, we have arrived at an inelastic formulation in which traction and body force rates are fictitious (depend on the inelastic strains), but the displacements are the actual ones. In order to apply equation (4.4.22) one has to be aware that although it looks like the elastic application of the boundary element technique,

the internal stresses still have to be computed by use of equations (2.4.1) and (2.4.5), i.e.

$$\dot{\sigma}_{ij} = \int_{\Gamma} u^*_{ijk}\, \dot{\bar{p}}_k\, d\Gamma - \int_{\Gamma} p^*_{ijk}\, \dot{u}_k\, d\Gamma + \int_{\Omega} u^*_{ijk}\, \dot{\bar{b}}_k\, d\Omega - C_{ijk\ell}\, \dot{\varepsilon}^a_{k\ell} \quad . \tag{4.4.23}$$

Another feature of this formulation is that in contrast with the two previous approaches, it needs computation of space derivatives of the inelastic strains (see expression (2.4.12)). This may be considered as a disadvantage for numerical implementation (since constant interpolation is ruled out) but, nevertheless, it is a valid procedure for formulating the B.E.M. to inelastic problems and still remains to be properly attempted.

Finally, the new tensors related to the fundamental solutions that appeared in this section are of the following form

$$\begin{aligned}\sigma^*_{ijk\ell} = \frac{G}{2\alpha\pi(1-\nu)r^\beta}\Big\{&\beta(1-2\nu)(\delta_{ij}r,_k r,_\ell + \delta_{k\ell}r,_i r,_j) \\ &+ \beta\nu(\delta_{\ell i}r,_j r,_k + \delta_{jk}r,_\ell r,_i + \delta_{ik}r,_\ell r,_j \\ &+ \delta_{j\ell}r,_i r,_k) - \beta\gamma r,_i r,_j r,_k r,_\ell \\ &+ (1-2\nu)(\delta_{ik}\delta_{\ell j} + \delta_{jk}\delta_{\ell i}) - (1-4\nu)\delta_{ij}\delta_{k\ell}\Big\}\end{aligned} \tag{4.4.24}$$

$$\begin{aligned}\varepsilon^*_{ijk\ell} = \frac{1}{4\alpha\pi(1-\nu)r^\beta}\Big\{&(1-2\nu)\big[\delta_{ik}\delta_{\ell j} + \delta_{jk}\delta_{\ell i} - \delta_{ij}\delta_{k\ell} \\ &+ \beta\delta_{ij}r,_k r,_\ell\big] + \beta\nu\big[\delta_{\ell i}r,_j r,_k + \delta_{jk}r,_\ell r,_i \\ &+ \delta_{ik}r,_\ell r,_j + \delta_{j\ell}r,_i r,_k\big] \\ &+ \beta\delta_{k\ell}r,_i r,_j - \beta\gamma r,_i r,_j r,_k r,_\ell\Big\}\end{aligned} \tag{4.4.25}$$

where $\alpha = 2, 1$; $\beta = 3, 2$; $\gamma = 5, 4$ for 3-D and plane strain respectively.

4.5 Half-Plane Formulations

The extension of the elastic half-plane boundary element formulation to inelastic problems follows the same procedure as in the Kelvin implementation.

If we consider the inelastic strains to be incompressible, the starting equation for the initial strain formulation is given by

$$C_{ij}\,\dot{u}_j = \int_\Gamma u^*_{ij}\,\dot{p}_j\,d\Gamma - \int_{\Gamma'} p^*_{ij}\,\dot{u}_j\,d\Gamma + \int_\Omega u^*_{ij}\,\dot{b}_j\,d\Omega + \int_\Omega \hat{\sigma}^*_{jki}\,\dot{\varepsilon}^a_{jk}\,d\Omega \quad (4.5.1)$$

in which for plane strain problems the complementary part of the tensor that multiplies the inelastic strain rates is

$$\hat{\sigma}^c_{jki} = \sigma^c_{jki} - \nu\sigma^c_{\ell\ell i}\,\delta_{jk} \quad (4.5.2)$$

whereas for plane stress

$$\hat{\sigma}^c_{jki} = \sigma^c_{jki}\,. \quad (4.5.3)$$

Equation (4.5.1) is valid for any location of the load point on condition that C_{ij} and the integral over Γ' be properly interpreted as discussed in Chapter 3.

By suitably modifying the inelastic strain rate integral, an initial stress equation without the condition of incompressibility of the inelastic strains can be equally obtained for plane strains

$$C_{ij}\,\dot{u}_j = \int_\Gamma u^*_{ij}\,\dot{p}_j\,d\Gamma - \int_{\Gamma'} p^*_{ij}\,\dot{u}_j\,d\Gamma + \int_\Omega u^*_{ij}\,\dot{b}_j\,d\Omega + \int_\Omega \varepsilon^*_{jki}\,\dot{\sigma}^a_{jk}\,d\Omega \quad (4.5.4)$$

where as explained in Section 4.4, plane stress problems can be dealt with by simply modifying the Poisson's ratio.

In order to accurately compute the stress rates at interior points, the derivatives of (4.5.1) are combined to produce the expressions for the total strain rates and then substituted into equation (2.4.5). Here one notices that, due to the non singular nature of the complementary tensors, the derivatives of the inelastic strain rate integral create exactly the same singularities obtained for the single Kelvin implementation. Hence, for plane strains one has

$$\dot{\sigma}_{ij} = \int_{\Gamma} u^*_{ijk}\, \dot{p}_k \, d\Gamma - \int_{\Gamma'} p^*_{ijk}\, \dot{u}_k \, d\Gamma + \int_{\Omega} u^*_{ijk}\, \dot{b}_k \, d\Omega + \int_{\Omega} \hat{\sigma}^*_{ijk\ell}\, \dot{\varepsilon}^a_{k\ell} \, d\Omega + f_{ij}(\dot{\varepsilon}^a_{k\ell}) \tag{4.5.5}$$

in which the inelastic strain integral is to be computed in the principal value sense and f_{ij} is the same free term obtained for the Kelvin formulation, i.e.,

$$f_{ij} = -\frac{G}{4(1-\nu)}\left[2\dot{\varepsilon}^a_{ij} + (1-4\nu)\dot{\varepsilon}^a_{\ell\ell}\,\delta_{ij}\right] . \tag{4.5.6}$$

In addition,

$$\hat{\sigma}^c_{ijk\ell} = \sigma^c_{ijk\ell} - \nu\sigma^c_{ijmm}\,\delta_{k\ell} \tag{4.5.7}$$

and

$$\sigma^c_{ijk\ell} = G\left(\frac{\partial \sigma^c_{k\ell i}}{\partial x_j} + \frac{\partial \sigma^c_{k\ell j}}{\partial x_i}\right) + \frac{2G\nu}{1-2\nu}\frac{\partial \sigma^c_{k\ell m}}{\partial x_m}\,\delta_{ij} \tag{4.5.8}$$

where the derivatives are taken with reference to the load point. These derivatives together with u^c_{ijk} and p^c_{ijk} were given in Chapter 3 Section 3.4.

An interesting feature of the half-plane implementation is that if the problem to be analysed satisfies the traction-free condition ($\dot{p}_k = 0$) over some part of the boundary $\Gamma - \Gamma'$, stresses at points located along this part of the boundary can be computed as if they were internal points. In order to validate equation (4.5.5) for such cases, only the expression of f_{ij} needs to be modified to take into consideration the limiting case $c = 0$. This expression can be easily obtained as follows; let us assume a semi-circular free body, of radius ρ, whose straight boundary is contained by the surface of the half-plane (see figure 4.5.1). If body forces are not considered, the application of a uniform plastic strain field ($\bar{\varepsilon}^p_{ij}$) to this body, will only produce displacements, internal stresses and tractions remain zero throughout the process.

The application of equation (4.5.5) to represent the stresses at the centre S of the semi-circle leads directly to

$$\int_{\Gamma'} p^*_{ijk}\, \bar{u}_k \, d\Gamma = \bar{\varepsilon}^p_{k\ell} \int_{\Omega} \hat{\sigma}^*_{ijk\ell} \, d\Omega + f_{ij}(\bar{\varepsilon}^p_{k\ell}) \qquad (4.5.9)$$

moreover, from the condition of existence of the principal value (see expression (4.3.11)), one can prove that

$$\int_{\Omega} \hat{\sigma}^*_{ijk\ell} \, d\Omega = 0 \quad . \qquad (4.5.10)$$

Hence,

$$f_{ij}(\bar{\varepsilon}^p_{k\ell}) = \int_{\Gamma'} p^*_{ijk}\, \bar{u}_k \, d\Gamma \qquad (4.5.11)$$

where the relevant boundary displacements (neglecting rigid body movements) can be computed by (see Appendix C)

$$\bar{u}_i = \rho(\bar{\varepsilon}^p_{ij} - \nu\bar{\varepsilon}^p_{kk}\,\delta_{ij})n_j \qquad (4.5.12)$$

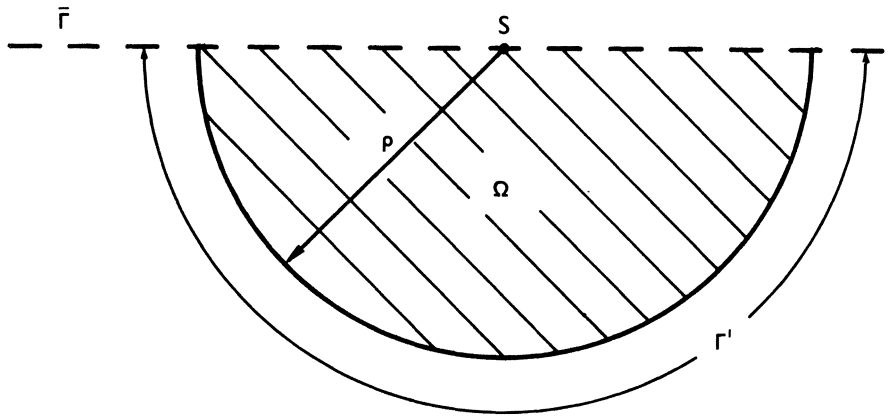

Fig. 4.5.1 Semi-circular free body under a constant plastic strain field.

in which n_j represents the direction cosines of the outward normal to the curved boundary.

Equation (4.5.11) therefore provides the required expression for f_{ij} when $c = 0$

$$f_{11} = f_{12} = 0$$
$$f_{22} = -\frac{G}{2(1-\nu)}(\dot{\varepsilon}^a_{22} - \dot{\varepsilon}^a_{11}) . \tag{4.5.13}$$

For the initial stress formulation the procedure is entirely similar and the equation equivalent to (4.5.5) is of the following form

$$\dot{\sigma}_{ij} = \int_{\Gamma} u^*_{ijk}\, \dot{p}_k\, d\Gamma - \int_{\Gamma'} p^*_{ijk}\, \dot{u}_k\, d\Gamma + \int_{\Omega} u^*_{ijk}\, \dot{b}_k\, d\Omega + \int_{\Omega} \varepsilon^*_{ijk\ell}\, \dot{\sigma}^a_{k\ell}\, d\Omega + g_{ij}(\dot{\sigma}^a_{k\ell}) \tag{4.5.14}$$

where $\varepsilon^c_{ijk\ell}$ is obtained from (4.5.8) by substituting σ^c_{jki} by ε^c_{jki},

$$g_{ij} = -\frac{1}{8(1-\nu)}\left[2\dot{\sigma}^a_{ij} + (1-4\nu)\dot{\sigma}^a_{\ell\ell}\,\delta_{ij}\right] \quad \text{for} \quad c > 0 \tag{4.5.15}$$

and

$$g_{11} = g_{12} = 0$$

$$g_{22} = -\frac{1}{4(1-\nu)}\left[\dot{\sigma}^a_{22} - \dot{\sigma}^a_{11}\right] \quad \text{for} \quad c = 0\ . \tag{4.5.16}$$

Plane stress problems can be handled by equations (4.5.5) and (4.5.14) if Poisson's ratio is modified as before, $\hat{\sigma}^*_{ijk\ell} = \sigma^*_{ijk\ell}$ and expression (4.5.6) is replaced by

$$f_{ij} = -\frac{G}{4(1-\bar{\nu})}\left[2\dot{\varepsilon}^a_{ij} + \dot{\varepsilon}^a_{\ell\ell}\,\delta_{ij}\right]\ . \tag{4.5.17}$$

Notice that expressions (4.5.13), (4.5.15) and (4.5.16) still remain valid.

4.6 Spatial Discretization

The spatial discretization of the equations previously presented is illustrated in this section for two dimensional problems. The boundary of the body is assumed to be represented by surface elements as discussed in Chapter 3 and the part of the domain in which non-zero inelastic strains are expected to develop is discretized using internal cells for integration. The body force term, though not causing any difficulty for implementation, is not considered for simplicity.

The discretization of the boundary integrals has been thoroughly discussed in Section 3.7 and the same procedure can be followed here. Consequently, emphasis will be given to the domain integrals of the inelastic terms.

It is instructive to start by assuming an initial strain formulation in which the inelastic strains are incompressible. Thus, let us now concentrate the attention to the following equation

$$C_{ij}\,\dot{u}_j + \int_\Gamma p^*_{ij}\,\dot{u}_j\,d\Gamma = \int_\Gamma u^*_{ij}\,\dot{p}_j\,d\Gamma + \int_\Omega \hat{\sigma}^*_{jki}\,\dot{\varepsilon}^a_{jk}\,d\Omega \qquad (4.6.1)$$

where the appropriate alterations for half-plane problems are implied.

For the domain discretization of equation (4.6.1) the Cartesian coordinates $\underset{\sim}{x}^{(j)}$ of points located within each cell Ω_j can be represented by the following equation

$$\underset{\sim}{x}^{(j)} = \bar{\underset{\sim}{M}}\,\underset{\sim}{x}^{(m)} \qquad (4.6.2)$$

where $\bar{\underset{\sim}{M}}$ represents the interpolation functions and $\underset{\sim}{x}^{(m)}$ the coordinates of some special points which define the geometry of the cell.

The inelastic strain rates are assumed to be interpolated within the cell in the form

$$\dot{\underset{\sim}{\varepsilon}}^{a(j)} = \bar{\underset{\sim}{N}}\,\dot{\underset{\sim}{\varepsilon}}^{a(n)} \qquad (4.6.3)$$

in which $\bar{\underset{\sim}{N}}$ stands for the interpolation functions and $\dot{\underset{\sim}{\varepsilon}}^{a(n)}$ for the values of the inelastic strain rates at a certain number of stress points (equivalent to nodal points in 2-D finite elements).

Assuming L boundary elements and Z internal cells, the discretized version of equation (4.6.1) for a boundary node S_i is given by

$$\underset{\sim}{C}(S_i)\,\dot{\underset{\sim}{u}}(S_i) + \sum_{j=1}^{L}\left(\int_{\Gamma_j} \underset{\sim}{p}^{*}\,\underset{\sim}{N}\,d\Gamma\right)\dot{\underset{\sim}{u}}^{(n)} = \sum_{j=1}^{L}\left(\int_{\Gamma_j} \underset{\sim}{u}^{*}\,\underset{\sim}{N}\,d\Gamma\right)\dot{\underset{\sim}{p}}^{(n)} + \sum_{j=1}^{Z}\left(\int_{\Omega_j} \hat{\underset{\sim}{\sigma}}^{*}\,\bar{\underset{\sim}{N}}\,d\Omega\right)\dot{\underset{\sim}{\varepsilon}}^{a(n)} \tag{4.6.4}$$

and the same form is valid for an internal stress point s_i ($\underset{\sim}{C} = \underset{\sim}{I}$) .

For general purposes it is convenient to compute the cell integrals by using a suitable numerical quadrature scheme; e.g., for triangular cells Hammer's integration formulae [1] can be used

$$\int_{\Omega_j} \hat{\underset{\sim}{\sigma}}^{*}\,\bar{\underset{\sim}{N}}\,d\Omega = \sum_{k=1}^{K} |J|_k\, W_k\, (\hat{\underset{\sim}{\sigma}}^{*}\,\bar{\underset{\sim}{N}})_k \tag{4.6.5}$$

where K is the number of integration points, W_k is the associated weighting factor and $|J|$ is the Jacobian of the coordinate transformation which allows for the representation of the interpolation functions in terms of a homogeneous coordinate system (ξ_1, ξ_2) . Note that these integrals present integrable singularities when the singular node (S_i) or point (s_i) lies on the cell Ω_j . Thus, some special care must be taken in such cases.

The application of equation (4.6.4) to all boundary nodes generates the following matrix relationship

$$\underset{\sim}{H}\,\dot{\underset{\sim}{u}} = \underset{\sim}{G}\,\dot{\underset{\sim}{p}} + \underset{\sim}{D}\,\dot{\underset{\sim}{\varepsilon}}^{a} \tag{4.6.6}$$

where matrices $\underset{\sim}{H}$ and $\underset{\sim}{G}$ are the same as those obtained for elastic analysis and matrix $\underset{\sim}{D}$ is due to the inelastic strain integral.

Computation of stress rates at internal points follows a similar procedure. Here, the equation equivalent to (4.6.1) is given by

$$\dot{\sigma}_{ij} = \int_{\Gamma} u^*_{ijk}\, \dot{p}_k \, d\Gamma - \int_{\Gamma} p^*_{ijk}\, \dot{u}_k \, d\Gamma + \int_{\Omega} \hat{\sigma}^*_{ijk\ell}\, \dot{\varepsilon}^a_{k\ell} \, d\Omega + f_{ij}(\dot{\varepsilon}^a_{k\ell}) \quad (4.6.7)$$

where as before the appropriate alterations for half-plane problems are implied.

Application of equation (4.6.7) in discretized form leads to

$$\begin{aligned} \dot{\underset{\sim}{\sigma}}(s_i) = &\sum_{j=1}^{L} \left(\int_{\Gamma_j} {}'\underset{\sim}{u}^*\, \underset{\sim}{N}\, d\Gamma \right) \dot{p}^{(n)} - \sum_{j=1}^{L} \left(\int_{\Gamma_j} {}'\underset{\sim}{p}^*\, \underset{\sim}{N}\, d\Gamma \right) \dot{\underset{\sim}{u}}^{(n)} \\ &+ \sum_{j=1}^{Z} \left(\int_{\Omega_j} {}'\hat{\underset{\sim}{\sigma}}^*\, \bar{\underset{\sim}{N}}\, d\Omega \right) \dot{\underset{\sim}{\varepsilon}}^{a(n)} + \underset{\sim}{C}'(s_i)\, \dot{\underset{\sim}{\varepsilon}}^a(s_i) \end{aligned} \quad (4.6.8)$$

for a stress point s_i .

As before, numerical integration schemes can be used for integrating over the cells. In this case, however, when the singular point s_i lies on the cell Ω_j some of the integrals are only possible in the principal value sense. Here we recall a general procedure devised by Telles and Brebbia [46] which provides indirect means of computing such principal values for any kind of interpolation functions or cells shape. This procedure is based on the application of a constant inelastic strain field to the discretized integral equations and is presented in Appendix A.

Equation (4.6.8) when applied to all internal stress points yields

$$\dot{\underset{\sim}{\sigma}} = \underset{\sim}{G}' \dot{\underset{\sim}{p}} - \underset{\sim}{H}' \dot{\underset{\sim}{u}} + (\underset{\sim}{D}' + \underset{\sim}{C}') \dot{\underset{\sim}{\varepsilon}}^a \qquad (4.6.9)$$

where $\underset{\sim}{C}'$ is a well defined matrix that represents the free terms (last term in eqn. (4.6.8)) and $\underset{\sim}{D}'$ is due to the inelastic strain integral. Matrices $\underset{\sim}{H}'$ and $\underset{\sim}{G}'$ correspond to the boundary integrals in a similar fashion to $\underset{\sim}{H}$ and $\underset{\sim}{G}$.

Note that equation (4.6.8) is only valid for internal stress points and possibly for stress points over the traction-free part of the boundary $\Gamma - \Gamma'$. Therefore, in order to compute the stress rates at boundary nodes, different expressions must be used. Such expressions are obtained by means of strain displacement relationships and traction rate values along each boundary element. They do not require any integration and are presented in Appendix B. Henceforth, such simple expressions are assembled into (4.6.9) and computation of stress rates at all stress points becomes possible in a unified manner.

It is obvious that what has been discussed here also applies for the initial stress equations. In this case, equations (4.6.6) and (4.6.9) are substituted by

$$\underset{\sim}{H} \dot{\underset{\sim}{u}} = \underset{\sim}{G} \dot{\underset{\sim}{p}} + \underset{\sim}{Q} \dot{\underset{\sim}{\sigma}}^a \qquad (4.6.10)$$

and

$$\dot{\underset{\sim}{\sigma}} = \underset{\sim}{G}' \dot{\underset{\sim}{p}} - \underset{\sim}{H}' \dot{\underset{\sim}{u}} + (\underset{\sim}{Q}' + \underset{\sim}{E}') \dot{\underset{\sim}{\sigma}}^a \qquad (4.6.11)$$

where the part of $\underset{\sim}{E}'$ that corresponds to the integral equations stands for the free terms g_{ij} and the equivalent part of $\underset{\sim}{Q}'$ together with $\underset{\sim}{Q}$ are due to the initial stress integrals. Notice that the principal values of $\underset{\sim}{Q}'$ can still be computed by applying equation (4.6.11) to represent a state of constant initial stresses, in much the same way as it is shown in Appendix A for the initial strain equation.

In order to minimize the computer effort for the solution of inelastic problems, let us reexamine equations (4.6.6) and (4.6.9). For a well-posed problem, a sufficient number of tractions and boundary displacements needs to be prescribed. The unknowns are then reordered leading to

$$\underset{\sim}{A}\ \dot{\underset{\sim}{y}} = \dot{\underset{\sim}{f}} + \underset{\sim}{D}\ \dot{\underset{\sim}{\varepsilon}}^{a} \tag{4.6.12}$$

and similarly,

$$\dot{\underset{\sim}{\sigma}} = -\ \underset{\sim}{A}'\ \dot{\underset{\sim}{y}} + \dot{\underset{\sim}{f}}' + \underset{\sim}{D}^{*}\ \dot{\underset{\sim}{\varepsilon}}^{a} \tag{4.6.13}$$

where $\underset{\sim}{D}^{*} = \underset{\sim}{D}' + \underset{\sim}{C}'$ and the contribution of the prescribed values is included in vectors $\dot{\underset{\sim}{f}}$ and $\dot{\underset{\sim}{f}}'$.

From the multiplication of equation (4.6.12) by $\underset{\sim}{A}^{-1}$ comes

$$\dot{\underset{\sim}{y}} = \underset{\sim}{K}\ \dot{\underset{\sim}{\varepsilon}}^{a} + \dot{\underset{\sim}{m}} \tag{4.6.14}$$

where

$$\underset{\sim}{K} = \underset{\sim}{A}^{-1}\ \underset{\sim}{D} \tag{4.6.15}$$

and

$$\dot{\underset{\sim}{m}} = \underset{\sim}{A}^{-1}\dot{\underset{\sim}{f}} \ . \tag{4.6.16}$$

Substituting (4.6.14) into (4.6.13) yields

$$\dot{\underset{\sim}{\sigma}} = \underset{\sim}{B}\ \dot{\underset{\sim}{\varepsilon}}^{a} + \dot{\underset{\sim}{n}} \tag{4.6.17}$$

in which

$$\underset{\sim}{B} = \underset{\sim}{D}^{*} - \underset{\sim}{A}'\underset{\sim}{K} \tag{4.6.18}$$

and

$$\dot{\underset{\sim}{n}} = \dot{\underset{\sim}{f}}' - \underset{\sim}{A}'\ \dot{\underset{\sim}{m}} \ . \tag{4.6.19}$$

Note that the elastic solution to the rate problem is given by the vectors $\dot{\underset{\sim}{m}}$ and $\dot{\underset{\sim}{n}}$.

From the above it is seen that equation (4.6.17) represents a single recursive expression which relates stress rates at selected boundary nodes and internal points to the corresponding inelastic strains and the elastic solution. Also, this expression is now independent of the boundary equation (4.6.14) and provides useful means of solving nonlinear material problems. This will be the subject of Chapter 5.

In terms of efficiently programming, it should be noted that initially matrix $\underset{\sim}{A}$ is assembled in the array of matrix $\underset{\sim}{B}$ and that once the system of equations is solved, equation (4.6.17) is generated in such a way that only matrix $\underset{\sim}{B}$ is actually formed. Thus, only $\underset{\sim}{K}$ and $\underset{\sim}{B}$ require storage.

Finally, the same matrix manipulations can be performed in the initial stress equations (4.6.10) and (4.6.11). In this case, however, a slight modification in equation (4.6.11) has proven to be convenient for elastoplastic problems and this will be discussed in Chapter 5. The initial stress equations are also employed in Chapter 6 where problems concerning viscoplasticity and creep are dealt with.

4.7 Internal Cells

Herein, for the numerical implementation of the equations presented in the previous sections, linear boundary elements and linear triangular cells have been chosen for both initial strain and initial stress formulations. The implementation of linear boundary elements has been discussed in Chapter 3 and the same procedure was followed here.

For linear triangular cells the interpolation functions are expressed in terms of a homogeneous coordinate system (ξ_1, ξ_2) as shown in figure 4.7.1 and the Jacobian $|J|$ indicated in expression (4.6.5) is simply twice the area of the triangle. In addition, the interpolation functions introduced in equation (4.6.2) are of the following form

$$\bar{\underset{\sim}{M}} = \left[\underset{\sim}{I}\,\xi_1 \quad \underset{\sim}{I}\,\xi_2 \quad \underset{\sim}{I}\,\xi_3\right] \tag{4.7.1}$$

where $\xi_3 = 1 - \xi_2 - \xi_1$, $\underset{\sim}{I}$ is the identity matrix of order two and the corresponding vector $\underset{\sim}{x}^{(m)}$ is formed by subvectors $\left[{}^{i}x_1 \quad {}^{i}x_2\right]^T$ for each stress point $i = 1, 2, 3$ located at the corners of the cell.

Similarly, the interpolation functions presented in equation (4.6.3) are given by

$$\bar{\underset{\sim}{N}} = \left[\underset{\sim}{I}\,\xi_1 \quad \underset{\sim}{I}\,\xi_2 \quad \underset{\sim}{I}\,\xi_3\right] \tag{4.7.2}$$

where $\underset{\sim}{I}$ is now the identity matrix of order three and the inelastic strain rates form subvectors of $\dot{\underset{\sim}{\varepsilon}}^{a(n)}$ of the form $\left[{}^{i}\dot{\varepsilon}^{a}_{11} \quad {}^{i}\dot{\varepsilon}^{a}_{12} \quad {}^{i}\dot{\varepsilon}^{a}_{22}\right]^T$, for each stress point i (see figure 4.7.1).

With reference to the Kelvin implementation, the computation of the domain integrals indicated in equations (4.6.4) and (4.6.8) has been carried out by a semi-analytical integration scheme [49]. In order to describe it, let us drop the standard tensor notation and express the interpolation functions in terms of the Cartesian coordinate system (x, y) as follows [2]

$$\xi_\alpha = \frac{1}{2A}\left(2A^o_\alpha + b_\alpha x + a_\alpha y\right) \tag{4.7.3}$$

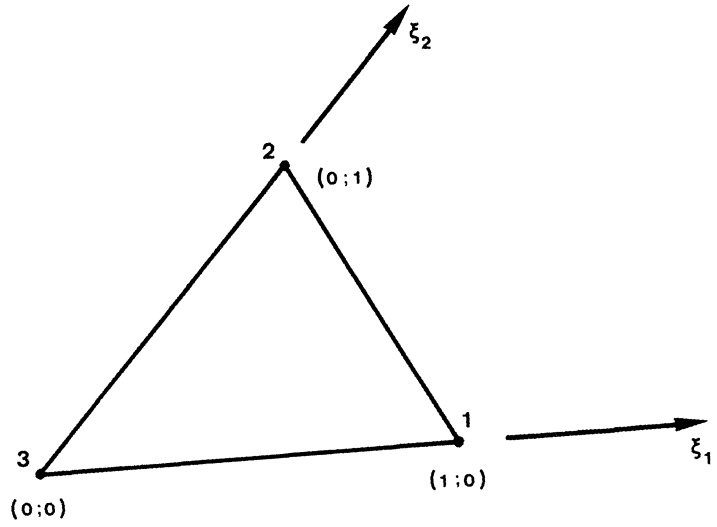

Fig. 4.7.1 Triangular cell and definition of intrinsic coordinate system (ξ_1, ξ_2).

where α represents the point to which the function refers and

$$a_\alpha = x_\gamma - x_\beta \quad ; \quad b_\alpha = y_\beta - y_\gamma \tag{4.7.4}$$

$$2A^o_\alpha = x_\beta y_\gamma - x_\gamma y_\beta \tag{4.7.5}$$

$$A = \text{area of triangle} = \frac{1}{2}(b_1 a_2 - b_2 a_1) \tag{4.7.6}$$

with $\alpha = 1, 2, 3$ for $\beta = 2, 3, 1$ and $\gamma = 3, 1, 2$.

For the total computation of matrix $\underset{\sim}{D}$ each cell will contribute with 2×9 matrices of the following form

$$\underset{\sim}{d} = \int_{\Omega_\Delta} \left\{ \left[\hat{\underset{\sim}{\sigma}}^* \xi_1 \quad \hat{\underset{\sim}{\sigma}}^* \xi_2 \quad \hat{\underset{\sim}{\sigma}}^* \xi_3 \right] \right\} d\Omega \tag{4.7.7}$$

where

$$\hat{\underset{\sim}{\sigma}}^* = \begin{bmatrix} \hat{\sigma}^*_{111} & 2\hat{\sigma}^*_{121} & \hat{\sigma}^*_{221} \\ \hat{\sigma}^*_{112} & 2\hat{\sigma}^*_{122} & \hat{\sigma}^*_{222} \end{bmatrix} . \tag{4.7.8}$$

To illustrate the present semi-analytical integration scheme the case when the singular node coincides with one of the cell points will be studied. Let us consider the typical expression

$$\underset{\sim}{d}^{\alpha} = \int_{\Omega_\Delta} \hat{\underset{\sim}{\sigma}}^* \, \xi_\alpha \, d\Omega \tag{4.7.9}$$

where $\underset{\sim}{d}^{\alpha}$ represents the 2×3 submatrix α of $\underset{\sim}{d}$.

In order to perform the integral, one can define a cylindrical coordinate system (r, ϕ) based at the singular point γ as shown in figure 4.7.2. In this system of coordinates the tensor $\hat{\sigma}^*_{jki}$ can be represented by

$$\frac{1}{r} \psi_{jki} \tag{4.7.10}$$

in which ψ_{jki} is a function of ϕ only.

Expression (4.7.9) can then be written as

$$\underset{\sim}{d}^{\alpha} = \lim_{\varepsilon \to 0} \int_{\phi_1}^{\phi_2} \int_{\varepsilon}^{R(\phi)} \underset{\sim}{\psi} \, \bar{\xi}_\alpha \, dr \, d\phi \tag{4.7.11}$$

where $\bar{\xi}_\alpha$ is the interpolation function with reference to the (r, ϕ) system

$$\bar{\xi}_\alpha = {}^{\gamma}\xi_\alpha + \frac{r}{2A} (b_\alpha \cos \phi + a_\alpha \sin \phi) \tag{4.7.12}$$

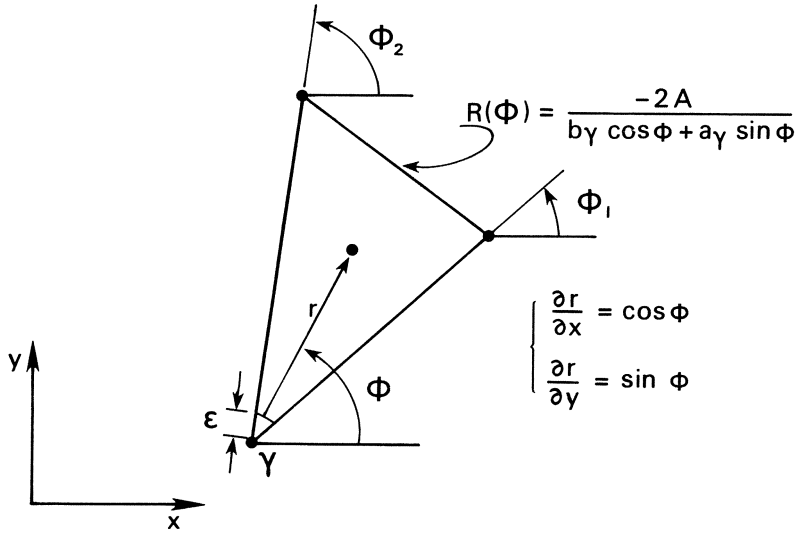

Fig. 4.7.2 Cylindrical coordinate system based at the singular point γ.

$^{\gamma}\xi_{\alpha}$ being the value of the interpolation function at the singular point γ , i.e.

$$^{\gamma}\xi_{\alpha} = \begin{cases} 0 & \text{for } \alpha \neq \gamma \\ 1 & \text{for } \alpha = \gamma \, . \end{cases} \tag{4.7.13}$$

Notice that $\underset{\sim}{\psi}$ does not depend on r and one can integrate (4.7.11) analytically with respect to r and take the limit for $\varepsilon \to 0$. The following expressions are then obtained

$$\underset{\sim}{d}^{\alpha} = A \int_{\phi_1}^{\phi_2} \underset{\sim}{\psi} \left\{ \frac{b_\alpha \cos\phi + a_\alpha \sin\phi}{(b_\gamma \cos\phi + a_\gamma \sin\phi)^2} \right\} d\phi, \quad \text{for} \quad \alpha \neq \gamma \qquad (4.7.14)$$

and

$$\underset{\sim}{d}^{\alpha} = - A \int_{\phi_1}^{\phi_2} \underset{\sim}{\psi} \left\{ \frac{1}{b_\gamma \cos\phi + a_\gamma \sin\phi} \right\} d\phi \ , \quad \text{for} \quad \alpha = \gamma \ . \qquad (4.7.15)$$

The advantage of integrating analytically with respect to r is now evident as very simple expressions are achieved and the singularity of the $\hat{\sigma}^*_{jki}$ tensor is removed. Integration with respect to ϕ does not present any problems and one can use standard one dimensional Gaussian quadrature formulae (five integration points has proved to be sufficient). This can be done by simply expressing the variable ϕ as follows

$$\phi = \frac{\eta}{2} (\phi_2 - \phi_1) + \frac{1}{2} (\phi_2 + \phi_1) \qquad (4.7.16)$$

where η is defined on the interval $[-1, 1]$.

Computation of matrix $\underset{\sim}{D}'$ follows the same pattern with the difference that each cell contributes with 3×9 matrices of the form

$$'\underset{\sim}{d} = \int_{\Omega_\Delta} \left\{ \left['\underset{\sim}{\hat{\sigma}}^* \xi_1 \quad '\underset{\sim}{\hat{\sigma}}^* \xi_2 \quad '\underset{\sim}{\hat{\sigma}}^* \xi_3 \right] \right\} d\Omega \qquad (4.7.17)$$

where

$$'\underset{\sim}{\hat{\sigma}}^* = \begin{bmatrix} \hat{\sigma}^*_{1111} & 2\hat{\sigma}^*_{1112} & \hat{\sigma}^*_{1122} \\ \hat{\sigma}^*_{1211} & 2\hat{\sigma}^*_{1212} & \hat{\sigma}^*_{1222} \\ \hat{\sigma}^*_{2211} & 2\hat{\sigma}^*_{2212} & \hat{\sigma}^*_{2222} \end{bmatrix} . \qquad (4.7.18)$$

Typically one can consider

$$'\underset{\sim}{d}^{\alpha} = \int_{\Omega_{\Delta}} '\hat{\underset{\sim}{\sigma}}^{*} \, \xi_{\alpha} \, d\Omega \ . \tag{4.7.19}$$

As before, in order to illustrate the semi-analytical process of integration, the case when the singular stress point coincides with one of the cell points will be studied. In this case, expression (4.7.19) presents a further difficulty for $\alpha = \gamma$, which means that integration is only possible in the principal value sense taking into consideration the contribution of all the adjacent cells connected to γ .

Introducing the cylindrical coordinate system of figure 4.7.2, the tensor $\hat{\sigma}^{*}_{ijk\ell}$ can be written as

$$\frac{1}{r^2} \psi_{ijk\ell} \tag{4.7.20}$$

where $\psi_{ijk\ell}$ is a function of ϕ only.

Expression (4.7.19) turns to be represented by

$$'\underset{\sim}{d}^{\alpha} = \lim_{\varepsilon \to 0} \int_{\phi_1}^{\phi_2} \int_{\varepsilon}^{R(\phi)} '\underset{\sim}{\psi} \frac{\bar{\xi}_{\alpha}}{r} \, dr \, d\phi \ . \tag{4.7.21}$$

For $\alpha \neq \gamma$, after integrating with respect to r and performing the limit for $\varepsilon \to 0$, expression (4.7.21) gives

$$'\underset{\sim}{d}^{\alpha} = -\int_{\phi_1}^{\phi_2} '\underset{\sim}{\psi} \left\{ \frac{b_{\alpha} \cos\phi + a_{\alpha} \sin\phi}{b_{\gamma} \cos\phi + a_{\gamma} \sin\phi} \right\} d\phi \ . \tag{4.7.22}$$

When $\alpha = \gamma$, integration of (4.7.21) regarding to r gives

$$'\underset{\sim}{d}^{\alpha} = \lim_{\varepsilon \to 0} \int_{\phi_1}^{\phi_2} '\underset{\sim}{\psi} \left\{ \ln \left(\frac{-2A}{b_{\gamma} \cos\phi + a_{\gamma} \sin\phi} \right) - 1 - \frac{\varepsilon}{2A} (b_{\gamma} \cos\phi + a_{\gamma} \sin\phi) - \ln(\varepsilon) \right\} d\phi \ . \tag{4.7.23}$$

To calculate the principal value let us first consider the following part of (4.7.23)

$$\underset{\sim}{\omega} = - \int_{\phi_1}^{\phi_2} {}'\underset{\sim}{\psi} \left[1 + \ln(\varepsilon)\right] d\phi \ . \qquad (4.7.24)$$

It is easily verified that in order to compute the contribution of all the adjacent cells connected to γ , one simply has to modify the integration limits in (4.7.24). This gives, due to an intrinsic property of $\psi_{ijk\ell}$ (see expression (4.3.11))

$$\underset{\sim}{\omega} = -\left[(1 + \ln(\varepsilon)\right] \int_{0}^{2\pi} {}'\underset{\sim}{\psi} \, d\phi = \underset{\sim}{0} \ . \qquad (4.7.25)$$

Once that the singular term has dropped, one can consider the rest of the expression (4.7.23) and take the limit for $\varepsilon \to 0$. The following expression then arises

$$'\underset{\sim}{d}^{\alpha} = \int_{\phi_1}^{\phi_2} {}'\underset{\sim}{\psi} \ln \left(\frac{-2A}{b_\gamma \cos\phi + a_\gamma \sin\phi} \right) d\phi \ . \qquad (4.7.26)$$

As before, one dimensional five points Gaussian quadrature formula can now be used to integrate (4.7.22) and (4.7.26).

The general case when the singular node or stress point γ is not coincident with one of the cell points follows the same process. Here, the use of a semi-analytical integration procedure is not so important since the integrals are always regular. Nevertheless, this procedure is still recommended in order to save computer time. Hence, with reference to figure 4.7.3 the integrals are split up and the following expressions are obtained

$$\underset{\sim}{d}^{\alpha} = \int_{\phi_1}^{\phi_3} \underset{\sim}{\psi} \int_{R_2(\phi)}^{R_3(\phi)} \bar{\xi}_\alpha \, dr \, d\phi + \int_{\phi_3}^{\phi_2} \underset{\sim}{\psi} \int_{R_1(\phi)}^{R_3(\phi)} \bar{\xi}_\alpha \, dr \, d\phi \qquad (4.7.27)$$

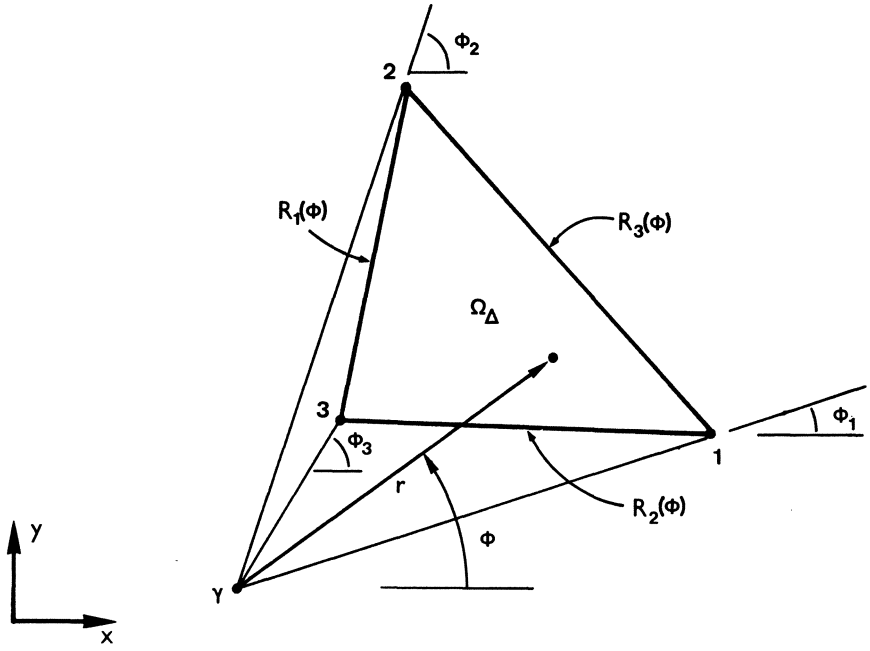

Fig. 4.7.3 Cylindrical coordinate system for semi-analytical integration. General case.

and

$$'\underset{\sim}{d}^{\alpha} = \int_{\phi_1}^{\phi_3} '\underset{\sim}{\psi} \int_{R_2(\phi)}^{R_3(\phi)} \frac{\bar{\xi}_\alpha}{r}\, dr\, d\phi + \int_{\phi_3}^{\phi_2} '\underset{\sim}{\psi} \int_{R_1(\phi)}^{R_3(\phi)} \frac{\bar{\xi}_\alpha}{r}\, dr\, d\phi \qquad (4.7.28)$$

where $\bar{\xi}_\alpha$ is given by expression (4.7.12) and

$$R_\alpha(\phi) = -\frac{2A|{}^{\gamma}\xi_\alpha|}{b_\alpha \cos\phi + a_\alpha \sin\phi} \quad . \qquad (4.7.29)$$

Note that ${}^{\gamma}\xi_\alpha$ is still the value of the interpolation function at the singular point γ and that expression (4.7.13) is not valid any more.

Since the tensors ε^*_{jki} and $\varepsilon^*_{ijk\ell}$ (Kelvin) can be cast into the form presented in (4.7.10) and (4.7.20), the same integration

scheme was here applied for the initial stress formulation.

With reference to the half-plane formulations, it has been shown that the complementary part of the expressions present no singularities when $c > 0$. Consequently, simple quadrature formulae can be used for the corresponding domain integrals. Herein, seven points Hammer's formula has been applied, but this number of points can be increased or reduced if necessary. The limiting case $c = 0$ has been seen to produce singularities of the same order as those present in Kelvin's, therefore the two parts of the fundamental solution are added up and the integrals are properly computed using the same integration scheme (semi-analytical) normally employed for the Kelvin part.

CHAPTER 5

ELASTOPLASTIC BOUNDARY ELEMENT ANALYSIS

5.1 Introduction

In this chapter the boundary element equations presented in the last chapter are employed to solve problems concerned with the inviscid or classical theory of plasticity. An application of the initial strain equations for incompressible plastic strains is first introduced in conjunction with the von Mises yield criterion and Mendelson's successive elastic solutions method [63]. This simple solution technique, also called "elastic predictor - radial corrector method" by Schreyer et al. [92], has proved to be very efficient and stable with reference to the load increment size. The initial stress equations, on the other hand, are more general and are here implemented to handle four different yield criteria (Tresca, Mises, Mohr-Coulomb and Drucker-Prager), with two different iterative routines. The first is a pure incremental technique comparable to what was used by Zienkiewicz et al. [93] for finite elements. The second deals with accumulated values of the initial stresses in a similar fashion to the initial strain implementation.

Several examples are presented to illustrate the applicability of boundary elements to elastoplastic problems and these also include some geotechnical problems solved by using the half-plane fundamental solution.

5.2 Some Simple Elastoplastic Relations

In Section 2.3 of Chapter 2 it was demonstrated that uniaxial

plastic behaviour is only possible if the yield criterion given by expression (2.3.13) is satisfied. Such expression is repeated here for completeness

$$F(\sigma, k) = \sigma - \sigma_o = 0 \ . \tag{5.2.1}$$

This yield condition was seen to be valid to describe uniaxial yield behaviour. For general stress states this sort of representation is generalized to handle any possible combination of stresses. In the present section, only the von Mises yield criterion will be considered and this can be written as follows [60 - 64, 68 - 71]

$$F(\sigma_{ij}, k) = \sqrt{3J_2} - \sigma_o = 0 \tag{5.2.2}$$

where J_2 is the second invariant of the stress deviator tensor (see Chapter 2 expression (2.2.15)) and as before k is a hardening parameter representing the total plastic work, i.e.

$$k = W^p = \int \sigma_{ij} \, d\varepsilon^p_{ij} \ . \tag{5.2.3}$$

As discussed before, plasticity is a path dependent phenomenon, therefore, it becomes necessary to compute the differentials or increments of plastic strain throughout the loading history and then obtain the accumulated strains by integration or summation. A suitable relation for the determination of the plastic strain increments is given by the well-known Prandtl-Reuss equations [60, 61, 63]

$$d\varepsilon^p_{ij} = S_{ij} \, d\lambda \tag{5.2.4}$$

where $d\lambda$ is a proportionality factor which may vary throughout the loading history, but is always positive.

In addition, it is convenient to define an equivalent or effective stress and an equivalent or effective plastic strain increment as

$$\sigma_e = \sqrt{3J_2} \tag{5.2.5}$$

and

$$d\varepsilon^p_e = \sqrt{\frac{2}{3}\, d\varepsilon^p_{ij}\, d\varepsilon^p_{ij}} \quad . \tag{5.2.6}$$

Note that for the uniaxial case presented in Section 2.3 $\sigma_e = \sigma$ and $d\varepsilon^p_e = d\varepsilon^p$. Moreover, the von Mises yield criterion can now be written as

$$\sigma_e - \sigma_o = 0 \tag{5.2.7}$$

which is entirely equivalent to expression (5.2.1).

With reference to equation (5.2.4) it is seen that the proportionality factor $d\lambda$ can be expressed in terms of the equivalent forms σ_e and $d\varepsilon^p_e$ if we square both sides of the equation as follows

$$d\varepsilon^p_{ij}\, d\varepsilon^p_{ij} = S_{ij}\, S_{ij}\, d\lambda^2 \tag{5.2.8}$$

which leads to

$$\left(\frac{3}{2}\, d\varepsilon^p_e\right)^2 = (\sigma_e\, d\lambda)^2 \tag{5.2.9}$$

or

$$d\lambda = \frac{3}{2}\,\frac{d\varepsilon^p_e}{\sigma_e} \quad . \tag{5.2.10}$$

For the initial strain implementaiton of the boundary element technique, the plastic strain increments were computed by using the

above expressions as follows [63]; let us assume that a loading path is found to reach a given state of stresses and accumulated plastic strains ε^p_{ij}. When the load is increased by a small amount, the additional plastic strains produced are $\Delta\varepsilon^p_{ij}$ and the total strains are given by

$$\varepsilon_{ij} = \varepsilon^e_{ij} + \varepsilon^p_{ij} + \Delta\varepsilon^p_{ij} \tag{5.2.11}$$

where ε^e_{ij} already includes the current load increment.

It is now convenient to define a modified total strain tensor of the form

$$\varepsilon'_{ij} = \varepsilon_{ij} - \varepsilon^p_{ij} \tag{5.2.12}$$

or

$$\varepsilon'_{ij} = \frac{1}{2G}\left(\sigma_{ij} - \frac{\nu}{1+\nu}\,\sigma_{kk}\,\delta_{ij}\right) + \Delta\varepsilon^p_{ij} \tag{5.2.13}$$

where expression (5.2.13) is simply (see expression (2.2.28))

$$\varepsilon'_{ij} = \varepsilon^e_{ij} + \Delta\varepsilon^p_{ij} \quad . \tag{5.2.14}$$

Expression (5.2.13) can also be written in deviatoric form as follows (note that $\Delta\varepsilon^p_{kk} = 0$)

$$e'_{ij} = \frac{S_{ij}}{2G} + \Delta\varepsilon^p_{ij} \tag{5.2.15}$$

in which

$$e'_{ij} = \varepsilon'_{ij} - \frac{\delta_{ij}}{3}\,\varepsilon'_{kk} \quad . \tag{5.2.16}$$

Recalling the Prandtl-Reuss equations given by (5.2.4), expression (5.2.15) yields

$$e'_{ij} = \left(1 + \frac{1}{2G\ \Delta\lambda}\right) \Delta\varepsilon^{p}_{ij} \quad . \tag{5.2.17}$$

By squaring both sides of (5.2.17) in a similar fashion to what was done for expressions (5.2.8) to (5.2.10), the following relation arises

$$1 + \frac{1}{2G\ \Delta\lambda} = \frac{\varepsilon_{et}}{\Delta\varepsilon^{p}_{e}} \tag{5.2.18}$$

where

$$\varepsilon_{et} = \sqrt{\frac{2}{3}\ e'_{ij}\ e'_{ij}} \quad . \tag{5.2.19}$$

Substituting (5.2.18) into (5.2.17) gives

$$\Delta\varepsilon^{p}_{ij} = \frac{\Delta\varepsilon^{p}_{e}}{\varepsilon_{et}}\ e'_{ij} \ . \tag{5.2.20}$$

From the above equation it is seen that in order to determine the actual magnitudes of the plastic strain increments, the equivalent plastic strain increment must be determined. Therefore, substituting the proportionality factor $\Delta\lambda$ given by (5.2.10) into expression (5.2.18) comes

$$1 + \frac{\sigma_e}{3G\ \Delta\varepsilon^{p}_{e}} = \frac{\varepsilon_{et}}{\Delta\varepsilon^{p}_{e}} \tag{5.2.21}$$

which gives

$$\Delta\varepsilon^{p}_{e} = \varepsilon_{et} - \frac{\sigma_e}{3G} \quad . \tag{5.2.22}$$

Since the condition expressed in (5.2.7) must be satisfied throughout the plastic process, σ_e can be substituted by σ_o in equation (5.2.22)

$$\Delta\varepsilon_e^p = \varepsilon_{et} - \frac{\sigma_o}{3G} \quad . \tag{5.2.23}$$

Note that σ_o corresponds to the uniaxial yield stress after the application of the current load increment, consequently, it is still unknown. This term, however, can be approximated by a truncated Taylor series about the preceeding value of σ_o (i.e., before the load increment is applied) as follows

$$^{k}\sigma_o = {}^{k-1}\sigma_o + {}^{k-1}H' \; \Delta\varepsilon_e^p + \ldots \tag{5.2.24}$$

where H' has been defined in Chapter 2, Section 2.3.

Substituting (5.2.24) into (5.2.23) and solving for $\Delta\varepsilon_e^p$ comes finally

$$\Delta\varepsilon_e^p = \frac{3G\,\varepsilon_{et} - \sigma_o}{3G + H'} \tag{5.2.25}$$

where the values of σ_o and H' are computed before the load increment.

The equations discussed here have been presented for the general 3-D case. For 2-D problems these equations are properly modified to account for plane strain or plane stress as indicated in Appendix D. This allows one to work with accumulated values of tractions, displacements and stresses in equations (4.6.14) and (4.6.17). Equation (4.6.14)can now be written as

$$\underset{\sim}{y} = \underset{\sim}{K}(\underset{\sim}{\varepsilon}^p + \Delta\underset{\sim}{\varepsilon}^p) + \underset{\sim}{m} \tag{5.2.26}$$

and equation (4.6.17)

$$\underset{\sim}{\sigma} = \underset{\sim}{B}(\underset{\sim}{\varepsilon}^p + \Delta\underset{\sim}{\varepsilon}^p) + \underset{\sim}{n} \tag{5.2.27}$$

where $\underset{\sim}{\varepsilon}^p$ represents the accumulated plastic strains up to (but not including) the corresponding to the current load increment $\Delta\underset{\sim}{\varepsilon}^p$ which are to be determined iteratively.

5.3 Initial Strain - Numerical Solution Technique

With reference to equations (5.2.26) and (5.2.27) one notices that vector $\underset{\sim}{m}$ represents the elastic solution to the boundary problem (tractions and displacements unknown) and that vector $\underset{\sim}{n}$ stands for the corresponding stresses. Therefore, load at first yield can be calculated by taking the most highly stressed boundary node or internal point and comparing its equivalent stress σ_e^{MAX} with the uniaxial yield stress of the material. The incremental process starts by reducing this stress value with a load factor defined as follows

$$\lambda_o = \frac{\sigma_o}{\sigma_e^{MAX}} \quad . \tag{5.3.1}$$

The load increment is then calculated and further values of the load factor are given by

$$\lambda_i = \lambda_{i-1} + \beta \tag{5.3.2}$$

where $\beta = \lambda_o \omega$; ω being the given value of the load increment with reference to load at first yield.

Equations (5.2.26) and (5.2.27) are now written as

$$\underset{\sim}{y} = \underset{\sim}{K}(\underset{\sim}{\varepsilon}^p + \Delta\underset{\sim}{\varepsilon}^p) + \lambda_i \underset{\sim}{m} \tag{5.3.3}$$

and

$$\underset{\sim}{\sigma} = \underset{\sim}{B}(\underset{\sim}{\varepsilon}^p + \Delta\underset{\sim}{\varepsilon}^p) + \lambda_i \underset{\sim}{n} \quad . \tag{5.3.4}$$

For a given value of λ_i , the plastic strain increment is determined iteratively at each selected boundary node and internal stress point as follows:

a) Compute stress (eqn. (5.3.4))

b) Calculate :

ε'_{ij} (eqn. (5.2.13))

ε_{et} (eqn. (5.2.19))

$\Delta\varepsilon^p_e \geq 0$ (eqn. (5.2.25))

c) Verify convergence, i.e.

Compare $\Delta\varepsilon^p_e$ calculated with its previous value.

d) Compute new estimate of $\Delta\varepsilon^p_{ij}$ (eqn. (5.2.20)).

e) Continue with next node or point and start with (b) until all nodes and points have been considered.

f) Go to a) for a new iteration.

Once convergence is obtained (within prescribed tolerance) for all selected nodes and points, $\Delta\underset{\sim}{\varepsilon}^p$ is added to $\underset{\sim}{\varepsilon}^p$ and its value is also used as an initial guess for the next load increment.

Note that for the whole incremental-iterative process to take place, only equation (5.3.4) is required. Equation (5.3.3) being used only once convergence is achieved and if boundary unknowns are requested by the user. Furthermore, matrices $\underset{\sim}{K}$ and $\underset{\sim}{B}$ as well as vectors $\underset{\sim}{m}$ and $\underset{\sim}{n}$ are generated only once at the beginning of the entire process, which represents a great saving in computer time.

5.4 Examples - Initial Strain Formulation

To outline the applicability of the formulation described in the previous sections, some examples were run and results have been compared with finite element and experimental analyses. Also, whenever possible, analytical solutions are included for checking the results.

5.4.1 Perforated Aluminium Strip - This plane stress problem (figure 5.4.1) is perhaps the most classical plasticity example and has been used to assess several alternative formulations.

Material parameters are as follows

$E = 7000.\ kg/mm^2$

$Y = 24.3\ kg/mm^2$

$H' = 0.032E$

$\nu = 0.2.$

Figure 5.4.1 shows the discretization used in this analysis. It is worth noting that the internal cells were confined to the region where plastic strains were predicted. This is a feature unique to BEM.

A comparison between experimental stresses obtained by Theocaris and Marketos [94] and the stresses obtained in the present analysis at the centre section is given in figure 5.4.2 for $\sigma_a = 11.5\ kg/mm^2$. Although computed stresses slightly differ near the hole, the results compare well with other plasticity formulations (e.g., see [95]). Plastic points for various values of $2\sigma_a/Y$ are shown in figure 5.4.3 together with the finite element plastic zones presented by Zienkiewicz and Cormeau [96] obtained by use of the mesh shown in figure 5.4.4.

5.4.2 Polystyrene Crazing Problem - In order to study the effect of voids in polystyrene strength, this example was run by Haward and Owen [97] using the finite element method. The geometry of the problem is given in figure 5.4.5 where boundary element and internal cell discretization is also shown. For the present comparison, plane strain

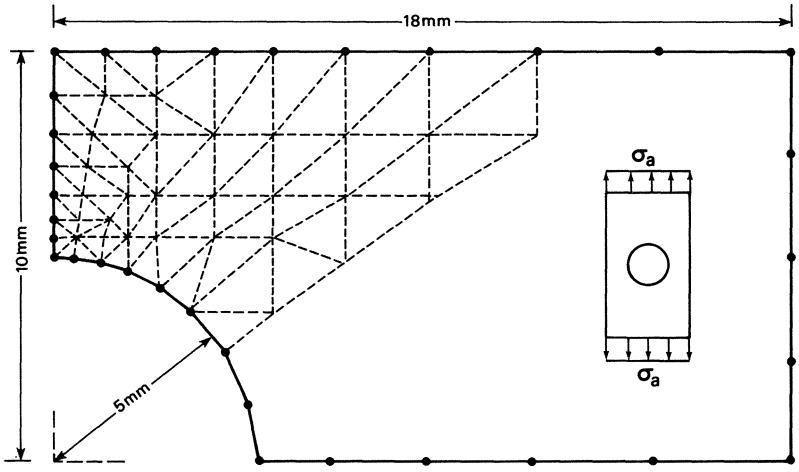

Fig. 5.4.1 Perforated aluminium strip. Boundary element and internal cell discretization.

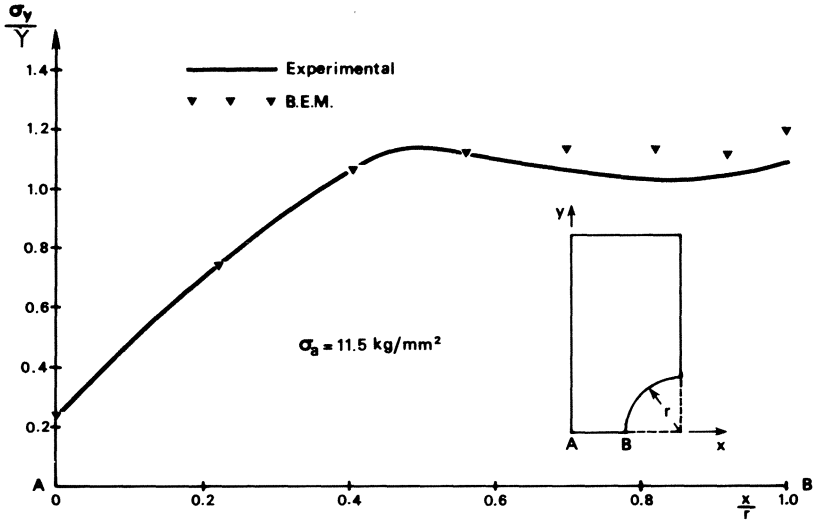

Fig. 5.4.2 Experimental and computed stresses (σ_y) at root of perforated aluminium strip.

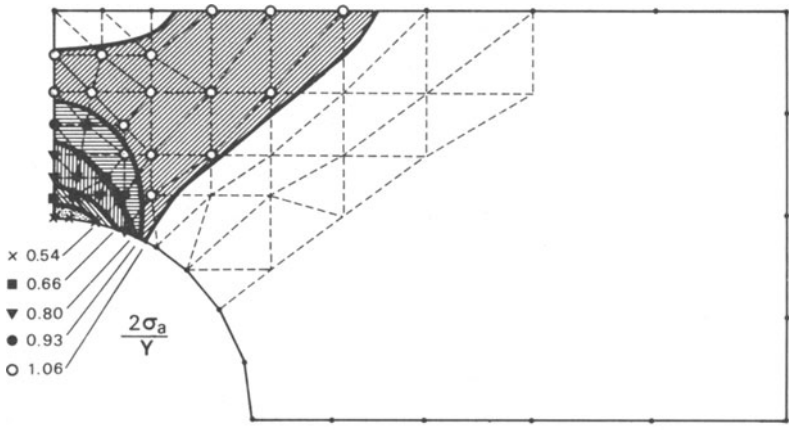

Fig. 5.4.3 Plastic points obtained by BEM and plastic zones obtained by FEM for various values of $2\sigma_a/Y$.

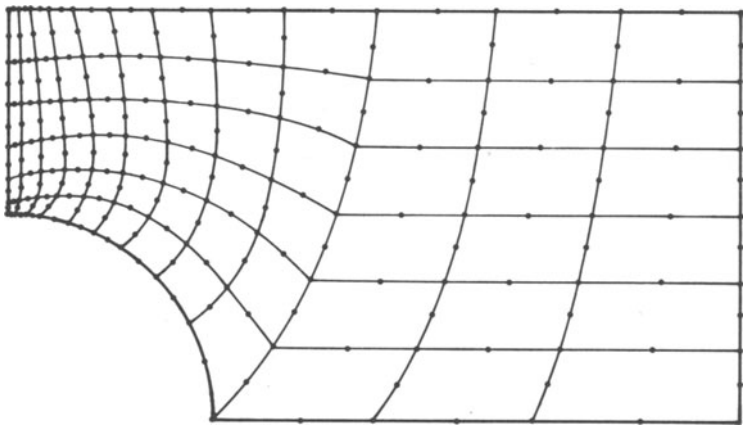

Fig. 5.4.4 Quadratic isoparametric finite element mesh used for perforated strip problem.

approximation was used in both FEM and BEM analyses, the former using quadratic isoparametric elements as depicted in figure 5.4.6.

Ideal plasticity was assumed with

$E = 42. \times 10^3$ MN/m^2

$\sigma_o = Y = 105.$ MN/m^2

$\nu = 0.33.$

Two loading conditions were considered. biaxial tension and uniaxial tension, both applied by prescribing displacements at the edges.

Figure 5.4.7a and b shows the results obtained by both programs for the two loading cases. As can be seen, agreement between the different formulations has been obtained.

5.4.3 Plane Strain Punch - This example consists of a rigid flat punch indented into a solid plane strain specimen (see figure 5.4.8). Finite element solutions with different material parameters were presented by Nayak and Zienkiewicz [98]. Boundary element results were calculated with the discretization shown in figure 5.4.8 (no boundary elements along symmetry axes) and by incrementing the rigid punch displacements.

For this comparison two different material properties were used; ideal plasticity (H' = 0) and strain softening (H' = - 0.1E). Mean pressure - displacement curves shown in figure 5.4.9 exhibit close agreement between finite element and boundary element results, despite the rather coarse discretization employed for the boundary element solution.

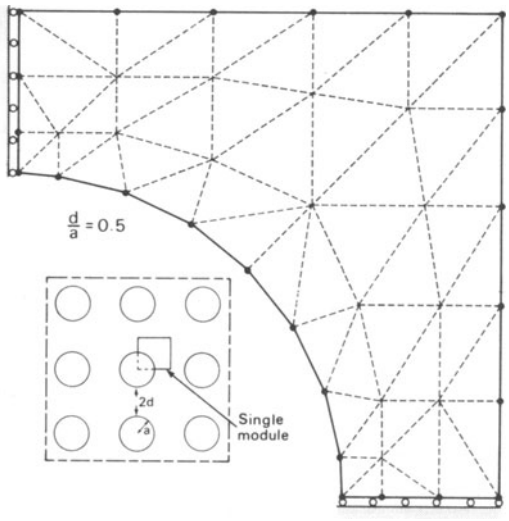

Fig. 5.4.5 Two dimensional cylindrical void model and discretization used for BEM.

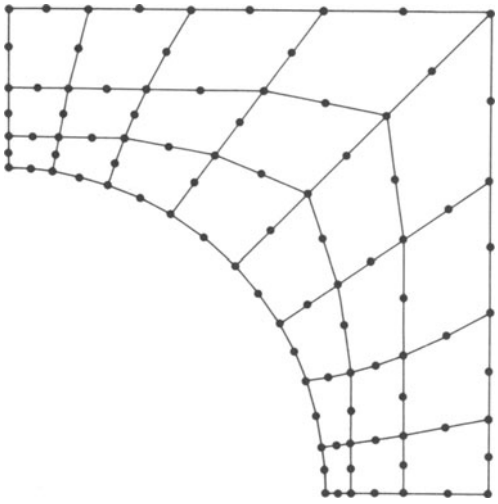

Fig. 5.4.6 Quadratic isoparametric finite element mesh used for polystyrene crazing problem.

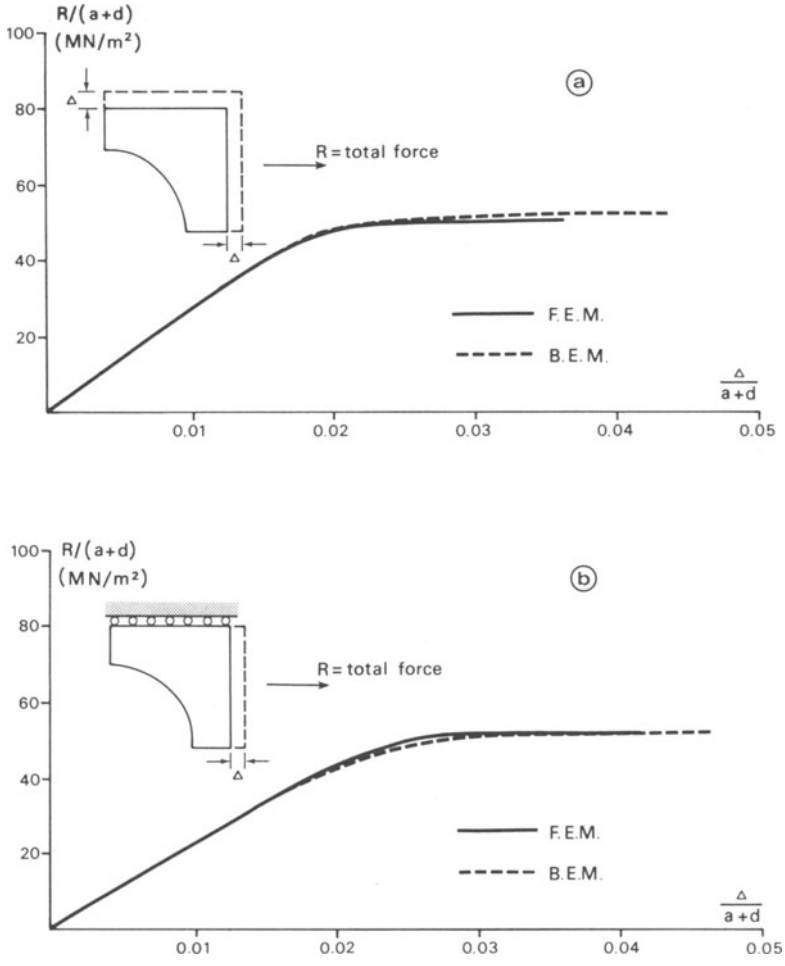

Fig. 5.4.7 Mean stress-strain curves for polystyrene crazing problem.

(a) biaxial tension

(b) uniaxial tension (fixed edge)

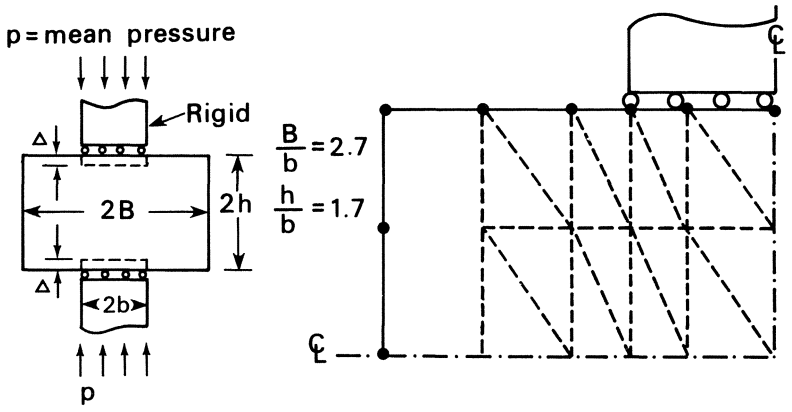

Fig. 5.4.8 Plane strain punch problem. Boundary element and internal cell discretization.

Plastic zones obtained for the strain softening case using FEM and the mesh shown in figure 5.4.10a. agree reasonably well with BEM plastified points as shown in figure 5.4.10b.

5.4.4 Thick Cylinder - In this example the plane strain expansion of a thick cylinder subjected to internal pressure is studied. Ideal plasticity is assumed with the following material parameters

$E = 12000.\ dN/mm^2$

$\sigma_o = 24.\ dN/mm^2$

$\nu = 0.3.$

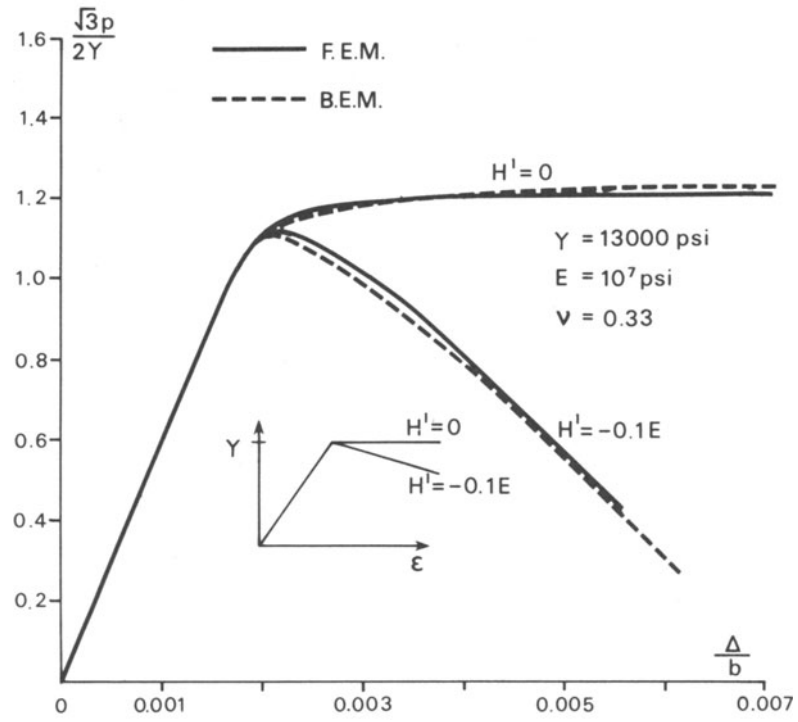

Fig. 5.4.9 Mean pressure-displacement curves for plane strain punch problem.

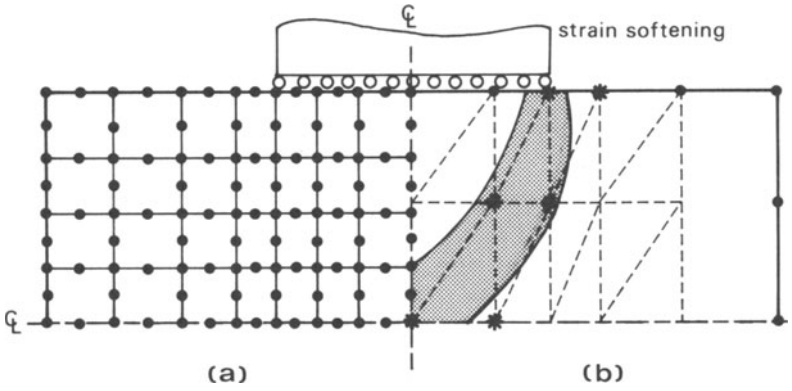

Fig. 5.4.10 Plane strain punch problem. (a) quadratic isoparametric finite element mesh. (b) comparison between plastic zones obtained by FEM and plastified points obtained by BEM (Δ/b = 0.0052)

Boundary element results computed without boundary discretization of the symmetry axes (see figure 5.4.11), are here compared with the analytical solution produced by Hodge and White [62].

Radial displacements over the outer boundary and circumferential stress distribution (plastic front at $r' = 1.6a$) exhibit good agreement with the analytical solution as shown in figure 5.4.12 and 5.4.13 respectively.

The applications shown in the present section clearly indicate the potentiality of boundary elements for solving plasticity problems. In all the examples the load increment was kept between 5% to 25% of the load at first yield and it was verified that the successive elastic solutions procedure employed is very stable with reference to the load increment size. Consequently, this procedure is recommended for Mises material problems. In the next section the stress-strain relations will be presented in a more general form and different yield criteria will be included for the initial stress implementation.

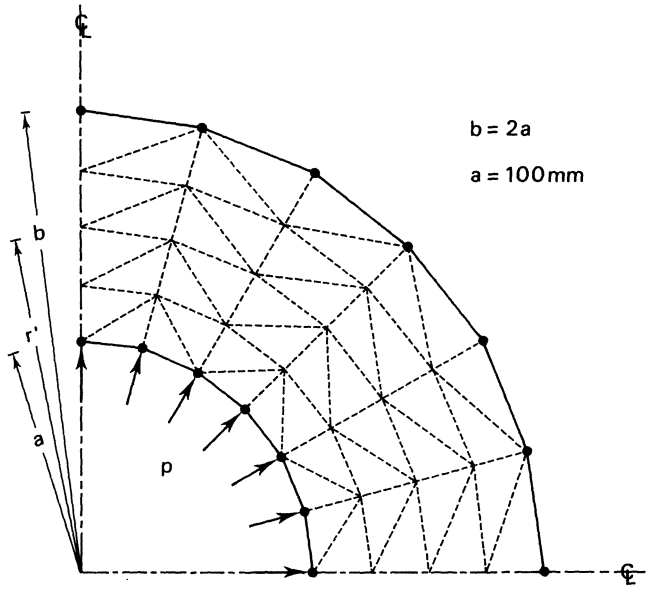

Fig. 5.4.11 Thick cylinder problem. Boundary element and internal cell discretization.

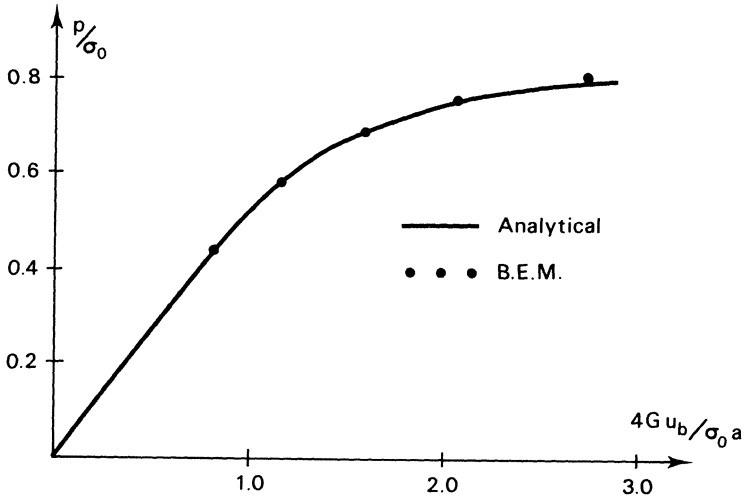

Fig. 5.4.12 Outer surface displacements for thick cylinder problem.

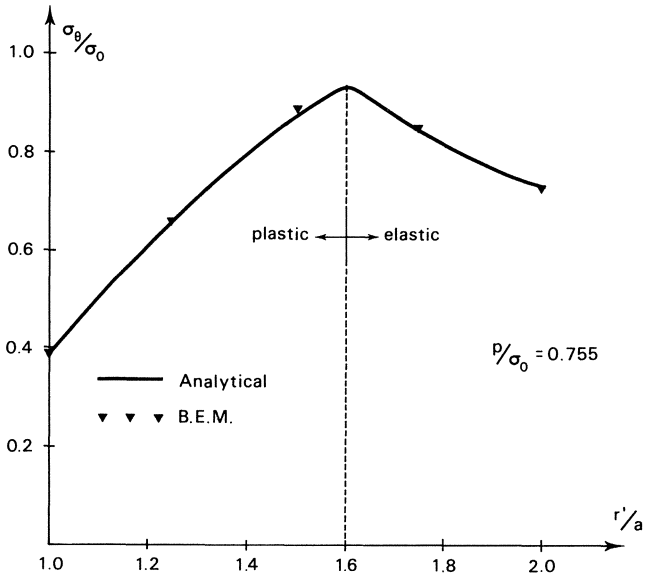

Fig. 5.4.13 Circumferential stress distribution in thick cylinder. Plastic front at r' = 1.6a.

5.5 General Elastoplastic Stress-Strain Relations

For the formulation of a theory which models elastoplastic material deformation, three requirements have to be met, these are:

a) Explicit elastic relationship between stress and strain before the onset of plastic deformation.

b) A yield criterion indicating the stress level at which plastic flow commences.

c) Relationship between stress and strain for post yield behaviour.

Requirement (a) has been thoroughly discussed in Chapter 2, Section 2.2. Therefore only (b) and (c) will be considered here.

The yield criterion for isotropic hardening can be written in general form as

$$F(\sigma_{ij}, k) = 0 \qquad (5.5.1)$$

where k is the work hardening parameter (see expression (5.2.3)) that gives the instantaneous position of the yield surface in the n-dimensional stress space.

On physical grounds, one can notice that the yield criterion to be independent of the orientation of the coordinate system employed, should be a function of the three stress invariants. It is common to represent two of these invariants as functions of the deviatoric stresses (see Chapter 2)

$$I_1 = \sigma_{kk}$$

$$J_2 = \frac{1}{2} S_{ij} S_{ij} \qquad (5.5.2)$$

$$J_3 = \frac{1}{3} S_{ij} S_{jk} S_{ki} \cdot$$

In the present work, instead of J_3 the alternative stress invariant α, known as the Lode angle [76] was used. This invariant has been introduced in Section 2.2 and is given by

$$-\frac{\pi}{6} \leq \alpha = \frac{1}{3} \sin^{-1}\left[-\frac{3\sqrt{3}}{2}\frac{J_3}{J_2^{3/2}}\right] \leq \frac{\pi}{6} \qquad (5.5.3)$$

By using these stress invariants, different yield criteria can be applied, such as [76]

Tresca :

$$2\sqrt{J_2}\cos\alpha - \sigma_o = 0 \qquad (5.5.4)$$

Von Mises :

$$\sqrt{3J_2} - \sigma_o = 0 \qquad (5.5.5)$$

Mohr-Coulomb :

$$\frac{I_1}{3}\sin\phi' + \sqrt{J_2}(\cos\alpha - \frac{1}{\sqrt{3}}\sin\alpha\sin\phi') - c'\cos\phi = 0 \qquad (5.5.6)$$

in which ϕ' is the angle of internal friction and c' is the cohesion of the material.

Drucker-Prager :

$$\alpha' I_1 + \sqrt{J_2} - K' = 0 \qquad (5.5.7)$$

where

$$\alpha' = \frac{2\sin\phi'}{\sqrt{3}(3-\sin\phi')} \quad ; \quad K' = \frac{6c'\cos\phi'}{\sqrt{3}(3-\sin\phi')} \quad . \tag{5.5.8}$$

Mohr-Coulomb hypothesis may be simulated by the Druker-Prager criterion in plane strains if α' and K' are written as [99]

$$\alpha' = \frac{\tan\phi'}{(9+12\ \tan^2\phi')^{\frac{1}{2}}} \quad ; \quad K' = \frac{3c'}{(9+12\ \tan^2\phi')^{\frac{1}{2}}} \quad . \tag{5.5.9}$$

For our practical purposes, equation (5.5.1) can then be written as

$$F(\sigma_{ij}, k) = f(\sigma_{ij}) - \psi(k) = 0 \tag{5.5.10}$$

where one can notice that $f(\sigma_{ij})$ is a scalar function of σ_{ij} which plays the role of an equivalent stress here designated by σ_e. As a consequence, we can define an equivalent plastic strain ε_e^p whose increment produces an increment in the plastic strain energy as follows

$$\sigma_e\, d\varepsilon_e^p = \sigma_{ij}\, d\varepsilon_{ij}^p = dk \quad . \tag{5.5.11}$$

Note that for the von Mises criterion $d\varepsilon_e^p$ defined above is given by expression (5.2.6).

In order to obtain the stress-strain relations for post yield behaviour, let us first rewrite equation (2.4.5) of Chapter 2 in incremental form

$$d\sigma_{ij} = C_{ijk\ell}\,(d\varepsilon_{k\ell} - d\varepsilon_{k\ell}^p) \quad . \tag{5.5.12}$$

Within the context of associated plasticity, the flow rule also known as normality principle [60, 68, 69], can be described by

$$d\varepsilon^{p}_{ij} = d\lambda \frac{\partial F}{\partial \sigma_{ij}} \tag{5.5.13}$$

where $d\lambda$ is a proportionality factor, termed the plastic multiplier. It should be pointed out that here the Prandtl-Reuss equations can also be simulated for the von Mises criterion, $d\lambda$ however would not be represented by expression (5.2.10) any more.

The substitution of (5.5.13) into (5.5.12) gives

$$d\sigma_{ij} = C_{ijk\ell}(d\varepsilon_{k\ell} - a_{k\ell}\, d\lambda) \tag{5.5.14}$$

in which

$$a_{k\ell} = \frac{\partial F}{\partial \sigma_{k\ell}} = \frac{\partial f}{\partial \sigma_{k\ell}} \tag{5.5.15}$$

When plastic yielding is occurring the stresses satisfy equation (5.5.10) which by differentiating gives

$$dF = a_{ij}\, d\sigma_{ij} - \frac{d\psi}{dk}\, dk = 0 \tag{5.5.16}$$

or, according to (5.2.3)

$$a_{ij}\, d\sigma_{ij} - \frac{d\psi}{dk}\, \sigma_{ij}\, d\varepsilon^{p}_{ij} = 0 \quad . \tag{5.5.17}$$

From the application of the normality principle to equation (5.5.17) results

$$a_{ij}\, d\sigma_{ij} - \frac{d\psi}{dk}\, \sigma_{ij}\, a_{ij}\, d\lambda = 0 \quad . \tag{5.5.18}$$

If we substitute (5.5.14) into the above equation and solve for $d\lambda$ comes

$$d\lambda = \frac{1}{\gamma} a_{ij}\, C_{ijk\ell}\, d\varepsilon_{k\ell} \tag{5.5.19}$$

where

$$\gamma' = a_{ij}\, C_{ijk\ell}\, a_{k\ell} + \frac{d\psi}{dk}\, \sigma_{ij}\, a_{ij} \ . \tag{5.5.20}$$

Before we go further the last term in expression (5.5.20) can be examined. It is easy to show that $f(\sigma_{ij})$ is a homogeneous function of degree one and this allows the application of Euler's theorem [80] as follows

$$\sigma_{ij} \frac{\partial f}{\partial \sigma_{ij}} = f(\sigma_{ij}) = \sigma_e \ . \tag{5.5.21}$$

The substitution of (5.5.21) and (5.5.11) into (5.5.20) yields

$$\gamma' = a_{ij}\, C_{ijk\ell}\, a_{k\ell} + \frac{d\psi}{d\varepsilon^p_e} \tag{5.5.22}$$

where $d\psi/d\varepsilon^p_e = H'$ if ψ is defined as the uniaxial yield stress.

Equation (5.5.19) can now be used to substitute $d\lambda$ in (5.5.14) providing the required incremental stress-strain relations

$$d\sigma_{ij} = C^{ep}_{ijk\ell}\, d\varepsilon_{k\ell} \tag{5.5.23}$$

in which

$$C^{ep}_{ijk\ell} = C_{ijk\ell} - \frac{1}{\gamma'} C_{ijmn}\, a_{mn}\, a_{op}\, C_{opk\ell} \ . \tag{5.5.24}$$

For the application of the above relations to the initial stress formulation, a further modification has proved to be convenient. Let us adopt the following notation (see expression (4.2.11))

$$d\sigma^e_{ij} = C_{ijk\ell}\, d\varepsilon_{k\ell} \tag{5.5.25}$$

where $d\sigma^e_{ij}$ stands for the components of the elastic stress increments (i.e., these represent the stress increment values as if a pure elastic problem were being solved).

Equation (5.5.23) can then be written in the following form

$$d\sigma_{ij} = d\sigma^e_{ij} - \frac{1}{\gamma'} C_{ijmn}\, a_{mn}\, a_{k\ell}\, d\sigma^e_{k\ell} \tag{5.5.26}$$

which means that the true stresses can be computed from the corresponding elastic stresses in incremental form. In addition to this, the increments of initial stress presented in Chapter 2 equation (2.4.7) can also be calculated by the relation

$$d\sigma^p_{ij} = d\sigma^e_{ij} - d\sigma_{ij} = \frac{1}{\gamma'} C_{ijmn}\, a_{mn}\, a_{k\ell}\, d\sigma^e_{k\ell} \tag{5.5.27}$$

where $d\sigma^p_{ij}$ corresponds to $d\sigma^a_{ij}$ with $d\varepsilon^a_{ij} = d\varepsilon^p_{ij}$.

All the expressions presented in this section are valid for the 3-D case. For 2-D problems the reader is referred to Appendix D for further details.

By simply examining equation (2.4.6) we notice that equation (4.6.11) can be applied for the computation of $d\sigma^e_{ij}$ if matrix $\underset{\sim}{E}'$ is replaced by

$$\bar{\underset{\sim}{E}} = \underset{\sim}{E}' + \underset{\sim}{I} \tag{5.5.28}$$

where $\underset{\sim}{I}$ is the identity matrix. This gives

$$d\underset{\sim}{\sigma}^e = \underset{\sim}{G}'\, d\underset{\sim}{p} - \underset{\sim}{H}'\, d\underset{\sim}{u} + \underset{\sim}{Q}^*\, d\underset{\sim}{\sigma}^p \tag{5.5.29}$$

in which

$$\underset{\sim}{Q}^* = \underset{\sim}{Q}' + \bar{\underset{\sim}{E}} \ . \tag{5.5.30}$$

Finally, it is worth mentioning that the problem of indeterminacy of the normality principle (see eqn. (5.5.13)) at the so-called "corners" of the yield surface (typical of Tresca and Mohr-Coulomb surfaces) has been overcome by adopting the simple procedure indicated in [98]. This consists of "rounding off" the corners whenever $|\alpha| > \left(\frac{\pi}{6} - \frac{\pi}{180}\right)$ and consequently avoids the singularity which occurs when $|\alpha| = \frac{\pi}{6}$.

5.6 Initial Stress- Outline of Solution Techniques

In order to minimize the computer effort for the initial stress formulation, equations (4.6.10) and (5.5.29) can be further manipulated as discussed in Section 4.6. This leads to

$$d\underset{\sim}{y} = \underset{\sim}{R}\, d\underset{\sim}{\sigma}^{p} + d\underset{\sim}{m} \tag{5.6.1}$$

and

$$d\underset{\sim}{\sigma}^{e} = \underset{\sim}{S}\, d\underset{\sim}{\sigma}^{p} + d\underset{\sim}{n} \tag{5.6.2}$$

where

$$\underset{\sim}{R} = \underset{\sim}{A}^{-1}\, \underset{\sim}{Q} \tag{5.6.3}$$

and

$$\underset{\sim}{S} = \underset{\sim}{Q}^{*} - \underset{\sim}{A}'\, \underset{\sim}{R}\ . \tag{5.6.4}$$

Note that as before vectors $d\underset{\sim}{m}$ and $d\underset{\sim}{n}$ represent the elastic solution to the incremental problem (actual solution in absence of plasticity). Furthermore, equations (5.6.1) and (5.6.2) remain valid if instead of incremental loading, the total load is applied. The only reason to proceed incrementally being the constitutive equations presented in (5.5.23). This enables us to compute load at first yield by simply scaling down the total elastic solution by a load factor λ_o. The incremental process starts at this load level and further values of the load factor are given by expression (5.3.2) of Section 5.3.

For elastoplastic solutions, equations (5.6.1) and (5.6.2) can therefore be applied as

$$\underset{\sim}{y} = \underset{\sim}{R}(\underset{\sim}{\sigma}^{p} + \Delta\underset{\sim}{\sigma}^{p}) + \lambda_i \underset{\sim}{m} \tag{5.6.5}$$

and

$$\underset{\sim}{\sigma}^{e} = \underset{\sim}{S}(\underset{\sim}{\sigma}^{p} + \Delta\underset{\sim}{\sigma}^{p}) + \lambda_i \underset{\sim}{n} \tag{5.6.6}$$

or alternatively for pure incremental relations,

$$\Delta\underset{\sim}{y} = \underset{\sim}{R}\ \Delta\underset{\sim}{\sigma}^{p} + \beta\ \underset{\sim}{m} \tag{5.6.7}$$

and

$$\Delta\underset{\sim}{\sigma}^{e} = \underset{\sim}{S}\ \Delta\underset{\sim}{\sigma}^{p} + \beta\ \underset{\sim}{n} \tag{5.6.8}$$

where in both cases vectors $\underset{\sim}{m}$ and $\underset{\sim}{n}$ correspond to the application of the total load and $\Delta\underset{\sim}{\sigma}^{p}$ stands for the current initial stress increment.

For a typical load increment (i.e., a given value of λ_i), the initial stress increment can be determined iteratively at each selected boundary node and internal point exhibiting plastic behaviour by two different processes. The former is in fact a pure incremental procedure. Once the load increment $\beta\underset{\sim}{n}$ has been applied, the initial stress increment corresponding to the solution of the elastic problem is computed and has to be applied back into the body, providing an elastic stress redistribution. This operation, again generates a new initial stress field to be redistributed elastically and so on. Iteration is halted when the contribution of the last initial stress increment can be neglected.

The above process is in essence comparable to what was presented in [93] for the finite element method and is summarized as follows:

a) Compute elastic stress increment by;

eqn. (5.6.8) if first iteration is being performed or

$\Delta\underset{\sim}{\sigma}^{e} = \underset{\sim}{S}\,\Delta\underset{\sim}{\sigma}^{p}$ otherwise.

b) Find true stress increment $\Delta\sigma_{ij}$ (eqn. (5.5.26)).

c) Verify convergence, i.e.;

compare $\Delta\varepsilon_{e}^{p}$ calculated with its accumulated value obtained during the current load increment to see if it can be neglected.

d) Calculate initial stress increment by;

$\Delta\sigma_{ij}^{p} = \Delta\sigma_{ij}^{e} - \Delta\sigma_{ij}$.

e) Accumulate values of initial stress and true stress;

$\sigma_{ij}^{p} = \sigma_{ij}^{p} + \Delta\sigma_{ij}^{p}$

$\sigma_{ij} = \sigma_{ij} + \Delta\sigma_{ij}$.

f) Continue with next node or point and start with (b) until all nodes and points have been considered.

g) Go to (a) for a new iteration.

Iterations are performed until convergence is obtained (within prescribed tolerance) at every selected node or point.

It is interesting to note that in order to avoid cumulative errors, $\Delta\underset{\sim}{\sigma}^{p}$ obtained at the end of iterations is applied together with $\beta\underset{\sim}{n}$ in eqn. (5.6.8) for the first iteration of the next load increment.

The second process, which proved to be less dependent on the load increment size but not always more economical, deals with

accumulated values of the elastic stress in a similar fashion to the procedure adopted for the initial strain implementation.

The initial stress increment is kept separate from its accumulated value until convergence is obtained as follows:

a) Compute elastic stress (eqn.(5.6.6))

b) Calculate elastic stress increment by;

$$\Delta\sigma^{e}_{ij} = \sigma^{e}_{ij} - \sigma_{ij} - \sigma^{p}_{ij} \ .$$

c) Find true stress increment $\Delta\sigma_{ij}$ (eqn. (5.5.26)).

d) Verify convergence, i.e.;

compare $\Delta\varepsilon^{p}_{e}$ with its previous value.

e) Calculate new estimate of initial stress increment by;

$$\Delta\sigma^{p}_{ij} = \Delta\sigma^{e}_{ij} - \Delta\sigma_{ij} \ .$$

f) Continue with next node or point and start with (b) until all nodes and points have been considered.

Once that convergence is obtained for all selected nodes and points, the true stress and initial stress increments are accumulated and the latter is also used as an initial guess for the next load increment.

Note that neither procedure requires computation of the boundary unknowns. Consequently equation (5.6.5) need only be used to print the boundary unknowns once convergence is achieved. In addition, if the body to be analysed is under an initial (in-situ) stress field, these stresses are simply added to the total stress vector at the beginning of the entire process. In this case load at first yield

cannot be computed by expression (5.3.1) any more, nevertheless any approximated value of λ_o can (provided it corresponds to a pure elastic state) be used to start the incremental process.

Before the application of the above algorithms to solve plasticity problems it should be pointed out that although solution procedures are incremental, always finite sized load increments are prescribed and this may create some drifts of the stress level beyond the yield surface. If load increments are kept sufficiently small this problem is practically eliminated, but if relatively large load increment sizes are to be permitted, special techniques of the type presented in references [98, 92, 100] have been found necessary to maintain the stresses on the yield surface. Basically, such techniques make use of a subincremental procedure which subdivides the increment of elastic stress into a number of subincrements. Consequently, relation (5.5.26) is always applied for small subincrement sizes. Also, once all subincrements have been considered, the satisfaction of equation (5.5.10) is verified and the final excess stress (if any) which still violates the yield criterion is added to the initial stress increment.

5.7 Examples - Kelvin Implementation

Following the solution algorithms presented in the last section, the results for a series of examples solved by the boundary element technique are now compared with analytical solutions where such solutions are available and with finite element results.

5.7.1 Notched Tensile Specimen - This example is one of the very early plasticity problems solved by using the finite element technique. Plane stress and plane strain results have been presented in several papers, creating a good opportunity to compare the boundary element computations.

Material parameters are as follows

$E = 7000.$ kg/mm

$\sigma_o = 24.3$ kg/mm

$\nu = 0.2$

$H' = 0.$ (von Mises yield criterion).

Plane stress analysis was carried out using the discretization shown in figure 5.7.1. Note that symmetry was taken into consideration without boundary discretization of the symmetry axes. This is due to a direct condensation process which automatically integrates over reflected elements and cells in such a way that the size of the final matrices corresponds to the reduced number of boundary elements and internal points presented.

Figure 5.7.2 gives the load-displacement curve for this case. It is seen that the curve remains nearly straight until very close to the limit load, when a sharp bend then occurs. Such behaviour was also observed by Yamada et al. [101] in an entirely similar problem. The limit load achieved by the boundary elements ($2\sigma_a/\sigma_o = 1.21$) coincides with the results presented by Nayak and Zienkiewicz [98] using four different finite elements to analyse the same problem. Their limit load was found to vary between $2\sigma_a/\sigma_o = 1.19 - 1.23$ and simple triangular, isoparametric linear, quadratic and cubic elements were used, all four meshes with approximately 97 nodes.

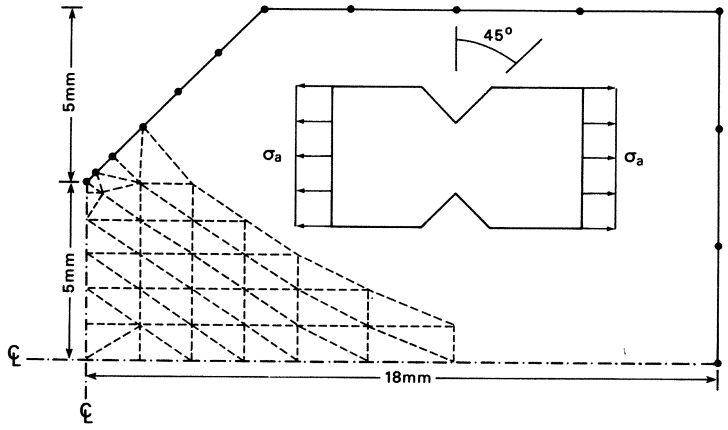

Fig. 5.7.1 Notched tensile specimen. Boundary element and internal cell discretization (plane stress case).

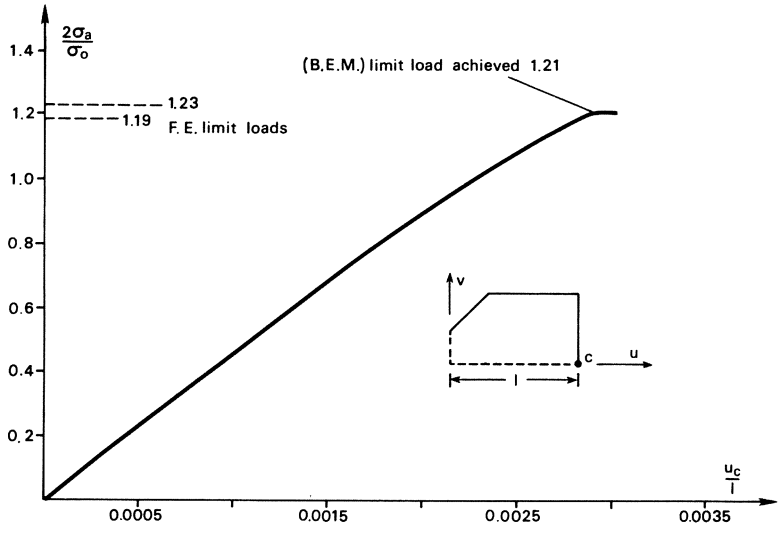

Fig. 5.7.2 Load-displacement curve for notched specimen in plane stress.

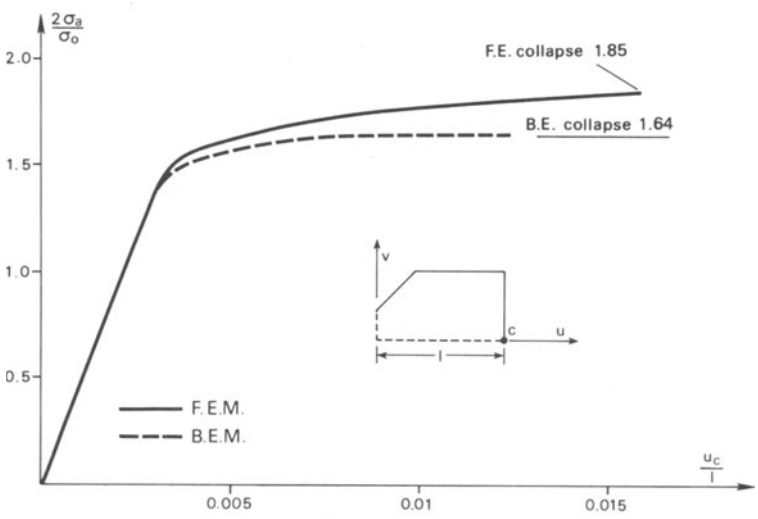

Fig. 5.7.3 Load-displacement curves for notched specimen in plane strain.

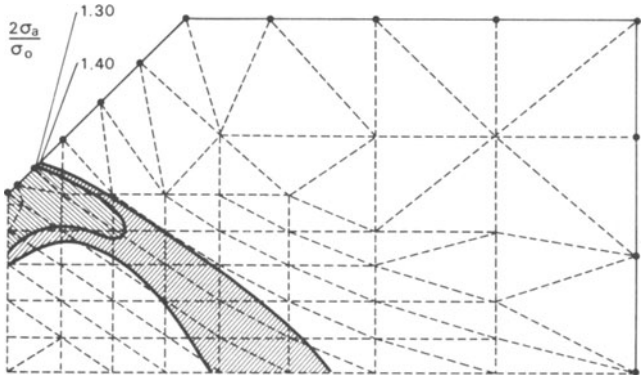

Fig. 5.7.4 Plastic zones obtained by BEM for different load levels (plane strain).

For the plane strain case, because of a large spread of plastic zone before limit load is achieved, the number of internal points and cells was increased from 33 and 51 to 59 and 97 respectively. Load-displacement curve is shown in figure 5.7.3 where the equivalent finite element results presented by Chen [64] are also given. The limit load obtained by BEM ($2\sigma_a/\sigma_o$ = 1.64) is below the value given by the finite element method ($2\sigma_a/\sigma_o$ = 1.85). But, as stated by Chen, bound theorems demonstrate that the maximum load should lie between 1.52 and 1.73, which supports the boundary element results.

Spread of plastic zones at lower load levels presented in figure 5.7.4 exhibits good agreement with finite element computations [93, 64] for the same problem.

5.7.2 Deep Circular Tunnel - This example was selected to emphasize the advantages of boundary elements over "domain"type techniques to solve infinite medium problems.

A circular excavation studied by Reyes [102] and later by Baker et al. [103] with linear displacement triangular and quadrilateral finite elements respectively is here compared with boundary element results.

The plane strain problem was analysed under the Drucker-Prager simulation of Mohr-Coulomb yield criterion (α' and K' given by expressions(5.5.9)) and by assuming the infinite domain to be initially subjected to a uniform stress field of 1 ksi vertical and 0.4 ksi in both horizontal directions (K_o = 0.4). For the present study, external loads corresponding to the relaxation of this in-situ stress field were applied over the surface of the opening.

The material (rock)was assumed to be perfectly plastic with

E = 500. ksi
c' = 0.28 ksi
ν = 0.2
ϕ' = 30^D .

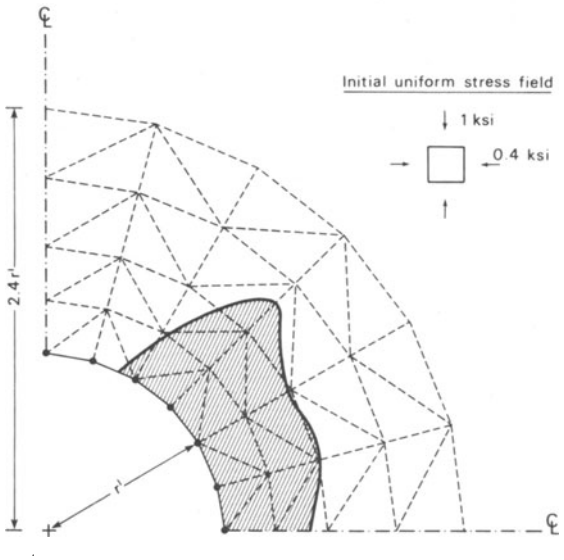

Fig. 5.7.5 Deep circular tunnel. Discretization used for BE results and total spread of plastic zone.

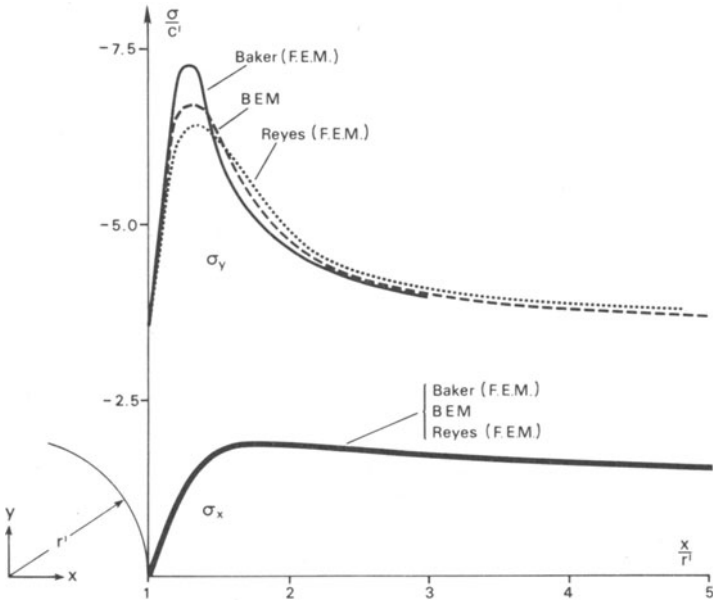

Fig. 5.7.6 Final stresses along the horizontal section through the medium.

Boundary element and internal cell discretization is presented in figure 5.7.5 where the plastic zone on complete removal of the in-situ stresses from the boundary of the cavity is also given.

Stresses along the horizontal section computed at the end of the relaxation process are compared with the corresponding results presented by Reyes and Baker in figure 5.7.6. Here, internal stresses outside the discretized region were calculated at simple internal points not connected to any internal cells.

It is important to note that the refinement of the two finite element meshes (about 253 nodes) should not lead to the differences in the σ_y values shown in figure 5.7.6. Although no reference was made by the authors, this discrepancy is probably due to the outer boundary conditions considered in the two analyses. The boundary element technique does not require any outer boundary discretization, but in order to study its influence in the results a quarter of a circle with radius equal to nine times the radius of the cavity was discretized using six boundary elements, this is approximately the extent of the finite element meshes. The outer circle was then considered to be free to displace, giving as a result a better agreement with Baker computations, A second alternative was carried out by prescribing zero displacements over the outer boundary, leading now to improved agreement with Reyes results.

5.7.3 Rough Punch - In this example the elastoplastic behaviour of a square block compressed by two opposite perfectly rough rigid punches is studied. The problem is analysed under plane strain condition and the material is considered to be perfectly plastic obeying the von Mises yield criterion.

By using a very refined mesh of 274 linear displacement triangular finite elements and 173 nodal points (see figure 5.7.7a), results to

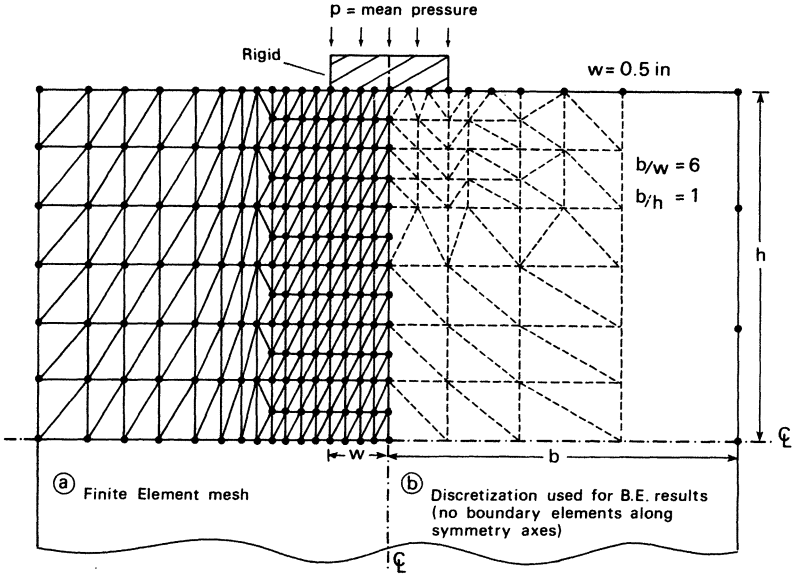

Fig. 5.7.7 Geometry of rough punch problem.

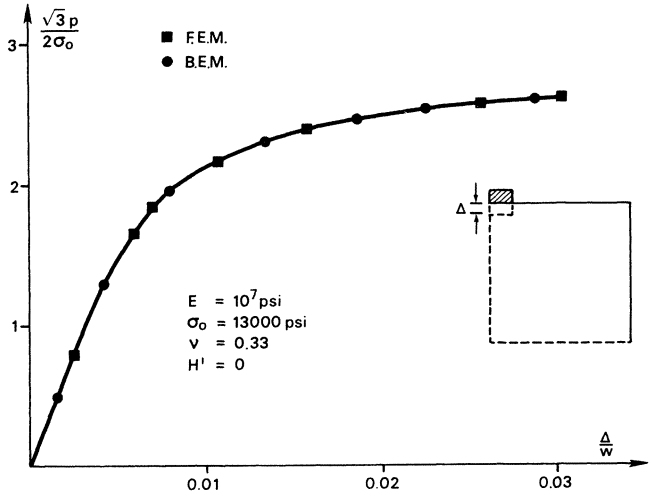

Fig. 5.7.8 Mean pressure-applied displacement curve for rough punch problem.

this problem were presented by Chen [104, 64]. The boundary element analysis was performed with the discretization shown in figure 5.7.7b, requiring less than one third of the FE data to run the problem.

The indentation process was developed by prescribing the flat punch displacements leading to the average pressure-applied displacement curve presented in figure 5.7.8. As can be seen, agreement between the two analyses has been thoroughly obtained, both methods slightly exceeding (4%) the theoretical limit load $\sqrt{3}p/2\sigma_o = 2.5$.

5.8 Examples - Half-Plane Implementation

In the present section the results of some applications of the half-plane implementation are compared with numerical and analytical solutions presented in the literature.

5.8.1 Strip Footing - In this example the plane strain analysis of a flexible strip footing under uniform loading is presented. The finite soil stratum was discretized taking full advantage of both, symmetry and free-surface condition, using the reduced number of 14 boundary elements and 42 internal points as shown in figure 5.8.1.

The soil was considered to be a perfectly plastic material, obeying the associated Mohr-Coulomb (M-C) criterion with

$$E = 30000.\ \text{psi}$$

$$c' = 10.\ \text{psi}$$

$$\nu = 0.3$$

$$\phi' = 20^{o}.$$

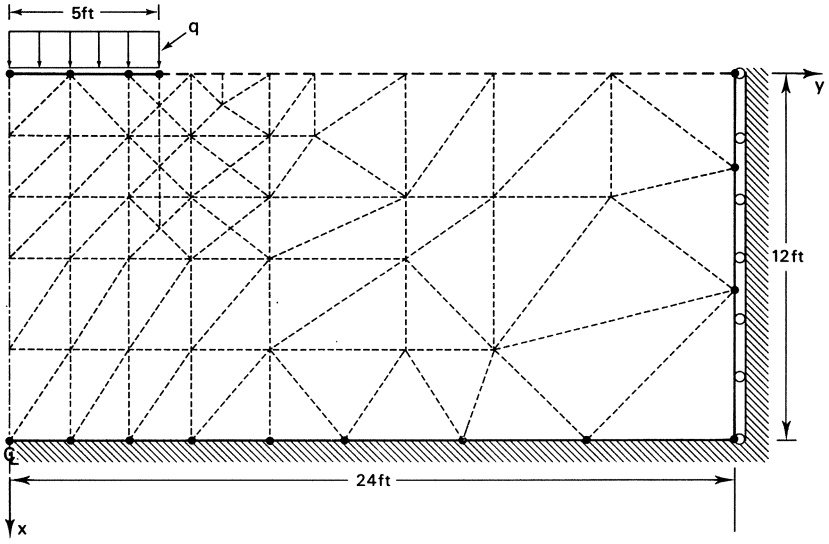

Fig. 5.8.1 Strip footing on elastoplastic soil. Discretization used for BE results.

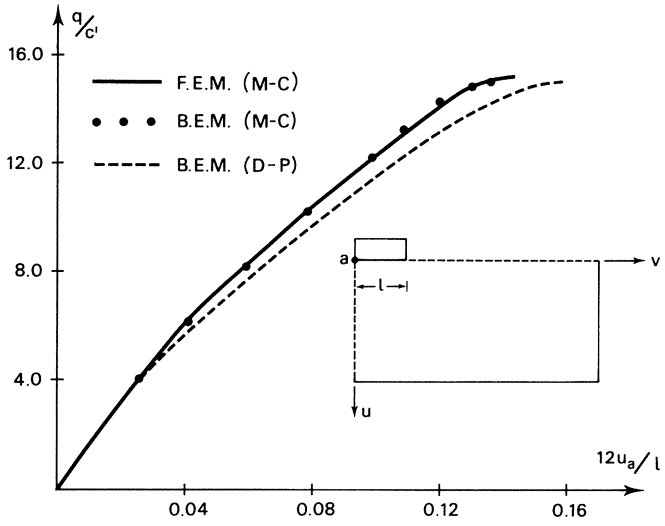

Fig. 5.8.2 Load-displacement curves for strip footing problem.

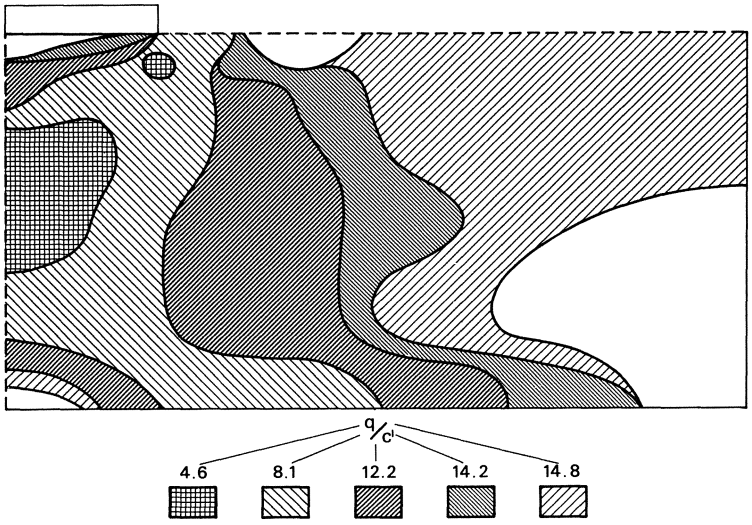

Fig. 5.8.3 Spread of plastic zones at different load levels. Mohr-Coulomb yield criterion.

An alternative solution was also obtained by using the associated Drucker-Prager (D-P) yield criterion given by expressions (5.5.7) and (5.5.9).

Ground surface displacements are presented in figure 5.8.2. Also included is the equivalent M-C finite element solution obtained by Zienkiewicz et al. [105] using quadratic isoparametric elements with 121 nodal points. The collapse loads achieved by the boundary element and finite element techniques (M-C) are $q/c' = 14.9$ and $q/c' = 15.1$ respectively, which agree well with the Prandtl solution (Chen [64]) $q/c' = 14.8$. As for the D-P results, it is seen that although the displacements were larger, the maximum load obtained was still not far from the previous ones.

Zones of yielding defined by the M-C solution are shown in figure 5.8.3. These zones compare well with the reported finite element computations.

5.8.2 Shallow Tunnel - In the last section the elastoplastic boundary element technique was applied to solve the problem of a deep circular excavation of radius r' in an inifinite medium. The great advantages of the technique were then pointed out when comparing results with different finite element solutions. Here, an analogous problem is studied by considering the tunnel to be shallow, located within a semi-infinite domain and with its centre at a depth of $5r'$.

As before, the rock-like material was assumed to follow the Drucker-Prager yield criterion (α' and K' as given in (5.5.9)), with the following characteristics

$$E = 500.\ \text{ksi}$$
$$c' = 0.28\ \text{ksi}$$
$$\nu = 0.2$$
$$\phi' = 30^{o}\ .$$

In order to produce a more realistic analysis, the semi-infinite medium was assumed to be initially under the in-situ linearly varying stress field given by the formulae

$$\sigma_v = \bar{\sigma}_v + \gamma h \qquad \text{(vertical stress)}$$
$$\sigma_h = 0.4\sigma_v \qquad \text{(horizontal stresses)}$$

where $\bar{\sigma}_v$ is a uniform pressure that may be due to an overburden of water or very weak material, γ is the unit weight of the rock and h is the distance from the ground surface.

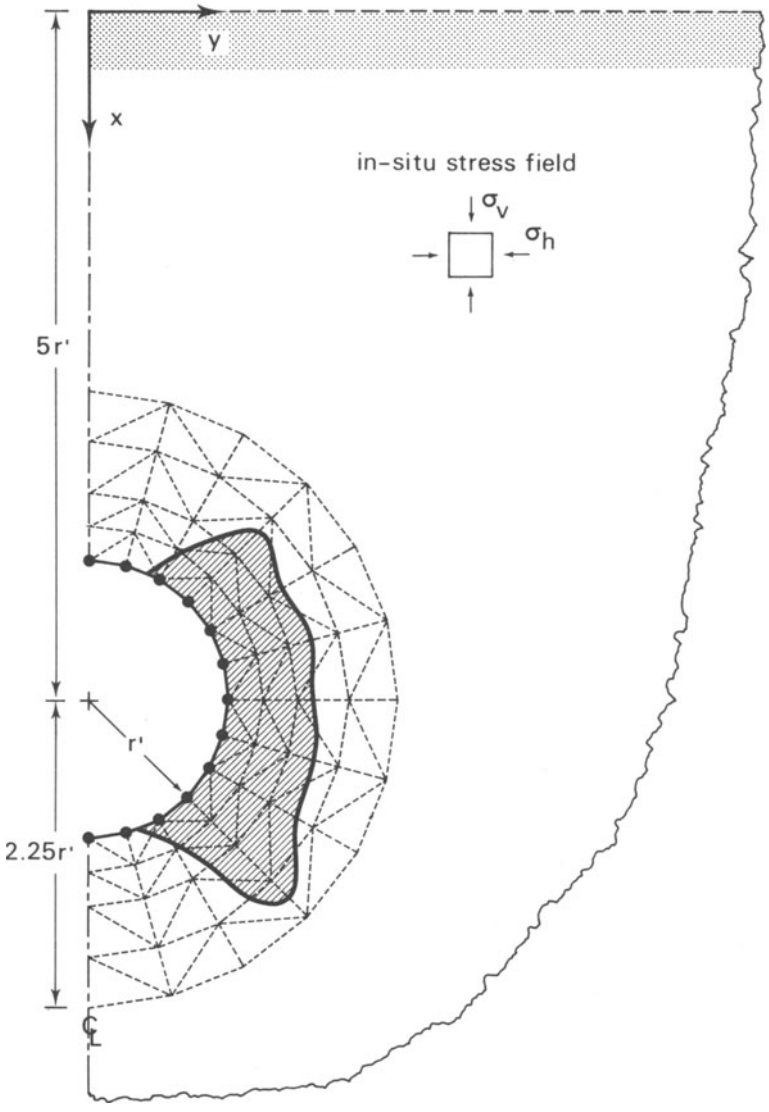

Fig. 5.8.4 Shallow circular tunnel problem. Discretization used for BE results and total spread of plastic zone.

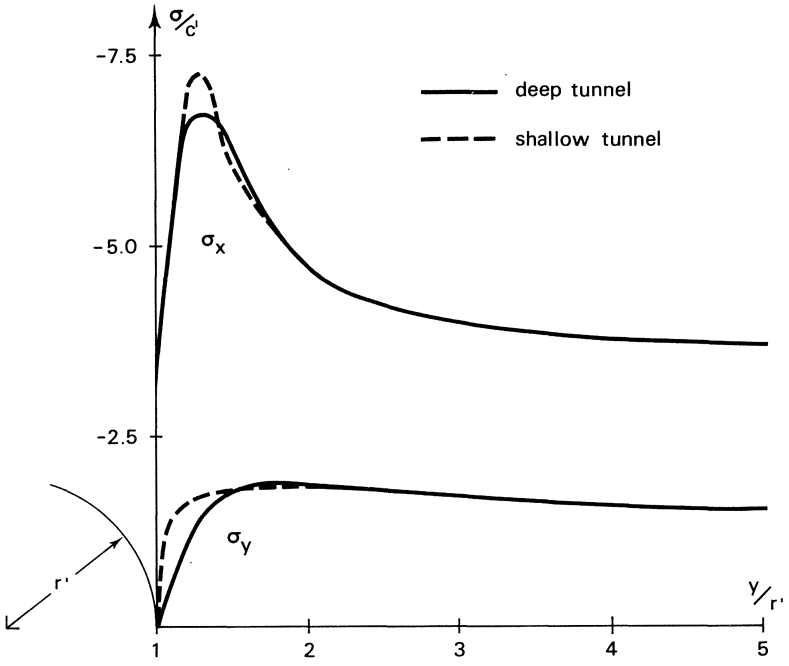

Fig. 5.8.5 Final stresses along the horizontal section through the medium.

To simulate the stress state adopted for the deep tunnel problem (σ_v = 1 ksi) at the depth of the excavation axis, the following values were chosen

$$\bar{\sigma}_v = 0.3 \quad \text{ksi}$$

$$\gamma = 8.9 \times 10^{-2} \quad \text{lb/in}^3$$

$$r' = 131. \quad \text{ft.}$$

The plane strain analysis was carried out by applying increments of external loads, corresponding to the relaxation of the in-situ stresses, over the boundary of the cavity. The discretization employed is depicted in figure 5.8.4 where the total extent of the plastic zone is also shown.

Final stresses along the horizontal section are presented in figure 5.8.5 with the equivalent results from the deep tunnel case (see Subsection 5.7.2) included for comparison. Note that stress values outside the internal cell region were computed at simple internal points.

The above example clearly indicates the powerfulness of the half-plane implementation. Problems of this sort can only be satisfactorily solved by using this technique, which requires neither ground surface nor outer boundary discretization.

CHAPTER 6

VISCOPLASTICITY AND CREEP USING BOUNDARY ELEMENTS

6.1 Introduction

In the present chapter an application of the boundary element equations to viscoplasticity is presented. The procedure can be used for creep problems as well. The Perzyna's [72-74] approach has been adopted since it is appropriate for computer applications and - as demonstrated in Chapter 2 - can be used to simulate pure elastoplastic solutions. The time-dependent solution is obtained by a simple Euler one step procedure [106-108] and some guide lines for the selection of the time step length are also discussed.

The examples presented and discussed at the end of the chapter point out the accuracy of the boundary element solution and illustrate the potentialities of the technique for these sort of nonlinear problems.

6.2 Rate Dependent Constitutive Equations

In this chapter we shall restrict ourselves to the solution of either creep or elastic/viscoplastic problems in the sense described by Perzyna [72]. It is worth mentioning that transient or steady state thermal strains could be equally considered by solving a coupled boundary element problem, following the procedure presented by Wrobel and Brebbia [109] for the thermal part of the problem.

With reference to Chapter 2 Section 2.3, the static yield criterion for isotropic hardening can now be written in general form as

$$F(\sigma_{ij}, k) = 0 \tag{6.2.1}$$

where as before k represents a hardening parameter which dictates the position of the static yield surface in the nine-dimensional stress space. This condition can be better visualized in the following form

$$f(\sigma_{ij}) = \psi(k) \tag{6.2.2}$$

in which $F = f - \psi$ and if the work hardening hypothesis is being adopted k is given by expression (5.2.3).

One can notice that the condition expressed in (6.2.1) or (6.2.2) does not differ from the corresponding yield condition for the so-called inviscid theory of plasticity. Therefore, the different expressions for F introduced in Section 5.5 can still be used. This encourages a further interpretation; let us designate the scalar function of $f(\sigma_{ij})$ by σ_e as before. Such designation allows for the definition of the equivalent plastic strain rate as follows (see expression (5.5.11))

$$\sigma_e \dot{\varepsilon}^p_e = \sigma_{ij} \dot{\varepsilon}^p_{ij} = \dot{k} \ . \tag{6.2.3}$$

Following the generalized normality principle due to Perzyna [72-74], the viscoplastic strain rates are given by

$$\dot{\varepsilon}^p_{ij} = \gamma < \Phi\left(\frac{F}{\psi}\right) > \frac{\partial F}{\partial \sigma_{ij}} \tag{6.2.4}$$

where γ, Φ and the symbol $< >$ have been defined and commented upon in Section 2.3.

Equation (6.2.4) can be further written as

$$\dot{\varepsilon}^{p}_{ij} = \gamma < \Phi\left(\frac{F}{\psi}\right) > \frac{\partial f}{\partial \sigma_{ij}} \tag{6.2.5}$$

which after multiplying both sides by σ_{ij} gives

$$\sigma_{ij}\,\dot{\varepsilon}^{p}_{ij} = \gamma < \Phi\left(\frac{F}{\psi}\right) > \sigma_{ij}\,\frac{\partial f}{\partial \sigma_{ij}} \quad . \tag{6.2.6}$$

Assuming that $f(\sigma_{ij})$ is homogeneous of degree one (a requirement satisfied by the yield criteria adopted here) and applying Euler's theorem [80] comes

$$\sigma_{ij}\,\dot{\varepsilon}^{p}_{ij} = \gamma < \Phi\left(\frac{F}{\psi}\right) > f(\sigma_{ij}) \quad . \tag{6.2.7}$$

Recalling definition (6.2.3), expression (6.2.7) can be finally represented by

$$\dot{\varepsilon}^{p}_{e} = \gamma < \Phi\left(\frac{F}{\psi}\right) > \tag{6.2.8}$$

a relation which for $F > 0$ leads to

$$f(\sigma_{ij}) = \psi(k)\left[1 + \Phi^{-1}\left(\frac{\dot{\varepsilon}^{p}_{e}}{\gamma}\right)\right] . \tag{6.2.9}$$

Equation (6.2.9) when compared to (6.2.2) clearly demonstrates the explicit dependence of the flow surface on the equivalent plastic strain rate.

As a further illustration, consider the following definition

$$\dot{\varepsilon}_{e} = \frac{\dot{\sigma}_{e}}{E} + \dot{\varepsilon}^{p}_{e} \tag{6.2.10}$$

in which E is the Young's modulus and $\dot{\varepsilon}_{e}$ stands for an equivalent measure of the total strain rate. Note that in uniaxial problems $\dot{\varepsilon}_{e}$, $\dot{\sigma}_{e}$ and $\dot{\varepsilon}^{p}_{e}$ become the actual total strain, stress and plastic strain rates if ψ is defined as the uniaxial yield stress.

The flow surface can now be written as

$$f(\sigma_{ij}) = \psi(k)\left[1 + \phi^{-1}\left(\frac{\dot{\varepsilon}_e - \dot{\sigma}_e/E}{\gamma}\right)\right] \qquad (6.2.11)$$

indicating the explicit dependence of $f(\sigma_{ij})$ on the rate of induced strains/stresses.

For creep problems the equivalent version of expression (6.2.8) is assumed to be (see Section 2.3)

$$\dot{\varepsilon}_e^c = K\,\sigma_e^m\,t^n \qquad (6.2.12)$$

where K is a material parameter and $\sigma_e = f(\sigma_{ij})$ represents the von Mises equivalent stress.

It is interesting to note that the time-hardening function t^n can be removed from (6.2.12) by the following transformation [110]

$$\bar{t} = \int_0^t \tau^n \, d\tau \qquad (6.2.13)$$

where $\bar{t}$ denotes a transformed time leading to

$$\frac{d\varepsilon_e^c}{d\bar{t}} = K\,\sigma_e^m \quad . \qquad (6.2.14)$$

This means that the problem can be solved in terms of a fictitious time which relates to the true time t by means of the inverse relation

$$t = \left[\bar{t}(n+1)\right]^{\frac{1}{n+1}} . \qquad (6.2.15)$$

Different time hardening functions can be equally transformed by the above procedure assuming that (6.2.12) is taken from experimental analysis under constant stress.

The creep strain rates can therefore be written as

$$\dot{\varepsilon}^{c}_{ij} = K \sigma_e^m \frac{\partial f}{\partial \sigma_{ij}} \tag{6.2.16}$$

where the dot indicates derivative with respect to $\bar{t}$ if $n \neq 0$.

Equation (6.2.16) corresponds to the Prandtl-Reuss equations and can be cast into the form of (6.2.5). In both cases the corresponding initial stress rates can be computed by the simple relation

$$\dot{\sigma}^{a}_{ij} = \gamma < \Phi > \bar{d}_{ij} \tag{6.2.17}$$

where

$$\bar{d}_{ij} = C_{ijk\ell} \frac{\partial f}{\partial \sigma_{k\ell}} . \tag{6.2.18}$$

Herein, for the boundary element implementation, the initial stress equations have been adopted since they present the advantage of handling compressible or incompressible inelastic strains in plane strain or plane stress problems with minor alterations. The relevant 2-D forms of the above relations are presented in Appendix D.

In order to apply equations (4.6.10) and (4.6.11) to the solution of time-dependent inelastic problems, the manipulations introduced in Section 4.6 can be performed resulting in the following matrix equations

$$\dot{\underset{\sim}{y}} = \underset{\sim}{R}\ \dot{\underset{\sim}{\sigma}}^{a} + \dot{\underset{\sim}{m}} \tag{6.2.19}$$

and

$$\dot{\underset{\sim}{\sigma}} = \underset{\sim}{V}\ \dot{\underset{\sim}{\sigma}}^{a} + \dot{\underset{\sim}{n}} \tag{6.2.20}$$

where vectors $\dot{\underset{\sim}{m}}$ and $\dot{\underset{\sim}{n}}$ are given in (4.6.16) and (4.6.19), matrix $\underset{\sim}{R}$ was defined in (5.6.3) and the new matrix $\underset{\sim}{V}$ is given by

$$\underset{\sim}{V} = \bar{\underset{\sim}{Q}} - \underset{\sim}{A}' \underset{\sim}{R} \tag{6.2.21}$$

in which

$$\bar{\underset{\sim}{Q}} = \underset{\sim}{Q}' + \underset{\sim}{E}' \tag{6.2.22}$$

From the above it is seen that (see expression (6.2.17)) equation (6.2.20) represents a system of ordinary differential equations for stresses at selected boundary nodes and internal points which can be solved by standard methods (provided it satisfies the Lipschitz condtion [106-108]), producing a unique solution to the time-dependent problem. A simple and efficient solution procedure for this matrix equation is the subject of the next section.

6.3 Solution Technique

For the solution of the examples presented in this chapter, a simple Euler one-step procedure [107] has been adopted in the following fashion; let us assume a load factor $\lambda(t)$ which is considered to be a known function of time. Equations (6.2.19) and (6.2.20) can be integrated on time to give

$$\underset{\sim}{y} = \underset{\sim}{R}\, \underset{\sim}{\sigma}^{a} + \lambda(t)\, \underset{\sim}{m} \tag{6.3.1}$$

and

$$\underset{\sim}{\sigma} = \underset{\sim}{V}\, \underset{\sim}{\sigma}^{a} + \lambda(t)\, \underset{\sim}{n} \tag{6.3.2}$$

where vectors $\underset{\sim}{m}$ and $\underset{\sim}{n}$ correspond to the elastic solution at some reference load level.

For the time marching procedure, equation (6.3.2) is applied after each discrete time step ($\Delta t = {}^{k+1}t - {}^{k}t$) with the value of the initial stresses being computed at selected boundary nodes and internal points by the Euler's formula

$$ {}^{k+1}\sigma^{a}_{ij} = {}^{k}\sigma^{a}_{ij} + \Delta t\, \gamma < {}^{k}\Phi > {}^{k}\bar{d}_{ij} \,. \qquad (6.3.3) $$

During this process one may have that $\lambda(t)$ is left constant for some time, creating a situation in which after a sufficient number of time steps has been applied, the values of "$\Delta t\, \dot{\varepsilon}^{p}_{e}$" or "${}^{k-1}\sigma_{e} - {}^{k}\sigma_{e}$" become vanishingly small everywhere. In such cases a stationary condition is deemed to have occurred and the time marching scheme can be stopped.

It is interesting to note that the time integration procedure does not require computation of the boundary unknowns. Consequently, equation (6.3.1) need only be used to print the boundary unknowns at some requested time/load values.

The success of this simple time integration scheme is dependent on the proper selection of the time step lengths. It has been known for quite some time [110] that ideally small time steps should be applied in the early stages of the computation (i.e., after the application of the load or load increment) and that these can be increased in size as stationary or steady state is approached.

Following the experience of many authors [110 - 113] with different spatial discretization techniques (mainly finite elements), the time step size should be controlled by a relation between accumulated and rate value of some variables to produce the above described automatic lengthening as asymptotic state is achieved. This can be considered at each node or point as follows

$$\Delta t \leq \eta_1 \frac{\varepsilon_e}{\dot{\varepsilon}^a_e} = \frac{\eta_1}{\dot{\varepsilon}^a_e} \left(\frac{\sigma_e}{E} + \varepsilon^a_e \right) \tag{6.3.4}$$

under the condition that

$$^{k+1}\Delta t \leq \eta_0 \, ^{k}\Delta t \tag{6.3.5}$$

where η_1 and η_0 are problem dependent parameters that should be chosen to compromise between computer time and accuracy. Normally, $0.01 \leq \eta_1 \leq 0.15$ and $1.2 \leq \eta_0 \leq 2$.

A drawback of relations (6.3.4) and (6.3.5) is that they do not guarantee complete stability of the explicit time integration scheme, particularly near to the steady state which produces large time step values. Useful bounds for the maximum time step length have been presented by Cormeau [114] for perfectly viscoplastic materials, these can be seen to correspond to the pure relaxation problem

$$\dot{\varepsilon}_{ij} = \frac{1}{2G} \left[\dot{\sigma}_{ij} - \frac{\nu}{1+\nu} \dot{\sigma}_{kk} \delta_{ij} \right] + \dot{\varepsilon}^a_{ij} = 0 \quad . \tag{6.3.6}$$

Herein, in addition to the above referred bounds, an approximate, yet general, limiting value for the time step has been adopted. It is expected that it will bring some light into the case of hardening/softening viscoplastic materials.

Recalling expression (6.2.10) in rearranged form one gets

$$\dot{\sigma}_e = g(t, \sigma_e) \tag{6.3.7}$$

where for $\dot{\varepsilon}_e = 0$,

$$g(t, \sigma_e) = - E \gamma < \Phi > \quad . \tag{6.3.8}$$

Equation (6.3.7) in equivalent stress form can be used to study a bound [106] for the stability condition of the simple Euler procedure adopted here. Thus, the coupling of equations (6.3.7) and (6.3.3) leads to the equivalent relation

$$^{k+1}\sigma_e = {}^{k}\sigma_e + \Delta t\, g(t, {}^{k}\sigma_e) . \qquad (6.3.9)$$

Let us now accept that throughout the time marching process truncation and roundoff errors have been committed. The global error at time ^{k}t is then given by

$$^{k}\rho = {}^{k}\sigma_e - {}^{k}\hat{\sigma}_e \qquad (6.3.10)$$

where $\hat{\sigma}_e$ represents the value of σ_e obtained through an exact integration on time of equation (6.3.7) which corresponds to the exact solution of equation (6.3.2).

Assuming that the error ρ is sufficiently small to allow a truncated Taylor's expansion of $g(t, \sigma_e)$ about $\hat{\sigma}_e$, comes

$$g(t, {}^{k}\sigma_e) = g(t, {}^{k}\hat{\sigma}_e) + {}^{k}\rho \frac{\partial g(t, {}^{k}\hat{\sigma}_e)}{\partial \sigma_e} + \ldots . \qquad (6.3.11)$$

The substitution of (6.3.10) for ^{k}t and ^{k+1}t in equation (6.3.9), together with (6.3.11) gives

$$^{k+1}\hat{\sigma}_e + {}^{k+1}\rho = {}^{k}\hat{\sigma}_e + {}^{k}\rho + \Delta t \left[g(t, {}^{k}\hat{\sigma}_e) - {}^{k}\rho\, \gamma\, E\, {}^{k}\left(\frac{\partial \Phi}{\partial \sigma_e}\right)\right] . \qquad (6.3.12)$$

If a stationary state is likely to have occurred,

$$^{k+1}\hat{\sigma}_e = {}^{k}\hat{\sigma}_e \quad ; \quad g(t, {}^{k}\hat{\sigma}_e) = 0 \qquad (6.3.13)$$

hence,

$$ {}^{k+1}\rho = {}^{k}\rho \left[1 - \Delta t \; \gamma \; E \; {}^{k}\left(\frac{\partial \Phi}{\partial \sigma_e} \right) \right] \; . \qquad (6.3.14) $$

In order to ensure that errors remain bounded (stability), one has that $|{}^{k+1}\rho| \leq |{}^{k}\rho|$, which gives

$$ \Delta t \leq \Delta t_{CRIT.} = \frac{2}{\gamma \frac{\partial \Phi}{\partial \sigma_e} E} \; . \qquad (6.3.15) $$

Taking into consideration that for work hardending viscoplastic materials

$$ \frac{\partial \Phi}{\partial \sigma_e} = \Phi' \left[\frac{1}{\psi} - \frac{\sigma_e}{\psi^2} \frac{d\psi}{dk} \frac{dk}{d\sigma_e} \right] \qquad (6.3.16) $$

where $\Phi' = d\Phi/d\left(\frac{F}{\psi}\right)$, one finally gets

$$ \Delta t \leq \Delta t_{CRIT.} = \frac{2\psi^2}{\gamma \Phi' \left(E \; \psi + \sigma_e \frac{d\psi}{d\varepsilon_e^p} \right)} \qquad (6.3.17) $$

in which for $\psi = \sigma_o$ one has $d\psi/d\varepsilon_e^p = H'$.

For creep problems the equivalent expression is

$$ \Delta t_{CRIT.} = \frac{2}{K \; E \; m \; \sigma_e^{m-1}} \qquad (6.3.18) $$

and if equation (6.2.12) is used instead, the term t^n should appear in the denominator producing the same critical time step obtained by Cormeau [114] and Irons [115] when $\nu \to 0.5$.

In order to study the effect of hardening in the critical time step let us consider the case $\Phi' = 1$, $d\psi/d\varepsilon_e^p = H' =$ constant. In this

case expression (6.3.17) simplifies as follows

$$\Delta t_{CRIT.} = \frac{2\sigma_o^2}{\gamma E (\bar{Y} + H' \varepsilon_e)} \qquad (6.3.19)$$

where the relation $\sigma_e = E(\varepsilon_e - \varepsilon_e^p)$ with ε_e = constant was used.

The above relation indicates that when $H' > 0$, the effect of hardening produces an initial reduction in the critical time step (when compared to the case $H' = 0$), and that as viscoplastic flow progresses this limit is increased with the square of σ_o. One can notice that this is not the case when $H' < 0$ (softening), here the time step limit is initially increased but diminishes as viscoplasticity develops, producing a reduction in the region of stability which must not be overlooked in such cases.

In the next section the results of some examples solved in the light of the theory presented in this chapter are compared with existing results taken from the literature.

6.4 Examples

An interesting feature of the elastic/viscoplastic theory (see Section 2.3 of Chapter 2) is that if the load is applied in small increments, allowing for stationary conditions to be achieved after each load step, a pure elastoplastic solution is obtained. The question of how small these increments should be taken still remains an open question and is in fact problem dependent. In the first example presented here this feature is fully explored for solving a current elastoplastic problem. But in the second and third applications, the

total load is applied in one step and two problems of the type power law creep and quasilinear viscoplastic are analysed.

In addition, a further test was carried out with the problem of a rigid punch (elastoplastic) in a strain softening material presented in Subsection 5.4.3. The results are not shown here for they are virtually the same as those presented in Chapter 5. Nevertheless, it should be pointed out that the stability criterion was successfully applied, avoiding premature instability as viscoplastic flow progressed beyond a certain stage.

6.4.1 Deep Beam - In the first example the elastoplastic behaviour of a simply supported deep beam under uniform load is studied by the viscoplastic boundary element technique. The discretization employed is shown in figure 6.4.1 and the material is assumed to obey the Tresca yield criterion with the following parameters

$$E = 30. \times 10^6 \text{ psi}$$

$$\sigma_o = 36. \times 10^3 \text{ psi}$$

$$\nu = 0.3$$

$$H' = 0. \quad \left(\phi\left(\frac{F}{\psi}\right) = \frac{F}{\psi} \; ; \; \gamma = 1. \text{ sec}^{-1} \right)$$

This problem has been analysed by Anand et al. [116] by using a mesh of 272 linear displacement triangular finite elements, which corresponds to 33% more elements on the boundary than the discretization used here.

A comparison of results is depicted in figure 6.4.2 where the load-midspan displacement curves, for both numerical techniques, are plotted together with the beam theory solution [62]. As can be seen,

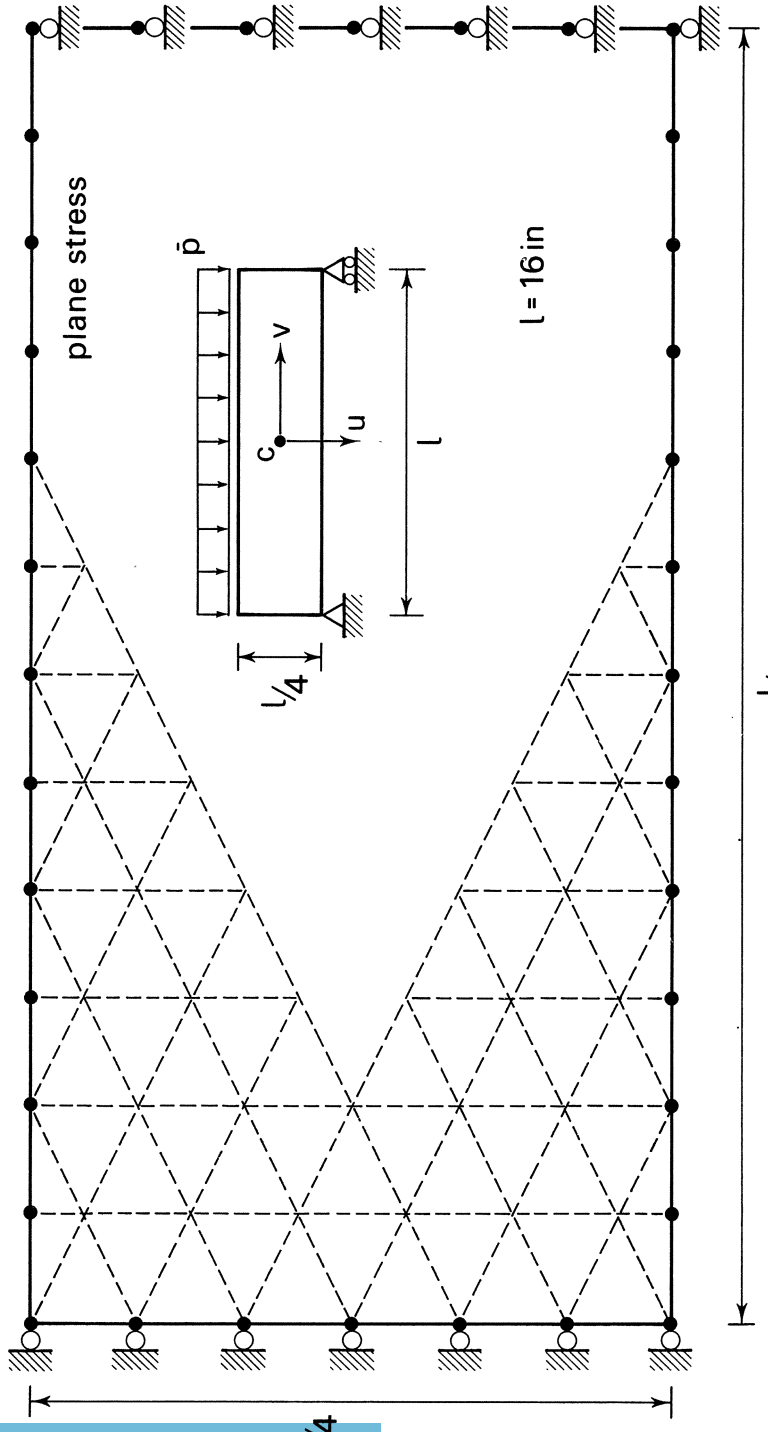

Fig. 6.4.1 Deep beam elastoplastic problem. Geometry and discretization used for BE results.

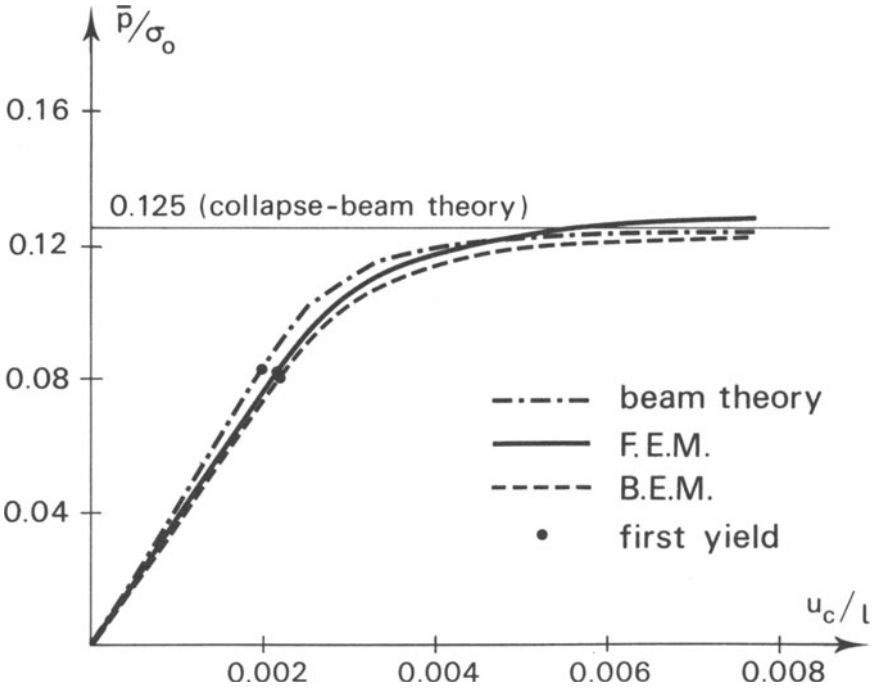

Fig. 6.4.2 Load-midspan displacement curves for deep beam problem.

the boundary element solution asymptotically approaches the limit load obtained by the beam theory, whereas the finite element resuls slightly exceed this load level. A vanishing small difference is already noticed in the elastic results, with the BE technique predicting a lower load value for initial yield and larger displacements for the same load level. The plastic zones produced by both techniques were in good agreement with the beam theory, therefore are not shown here.

A further confirmation of the BE results was obtained by solving the same example using the pure elastoplastic implementation of Chapter 5 (initial stress approach). Remarkable agreement was then achieved in every aspect of the solution (differences within prescribed tolerance for convergence/stationarity).

6.4.2 Thin Disc - Accurate bounds for the creep problem of a thin disc with a central rigid insert under constant external edge load were produced by Sim [117]. These were obtained by direct time integration of the analytical solution and presented in dimensionless form using the so-called "reference stress" technique. In order to test the boundary element performance in the same problem, the following material parameters were chosen

$$E = 17. \times 10^6 \text{ psi}$$

$$\nu = 0.33$$

$$\dot{\varepsilon}^c_e = 5.8 \times 10^{-18} \sigma_e^{4.4} \quad . \quad \text{(units : lb, in and sec.)}$$

The geometry and load value are given in figure 6.4.3 where the boundary element and internal cell discretization is also shown. Notice that improved axial symmetry was obtained by avoiding boundary discretization of the symmetry axes.

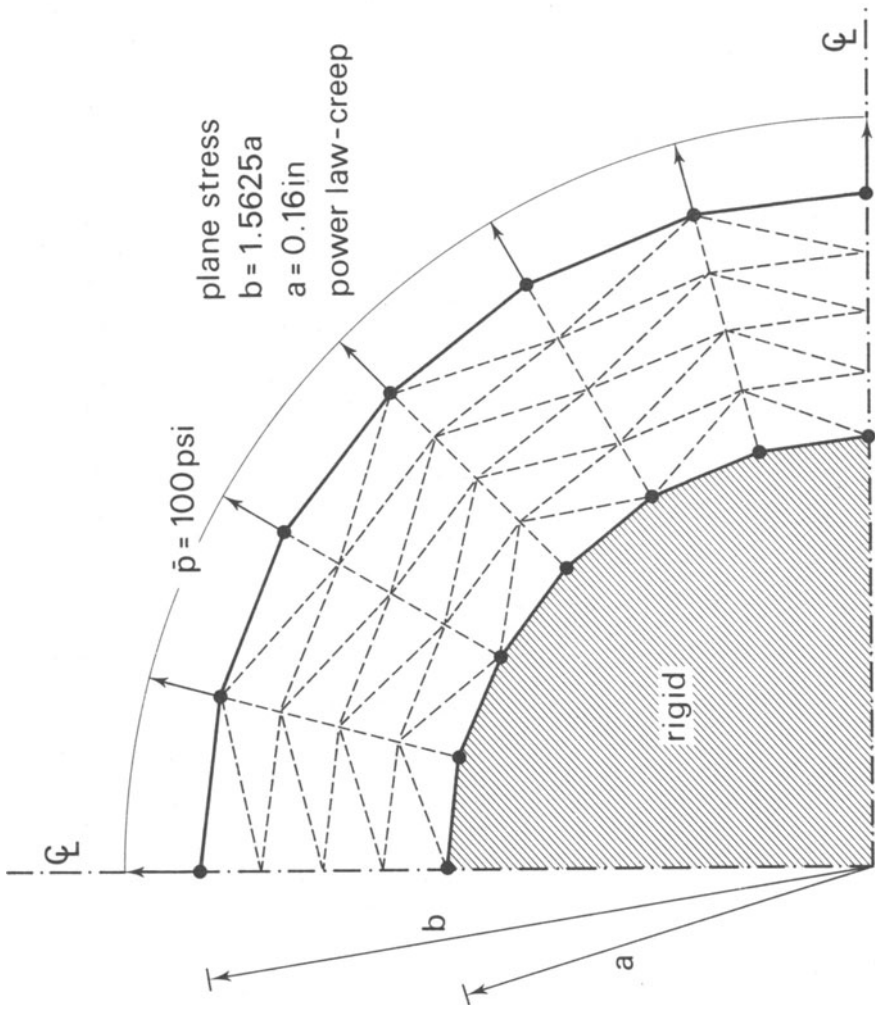

Fig. 6.4.3 Geometry of thin disc problem including boundary element and internal cell discretization.

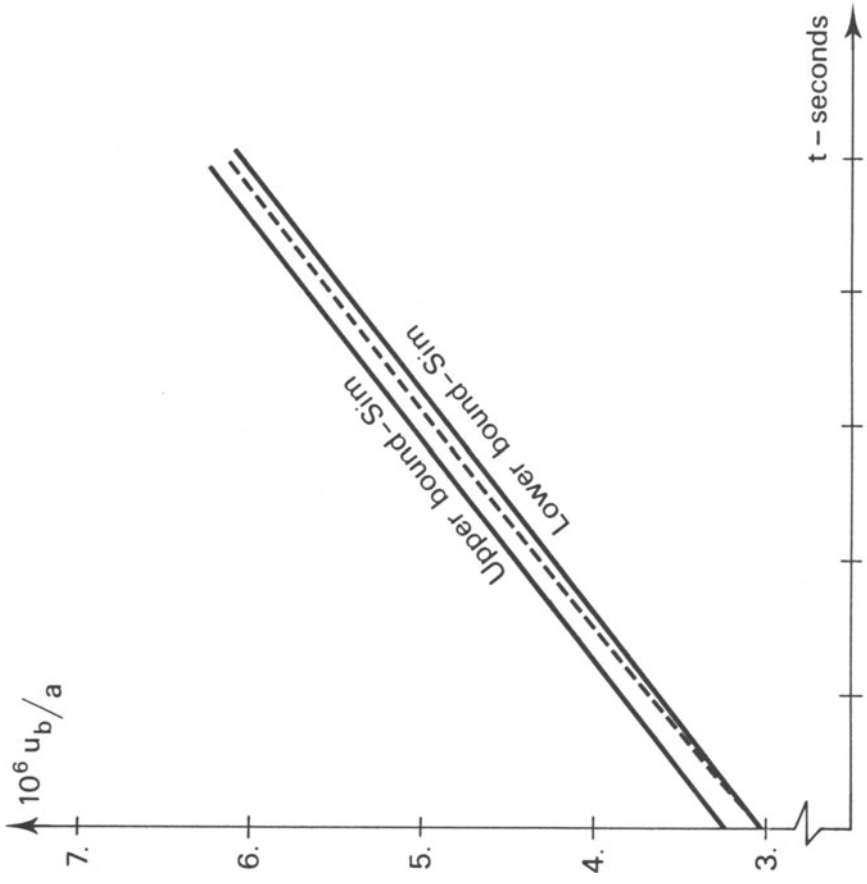

Fig. 6.4.4 Variation of outer boundary radial displacement with time for thin disc problem.

Radial displacements computed over the outer boundary are plotted against time for comparison with the solution bounds in figure 6.4.4. As expected, the boundary element technique produces a flat curve which lies within the narrow space between the two limiting lines taken from the reference. It is interesting to note that the slope of these parallel lines was calculated for an approximate stationary condition in which the variation of the displacement rates was 1%. Consequently, the same stationarity criterion was adopted here, generating the final straight part of the curve.

6.4.3 Plate Under Thermal Shrinkage - In this example the analysis of a rectangular plate, bonded on one edge to a rigid support and subjected to a sudden uniform temperature drop is presented. The thermal shrinkage was assumed to be such that $\varepsilon^{T}_{ij} = -0.01\ \delta_{ij}$. The problem can be properly solved by prescribing tangential displacements corresponding to $\varepsilon_{ij} = -\varepsilon^{T}_{ij}$ over the fixed edge and computing the final displacements by simple superposition.

The material was assumed to be quasilinear $(\Phi(F/\psi) = F/\psi)$ ideal viscoplastic, obeying the von Mises criterion.

Due to symmetry, only half the plate was discretized using 26 boundary elements and 17 internal points located in the region near to the restrained edge as shown in figure 6.4.5. Also included is the plastic zone produced by the instantaneous cooling process.

Finite element results for this problem have been presented by Zienkiewicz and Cormeau [112]. They used a mesh of 96 quadrilateral elements which was equivalent in size to the boundary element discretization over the bonded edge (A-B), but presented more refinement over the opposite edge (C-D).

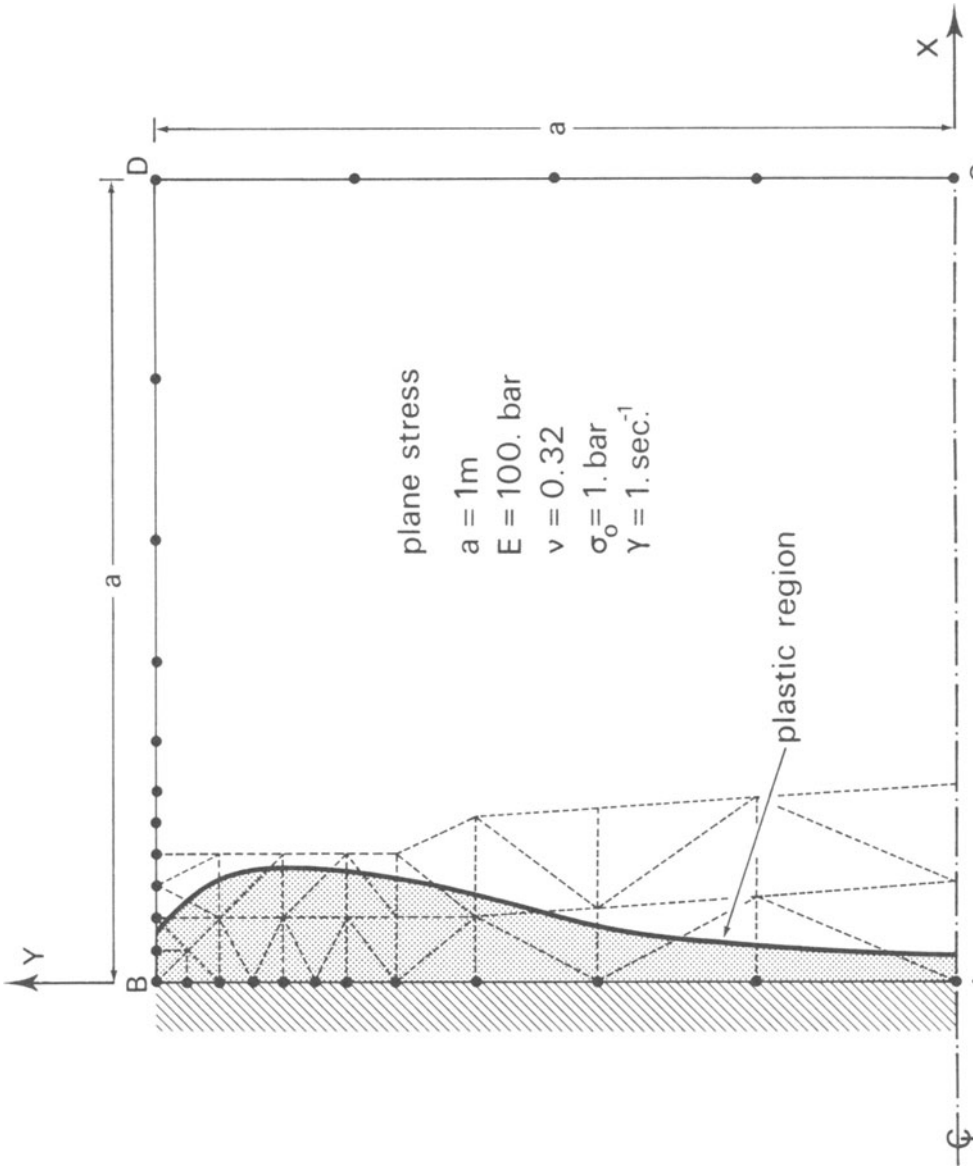

Fig. 6.4.5 Discretization for rectangular plate under thermal shrinkage and total extent of plastic region.

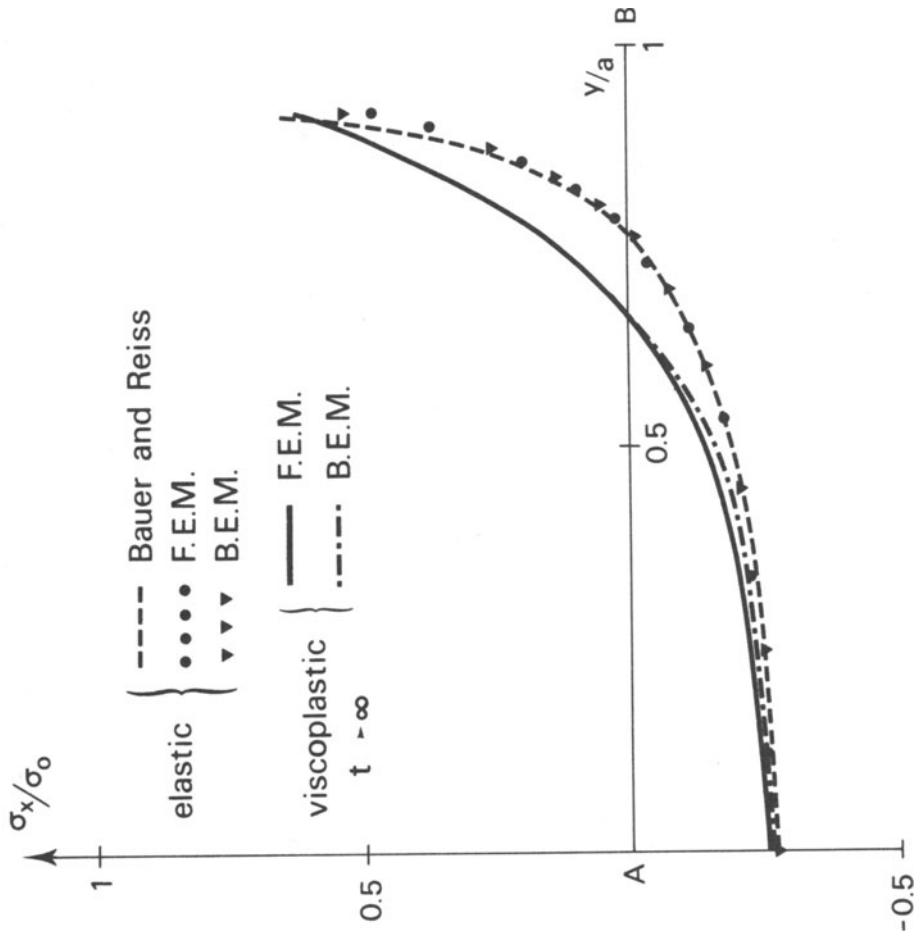

Fig. 6.4.6 Variation of σ_x over fixed edge for t = 0 and asymptotic state.

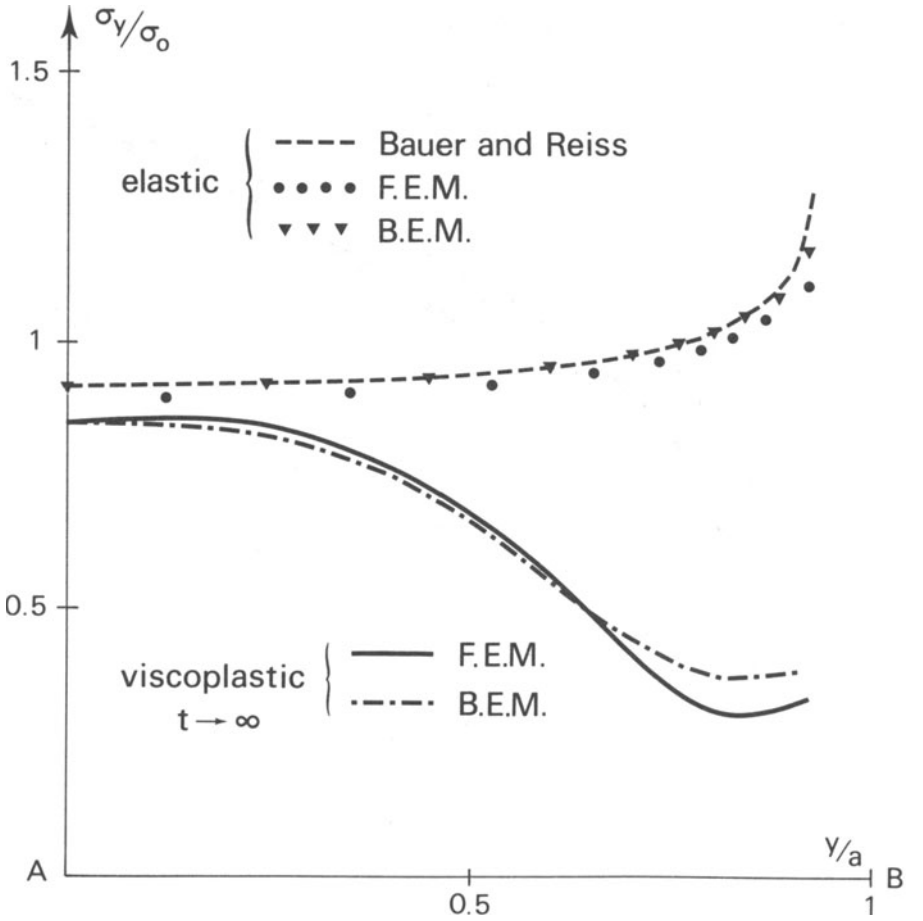

Fig. 6.4.7 Variation of σ_y over fixed edge for $t = 0$ and asymptotic state.

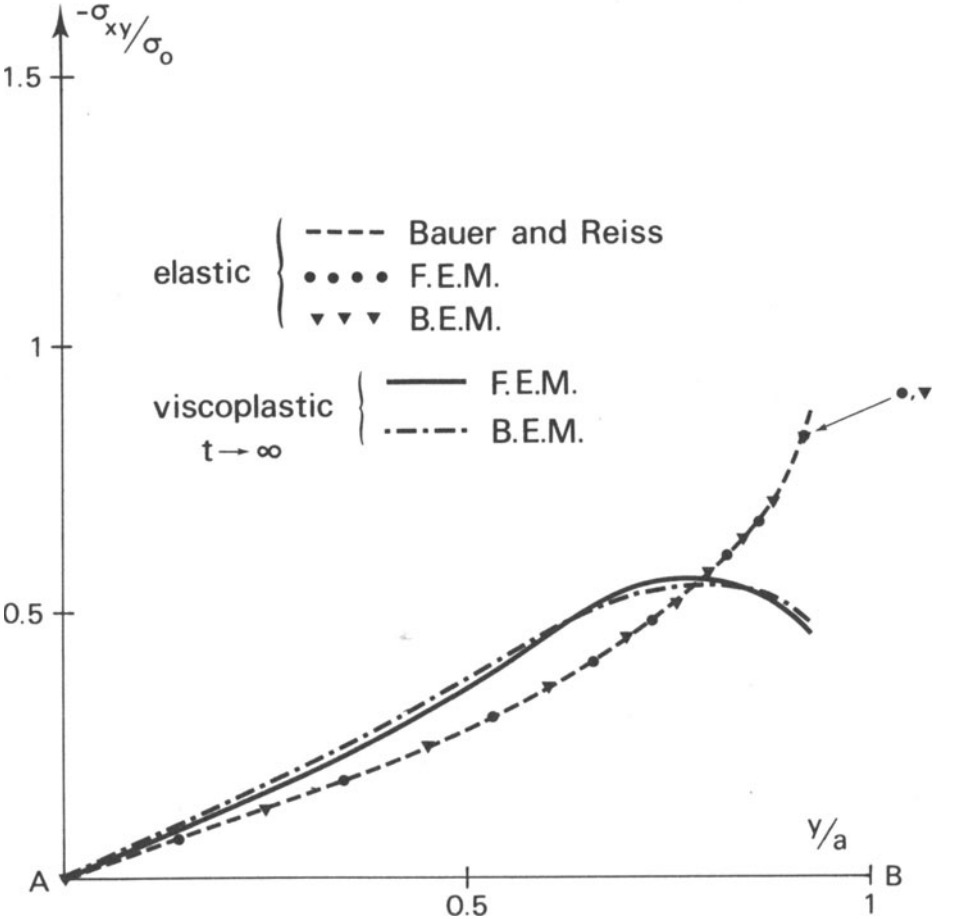

Fig. 6.4.8 Variation of σ_{xy} over fixed edge for $t = 0$ and asymptotic state.

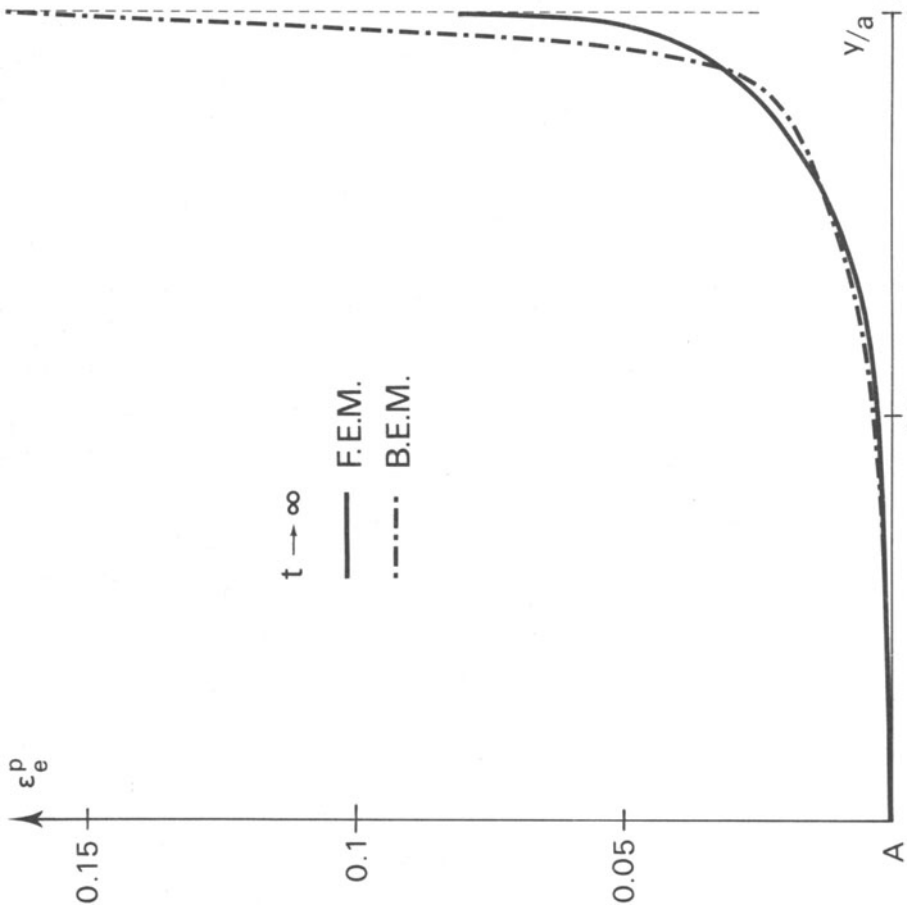

Fig. 6.4.9 Equivalent plastic strain distribution over bonded edge at stationary state.

An interesting comparison of results is depicted in figures 6.4.6 to 6.4.8 where the stresses computed at the fixed edge are shown for times $t = 0$ (elastic) and $t \to \infty$ when stationary condition is achieved. These include not only the FE and BE results, but also the sufficiently refined elastic finite difference solution produced by Bauer and Reiss [118], which provides a useful reference result for $t = 0$.

It is worth mentioning that neither method can predict the infinite value of the elastic stresses at the corners of the fixed edge. Consequently, a localized perturbation in the solutions is expected in the vicinity of corner B. Nevertheless, even though we neglect the results near to the singular node, one can notice that the boundary elements tend to produce a better representation of the singular behaviour than the finite elements. This difference may be partly explained by the fact that the FE stresses were calculated at the Gauss points (2×2 integration) and is particularly apparent in figure 6.4.7 where the σ_y stresses are noticeably unequal over a large range.

A final comparison is presented in figure 6.4.9 in which the equivalent plastic strains computed by the boundary element technique are indicating a more severe concentration of plasticity near the corner than the finite element results.

CHAPTER 7

GENERAL DISCUSSION AND CONCLUSIONS

The present work was primarily concerned with the application of the direct boundary element method to solve inelastic problems in continuum mechanics. In spite of this, Chapter 3 presented the complete formulation of the technique for pure elastic problems. This included not only the implementation of the Kelvin fundamental solutions (3-D and 2-D plane strain/stress) but also the complete expressions of a new fundamental solution suitable for half-plane type problems. In addition, the numerical discretization of the integral equations was discussed in detail for 2-D problems and the results of some classical examples were presented to illustrate the applicability of the half-plane boundary element technique.

From the examples shown in the above referred chapter, it was readily seen that such a solution procedure is more accurate than discretizing the semi-plane using finite elements or even using the Kelvin fundamental solution, which would necessitate defining a closed boundary or using elements tending to infinity. Here, some further comments regarding the computational efficiency of the procedure can be made; first of all, since the tensors corresponding to the half-plane fundamental solution ($c > 0$) are longer than those of Kelvin's, one should expect a certain increase in computer time for the numerical integrals. This difference, however, is compensated by three important features of the solution. In the first place, integration over the traction-free part of $\Gamma-\Gamma'$ is now unnecessary and furthermore, one

of the boundary integrals is always performed over Γ' only, which also provides some saving in computer time. Secondly, when $c = 0$ the resulting expressions (see (3.3.22) and (3.3.23)) are shorter than the Kelvin counterparts. Finally, the resulting system of equations is usually of a reduced size since the boundary may be left "open" in many cases. Therefore, the half-plane boundary element procedure is found to combine both, accuracy and computational efficiency for problems concerning the semi-plane.

It is interesting to note that the half-plane implementation can also be used for bounded bodies where the boundary Γ is entirely located within the semi-plane $x_1 > 0$ ($\Gamma \equiv \Gamma'$). In such cases the results produced are in every aspect equivalent to the solution obtained by using the Kelvin implementation, but the computer time required would be larger than the standard boundary element solution, since all the above mentioned compensations disappear. This feature, however, has been explored during the course of this research for debugging the computer programs.

Following the original purpose of this work, the extension of the boundary element equations to handle inelastic problems (3-D and 2-D) was thoroughly discussed in Chapter 4. Here, a proper procedure for obtaining the complete expressions for stresses at internal points was presented and three alternative formulations were proposed; namely initial strain, initial stress and fictitious tractions and body forces. In order to outline the potentiality of the boundary element method,the 2-D case was taken further and the spatial discretization of the initial strain/stress equations was presented in matrix form. To this end, the apparent difficulty in computing the principal values of the domain integrals (associated with

the inelastic terms), was overcome by employing two different procedures. The first is outlined in Appendix A and is entirely general, the second consists of actually evaluating the integrals by employing a semi-analytical integration scheme which proved to be accurate and efficient for the case of triangular cells with linear interpolation functions. It should be pointed out that both procedures were originally implemented in the initial strain computer program and, for the cases studied, the latter has required slightly less computer time for the total computation of matrix $\underset{\sim}{B}$. Therefore, the same semi-analytical integration procedure was used for the initial stress formulation. It is expected that, because of its generality, the former procedure can be used for higher order cells where a semi-analytical scheme may be difficult to implement.

The application of the boundary element equations to plasticity problems was the object of Chapter 5, where a complete description of the different solution techniques adopted was given. The examples presented indicate a good performance of the boundary element technique when compared to finite element results for the same problems. A considerable reduction in the amount of data required to run a problem can be achieved for the same degree of accuracy. Internal cells, for instance, are only needed in the region of plasticity and they do not require any special connectivity as the problem unknowns are originally defined on the boundary of the body.

Problems such as applied displacements, strain softening and stress concentration were seen to be solved by using a relatively small system of equations and achieving an accuracy only obtained with more complex finite element grids. In addition, bodies with

boundary at infinity can be properly modelled by using boundary elements. This property is of great significance in problems connected with foundations, mining engineering, tunnels, etc., and is, without doubt, a great advantage of the elastoplastic boundary element technique for problems concerning infinite or semi-infinite regions.

Also, from the examples presented and many other tests performed during the period of this research, some interesting features of boundary elements were observed. Among these features it is worth mentioning that the consideration of symmetry without actually discretizing the symmetry axes often leads to improved results when compared to the alternative procedure which define such axes as physical boundaries. In addition, as already indicated in references [2, 24], the elastic boundary element technique is applicable to incompressible materials (i.e., $\nu = 0.5$). Herein, this property is retained in the initial strain formulation and this is naturally possible due to the elastoplastic relations employed (plastic strain increments are computed from the modified total strains).

Another important characteristic of the implementations described is that they overcome the well-known disadvantage of finite elements first reported by Nagtegaal et al. [120] ; i.e., the occasional impossibility of representing properly the limit load due to the severe constraints created by the incompressibility of the plastic strains. This difficulty is always present when internal strains are computed from the derivatives of the interpolated displacements within the finite elements, and is effectively noticeable in 3-D and plane strain problems.

The marked difference between the BE and FE collapse loads depicted in figure 5.7.3 of example 5.7.1 (notched tensile specimen in plane strain) may well be explained by the above argument.

Still with reference to the pure elastoplastic BE formulations, a question is now posed;

Which procedure is more efficient?

The answer can only be obtained in the light of experience. Regarding to precision, the examples solved show that if load increment is kept small, the initial strain and both initial stress processes lead to entirely equivalent results (differences within the prescribed tolerance for convergence). Nevertheless, with relation to computer time, the initial strain version has proved to be faster than the initial stress. This difference, however, seems to be markedly due to the fact that in contrast with the initial strain program which is restricted to von Mises yield criterion, both versions of the initial stress routine are more general and can handle four different yield criteria.

As load increment was increased, the initial strain and the second initial stress versions exhibited more stable results than the former initial stress procedure, despite special techniques to avoid stress drifts beyond the yield surface. But in some of the examples run with relatively large load increments, the pure incremental form of the initial stress program produced equally reliable results, requiring less computer time than its second version.

The above discussion demonstrates the equivalence of the three processes and furthermore shows that the efficiency of the procedure is problem dependent. Ideally, all three options should be available for a general case.

Example No.	Title	Load increment ω (%)
5.4.1	Perforated Aluminium Strip	5.
5.4.2	Polystyrene Crazing Problem	25.
5.4.3	Plane Strain Punch	25.
5.4.4	Thick Cylinder	5.
5.7.1	Notched Tensile Specimen	12.5
5.7.2	Deep Circular Tunnel	20. †
5.7.3	Rough Punch	25.
5.8.1	Strip Footing	12.5
5.8.2	Shallow Tunnel	20. †
$\omega = \beta/\lambda_o$ (see expression (5.3.2))		
† approximated value		

Table 7.1 Load increments with reference to load at initial yield.

In order to complement the examples shown in Chapter 5, table 7.1 presents the load increment values adopted with reference to load at first yield. It should be noted that in the examples where a limit load was obtained, the load increment was subdivided further near to the collapse situation. This provided a more accurate estimate of the load bearing capacity.

According to the experience of the examples it was also observed that in cases where stress singularities (i.e., $\sigma_{ij} \to \infty$) occur at certain points (the edge of a rigid punch for instance), the value of the load increment could be increased to 50% or more without any significant change in the overall solution. Such

cases can be identified by an initial localized plastic region which starts to increase at much higher load levels. The rough punch problem (example 5.7.3) was found to be a typical case.

As for the number of iterations, a limiting value is left to be specified. This maximum should be such that under normal circumstances, when this number of iterations is achieved, a collapse situation is deemed to have occurred. This is often the case in problems where non-zero tractions instead of displacements are prescribed, and the material is perfectly plastic. Therefore, such a maximum number should be large enough to produce an accurate limit load. For the majority of problems solved, 200 iterations have been sufficient, but this could be increased to 300 if necessary.

The inclusion of time-dependent effects was accomplished in Chapter 6. This chapter presented a complete solution technique for viscoplastic problems using the constitutive equations due to Perzyna. The procedure is simple to implement numerically and is capable of handling pure creep problems in the same fashion. Also, elastoplastic solutions can be obtained by applying small load increments followed by stationary conditions.

The examples discussed illustrate the potentialities of the formulation and demonstrate that solutions for these classes of problems which were until recently the object of the finite element method as the only efficient alternative, are now possible within the context of the boundary element technique.

Since the boundary element equations are basically the same as those in Chapter 5, the same characteristics concerning symmetry and load bearing capacity are retained here. However, with reference to

the limit load when non-zero tractions are prescribed instead of displacements, a collapse situation is now characterized by $\dot{\varepsilon}_e^p \neq 0$ as $t \to \infty$. Consequently, when simulating pure elastoplastic solutions, a limiting number of time steps is desirable. According to the author's experience, a good number of these problems can be solved by adopting a constant time step length equal to the stability limit (note that stability does not guarantee accuracy). In such cases a maximum number of 200 time steps was found sufficient. Example 6.4.1 (deep beam) belongs to this class and was here solved by prescribing load increments of 6.25% of the load at first yield.

So far in this chapter, no comparison between the computer time required for the BE and FE solutions has been made. This is because such information was not readily available for the finite element results. Regarding example 6.4.3 (plate under thermal shrinkage), the computer time for the FE solution is given in reference [119], where a CDC 7600 was used. Herein, all the computer codes were implemented in the IBM 360/195 of the Rutherford Laboratory. Thus, a comparison of the overall solution times is given in Table 7.2 below.

Method	Computer	CPU time (sec.)	No. time steps
FE	CDC 7600	20.	69
BE	IBM 360/195	10.9	91

Table 7.2 Comparison between computer time for example 6.4.3.

It is worth mentioning that the finite element solution was computed by adopting a time step size control similar to what was presented in expressions (6.3.4) and (6.3.5) ($\eta_1 = 0.03$ and $\eta_o = 1.5$ for both methods) and that the same time step limit was employed for both solutions. Therefore, the fact that the BE solution required a larger number of time steps to achieve stationary condition is entirely explicable by the better representation of the singularity at the corners of the bonded edge and also by the exagerated stationarity criterion adopted here, i.e. $({}^{k+1}\varepsilon^p_e - {}^{k}\varepsilon^p_e) \leq 0.0001\ {}^{k}\varepsilon^p_e$. However, even though the number of time steps were larger, the BE solution is seen to be very efficient. Notice that the CDC computer is faster than the IBM, which makes the difference in equivalent CPU time even more pronounced.

In order to provide some comparison between the computational efficiency of the different solution procedures described throughout this work, the elastoplastic example 5.4.2 (polystyrene crazing problem - uniaxial tension) was solved by the initial strain, both initial stress and the "viscoplastic" procedures. The total number of iterations/time steps, together with the average number per displacement increment are presented in table 7.3. It should be noted that for the viscoplastic simulation, constant time steps equal to the stability limit were applied. In this case, the final resultant load obtained (see fig. 5.4.7b) differ from the pure elastoplastic solutions (initial strain/stress) by 0.4%, which shows that the accuracy of the solution did not deteriorate much. However, by using $\Delta t = \Delta t_{CRIT}/2$ this difference dropped to less than 0.1%, but the total number of time steps increased to 170 and its average per displacement increment became 18.89.

Procedure	n	$\bar{n}$
initial strain	158	17.56
first initial stress	157	17.44
second initial stress	156	17.33
"viscoplastic"	86	9.56

n = total number of iterations or time steps.

$\bar{n}$ = average number per displacement increment.

Table 7.3 Comparison between different procedures for the solution of example 5.4.2 (uniaxial tension case).

The computer time required for the total solution of the problem is presented in table 7.4. These values correspond to table 7.3 and clearly indicate that the viscoplastic simulation for pure plasticity problems can, in some cases, result in the most efficient procedure. Nevertheless, this should not be taken too far, since accuracy is not guaranteed by a constant time step equal to the stability limit.

Procedure	CPU time (sec.)
initial strain	11.8
both in. stress	12.4
"viscoplastic"	11.1

Table 7.4 Comparison between total computer time corresponding to table 7.3.

It is worth mentioning that although the applications described in these notes were restricted to associated plastic/viscoplastic material behaviour, this does not constitute any limitation to the

boundary element technique. Non-associated plasticity or viscoplasticity can be implemented with equal ease and the same can be said about kinematic hardening models under cyclic or repetitive loading conditions. All the equations introduced in Chapter 4 remain valid for such cases.

An interesting remark concerning inelastic applications of the boundary element method is that non-homogeneous problems can also be included. Here, two different procedures can be followed. The first possibility is by introducing subregions [1, 2, 23-25], which consists of defining internal boundaries limiting homogeneous regions within the body. Another valid procedure would be utilizing the internal cells to integrate an initial stress field which compensates for the different material constants. This second possibility appears to be promising, since both initial stress fields can be considered in a unified manner. However, further tests regarding to accuracy and computational efficiency will indicate the most suitable process.

Finally, with reference to extending the present work, axisymmetric inelastic problems can be dealt with by using the appropriate fundamental solution [122, 123] and following exactly the same procedures presented here. An initial attempt to formulate the boundary element technique for this sort of problems has recently been reported by the present author and co-workers in reference [121].

REFERENCES

1. BREBBIA, C.A. (1978). The Boundary Element Method for Engineers. Pentech Press, London.

2. BREBBIA, C.A. and WALKER, S. (1980). The Boundary Element Techniques in Engineering. Newes-Butterworths, London.

3. CRUSE, T.A. (1977). Mathematical Foundations of the Boundary Integral Equation Method in Solid Mechanics. Report No. AFOSR-TR-77-1002, Pratt and Whitney Aircraft Group.

4. JASWON, M.A. and SYMM, G.T. (1977). Integral Equation Methods in Potential Theory and Elastostatics. Academic Press, London.

5. SWEDLOW, J.L. and CRUSE, T.A. (1971). Formulation of Boundary Integral Equations for Three Dimensional Elastoplastic Flow. Int. J. Solids Structures, 7 : 1673 - 1683.

6. MENDELSON, A. (1973). Boundary Integral Methods in Elasticity and Plasticity. Report No. NASA TN D-7418, NASA.

7. RICCARDELLA, P.C. (1973). An Implementation of the Boundary Integral Technique for Planar Problems in Elasticity and Elastoplasticity. Report No. SM-73-10, Dept. Mech. Engng., Carnegie Mellon Univ., Pittsburg.

8. MENDELSON, A. and ALBERS, L.U. (1975). Application of Boundary Integral Equations to Elastoplastic Problems. In Boundary Integral Equation Method : Computational Applications in Applied Mechanics, (CRUSE and RIZZO eds.), ASME, New York : 47-84.

9. MUKHERJEE, S. (1977). Corrected Boundary Integral Equations in Planar Thermoelastoplasticity. Int. J. Solids Structures, 13:331-335.

10. BUI, H.D. (1978). Some Remarks About the Formulation of Three Dimensional Thermoelastoplastic Problems by Integral Equations. Int. J. Solids Structures, 14 : 935-939.

11. SMITH, G.D. (1978). Numerical Solution of Partial Differential Equations : Finite Difference Methods. 2nd ed., Clarendon Press, Oxford.

12. SOUTHWELL, R.V. (1946). Relaxation Methods in Theoretical Physics. Oxford Univ. Press, London.

13. TURNER, M.J.; CLOUGH, R.W.; MARTIN, H.C. and TOPP, L.J. (1956). Stiffness and Deflection Analysis of Complex Structures. J.Aero.Sci., 23 : 805-823.

14. CLOUGH, R.W. (1960). The Finite Element in Plane Stress Analysis. Proc. 2nd A.S.C.E. Conf. on Electronic Computation, Pittsburg, Pa.

15. ZIENKIEWICZ, O.C. (1977). The Finite Element Method. 3rd ed., McGraw Hill, London.

16. ODEN, J.T. (1972). Finite Elements of Nonlinear Continua. McGraw Hill, New York.

17. WATSON, J.O. (1972). The Analysis of Thick Shells with Holes by Integral Representation of Displacement. Ph.D. Thesis, University of Southampton.

18. BUTTERFIELD, R. and BANERJEE, P.K. (1971). The Problem of Pile Cap-Pile Group Interaction. Géotechnique, 21 : 135-142.

19. RIZZO, F.J. (1967). An Integral Equation Approach to Boundary Value Problems of Classical Elastostatics. Q. Appl. Math., 25 : 83-95.

20. CRUSE, T.A. (1969). Numerical Solutions in Three Dimensional Elastostatics. Int. J. Solids Structures, 5 : 1259-1274.

21. CRUSE, T.A. (1972). Application of the Boundary Integral Equation Solution Method in Solid Mechanics. In Variational Methods in Engineering, (BREBBIA and TOTTENHAM eds.), Southampton University Press., Vol. 2 : 9/1-9/29.

22. CRUSE, T.A. (1974) An Improved Boundary Integral Equation Method for Three Dimensional Elastic Stress Analysis. Comp. & Structures, 4 : 741-754.

23. LACHAT, J.C. and WATSON, J.O. (1977). Progress in the Use of Boudary Integral Equations Illustrated by Examples. Computer Meth. Appl. Mech. Engng., 10 : 273-289.

24. LACHAT, J.C. (1975). A Further Development of the Boundary Integral Technique for Elastostatics. Ph.D. Thesis, University of Southampton.

25. NAKAGUMA, R.K. (1979). Three Dimensional Elastostatics Using the Boundary Element Method. Ph.D. Thesis, University of Southampton.

26. LOVE, A.E.H. (1944). A Treatise on the Mathematical Theory of Elasticity. Dover, New York.

27. CRUSE, T.A. (1978). Two Dimensional BIE Fracture Mechanics Analysis. Appl. Math. Modelling, 2 : 287-293.

28. ZABREYKO, P.P. et al. (1975). Integral Equations - A Reference Text. Noordhoff, Holland.

29. FREDHOLM, I. (1903). Sur une Classe d'Equations Fonctionelles. Acta Math., 27 : 365-390.

30. KUPRADZE, V.D. (1965). Potential Methods in Theory of Elasticity. Israel Program for Scientific Translations. Jerusalem.

31. KELLOGG, O.D. (1929). Foundations of Potential Theory. Springer, Berlin.

32. SOMIGLIANA, C. (1886). Sopra l'Equilibrio di un Corpo Elastico Isotropo. Il Nuovo Ciemento, t. 17-19.

33. MIKHLIN, S.G. (1962). Singular Integral Equations . Amer. Math. Soc. Trans. Series 1, 10 : 84-197.

34. MUSKHELISHVILI, N.I. (1953). Singular Integral Equations. Noordhoff, Holland.

35. BETTI, E. (1872). Teoria dell Elasticita. Il Nuovo Ciemento, t.7-10.

36. CRUSE, T.A. and RIZZO, F.J. (eds.) (1975). Boundary Integral Equation Method : Computational Applications in Applied Mechanics. ASME, AMD - Vol. 11, New York.

37. CRUSE, T.A.; LACHAT, J.C.; RIZZO, F.J. and SHAW, R.P. (eds.) (1977). First Int. Symp. on Innovative Numerical Analysis in Applied Engineering Science. CETIM, Versailles.

38. BREBBIA, C.A. (ed.) (1978). Recent Advances in Boundary Element Methods. Pentech Press, London.

39. BANERJEE, P.K. and BUTTERFIELD, R. (eds.) (1979). Developments in Boundary Element Methods - Vol. 1. Applied Science Publishers, London.

40. BREBBIA, C.A. (ed.) (1980). New Developments in Boundary Element Methods. CML Publications, Southampton.

41. SHAW, R.P. et. al. (eds.) (1980). Innovative Numerical Analysis for the Engineering Sciences. University Press of Virginia, Charlottesville.

42. BREBBIA, C.A. (ed.) (1981). Progress in Boundary Elements - Vol. 1. Pentech Press, London.

43. BREBBIA, C.A. (ed.) (1981). Boundary Element Methods. Springer Verlag, Berlin.

44. MINDLIN, R.D. (1936). Force at a Point in the Interior of a Semi-infinite Solid. Physics, 7:195-202.

45. KUMAR, V. and MUKHERJEE, S. (1977). A Boundary Integral Equation Formulation for Time-Dependent Inelastic Deformation in Metals., Int. J. Mech. Sci., 19:713-724.

46. TELLES, J.C.F. and BREBBIA, C.A. (1979). On the Application of the Boundary Element Method to Plasticity. Appl. Math. Modelling., 3:466-470.

47. BANERJEE, P.K. and MUSTOE, G.G. (1978). The Boundary Element Method for Two Dimensional Problems of Elastoplasticity. In Recent Advances in Boundary Element Methods, (BREBBIA, ed.) University of Southampton, Southampton : 283-300.

48. MUKHERJEE, S. and KUMAR, V. (1978). Numerical Analysis of Time Dependent Inelastic Deformation in Metallic Media Using the Boundary Integral Equation Method. Trans. ASME, J. Appl. Mech., 45 : 785-790.

49. TELLES, J.C.F. and BREBBIA, C.A. (1980). The Boundary Element Method in Plasticity. Proc. 2nd Int. Seminar on Recent Advances in Boundary Element Methods, (BREBBIA, ed.), University of Southampton, Southampton : 295-317.

50. BANERJEE, P.K. and CATHIE, D.N. (1980). A Direct Formulation and Numerical Implementation of the Boundary Element Method for Two Dimensional Problems of Elastoplasticity. Int. J. Mech. Sci., 22 : 233-245.

51. CATHIE, D.N. (1980). On the Implementation of Elastoplastic Boundary Element Analysis. Proc. 2nd Int. Seminar on Recent Advances in Boundary Element Methods, (BREBBIA, ed.), University of Southampton, Southampton : 318-334.

52. TELLES, J.C.F. and BREBBIA, C.A. (1980). Elastoplastic Boundary Element Analysis. Proc. Europe - U.S. Workshop on Nonlinear Finite Element Analysis in Structural Mechanics, (Wunderlich et al., eds.), Ruhr-University Bochum, Germany : 403-434.

53. RZASNICKI, W. and MENDELSON, A. (1975). Application of Boundary Integral Method to Elastoplastic Analysis of V-Notched Beams. Int. J. Fracture, 11 : 329-342.

54. CHAUDONNERET,M. (1977). Méthode des Équations Intégrales Appliquées a la Résolution de Problèmes de Viscoplasticité. J. Mécanique Appliquée, 1 : 113-132.

55. MORJARIA, M. and MUKHERJEE, S. (1980). Improved Boundary Integral Equation Method for Time Dependent Inelastic Deformation in Metals. Int. J. Num. Meth. Engng., 15:97-111.

56. TELLES, J.C.F. and BREBBIA, C.A. (1981). New Developments in Elastoplastic Analysis. Proc. 3rd. Int. Seminar on Recent Advances in Boundary Element Methods, (BREBBIA, ed.), California, Irvine : 350-370.

57. MORJARIA, M. and MUKHERJEE, S. (1981). Numerical Analysis of Planar Time Dependent Inelastic Deformation of Plates with Cracks by the Boundary Element Method. Int. J. Solids Structures, 17 : 127-143.

58. TELLES, J.C.F. and BREBBIA, C.A. (1981). Elastic/Viscoplastic Problems Using Boundary Elements. Int. J. Mech. Sci., in Press.

59. TELLES, J.C.F. and BREBBIA, C.A. (1981). Boundary Element Solution for Half-Plane Problems. Int. J. Solids Structures, 17 : 1149-1158.

60. HILL, R. (1950). The Mathematical Theory of Plasticity. Clarendon Press, Oxford.

61. FORD, H. and ALEXANDER, J.M. (1977). Advanced Mechanics of Materials. 2nd ed., Ellis Horwood, Chichester.

62. PRAGER, W. and HODGE, P.G. (1968). Theory of Perfectly Plastic Solids. Dover, New York.

63. MENDELSON, A. (1968). Plasticity : Theory and Application. Macmillan, New York.

64. CHEN, W.F. (1975). Limit Analysis and Soil Plasticity. Elsevier, Amsterdam.

65. LIN, T.H. (1968). Theory of Inelastic Structures. Wiley, New York.

66. PENNY, R.K. and MARRIOTT, D.L. (1971). Design for Creep. McGraw-Hill, London.

67. ODQVIST, F.K.G. (1974). Mathematical Theory of Creep and Creep Rupture. 2nd ed., Clarendon Press, Oxford.

68. MALVERN, L.E. (1969). Introduction to the Mechanics of a Continuous Medium. Prentice-Hall, New Jersey.

69. FUNG, Y.C. (1965). Foundations of Solid Mechanics. Prentice-Hall, New Jersey.

70. JOHNSON, W. and MELLOR, P.B. (1962). Plasticity for Mechanical Engineers. Van Nostrand, London.

71. OLSZAK. W.; MROZ, Z. and PERZYNA, P. (1963). Recent Trends in the Development of the Theory of Plasticity. Pergamon Press - PWN, Oxford-Warsaw.

72. PERZYNA, P. (1966). Fundamental Problems in Viscoplasticity. Adv. Appl. Mech., 9 : 243-377.

73. PERZYNA, P. (1963). The Constitutive Equations for Rate Sensitive Plastic Materials. Quart. Appl. Math., 20 : 321-332.

74. OLSZAK, W. and PERZYNA, P. (1970). Stationary and Non Stationary Visco-Plasticity. In Inelastic Behaviour of Solids, (KANNINEN, et al. eds.), McGraw-Hill : 53-75.

75. TIMOSHENKO, S.P. and GOODIER, J.N. (1970). Theory of Elasticity. 3rd ed., McGraw-Hill, Tokyo.

76. NAYAK, G.C. and ZIENKIEWICZ, O.C. (1972). Convenient Form of Stress Invariants for Plasticity. Proc. Am. Soc. Civ. Engrs., J. Struct. Div., 98 : 949-954.

77. BESSELING, J.F. (1958). A Theory of Elastic, Plastic and Creep Deformations of an Initially Isotropic Material Showing Anisotropic Strain Hardening, Creep Recovery, and Secondary Creep. Trans. ASCE, J. Appl. Mech., 25 : 529-536.

78. OWEN, D.R.J.; PRAKASH, A. and ZIENKIEWICZ, O.C. (1974). Finite Element Analysis of Nonlinear Composite Materials by use of Overlay Stystems. Computer and Struct., 4 : 1251-1267.

79. MELAN, E. (1932). Der Spannungszustand der durch eine Einzelkraft im Innern beanspruchten Halbscheibe. Z. Angew. Math. Mech., 12 : 343-346.

80. WYLIE, C.R. (1975). Advanced Engineering Mathematics. 4th ed., McGraw-Hill, Tokio.

81. GRADSHTEYN, I.S. and RYZHIK, I.M. (1965). Table of Integrals, Series and Products. Academic Press, London.

82. POULOS, H.G. and DAVIS, E.H. (1974). Elastic Solutions for Soil and Rock Mechanics. Wiley, New York.

83. HARTMANN, F. (1980). Computing the C-Matrix in Non-Smooth Boundary Points. Proc. 2nd Int. Seminar on Recent Advances in Boundary Element Methods, (BREBBIA, ed.), University of Southampton, Southampton : 367-379.

84. RIZZO, F.J. and SHIPPY, D.J. (1977). An Advanced Boundary Integral Equation Method for Three Dimensional Thermoelasticity. Int. J. Num. Meth. Engng., 11 : 1753-1768.

85. DANSON, D.J. (1981). A Boundary Element Formulation of Problems in Linear Isotropic Elasticity with Body Forces. Proc. 3rd Int. Seminar on Recent Advances in Boundary Element Methods, (BREBBIA, ed.), California, Irvine : 105-122.

86. MANSUR, W.J.; HALBRITTER, A.L. and TELLES, J.C.F. (1979). Boundary Element Method-Formulation for Two Dimensional Elasticity. Commemorative Annals of the 15th Anniversary of COPPE-UFRJ, (COPPE-UFRJ ed. in Portuguese), Rio de Janeiro : 1-22.

87. CHAUDONNERET, M. (1978). On the Discontinuity of the Stress Vector in the Boundary Integral Equation Method for Elastic Analysis. Proc. 1st Int. Seminar on Recent Advances in Boundary Element Methods, (BREBBIA, ed.), Southampton : 185-194.

88. TELLES, J.C.F.; MANSUR, W.J. and HALBRITTER, A.L. (1978). The Boundary Element Method Applied to Two Dimensional Linear Elasticity. Proc. 2nd. Symposium on Computational Systems for Civil Engineering, (CESP ed. in Portuguese), São Paulo : 303-314.

89. JEFFERY, G.B. (1920). Plane Stress and Plane Strain in Bipolar Coordinates. Trans. Roy. Soc. (London), Ser. A, 221 : 265-293.

90. MINDLIN, R.D. (1948). Stress Distribution Around a Hole Near the Edge of a Plate Under Tension. Proc. Soc. Exptl. Stress. Anal., 5 : 56-68.

91. WATSON, J.D. (1979). Advanced Implementation of the Boundary Element Method for Two and Three Dimensional Elastostatics. Chapter 3 in [39].

92. SCHREYER, H.L.; KULAK, R.F. and KRAMER, J.M. (1979). Accurate Numerical Solutions for Elastic-Plastic Models. Trans. ASME, J. Pressure Vessel Technology, 101 : 226-234.

93. ZIENKIEWICZ, O.C.; VALLIAPPAN, S. and KING, I.P. (1969). Elasto-Plastic Solutions of Engineering Problems, Initial Stress Finite Element Approach. Int. J. Num. Meth. Engng., 1 : 75-100.

94. THEOCARIS, P.S. and MARKETOS, E. (1964). Elastic-Plastic Analysis of Perforated Thin Strips of a Strain Hardening Material. J. Mech. Phys. Solids, 12 : 377-390.

95. BATHE, K.J.; OZDEMIR, H. and WILSON, E.L. (1974). Static and Dynamic Geometric and Material Non-Linear Analysis. Report No. UCSESM74-4, Dept. Civil Engng., Univ. of California, Berkeley.

96. ZIENKIEWICZ, O.C. and CORMEAU, I.C. (1974). Viscoplasticity, Plasticity and Creep in Elastic Solids, a Unified Numerical Solution Approach. Int. J. Num. Methods Engng, 8 : 821-845.

97. HAWARD, R.N. and OWEN, D.R.J. (1973). The Yielding of a Two Dimensional Void Assembly in an Organic Glass. J. Materials Sci., 8 : 1136-1144.

98. NAYAK, G.C. and ZIENKIEWICZ, O.C. (1972). Elasto-Plastic Stress Analysis : a Generalization for Various Constitutive Relations Including Strain Softening. Int. J. Num. Methods Engng., 5 : 113-135.

99. DRUCKER, D.C. and PRAGER, W. (1952). Soil Mechanics and Plastic Analysis or Limit Design. Q. Appl. Math., 10 : 157-165.

100. BUSHNELL, D. (1977). A Strategy for the Solution of Problems Involving Large Deflections, Plasticity and Creep. Int. J. Num. Methods Engng., 11 : 683-708.

101. YAMADA, Y.; YOSHIMURA, N. and SAKURAI, T. (1968). Plastic Stress-Strain Matrix and its Application for the Solution of Elastic-Plastic Problems by the Finite Element Method. Int. J. Mech. Sci., 10 : 343-354.

102. REYES, S.F. and DEERE, D.U. (1966). Elastic-Plastic Analysis of Underground Openings by the Finite Element Method. Proc. 1st.Int. Congr. Rock Mechanics, Lisbon : 477-483.

103. BAKER, L.E.; SHANDU, R.S. and SHIEH, W.Y. (1969). Application of Elastoplastic Analysis in Rock Mechanics by Finite Element Method . Proc. 11th Symp. Rock Mechanics., (SOMERTON, ed.) University of California, Berkeley: 237-251.

104. CHEN, A.C.T. and CHEN, W.F. (1975). Constitutive Equations and Punch-Indentation of Concrete. Proc. Am. Soc. Civ. Engrs., J. Engng. Mech. Div., 101 : 889-906.

105. ZIENKIEWICZ, O.C.; HUMPHESON, C. and LEWIS, R.W. (1975). Associated and Non-Associated Visco-Plasticity and Plasticity in Soil Mechanics. Géotechnique, 25 : 671-689.

106. DAHLQUIST, G. and BJÖRCK, A. (1974). Numerical Methods. Prentice-Hall, New Jersey.

107. GEAR, C.W. (1971). Numerical Initial Value Problems in Ordinary Differential Equations. Prentice-Hall, New Jersey.

108. LAMBERT, J.D. (1973). Computational Methods in Ordinary Differential Equations. Wiley, London.

109. WROBEL, L.C. and BREBBIA, C.A. (1981). Time-Dependent Potential Problems. Chapter 6 in [42].

110. PENNY, R.K. (1967). The Creep of Spherical Shells Containing Discontinuities. Int. J. Mech. Sci., 9 : 373-388.

111. PENNY, R.K. and HAYHURST, D.R. (1969). The Deformations and Stresses in a Stretched Thin Plate Containing a Hole During Stress Redistribution Caused by Creep. Int. J. Mech. Sci., 11 : 23-39.

112. ZIENKIEWICZ, O.C. and CORMEAU, I.C., (1973). Viscoplasticity and Plasticity, an Alternative for Finite Element Solution of Material Nonlinearities. Proc. Colloque Meth. Calcul. Scie. Tech., IRIA, Paris : 171-199.

113. SUTHERLAND, W.H. (1970). AXICRIP - Finite Element Computer Code for Creep Analysis of Plane Stress, Plane Strain and Axisymmetric Bodies. Nucl. Eng. and Design, 11 : 269-285.

114. CORMEAU, I. (1975). Numerical Stability in Quasi-Static Elasto/Viscoplasticity. Int. J. Num. Meth. Engng., 9 : 109-127.

115. IRONS, B. and TREHARNE, G. (1971). A Bound Theorem in Eigenvalues and its Practial Applications. Proc. 3rd Conf. Matrix Meth. Struct. Mech., Wright-Patterson A.F.B., Ohio : 245-254.

116. ANAND, S.C.; LEE, S.L. and ROSSOW, E.C. (1970). Finite Element Analysis based upon Tresca Yield Criterion. Ingenieur - Archiv, 39 : 73-86.

117. SIM, R.G. (1972). Reference Results for Plane Stress Creep Behaviour. J. Mech. Engng. Sci., 14 : 404-410.

118. BAUER, F. and REISS, E.L. (1970). On the Numerical Determination of Shrinkage Stresses. Trans. ASME, J. Appl. Mech., March : 123-127.

119. CORMEAU, I.C. (1976). Viscoplasticity and Plasticity in the Finite Element Method. Ph.D. Thesis, University College of Swansea.

120. NAGTEGAAL, J.C.; PARKS, D.M. and RICE, J.R. (1974). On Numerically Accurate Finite Element Solutions in the Fully Plastic Range. Comp. Meth. Appl. Mech. Engng., 4 : 153-177.

121. DOBLARE, M.; TELLES, J.; BREBBIA, C. and ALARCON, E. (1981). Boundary Element Formulation for Elastoplastic Analysis of Axisymmetrical Bodies. Paper Presented at the 3rd Int. Seminar on Recent Advances in Boundary Element Methods. California, Irvine.

122. CRUSE, T.A.; SNOW, D.W. and WILSON, R.B. (1977). Numerical Solutions in Axisymmetric Elasticity. Comp.and Structures, 7 : 445-451.

123. KERMANIDIS, T. (1975). A Numerical Solution for Axially Symmetrical Elasticity Problems. Int. J. Solids Structures, 11 : 493-500.

APPENDIX A

INDIRECT COMPUTATION OF PRINCIPAL VALUES

In what follows a simple and general numerical procedure to calculate the principal values of the inelastic strain integrals is proposed [46]. It is expected that it will allow higher order interpolation functions to be used and consequently the numerical approximations would be improved.

For simplicity and without loss of generality for the three dimensional case, equation (4.6.9) of Chapter 4 will only be considered. This equation is repeated here for completeness

$$\dot{\underset{\sim}{\sigma}} = \underset{\sim}{G'}\,\dot{\underset{\sim}{p}} - \underset{\sim}{H'}\,\dot{\underset{\sim}{u}} + (\underset{\sim}{D'} + \underset{\sim}{C'})\,\dot{\underset{\sim}{\varepsilon}}^{a} \qquad (A.1)$$

where in order to concentrate the attention to the domain integrals, the expressions for stresses at boundary nodes (see Appendix B) are not included.

To understand better the difficulties that arise in computing matrix $\underset{\sim}{D'}$, let us consider the triangular cell with linear interpolation functions of figure 4.7.1. In this case, with reference to expression (4.7.17), one notices that if the internal point where the stress rates are to be calculated is different from points 1, 2 or 3 (herein it is assumed that no internal point is located inside cells), no difficulty arises and one can integrate numerically as usual. When the singular point coincides with one of the corner points, point 2 for instance, no standard integration over the cell, corresponding to integrands where ξ_2 appears, is permissible and we need to calculate

the principal value taking into consideration all the adjacent cells connected to point 2. Integration where ξ_1 and ξ_3 appear will be allowable because although r assumes zero value at point 2, the interpolation functions are also zero at this point.

One can easily verify that for any kind of interpolation functions or cells shape, always a 3 × 3 block corresponding to each internal point remains to be calculated in matrix $\underset{\sim}{D}'$. The analytical calculation of such principal values may produce complex limiting expressions, but it is here proposed to compute these blocks by a numerical procedure based on the fact that a free body, under the application of an inelastic strain field, will have no internal stresses if the field satisfies the compatibility conditions [75] (see equation (2.2.26)). Constant inelastic strains satisfy this requirement, and the boundary displacements can be determined as functions of the differences between the Cartesian coordinate of the boundary node under consideration and a reference point which is supposed to be fixed with zero rotations (Appendix C presents such expressions).

In this case, equation (A.1) assumes the form

$$(\underset{\sim}{D}' + \underset{\sim}{C}')\underset{\sim}{\bar{\varepsilon}}^a = \underset{\sim}{H}' \underset{\sim}{\bar{u}}. \qquad (A.2)$$

As before, let us call $(\underset{\sim}{D}' + \underset{\sim}{C}')$ by $\underset{\sim}{D}^*$ where $\underset{\sim}{C}'$ is known but the above mentioned 3 × 3 submatrices of $\underset{\sim}{D}'$ are to be determined. Furthermore, $\underset{\sim}{C}'$ is non-zero only where $\underset{\sim}{D}'$ is unknown, which means that all the terms of $\underset{\sim}{D}^*$ other than the unknown 3 × 3 blocks are equal to the corresponding $\underset{\sim}{D}'$ terms.

Hence, equation (A.2) can be written as

$$\underset{\sim}{D}^* \underset{\sim}{\bar{\varepsilon}}^a = \underset{\sim}{H}' \underset{\sim}{\bar{u}} \qquad (A.3)$$

or, in expanded form

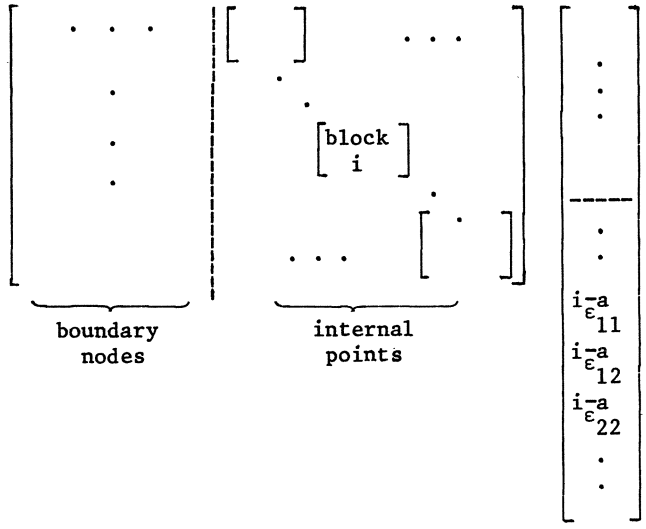

$$= \underset{\sim}{H}' \bar{\underset{\sim}{u}} \quad . \qquad (A.4)$$

Since equation (A.4) is valid for any constant inelastic field, one can first assume that $\bar{\varepsilon}^a_{11} = 1$ while $\bar{\varepsilon}^a_{12} = \bar{\varepsilon}^a_{22} = 0$. This will produce a series of independent equations which give the terms of the first columns of all the 3 x 3 blocks.

The same procedure can be used for $\bar{\varepsilon}^a_{12} = 1$; $\bar{\varepsilon}^a_{11} = \bar{\varepsilon}^a_{22} = 0$ and for $\bar{\varepsilon}^a_{22} = 1$; $\bar{\varepsilon}^a_{11} = \bar{\varepsilon}^a_{12} = 0$, and they will give respectively all the terms of the second and third columns of the unknown blocks.

The above numerical scheme allows for the computation of the principal values together with the corresponding free terms. However, one of the advantages of the boundary element technique applied inelastic problems is that the domain discretization is only necessary where inelastic strains actually occur. The present procedure appears to loose this advantage because the entire domain has to be discretized to consider the constant inelastic strain fields.

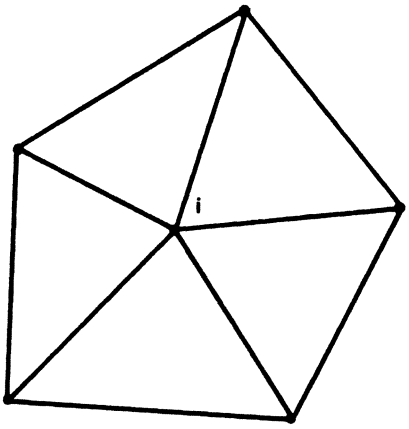

Fig. A.1 Internal region corresponding to all adjacent cells connected to the stress point i.

To avoid this disadvantage a somewhat less restrictive implementation can be used. It has been shown that only the cells connected to the singular point need to be considered to determine the corresponding unknown submatrix. Let us consider the part of the domain formed by such cells as shown in figure A.1. One can apply equation (A.3) to this small region where point i is the only interior point and proceed as before to calculate the three columns of the corresponding unknown block.

In this case equation (A.3) gives

$$\begin{bmatrix} \cdots & \vdots & \text{block} \\ \cdots & \vdots & i \\ \cdots & \vdots & \end{bmatrix}_{3 \times 3\ (n+1)} \begin{bmatrix} \\ \vdots \\ \\ \hline i_{\bar{\varepsilon}^a_{11}} \\ i_{\bar{\varepsilon}^a_{12}} \\ i_{\bar{\varepsilon}^a_{22}} \end{bmatrix} = i_{\underset{\sim}{H}'}\, \bar{\underset{\sim}{u}} \qquad (A.5)$$

where n is the number of internal cells connected to point i and $i_{\underset{\sim}{H}'}$ as well as $\bar{\underset{\sim}{u}}$ are defined over the boundary of this small region. It should be noted that for computational purposes the contribution of each cell to block i is obtained while actually computing matrix $'\underset{\sim}{d}$; i.e., after performing the allowable integrals over the cell, the same routine that performs the boundary integrals of $\underset{\sim}{h}'$ is called to integrate over the opposite side of the cell. The appropriate operations are then carried out and matrix $'\underset{\sim}{d}$ becomes ready to be assembled in complete form, including not only the principal values but also the partial contribution of the corresponding terms of $\underset{\sim}{C}'$.

The use of constant strain fields to compute the principal values of the inelastic strain integrals offers many computational advantages, since it is independent of the type of cells and allows the use of higher order interpolation functions without any increase in complexity.

APPENDIX B

STRESS RATES AT BOUNDARY NODES

Figure B.1 presents a linear boundary element with reference to its local coordinate system.

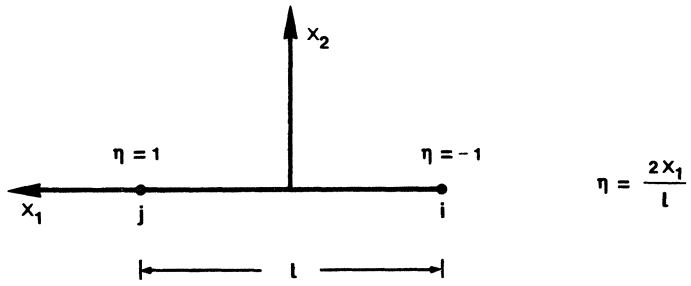

Fig. B.1 Linear boundary element and local coordinate system.

The interpolation functions can be written as

$$N_i = \frac{1}{2}(1-\eta) \tag{B.1}$$

$$N_j = \frac{1}{2}(1+\eta) \ . \tag{B.2}$$

Displacement rates over the boundary element can be calculated using expressions (B.1) and (B.2)

$$\dot{u}_1(\eta) = N_i \ {}^{i}\dot{u}_1 + N_j \ {}^{j}\dot{u}_1 \tag{B.3}$$

$$\dot{u}_2(\eta) = N_i \ {}^{i}\dot{u}_2 + N_j \ {}^{j}\dot{u}_2 \tag{B.4}$$

where ${}^{i}\dot{u}_1$, ${}^{i}\dot{u}_2$ and ${}^{j}\dot{u}_1$, ${}^{j}\dot{u}_2$ are the nodal displacement rates at nodes i and j with reference to the local axes.

The component of the total strain rate tensor along the element axis is easily evaluated as

$$\dot{\varepsilon}_{11} = \frac{\partial \dot{u}_1}{\partial x_1} = \frac{1}{\ell}({}^{j}\dot{u}_1 - {}^{i}\dot{u}_1) \quad . \tag{B.5}$$

The traction rate vector in the local coordinate system will give directly two components of the stress rate tensor at any of the two boundary nodes. In what follows the computation of the only unknown component of the stress rate tensor at node j will be presented, but the same procedure is applicable to node i .

The components of the traction rate vector at node j give

$${}^{j}\dot{\sigma}_{22} = {}^{j}\dot{p}_2 \tag{B.6}$$

$${}^{j}\dot{\sigma}_{12} = {}^{j}\dot{p}_1 \quad . \tag{B.7}$$

Starting with the plane strain case, one can write expression (2.4.5) ($\dot{\hat{\theta}} = 0$) for ${}^{j}\dot{\sigma}_{22}$ as follows

$$\frac{{}^{j}\dot{\sigma}_{22}}{2G} = {}^{j}\dot{\varepsilon}_{22} + \frac{\nu}{1-2\nu}\,{}^{j}\dot{\varepsilon}_{kk} - {}^{j}\dot{\varepsilon}^{a}_{22} \tag{B.8}$$

which gives

$${}^{j}\dot{\varepsilon}_{22} = \frac{1}{1-\nu}\left[(1-2\nu)\left(\frac{{}^{j}\dot{\sigma}_{22}}{2G} + {}^{j}\dot{\varepsilon}^{a}_{22}\right) - \nu\,\dot{\varepsilon}_{11}\right] \quad . \tag{B.9}$$

Rewriting expression (2.4.5) for ${}^{j}\dot{\sigma}_{11}$ and substituting ${}^{j}\dot{\varepsilon}_{22}$ calculated above, we find

$${}^{j}\dot{\sigma}_{11} = \frac{1}{1-\nu}\,(2G\dot{\varepsilon}_{11} + \nu\,{}^{j}\dot{\sigma}_{22}) + 2G\left(\frac{\nu}{1-\nu}\,{}^{j}\dot{\varepsilon}^{a}_{22} - {}^{j}\dot{\varepsilon}^{a}_{11}\right) \quad . \tag{B.10}$$

Proceeding as before, but using equation (2.4.5) for plane stress, the following expression arises

$$\dot{j\sigma}_{11} = \frac{1}{1-\bar{\nu}} (2G\dot{\varepsilon}_{11} + \bar{\nu}\, \dot{j\sigma}_{22}) - \frac{2G}{1-\bar{\nu}} \dot{j\varepsilon}^{a}_{11} \qquad (B.11)$$

where

$$\bar{\nu} = \nu/(1+\nu) \ . \qquad (B.12)$$

For the initial stress formulation the procedure is analogous. The final expression is given by (plane strain)

$$\dot{j\sigma}_{11} = \frac{1}{1-\nu} (2G\dot{\varepsilon}_{11} + \nu \dot{j\sigma}_{22}) + \frac{\nu}{1-\nu} \dot{j\sigma}^{a}_{22} - \dot{j\sigma}^{a}_{11} \qquad (B.13)$$

where for plane stress ν is replaced by $\bar{\nu}$. Note that the condition of incompressibility of the inelastic strains is not included any more.

Replacing j by i in (B.10), (B.11) and (B.13), the equivalent expressions for node i are obtained.

It should be noticed that after performing the required coordinate transformations (local to global axes), the above expressions become ready to be assembled into the corresponding global matrices. Here, the contribution of adjacent elements to the common boundary nodes is automatically averaged for non-double nodes.

APPENDIX C

DISPLACEMENTS DUE TO CONSTANT INELASTIC STRAIN FIELDS

Recalling expression (2.2.24) of Chapter 2, one can easily verify that the displacements of any boundary node in a free body due to a constant inelastic strain field can be calculated with reference to a point which has zero displacements and zero rotations by simply using the total strain components, i.e.

$$\bar{u}_i = \bar{\varepsilon}_{ij} \Delta x_j \tag{C.1}$$

where Δx_j is the difference between the j coordinate of the node and the reference point.

In plane strain problems, because of $\dot{\hat{\theta}} = 0$ and $\varepsilon_{33} = 0$ conditions, the following relation arises

$$\bar{\varepsilon}_{ij} = \bar{\varepsilon}^a_{ij} - \nu \bar{\varepsilon}^a_{kk} \delta_{ij} \, . \tag{C.2}$$

For the plane stress case, the equivalent expression is simply

$$\bar{\varepsilon}_{ij} = \bar{\varepsilon}^a_{ij} \, . \tag{C.3}$$

Expression (C.1) together with (C.2) or (C.3) provides the required expressions for the displacements.

APPENDIX D

SOME PARTICULAR EXPRESSIONS FOR 2-D INELASTIC PROBLEMS

With reference to the initial strain formulation of Section 5.2, the following expressions are valid for 2-D plasticity problems:

$$\sigma_z = \begin{cases} \nu(\sigma_x + \sigma_y) + E(\varepsilon_x^p + \varepsilon_y^p + \Delta\varepsilon_x^p + \Delta\varepsilon_y^p) & \text{(plane Strain)} \\ 0 & \text{(plane stress)} \end{cases} \tag{D.1}$$

$$\begin{aligned} \varepsilon'_x &= \frac{1}{E}\left[\sigma_x - \nu(\sigma_y + \sigma_z)\right] + \Delta\varepsilon_x^p \\ \varepsilon'_{xy} &= \frac{\sigma_{xy}}{2G} + \Delta\varepsilon_{xy}^p \\ \varepsilon'_y &= \frac{1}{E}\left[\sigma_y - \nu(\sigma_x + \sigma_z)\right] + \Delta\varepsilon_y^p \end{aligned} \tag{D.2}$$

$$\varepsilon'_z = \begin{cases} \varepsilon_x^p + \varepsilon_y^p & \text{(plane strain)} \\ -\left[\frac{\nu}{E}(\sigma_x + \sigma_y) + \Delta\varepsilon_x^p + \Delta\varepsilon_y^p\right] & \text{(plane stress)} \end{cases}$$

$$\varepsilon_{et} = \frac{\sqrt{2}}{3}\sqrt{(\varepsilon'_x - \varepsilon'_y)^2 + (\varepsilon'_y - \varepsilon'_z)^2 + (\varepsilon'_z - \varepsilon'_x)^2 + 6(\varepsilon'_{xy})^2} \tag{D.3}$$

$$\begin{aligned} \Delta\varepsilon_x^p &= \frac{\Delta\varepsilon_e^p}{3\varepsilon_{et}}(2\varepsilon'_x - \varepsilon'_y - \varepsilon'_z) \\ \Delta\varepsilon_{xy}^p &= \frac{\Delta\varepsilon_e^p}{\varepsilon_{et}}\varepsilon'_{xy} \\ \Delta\varepsilon_y^p &= \frac{\Delta\varepsilon_e^p}{3\varepsilon_{et}}(2\varepsilon'_y - \varepsilon'_z - \varepsilon'_x) \,. \end{aligned} \tag{D.4}$$

For the initial stress formulation of Chapter 5 it is convenient to write a_{ij} in vector form as follows

$$\underset{\sim}{a} = \begin{Bmatrix} a_{11} \\ 2a_{12} \\ a_{22} \\ a_{33} \end{Bmatrix} . \qquad (D.5)$$

In addition, $\bar{d}_{ij}$ defined in Chapter 6 expression (6.2.18) can be represented for plane strain in the following form

$$\underset{\sim}{\bar{d}} = 2G \begin{Bmatrix} a_{11} + \omega \\ a_{12} \\ a_{22} + \omega \\ a_{33} + \omega \end{Bmatrix} \quad ; \quad \omega = \frac{\nu}{1-2\nu} (a_{11} + a_{22} + a_{33}) \qquad (D.6)$$

whereas for plane stress

$$\underset{\sim}{\bar{d}} = 2G \begin{Bmatrix} a_{11} + \omega \\ a_{12} \\ a_{22} + \omega \\ 0 \end{Bmatrix} \quad ; \quad \omega = \frac{\bar{\nu}}{1-2\bar{\nu}} (a_{11} + a_{22}) . \qquad (D.7)$$

The above vectors allow expression (5.5.22) and (5.5.26) to be written as

$$\gamma' = \underset{\sim}{a}^T \bar{\underset{\sim}{d}} + \frac{d\psi}{d\varepsilon^p_e} \tag{D.8}$$

and

$$\begin{Bmatrix} d\sigma_x \\ d\sigma_{xy} \\ d\bar{\sigma}_y \\ d\sigma_z \end{Bmatrix} = \begin{Bmatrix} d\sigma^e_x \\ d\sigma^e_{xy} \\ d\sigma^e_y \\ d\sigma^e_z \end{Bmatrix} - \frac{1}{\gamma'} \bar{\underset{\sim}{d}} \underset{\sim}{a}^T \begin{Bmatrix} d\sigma^e_x \\ d\sigma^e_{xy} \\ d\sigma^e_y \\ d\sigma^e_z \end{Bmatrix} \tag{D.9}$$

in which

$$d\sigma^e_z = \begin{cases} \nu(d\sigma^e_x + d\sigma^e_y) & \text{(plane strain)} \\ \\ 0 \ . & \text{(plane stress)} \end{cases} \tag{D.10}$$

Also, expression (6.2.17) is now of the form

$$\begin{Bmatrix} \dot{\sigma}^a_x \\ \dot{\sigma}^a_{xy} \\ \dot{\sigma}^a_y \\ \dot{\sigma}^a_z \end{Bmatrix} = \gamma \langle \phi \rangle \ \bar{\underset{\sim}{d}} \tag{D.11}$$

where it should be noted that σ_z is computed by the following relation

$$\sigma_z = \begin{cases} \nu(\sigma_x + \sigma_y + \sigma^a_x + \sigma^a_y) - \sigma^a_z & \text{(plane strain)} \\ \\ 0 \ . & \text{(plane stress)} \end{cases} \tag{D.12}$$

Finite Element Systems

A Handbook

Editor: **C. A. Brebbia**

2nd revised edition. 1983. Approx. 300 figures.
Approx. 500 pages
Cooperation with Computational Mechanics Centre, Southampton
ISBN 3-540-12118-8

The finite element method has become, because of its versatility, one of the most important tools used by engineers. However, there are at present so many different finite element systems that users often find it difficult to appreciate the advantages or disadvantages of a system for a particular problem that they want to solve.
This handbook contains descriptions of over 30 of the most well known finite element systems available, plus some special systems. The capability and facilities of the systems are described and examples of their use are given. One important feature of the Handbook is the tables giving essential information on the elements provided in a system, the type of material models available, the computer system the programs will run on, names and addresses of system providers, etc. The volume also provides information on pre- and post-processing packages.
This work is an essential reference for engineers who need up-to-date information on finite element systems and who wish to select the most appropriate finite element system for their work.

Engineering Software III

Proceedings of the 3rd International Conference, Imperial College, London, England, April 1983

Editor: **R. A. Adey**

1983. Approx. 200 figures. Approx. 1000 pages
Cooperation with Computational Mechanics Centre, Southampton
Distribution rights for all countries:
Springer-Verlag Berlin Heidelberg New York Tokyo

The theme of these conference proceedings is the use and application of computers in engineering. Many abbreviations have been invented to describe the use of computers, such as CAD, CAM, CADMAT etc., but the term which best describes the scope of the conference proceedings is Computer Aided Engineering, CAE.

Springer-Verlag
Berlin
Heidelberg
New York
Tokyo

Boundary Element Methods

Proceedings of the Third International Seminar, Irvine, California, July 1981
Editor: **C. A. Brebbia**
Seminar sponsored by the International Society for Computational Methods in Engineering
1981. 232 figures. XXIV, 622 pages. ISBN 3-540-10816-5

From the Contents: Potential and Fluid Flow Problems. – Elasticity Problems. – Geomechanics. – Material Problems. – Numerical Techniques and Mathematical Principles. – Coupling of Boundary and Finite Element Methods.

Boundary Element Methods in Engineering

Proceedings of the Fourth International Seminar, Southampton, England, September 1982
Editor: **C. A. Brebbia**
Seminar sponsored by the International Society for Computational Methods in Engineering
1982. 291 figures. X, 649 pages. ISBN 3-540-11819-5

Contents: Basic Principles. – Potential Problems. – Solid Mechanics. – Stress Concentration and Fracture Mechanics. – Plate Bending Problems. – Applications. – Combination with Other Techniques.

Computational Methods and Experimental Measurements

Proceedings of the International Conference, Washington, DC, July 1982
Sponsored by the International Society for Computational Methods in Engineering
Editors: **G. A. Keramidas, C. A. Brebbia**
1982. XIV, 838 pages
Cooperation with Computational Mechanics Centre, Southampton
ISBN 3-540-11648-6

Contents: Keynote Address. – System Identification. Water Resources. – Data Identification. Atmospheric Fluid Dynamics. – Material Identification. Geophysical Fluid Dynamics. – Structural Dynamics. Fluid Dynamics. – Structural Application. Wave & Structures. – Soil Dynamics. Fluid-Structure Interaction. – Geomechanics. – Free-Surface Flow. – Structural Applications. Sediment Transport. – Fracture Mechanics. Heat Transfer. – Structures. Fluid Mechanics.

Nonlinear Finite Element Analysis in Structural Mechanics

Proceedings of the Europe–U. S. Workshop
Ruhr-Universität, Bochum, Germany, July 28–31, 1980
Editors: **W. Wunderlich, E. Stein, K.-J. Bathe**
1981. 272 figures. XIII, 777 pages. ISBN 3-540-10582-4

This proceedings volume contains the 38 papers presented at the Europe–U. S. Workshop held at the Ruhr-University, Bochum in August 1980. They give an overview of the current state of the art in nonlinear finite element analysis in those areas of structural mechanics where research has been most active and further progress can be expected in the future.

Springer-Verlag
Berlin
Heidelberg
New York
Tokyo

Lecture Notes in Engineering

Edited by C.A. Brebbia and S.A. Orszag

Vol. 1: J.C.F. Telles,
The Boundary Element Method
Applied to Inelastic Problems
IX, 243 pages. 1983

Vol. 2: Bernard Amadei,
Rock Anisotropy and
the Theory of Stress Measurements
XVII, 479 pages. 1983